TECHNISCHE UNIVERSITÄT MÜNCHEN

Wissenschaftszentrum Weihenstephan für Ernährung, Landnutzung und Umwelt (WZW)

Lehrstuhl für Biochemische Pflanzenpathologie

Loss of S-NITROSOGLUTATHIONE REDUCTASE 1 (GSNOR1) function leads to an altered DNA and histone methylation pattern in *Arabidopsis thaliana*

Eva Rudolf

Vollständiger Abdruck der von der Fakultät Wissenschaftszentrum Weihenstephan für Ernährung, Landnutzung und Umwelt der Technischen Universität München zur Erlangung des akademischen Grades eines

Doktors der Naturwissenschaften

genehmigten Dissertation.

Vorsitzender: Prof. Dr. Frank Johannes

Prüfer der Dissertation: 1. Prof. Dr. Jörg Durner

2. apl. Prof. Dr. Ramon A. Torres Ruiz

Die Dissertation wurde am 30.01.2020 bei der Technischen Universität München eingereicht und durch die Fakultät Wissenschaftszentrum Weihenstephan für Ernährung, Landnutzung und Umwelt am 20.04.2020 angenommen.

To my family, Florian and Tobias.

Publications and conference contributions related to this thesis:

Izabella Kovacs, Alexandra Ageeva, **Eva König** and Christian Lindermayr, 2016. Chapter Two – S-Nitrosylation of Nuclear Proteins: New Pathways in Regulation of Gene Expression. In Advances in Botanical Research edited by David Wendehenne. Nitric Oxide and Signaling in Plants. Academic Press, 77, 15–39.

Eva Rudolf, Markus Wirtz, Ignasi Forné and Christian Lindermayr. S-Nitrosothiols as architect of the methylome in *Arabidopsis thaliana.* EMBO Conference - Chromatin and Epigenetics 2017, Heidelberg, Germany, Poster.

Eva Rudolf, Alexandra Ageeva-Kieferle, Alexander Mengel, Ignasi Forné, Rüdiger Hell, Axel Imhof, Markus Wirtz, Jörg Durner and Christian Lindermayr. Post-translational modification of histones: Nitric oxide modulates chromatin structure. Symposium - From Proteome to Phenotype: role of post-translational modifications 2017, Edinburgh, United Kingdom, Oral presentation.

Alexandra Ageeva-Kieferle, **Eva Rudolf** and Christian Lindermayr, 2019. Redox-Dependent Chromatin Remodeling: A New Function of Nitric Oxide as Architect of Chromatin Structure in Plants. Frontiers in Plant Science, 10, 625.

Christian Lindermayr, **Eva Rudolf**, Jörg Durner and Martin Groth, 2020. Interaction between metabolism and chromatin in plant models. Molecular Metabolism, 38, 100951.

Eva Rudolf, Patrick Hüther, Ignasi Forné, Elisabeth Georgii, Yongtao Han, Markus Wirtz, Rüdiger Hell, Axel Imhof, Claude Becker, Jörg Durner and Christian Lindermayr. S-Nitrosoglutathione reductase regulates demethylation and expression of transposable elements and stress-responsive genes. In progress.

Other publications and conference contributions:

Felicitas Groß, **Eva König,** Jörg Durner and Jeremy Astier. Nitric oxide production in *Arabidopsis thaliana*. 5th Plant NO Club Meeting 2014, Munich, Germany, Poster.

Zsuzsanna Kolbert, Árpád Molnár, Dóra Oláh, Gábor Feigl, Edit Horváth, László Erdei, Attila Ördög, **Eva Rudolf**, Teresa K. Barth and Christian Lindermayr, 2019. S-Nitrosothiol Signaling Is involved in Regulating Hydrogen Peroxide Metabolism of Zinc-Stressed Arabidopsis. Plant and Cell Physiology. 60, 2449–2463.

Table of Contents

Summary

Nitric oxide (NO) is a key signaling molecule in plant physiology. S-Nitrosoglutathione (GSNO) represents one of the major transport forms of NO in biological systems and plays a fundamental role in various aspects of plant biology. GSNO regulates protein functions via transnitrosation as well as gene expression, and epigenetic processes such as histone acetylation. The intracellular level of GSNO, and hence, protein S-nitrosation, is controlled by S-NITROSOGLUTATHIONE REDUCTASE 1 (GSNOR1) in *Arabidopsis thaliana*. In this way, *At*GSNOR1 controls S-nitrosothiol (RSNO) levels and regulates NO signaling. In this study, the effect of the physiological NO-donor GSNO as well as enhanced endogenous RSNO/GSNO levels using the *Atgsnor1-3* mutant on the methylation cycle, DNA and histone methylation in *Arabidopsis* is reported. The methylation cycle provides the major methyl donor S-adenosylmethionine (SAM) for DNA and histone methylation catalyzed by methyltransferases (MTs). Upon methyl transfer, SAM is converted to S-adenosylhomocysteine (SAH), which *per se* functions as competitive inhibitor of SAM-dependent MTs. In this regard, the SAM/SAH ratio (methylation index, MI) is considered as a metabolic indicator of the organismal methylation status. Here, the inhibition of SAH HYDROLASE 1 (*At*SAHH1) by GSNO was demonstrated *in vitro*. Interestingly, exogenous GSNO treatment of 7-day old seedlings resulted in a diminished MI. However, H3K9me2 and DNA methylation as assayed by immunoblotting and chop-PCR, respectively, were not significantly changed. The same has been observed in dihydroxypropyladenine (DHPA, inhibitor of SAHH; control treatment) treated seedlings. In contrast, loss of *At*GSNOR1 function resulted in an enhanced MI. Accordingly, enhanced levels of H3K9me2 and H3.1K27me2 were determined by LC-MS/MS in *Atgsnor1-3*. H3K9me2 increase was confirmed by immunoblotting. In *Arabidopsis*, H3K9me2 is functionally linked to non-CG DNA methylation and both marks seem to be particularly sensitive to an altered MI, whereas other marks are less effected. In this regard, whole genome bisulfite sequencing (WGBS) revealed that methylated regions (DMRs) in non-CG context are hypermethylated in *Atgsnor1-3*. Interestingly, also DMRs in CG-context *per se* mainly located in gene bodies were to a large extent hypermethylated. These data suggest that *At*GSNOR1 functions as an epigenetic regulator of DNA and histone methylation in a modification specific manner by impairing the MI. Genomic feature annotation showed that the identified DMRs are mainly mapped to protein coding genes (PCGs in their genic, 3kb up- or 3kb down-stream flanking region) and TEs. Hence, an integrative analysis of WGBS and RNA-seq data was performed. Consistent with the enhanced DNA methylation, RNA-seq data indicated that TEs (expression analysis on family level performed) were mainly repressed in *Atgsnor1-3*. In turn, alteration in DNA methylation of protein encoding genes is poorly correlated with gene expression differences. Furthermore, the *Atsahh1* mutant was assayed in parallel and used as control. *At*SAHH1

is responsible for SAH removal, and blocking of SAHH activity led to increased SAH levels, decreased SAM/SAH ratio, and to decreased DNA and H3K9me2 methylation levels.

Abbreviations

The International System of Units (SI) and SI derived units were used[1].

At	*Arabidopsis thaliana*	MR	methylated regions
CMT	CHROMOMETHYLASE	MS	METHIONINE SYNTHASE
Col-0	Columbia	MTA	methylthioadenosine
CysNO	*S*-nitrosocysteine	MTs	methyltransferases
DHPA	dihydroxypropyladenine	NO	nitric oxide
DME	DEMETER (DNA demethylase)	PCGs	protein coding genes
DMG	differentially methylated genes	PR1	PATHOGENESIS-RELATED GENE 1
DMR	differentially methylated region	PRMT	PROTEIN ARGININE MT
DMT	DNA methyltransferase	*Pst*	*Pseudomonas syringae pv. tomato*
DNIC	dinitrosyl-iron complex	PTM	post-translational modification
DRM	DOMAIN REARRAGNED METHYLASE	RdDM	RNA-directed DNA methylation
exGSNO	NO-exhausted GSNO	RNS	reactive nitrogen species
gbM	gene body methylation	ROS	reactive oxygen species
GSH	glutathione	ROS	REPRESSOR OF SILENCING
GSNO	S-nitrosoglutathione	RSNO	S-nitrosothiol
GSNOR1	GSNO REDUCTASE 1	SAH	S-adenosylhomocysteine
GUS	β-GLUCURONIDASE	SAHH	SAH HYDROLASE
H3K9me2	histone H3 lysine 9 di-methylation	SAM	S-adenosylmethionine
Hcys	homocysteine	SHH1	SAWADEE HOMEODOMAIN
HDM	histone demethylase		HOMOLOGUE 1
HMT	histone methyltransferases	SMM	S-methylmethionine
HOG	HOMOLOGY-DEPENDENT GENE	SNP	sodium nitroprusside
	SILENCING	SUVH	SU(VAR)3-9 HOMOLOG
JHDM	Jumonji C domain HDM (JMJ)	TCA	tricarboxylic acid cycle
kd	knock-down	TE	transposable element
ko	knock-out	TET	TEN ELEVEN TRANSLOCATION
LSD	lysine specific demethylase	TGS	transcriptional gene silencing
MAT	METHIONINE S-ADENOSYLTRANSFERASE	TRX	THIOREDOXIN
MET1	DNA METHYLTRANSFERASE 1	WGBS	whole genome bisulfite sequencing
MI	methylation index (SAM/SAH ratio)	α-KG	α-ketoglutaric acid

List of Figures and Tables

Figures

Tables

Supplemental Figures

Supplemental Tables

1 Introduction

1.1 Nitric oxide in plants

Nitric oxide (NO) is a ubiquitous signaling molecule with pleiotropic functions throughout the lifespan of plants. Indeed, NO is involved in several physiological processes, including growth and development, biotic and abiotic stress response as well as in iron homeostasis[2–5]. The multifunctional role of NO is based on its chemical properties, cellular environment, and compartmentation[6]. As a result, NO has been described as cytoprotective and/or signaling as well as cytotoxic molecule depending to a large extent on its local concentration, which is affected by its rate of synthesis, displacement, and removal[7,8]. In plants, NO is endogenously produced in different cellular compartments including cytosol, peroxisomes, mitochondria, and chloroplasts[9], under both physiological and stress conditions[10]. In general, two main pathways for NO production have been described[10–12]. The reductive pathway is based upon the reduction of nitrite to NO, while the oxidative route is based on the oxidation of aminated molecules such as L-arginine, polyamines, or hydroxylamine (Figure 1)[10]. Although NO biosynthesis has not been described in the nucleus, NO can cross the nuclear membrane or enter through nuclear pores because of its lipophilic character. Moreover, NO can be transferred into the nucleus through S-nitrosated proteins or S-nitrosated low molecular weight thiols, such as S-nitrosoglutathione (GSNO) or S-nitrosocysteine (CysNO)[6]. In this regard, a number of nuclear proteins undergoing S-nitrosation have been identified using the biotin switch technique[13].

The radical nature of NO promotes its interaction with different macromolecules to transduce its bioactivity[14]. Endogenously synthesized or exogenously applied NO is able to react with other radicals, including reactive oxygen species (ROS), resulting in the formation of reactive nitrogen species (RNS; RNS formation is summarized in Ref.[9]) or with metals forming metal-nitrosyl complexes such as dinitrosyl-iron complexes (DNIC; formed by the interaction between NO, iron, and thiol-containing ligands such as glutathione (GSH), cysteine, or protein thiols)[15].

NO and RNS exert their biological function through post-translational modifications (PTMs), including tyrosine nitration, metal nitrosylation, and S-nitrosation (also referred as S-nitrosylation; for formation and denitrosation mechanisms see Figure 1). In general, those NO-mediated PTMs have profound effects on the function of target proteins by regulating their activities, subcellular localization, structure, or interaction with biomolecules[16–18]. Protein S-nitrosation is considered as the chief among those NO-mediated PTMs[5]. Proteome-wide studies identified putatively S-nitrosated proteins involved in numerous aspects of plant biology, such as plant immune response, the antioxidant system, metabolic processes, and transcription factors. Consequently, NO has been found to induce diverse physiological responses and/or signaling processes, including alteration of gene expression[6,19,20], metabolic changes[21], and phytohormone signaling[22,23].
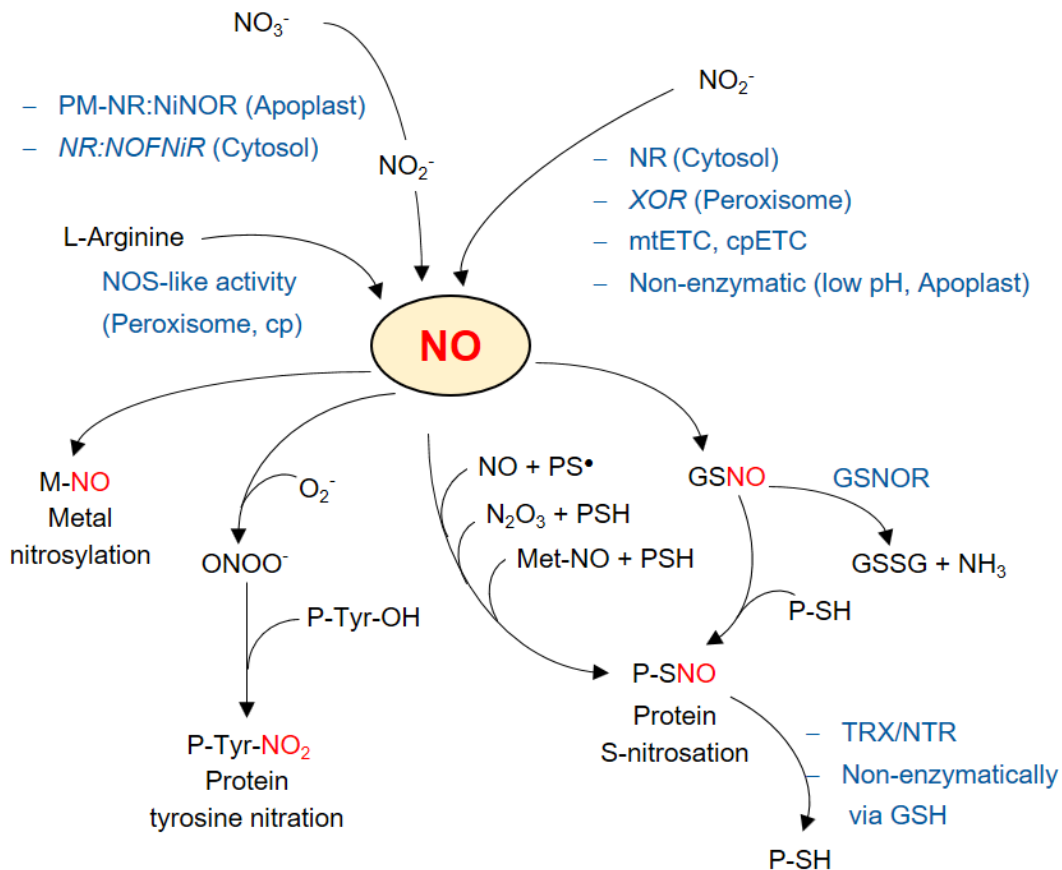
Figure 1. NO transduce its bioactivity via PTMs. <u>NO biosynthesis:</u> Nitrite-based NO production is catalyzed by cytosolic NR[11], peroxisomal XOR[24–26], mtETC[27], cpETC[28] or non-enzymatically in the apoplast favored by high nitrite levels and low pH[29]. Furthermore, NO production occurs via coupled systems where NR reduce nitrate for nitrite-based NO production such as the PM-NR:NiNOR[30] or NR:NOFNiR system[31–33]. Arginine-dependent NO production similar to the NOS activity present in animals was observed in chloroplasts and peroxisomes[10]. NO sources under debate in higher plants are given in italics. NO production in plants is reviewed by Ref.[10,12,33]. Peroxynitrite formation causes <u>protein tyrosine nitration</u>[16]. <u>Protein S-nitrosation</u> is the reversible, covalent addition of a NO moiety to a protein cysteine thiol. Since NO itself does not react with thiols or thiolates under biological conditions, modification of thiols by NO requires either prior oxidation of NO (to give a NO$^+$-donor, such as N_2O_3; S-nitrosation) or of the thiol (to give a thiyl radical; S-nitrosylation). Further mechanisms are transnitrosation mediated by GSNO or metal-mediated protein-SNO formation[17,34]. <u>Protein denitrosation</u> takes place via enzymatic mechanisms involving GSNOR or the TRX/NTR system or via non-enzymatic mechanism with GSH as denitrosylating agent. GSNOR indirectly impact the level of protein nitrosation by controlling the intracellular GSNO level[34]. Modified from Ref.[35]. <u>Abbreviations:</u> cp, chloroplast; ETC, electron transport chain; GSH, glutathione; GSNO, S-nitrosoglutathione; GSNOR, GSNO REDUCTASE; GSSG, oxidized GSH; Met-NO, metal-nitrosyl complex; mt, mitochondria; N_2O_3, dinitrogen trioxide; NH$_3$, ammonia; NO, nitric oxide; NO$^+$, nitrosonium cation; NOS, NITRIC OXIDE SYNTHASE; NR, NITRATE REDUCTASE; NR:NOFNiR, NR:NO-FORMING NITRITE REDUCTASE; O$_2^-$, superoxide; ONOO$^-$, peroxynitrite; PM-NR:NiNOR plasma membrane bound NR:NITRITE-NO REDUCTASE; PS·, protein thiyl radical; PSH, protein cysteine thiol; TRX/NTR, THIOREDOXIN/ NADPH-THIOREDOXIN REDUCTASE; XOR, XANTHINE OXIDOREDUCTASE.

In addition to NO-mediated modification of proteins, other biomolecules can undergo functional modifications mediated by NO-derived molecules and participate in the complex NO signaling network, including fatty acids, 3´,5´-cyclic guanosine monophosphate, nucleic acids, and phytohormones (e.g. cytokinins)[22,23,35,36]. The wide variety of NO sources and biological effects suggest the requirement of removal/ turnover mechanisms in plants to control the levels of NO as well as its reactivity and signaling function. Concerning the turnover of NO, the following points must be

considered. As mentioned above, NO can react with ROS yielding to RNS. Depending on the concentration and radical involved, NO may act either as an antioxidant or as source of RNS with even greater oxidizing potential[9]. For instance, under stress conditions both NO and superoxide levels increase and stimulate peroxynitrite formation, a toxic RNS causing tyrosine nitration[16]. In addition, NO can react chemically with oxygen, generating mainly nitrite and also nitrate, which can be in turn metabolized to NO in the reductive NO production pathway[10–12]. In addition, NO/RNS are enzymatically scavenged by non-symbiotic phytoglobins known to mediate the enzymatic conversion of NO into nitrate[37], and by thiol-dependent peroxidases, such as the *Arabidopsis* PEROXIREDOXIN IIE, which reduces peroxynitrite to nitrite[9]. Further, NO/RNS can react with GSH to produce GSNO, which is metabolized by GSNO REDUCTASE (GSNOR)[38,39].

1.2   S-Nitrosoglutathione is an intracellular mobile NO reservoir

Whereas NO is a short-lived free-radical that restrict its effect to the local microenvironment, S-nitrosated glutathione (GSNO) is a more stable redox form of NO[38,39]. Hence, GSNO is regarded as an intracellular mobile NO reservoir[14], which can directly release NO in the presence of metal ions, such as copper and iron, and reductants, such as ascorbate or GSH[8]. Therefore, GSNO is widely used as an *in vivo* NO-donor[40], although NO formations may not be the major mechanism of GSNO decay proposing other effects of GSNO in biological processes[41]. Instead, GSNO can transnitrosate proteins, thereby regulating their function[18,39]. GSNO can be chemically synthesized from the reaction between GSH and nitrous acid *in vitro*. However, the exact mechanism of *in vivo* GSNO formation remains unclear[14,34,41]. NO itself does not directly react with GSH to GSNO[14,34,41]. GSNO formation under aerobic conditions is considered to occur either through S-nitrosation of GSH by dinitrogen trioxide (N_2O_3) or by S-nitrosylation of a glutathionyl radical, generated probably under stress, by NO[41], as illustrated in Figure 2. Moreover, GSNO can be generated by the transnitrosation between S-nitrosothiols (RSNOs) and GSH[14,41]. GSNO degradation occur in non-enzymatic and enzymatic processes. GSNO, like other RSNOs, are light-, temperature- and redox-sensitive compounds that might be non-enzymatically degraded[39]. In addition, transnitrosation is an important mechanism leading to the decay of GSNO[41]. In plants, GSNOR- and THIOREDOXIN-mediated denitrosation have emerged as key mechanism for denitrosation of GSNO and protein-SNOs, respectively[34]. GSNOR is an evolutionarily conserved enzyme that was shown to be involved in GSNO metabolism catalyzing the NADH-dependent reduction of GSNO to GSSG (oxidized GSH) and ammonia in the presence of GSH[38,39].
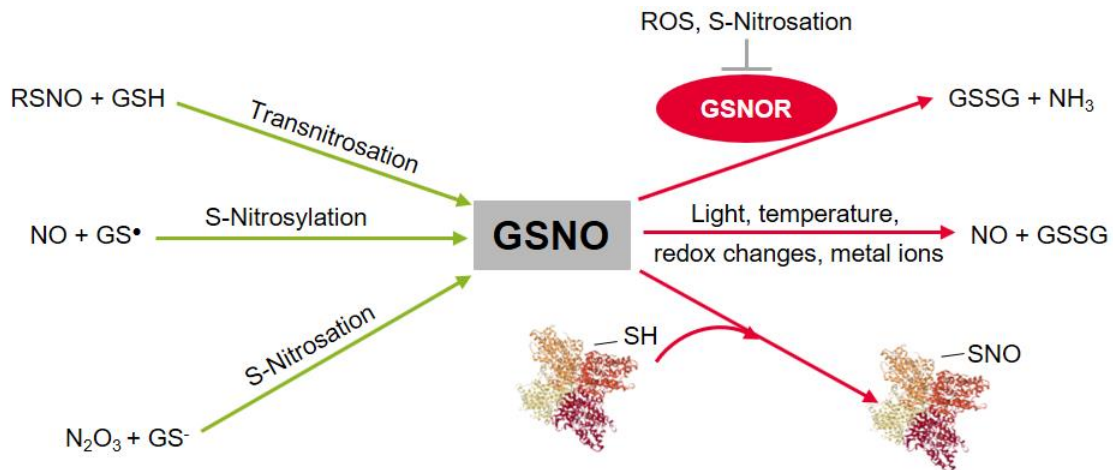
Figure 2. S-Nitrosoglutathione turnover in plants. The GSNO level is regulated either by its production (green arrows) or degradation (red arrows). GSNO is generated through <u>transnitrosation</u> between RSNOs and GSH. <u>S-Nitrosylation</u> is the reaction of NO with a glutathionyl radial generated under stress conditions. N_2O_3 transfer its NO^+ group to a thiolate forming GSNO in a reaction termed <u>S-nitrosation</u>. <u>Decomposition</u> of GSNO can either occur non-enzymatically, enzymatically by GSNOR, or by transnitrosation processes targeting proteins[14,38,39]. ROS-dependent inhibition of *At*GSNOR1[39,42] and inhibition by S-nitrosation of *At*GSNOR1[43] have been reported. Modified from Ref.[14]. *Abbreviations:* GS·, glutathionyl radical; GS⁻, glutathione thiolate; GSH, glutathione; GSNO, S-nitrosoglutathione; GSNOR, GSNO reductase; GSSG, oxidized GSH; NH_3, ammonia; N_2O_3, dinitrogen trioxide; NO, nitric oxide; SH, thiol; ROS, reactive oxygen species; RSNO, S-nitrosothiol.

The *Arabidopsis* genome encodes a single-copied *GSNOR* gene. Loss of *At*GSNOR1 leads to elevated levels of NO, nitrate, nitrite, RSNOs, and a proteome-wide increased S-nitrosation[42,44–49]. Hence, *At*GSNOR1 is considered to control intracellular levels of both GSNO and indirectly protein-SNOs[45]. *At*GSNOR1 deficiency causes pleiotropic plant growth and development defects, impaired plant disease responses, heat sensitivity, and resistance to cell death[14,38,39]. The *At*GSNOR1 deficient mutant (*Atgsnor1-3*; also named *Athot5-2*) is an important tool allowing a direct functional analysis of enhanced RSNO/GSNO levels under physiological conditions in *Arabidopsis*. Since this mutant affects the main GSNO enzymatic degradation pathway, and thereby indirectly control the total RSNO pool, the observed effects are supposed to directly reflect GSNO bioactivity[14,39]. Interestingly, *At*GSNOR1 activity is inhibited by S-nitrosation[43], proposing that GSNO regulate its own scavenging by GSNOR activity to establish a fine-tuning mechanism of GSNO homeostasis in the cell[14]. Additionally, *At*GSNOR1 is inhibited by oxidative PTMs suggesting a direct crosstalk between ROS- and RNS-signaling[39,42]. Recently, S-nitrosation induced selective autophagy of *At*GSNOR1, which is relevant to hypoxia responses, was reported[50].

So far, the physiological impact of GSNOR in regulating RSNO/GSNO levels has been well described during plant growth and development, in plant responses to different environmental stresses, as well as nitrogen metabolism, and photosynthesis (see Ref.[14,38,39] and references therein). Moreover, transcriptomic, S-nitrosoproteomic, and targeted metabolomic analysis gave insights into the regulatory function of GSNO/GSNOR on cellular processes[39].

1.3 NO-mediated regulation of gene expression

A number of large-scale transcriptomic analysis demonstrated that exogenous application of NO donors or gaseous NO fumigation and endogenous altered NO levels in mutants with impaired NO homeostasis, including *Atgsnor1-3*, resulted in profound transcriptional reprogramming in *Arabidopsis*[6,19,20]. These studies have identified thousands of NO-responsive genes, most of which are related to biotic and abiotic stress response, signal transduction, hormone biosynthesis and signaling, transcription factors, photosynthesis, cellular transport, and basic metabolism. Growing evidence suggest that NO-induced transcriptional changes are regulated via several mechanisms in mammals as well as in plants (Figure 3).
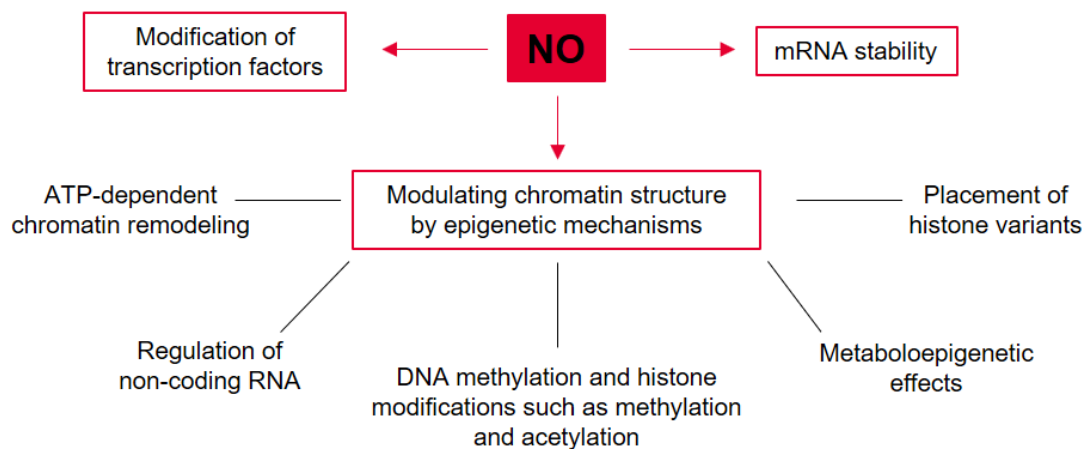
Figure 3. Proposed mechanisms of NO-mediated regulation of gene expression in *Arabidopsis*. Given that NO effect gene transcription in plants, the question arises how does NO alter the transcriptome *in planta*. Here, possible mechanisms are summarized.

Apart from NO-induced transcriptional changes of transcription factors[51], NO control gene transcription by its regulatory function on transcription factors (reviewed by Ref.[19,20]). For instance, in the *At*NPR1/*At*TGA1 system S-nitrosation induce translocation of *At*NPR1 to the nucleus and *At*TGA1 enhances its binding activity towards DNA upon S-nitrosation[52,53]. In contrast, DNA binding activity of *At*MYB transcription factors is negatively regulated by S-nitrosation[54,55]. Moreover, NO can effect gene expression on post-transcriptional level by inducing the stabilization of mRNA containing CU-rich elements in human cells[56].

Several lines of evidence demonstrate that NO regulate gene expression via modification of the chromatin structure and/or DNA accessibility[6]. In general, the distinct chromatin states that modulate access to DNA for transcription are regulated by multiple epigenetic mechanisms, including DNA methylation, covalent modifications of core histones such as methylation and acetylation, ATP-dependent chromatin remodeling, placement of histone variants, non-coding RNAs, and metaboloepigenetic effects (Figure 3)[57,58]. For instance, NO functions as regulator of gene expression by altering histone PTMs in human cancer cells[59]. Further, S-nitrosation of HISTONE DEACETYLASE 2

induced its release from chromatin resulting in increased histone acetylation accompanied by transcriptional activation[60]. In *Arabidopsis*, GSNO treatment induced histone hyperacetylation by inhibition of total histone deacetylase activity, and therefore, controlling the expression of target genes, most of which are related to stress response[40]. Further, the plant-specific histone deacetylases HDT1/2 regulating the expression of *GIBBERELLIN 2-OXIDASE2* by histone acetylation[61] were identified as target for S-nitrosation[13]. DNA hypomethylation concomitant with transcriptional activation of TEs was observed in rice upon sodium nitroprusside (SNP; NO-donor) treatment[62]. Furthermore, NO-induced enrichment of the silencing H3K9me2 methylation mark by inhibiting Jumonji C domain-containing demethylases was observed in human cells[59,63].

In addition, NO could affect transcription by metaboloepigenetic processes. Chromatin-modifying enzymes depend on the availability of intermediate metabolites of the methylation and tricarboxylic acid (TCA) cycle[57,64]. Interestingly, NO induces transcriptional and metabolic reprogramming affecting the TCA[21,65,66] and methylation cycle[65–68]. Moreover, enzymes involved in those metabolic pathways are identified as targets for NO-mediated PTMs[44,69,78,79,70–77]. Furthermore, altered placement of histone variants can modify biophysical features of the nucleosome impacting transcription[80]. Interestingly, NO induces transcriptional changes of several genes encoding histone variants[42,65,66] suggesting NO-induced altered placement of histone variants. In addition, non-coding RNAs are regulators of gene expression by a variety of mechanisms such as chromatin remodeling. Of note, several non-coding miscellaneous RNAs, which are supposed to be involved in post-transcriptional RNA processing[81], were identified in roots in response to GSNO[82].

1.4   Chromatin methylation and metaboloepigenetic

In eukaryotic cells, DNA is packaged into chromatin by wrapping 146 base pairs of DNA around an octamer of four core histones, namely H2A, H2B, H3, H4. The resulting nucleosomes together with associated non-histone proteins and RNA comprise the chromatin. The N-terminal tails of histones are subjected to covalent modifications such as methylation and acetylation. DNA bases can be covalently modified, with the most commonly studied modification being methylation at the five position of cytosine (5-methylcytosine)[83]. Those epigenetic marks are written or erased by the activity of chromatin-modifying enzymes, which are partly regulated by the bioavailability of their substrates and cofactors (Figure 4). The crosstalk between the metabolic state of a cell and epigenetic possesses is termed metaboloepigenetics[57,84].
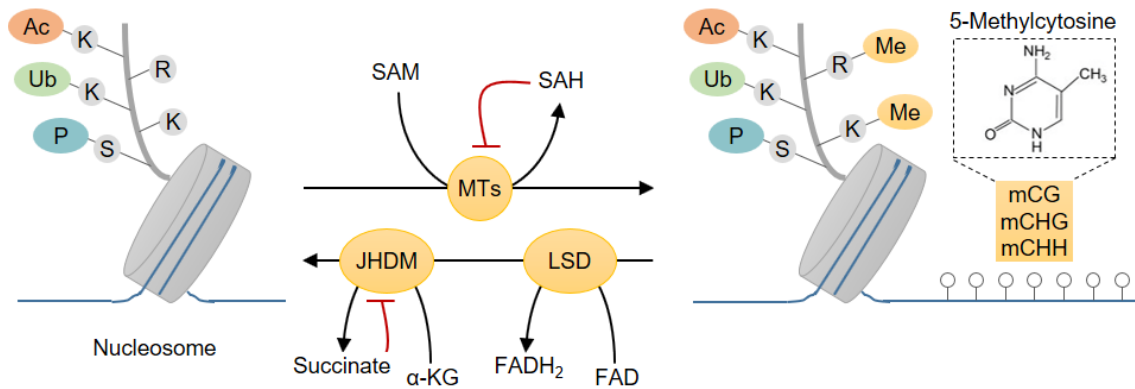
Figure 4. Metabolites are involved in methylation and demethylation of chromatin. Chromatin methylation is catalyzed by DNA and histone MTs using SAM as methyl donor[58,85]. Histone demethylation is catalyzed by JHDM and LSD histone demethylases, which use α-KG and FAD as cofactors, respectively[86,87]. <u>Abbreviations:</u> Ac, acetylation; FAD, flavin adenine dinucleotide; JHDM, Jumonji C domain-containing demethylase; K, lysine; LSD, lysine-specific demethylase; mC, 5-methylcytosine; me, methylation; MTs, methyltransferases; P, phosphorylation; R, arginine; S, serine; SAH, S-adenosylhomocysteine; SAM, S-adenosylmethionine; Ub, ubiquitination; α-KG, α-ketoglutaric acid. Modified from Ref.[57,84].

1.4.1 Histone lysine methylation and demethylation in *Arabidopsis*

Histone lysine methylation, which has important roles in transcriptional regulation and genome stability, occur at different degrees (mono-, di- and tri-methylation) on their target lysine residues on histone H3 (H3K4, H3K9, H3K27, H3K36). In general, methylation of histone H3K4 and H3K36 is associated with transcriptional activation, whereas methylation of H3K9 and H3K27 are characteristic repressive epigenetic marks. Histone lysine methylation is written by SAM-dependent histone (lysine) methyltransferases (H(K)MTs) and erased by histone demethylases (HDM)[88,89]. HKMTs contain the catalytic SET domain, which is evolutionarily conserved. The *Arabidopsis* genome encodes 49 different SET domain group (SDG) proteins, which are grouped into five distinct phylogenetic classes[85]. To date, a number of SDGs have been functionally identified in plants (reviewed by Ref.[88–90]). For instance, proteins of the Class V subgroup, which consists of 14 proteins in *Arabidopsis* (*At*SUVH1-9, *At*SUVR1-5), play an essential role in the establishment of the heterochromatic mark H3K9me, and hence, in transcriptional silencing with the exception of *At*SUVH1 and *At*SUVH3 having an anti-silencing function in *Arabidopsis*[58,91,92]. In general, mutations of *AtSDG* genes resulted in phenotypic abnormalities due to the improper regulation of important developmental genes[85], impaired pathogen defense[93], and altered DNA methylation[94].

Two classes of HDM have been identified in plants[88,89,95], namely the lysine-specific demethylase family (LSD) and the JHDM family (also named JMJ)[87]. In *Arabidopsis* four FAD-dependent LSD family members (*At*FLD, *At*LDL1/2/3) are present and demethylate H3K4me1/2[89,96]. Functional characterization of *At*LSD family members in plants demonstrated that they are involved in flowering, seed dormancy, and the RdDM pathway[91,97]. JHDMs catalyze demethylation through a ferrous ion (Fe(II)) and α-ketoglutaric acid (α-KG)-dependent oxidative reaction[87]. JHDMs have demethylase activities towards mono-, di-, tri-methylated lysines and a subset of JHDMs act as histone methyl-arginine demethylases[98]. The

common structural motif of this protein family is a 2-histidine-1-carboxylate facial traid that coordinates a non-heme Fe(II) at the catalytic center, which is used for substrate and cofactor binding[99]. *Arabidopsis* contain 21 JHDM proteins, which are subdivided into five groups based on their Jumonji C domain sequences and domain architectures. Members of the same group show similar target specificity for histone. To date, about half of these genes have been functionally characterized and they have been found to be involved in various aspects of plant biology, including plant growth and development, as well as in epigenetic processes such as DNA methylation, TE silencing, gene silencing, and RNA silencing (Ref.[100–104] and references therein). For instance, mutations in *AtJMJ25* (also named *AtIBM1*, *INCREASE IN BONSAI METHYLATION 1*; member of JHDM2/KDM3 group) leads to induced ectopic H3K9me2 methylation, and concomitantly, to enhanced gene body methylation[101,105] reflecting the mutual enhancement of H3K9me2 and DNA methylation[91].

1.4.2   DNA methylation and demethylation in *Arabidopsis*

Cytosine DNA methylation is an evolutionarily conserved chromatin modifications that contributes to gene regulation, silencing of transposable elements (TEs; transposons) and other repeats, genome structure and integrity, chromosome interactions, and regulation of RNA processing[58,89]. Additionally, a proper DNA methylation pattern is important for plant development and plant responses to various stress conditions[58]. Plant DNA methylation occurs in all sequence contexts, namely the symmetric CG and CHG context and the asymmetric CHH context (where H represents A, T or C), and displays distinct genomic pattering within genes, repeated regions, and TEs. Briefly, the genome of *A. thaliana* possesses extensive DNA methylation in all sequence contexts of TEs and other repetitive DNA sequences, which are primarily found in the heterochromatin, but also in small patches in euchromatin, leading to transcriptional gene silencing (TGS)[58,91]. In contrast, gene body methylation (gbM) mainly exists in CG context. A clear functional role of gbM has to be identified, however, various functions of gbM such as regulation of expression and splicing has been proposed (reviewed by Ref.[106]). Promoter methylation is typically associated with gene repression, however, exceptions exists where promoter methylation is required for gene expression[58]. Generally spoken, the downstream factors that perceive DNA methylation to mediate these divergent transcriptional effects are poorly understood. Only recently, a DNA methylation reader complex that enhances gene transcription was found[92].

In *Arabidopsis*, DNA methylation of each sequence context can be maintained or established *de novo* by DNA methyltransferase (DMTs) using SAM as the methyl donor through distinct pathways (Figure 6). *De novo* DNA methylation in all sequence contexts is catalyzed by DOMAIN REARRANGED METHYLASE 2 (*At*DRM2) by a process known as RNA-directed DNA methylation (RdDM, reviewed by

Ref.[58,107]). Once established, DNA methylation is maintained via different mechanisms depending on the cytosine context and setting (euchromatin versus heterochromatin), as reviewed by Ref.[58,91,108].
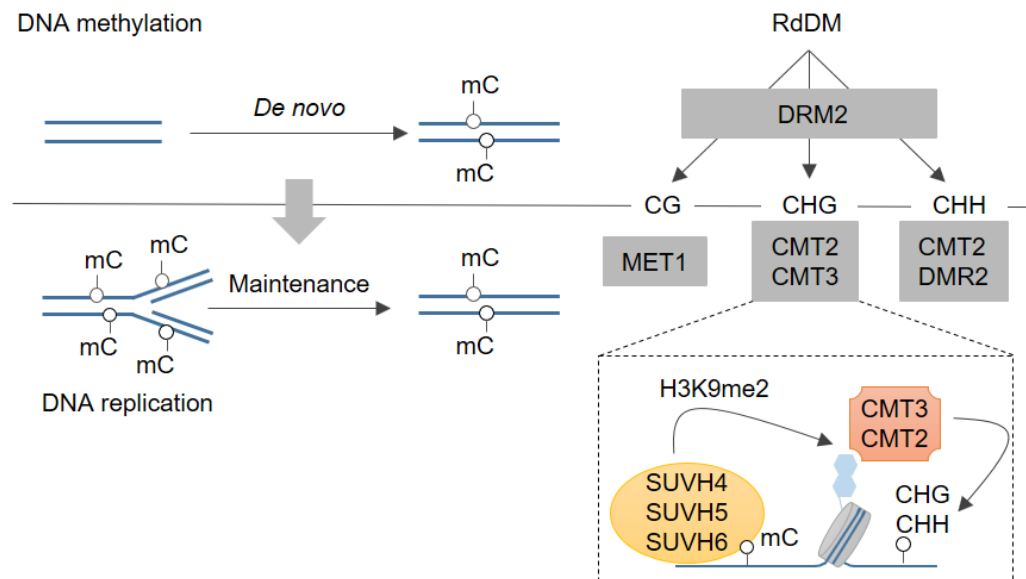
Figure 5. DNA methylation pathways in *Arabidopsis*. For details see text. Modified from Ref.[58]. Abbreviations: CMT2/3, CHROMOMETHYLASE 2/3; DRM2, DOMAIN REARRANGED METHYLASE 2; mC, cytosine methylation; MET1, DNA METHYLTRANSFERASE 1; RdDM, RNA-directed DNA methylation; SUVH4/5/6, SU(VAR)3-9 HOMOLOG 4/5/6.

Following DNA replication, CG methylation is maintained by DNA METHYLTRANSFERASE 1 (*At*MET1), and CHG methylation is maintained by CHROMOMETHYLASE 2 (*At*CMT2) and *At*CMT3. Maintenance of CHH methylation occurs either via *At*DRM2 through persistent *de novo* methylation via RdDM mainly at euchromatic sites or via *At*CMT2 in the heterochromatin. In the CMT2-CMT3 maintenance pathway, a reinforcing loop between DNA methylation and H3K9me2 perpetuates both epigenetic marks. In short, *At*CMT3 and *At*CMT2 are targeted by H3K9me2 through their bromo-adjacent homology domain and chromodomain to catalyzes non-CG DNA methylation, and, in turn, methylated DNA recruits the H3K9 SU(VAR)3-9 HOMOLOGs 4/5/6 (*At*SUVH4/5/6) methyltransferases through their SUPPRESSOR OF VARIEGATION ENHANCER of ZESTE and TRITHORAX and RING finger-associated domain[58,91,108]. Of note, *At*SUVH4/6 bind to CHH and CHG, whereas *At*SUVH5 binds in all contexts. The RdDM pathway is also interwoven with H3K9me2 due to the plant-specific DNA-DEPENDENT RNA POLYMERASES IV (*At*Pol IV; catalyze small interfering RNA biogenesis guiding RdDM) is recruited to RdDM loci by SAWADEE HOMEODOMAIN HOMOLOGUE 1 (*At*SHH1), which binds H3K9me2[58].
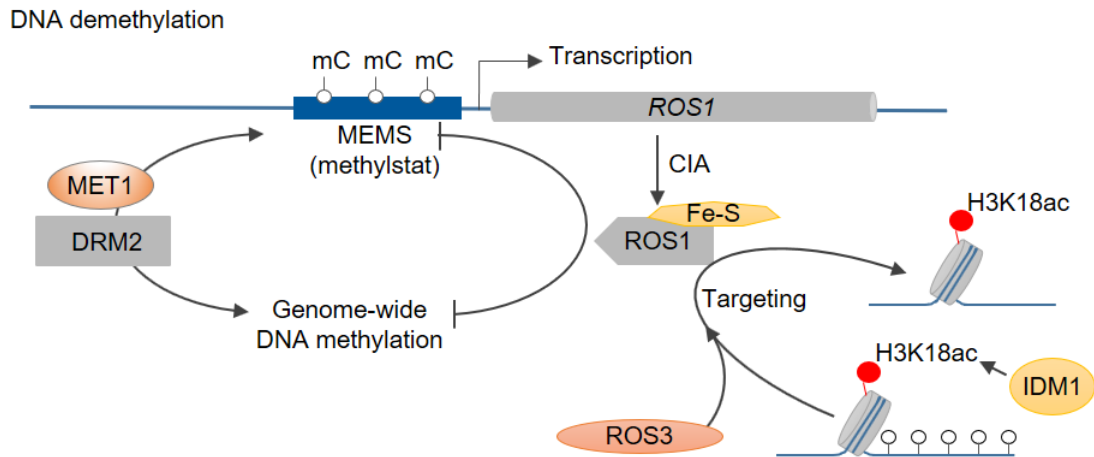
Figure 6. DNA demethylation in *Arabidopsis*. DNA demethylation mediated by ROS1, the major DNA demethylase in *Arabidopsis*. The cellular methylation status is monitored by means of the methylation level of MEMS within the promoter region of *At*ROS1. MEMS is targeted by *At*DRM2/RdDM, *At*MET1, and *At*ROS1 itself. *At*ROS1 expression is positively regulated by DNA methylation of MEMS attaining a dynamic balance between DNA methylation and demethylation in the cell[109,110]. *At*ROS1 is recruited to a subset of demethylation target loci by the IDM complex, in which *At*IDM1 catalysis acetylation of H3K18 to create a permissive chromatin environment for *At*ROS1[111]. Additionally, *At*ROS3 guides *At*ROS1 to a subset of its target loci[112]. Fe-S cluster assembly via CIA pathway is required for active DNA demethylation, because the Fe-S motif is crucial for *At*ROS1/*At*DME activities. In this regard, deficiencies in the CIA pathway resulted in hypermethylation[113]. Modified from Ref.[58,114]. Abbreviations: CIA, cytosolic Fe-S assembly; DRM2, DOMAIN REARRANGED METHYLASE 2; Fe-S, iron-sulfur cluster; IDM, increased DNA methylation complex; mC, cytosine methylation; MEMS, DNA methylation monitoring sequence; MET1, DNA METHYLTRANSFERASE 1; ROS1/3, REPRESSOR OF SILENCING 1/3.

DNA demethylation occurs either by active or passive processes. The latter refers to the loss of methylation marks in newly synthesized DNA during DNA replication due to the lack of DMT activities or deprivation of the methyl donor SAM. Active DNA demethylation in plants is driven by closely related DNA glycosylases such as the REPRESSOR OF SILENCING 1 (*At*ROS1), which recognize DNA methylcytosines and initiate DNA demethylation through a base excision repair process in a replication-independent manner (see Figure 6 for details; reviewed by Ref.[58,114]).

1.4.3 Metabolic regulation of DNA and histone methylation

From bacteria to humans, methylation is sensitive to cellular metabolic status[115]. Both the methylation cycle and the tricarboxylic acid (TCA) cycle provide substrates for enzymes involved in DNA and histone methylation. Indeed, methylation is directly linked to intermediary metabolism with S-adenosylmethionine (SAM) acting as the main methyl donor for transmethyl reactions catalyzed by methyltransferases, which methylate DNA, RNA, lipids, histones, and cellular metabolites (Figure 7)[116]. Each transmethyl reaction consumes SAM and releases the by-product S-adenosylhomocysteine (SAH). SAH, a competitive inhibitor of methyltransferases, is then recycled to homocysteine (Hcys) and adenosine by S-ADENOSYLHOMOCYSTEINE HYDROLASE (SAHH). The equilibrium of this reversible reaction favoring SAH is driven towards hydrolysis of SAH due to removal of its products by down streaming enzymes. METHIONINE SYNTHASE (MS) catalyzes the methylation of Hcys to methionine using methyl-tetrahydrofolate (CH_3-THF), which are derived from the transsulfuration pathway and the

folate cycle, respectively. Then, METHIONINE S-ADENOSYLTRANSFERASE (MAT) catalyzes the adenylation of methionine to SAM to close the methylation cycle[116,117]. The recycling mechanism is crucial for maintaining an adequate methylation index (MI; SAM/SAH ratio), which is regarded as an indicator of the cellular methylation state.
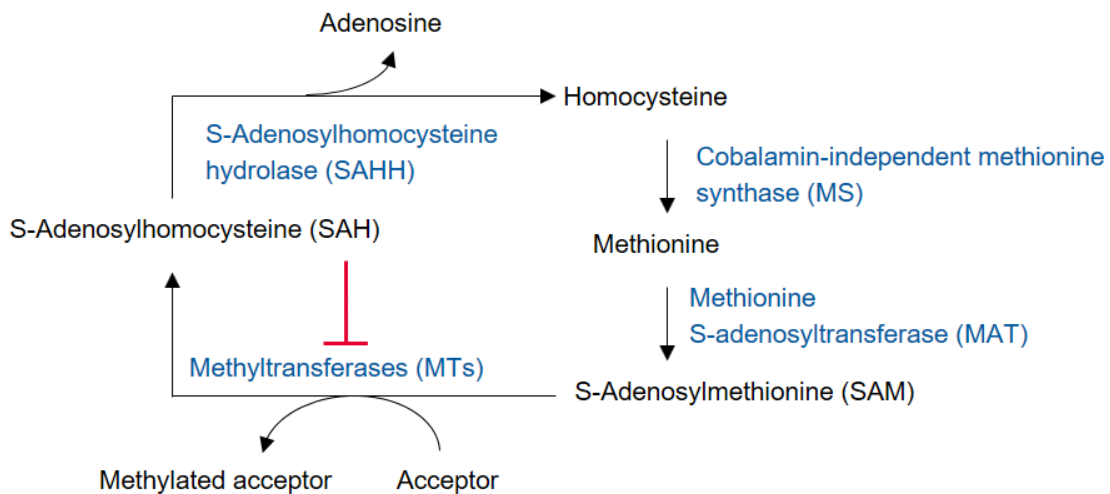
Figure 7. Schematic representation of the methylation cycle. See text for details.

In plants and in the animal system numerous studies reported that SAM and SAH levels regulate DNA and histone methylation (Ref.[57,118,119] and references therein). For instance, the importance of SAHH activity towards DNA and histone methylation has been previously demonstrated (Ref.[120–122] and references therein). The *Arabidopsis* genome encodes two *SAHH* isoforms, however, *AtSAHH*1 is primarily supposed to play a role in maintaining TGS and DNA methylation at numerous targets compared to *At*SAHH2[120,123]. *Atsahh1* knock-down mutants (*Atsahh1-kd;* knockout is zygotic lethal[123]) possessed a decreased MI[123,124], DNA and H3K9me2 hypomethylation concomitant with the release of transcriptional silencing at transgene reporters[120,123], repetitive DNA sequences such as ribosomal DNA and 180-bps repeats[120,123,124], and transposons[121,125]. Similarly, the expression of antisense RNA of *SAHH* in tobacco plants resulted in a loss of DNA methylation in repetitive elements[126]. Other studies employed a selective reversible inhibitor of SAHH, namely dihydroxypropyladenine (DHPA). In tobacco DHPA caused accumulation of SAH and DNA hypomethylation[122,127,128]. In *Arabidopsis*, the application of DHPA reduced levels of DNA and histone methylation at endogenous repeats[120].

Moreover, *At*MAT4 is an important epigenetic regulator. Mutations in *AtMAT4* caused decreased SAM levels, CHG/CHH and H3K9me2 hypomethylation, and activation of TEs[129]. Similarly, the *AtMS1* mutation resulted in a decreased MI, DNA and H3K9me2 hypomethylation[118]. Interestingly, overexpression of *AtMETS1* (here abbreviated as *35S::AtMS1*) is accompanied by a genome-wide global increase in DNA methylation[130]. Of note, the MI and histone methylation levels were not analyzed in *35S::AtMS1* plants.

Furthermore, inhibition of folate biosynthesis by sulfamethazine or by a mutation in *FOLYLPOLY-GLUTAMATE SYNTHETASE 1* (*AtFPGS1*) resulted in an impaired methylation cycle, and continuatively in DNA and H3K9me2 hypomethylation and TE activation[131,132]. A mutation in *METHYLENETETRA-HYDROFOLATE DEHYDROGENASE 1 (AtMTHFD1;* folate cycle) caused accumulation of SAH, genome-wide DNA hypomethylation, loss of H3K9me2, and transposon reactivation[133]. Mutation in the *MORE SULPHUR ACCUMULATION 1* (*AtMSA1*) was recently identified to be crucial for SAM production and DNA methylation[134] demonstrating an interrelationship between Sulphur homeostasis and epigenetic processes in plants (reviewed by Ref.[119]). These studies demonstrate that an altered MI affect DNA and histone methylation marks in a modification specific manner most pronounced in non-CG DNA methylation and H3K9me2[118].

The TCA cycle intermediate α-KG and the electron carrier FAD serve as essential substrates and co-factors for epigenetic enzymes involved in DNA and histone methylation. The redox cofactor FAD is required by members of the lysine-specific histone demethylase family (LSD)[135]. In animal cells, accumulation of FAD activated LSD1 activity and resulted in demethylation of repressive H3K9me2 sites[136,137]. The JHDMs require iron (Fe(II)) and the TCA cycle intermediate α-KG as cofactors to demethylate methylated lysine residues by an oxidative mechanism[87]. Additionally, intermediates of the TCA cycle downstream of α-KG inhibit JHDMs *in vitro*, namely fumarate and succinate[138]. In this regard, studies in human cell lines revealed that reduced α-KG levels resulted in diminished JHDM activities with increased histone methylation levels. Whereas increased succinate and fumarate levels resulted in hypermethylation of histone H3[138]. However, studies on the metabolic regulation of JHDM and LSD demethylases in plants remain elusive.

1.5 Epigenetic effects of NO on DNA and histone methylation

Until now, regulation of epigenetic processes by NO has mostly been addressed in mammals (reviewed by Ref.[139–142]). In plants, the role of NO as epigenetic regulator is an emerging research field[6]. However, NO is supposed to be an epigenetic regulator of DNA and histone methylation in plants based on S-nitrosoproteomic studies, transcriptomic profiling, and metabolic analysis using NO-donors and mutants with impaired NO homeostasis. Furthermore, mechanisms how NO affect epigenetic processes can be concluded based on observations in the animal field. In the following paragraphs the regulatory function of NO on DNA and histone methylation and metaboloepigenetic processes (focus on methylation cycle) is discussed. A summary is given in Figure 8.
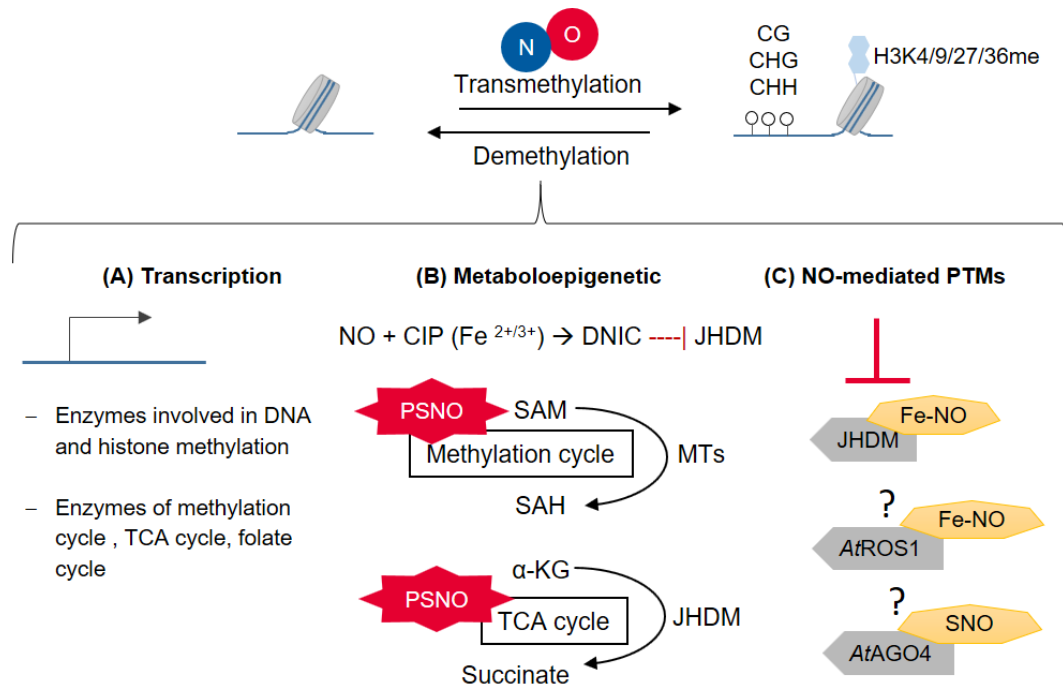
Figure 8. Epigenetic effects of NO on DNA and histone methylation.(A) NO alters the expression level of chromatin-modifying enzymes and proteins involved in metabolic pathways providing substrates and cofactors for those in *Arabidopsis*. **(B)** NO affects metaboloepigenetic processes. Proteins involved in the methylation[44,69–72] and TCA cycle[44,69–72,78,79] are targets for S-nitrosation in *Arabidopsis*. NO-induced metabolic reprogramming affecting the methylation cycle[67] and the TCA cycle[21,143,144] in plants was reported. NO reduce iron cofactor availability via DNIC formation affecting the functionality of JHDMs in mammals[63]. **(C)** NO-mediated post-translational modifications. Fe(II)-dependent plant JHDMs might be targets for metal nitrosylation based on studies in the mammalian field[63]. Further, the iron-sulfur clusters of *At*ROS1 DNA demethylase might be targeted by NO. *At*AGO4 (RdDM component) was identified as putative S-nitrosated in a proteome-wide approach[44]. Abbreviations: *At*AGO4, ARGONAUTE 4; CIP, chelatable iron pool; DNIC, dinitrosyl-iron complex; H3K4me, histone H3 lysine 4 methylation; MTs, methyltransferases; NO, nitric oxide; JHDM, Jumonji C domain-containing demethylase; PSNO, protein S-nitrosothiol; PTM, post-translational modification; RdDM, RNA-directed DNA methylation; ROS1, REPRESSOR OF SILENCING 1; SAH, S-adenosylhomocysteine; SAM, S-adenosylmethionine; TCA, tricarboxylic acid; α-KG, α-ketoglutaric acid.

1.5.1 NO affects DNA and histone methylation pathways

In the animal field, NO has been shown to directly and indirectly affect DNA and histone methylation (reviewed by Ref.[139–142]). Indeed, NO induces transcriptional changes of DNA and histone methyltransferases and demethylases. For instance, all of the known H3K9me HDMs were upregulated at the mRNA level in response to NO in human cells, remarkably, these response was not accompanied by decreases in H3K9me levels[63]. The expression levels of HMTs are differentially controlled by NO. Upon treating cells with NO, the expression levels of SETDB2 and SUV39H2 (tri-methylate H3K9) increased, while the levels of G9a (di-methylates H3K9) decreased[63,139]. Application of the NO donor RRX-001 decreased the expression of DMTs in mammalian cells and diminished global DNA methylation levels[145]. Conversely, exposure of mammalian cells to NO-donor SNAP did not increase the expression of DMTs[146]. Furthermore, NO-induced alteration in enzymatic activities of chromatin-modifying enzymes were observed. For instance, the activity of DMTs increased when NO was applied directly on a nuclear protein extract[146]. In this regard, endogenously produced NO upon *Helicobacter*

pylori treatment was associated with increased DMT activity and an increase in DNA methylation[147]. Moreover, NO inhibit mononuclear non-heme iron dioxygenases such as JHDM and TEN-ELEVEN TRANSLOCATION (TET; DNA demethylase) enzymes by the formation of a nitrosyl-iron complex with their catalytic non-heme iron[63,148]. Moreover, NO-mediated enzymatic degradation of the H3K9 tri-methylating HMT SUV39H1 resulted in decreased H3K9me3 levels[149]. Taken together, NO has emerged as an important regulator of epigenetic methylation processes on different levels (transcription, activity, and degradation of chromatin-modifying enzymes) in mammalians.

In plants, the exposure to high concentrations of the NO-donor sodium nitroprusside (SNP) induced DNA hypomethylation in rice going along with altered expression of chromatin remodeling enzymes[62]. Interestingly, the expression levels of many genes encoding proteins involved in DNA or histone methylation were altered upon exogenous NO application or in plants with impaired NO homeostasis (Table 1).

Table 1. NO-induced transcriptional changes of genes related to DNA and histone methylation. Previously reported transcriptomic analysis were screened for differentially expressed genes involved in DNA and histone methylation. For abbreviations refer to Chapter 7.3.

Treatment	Up/down	Function/ pathway	Gene
Irrigation of 4-week-old plants with 1 mM SNP; Microarray analysis[150]	Up	RdDM	HSP90-2, HSP90-4
Spray-treatment of three-week-old plants with 0.5 mM SNP; Microarray analysis[151]	Up	RdDM	AGO2
		DNA demethylation	DRE2
		Histone methylation:	JMJ13
Infiltration of 4-week-old leaves with 1 mM CysNO; RNA-seq analysis[65]	Up	RdDM	DCL1, STABILIZED1, RDM16, HSP90-1
		CHG/CHH methylation	CMT2
		DNA demethylation	DRE2, NBP35
		DNA and H3K9me2 linking	AGDP1
		Histone methylation	SUVR3/SDG20, JMJ13, JMJ21, JMJ26, JMJ29
	Down	RdDM	NRPD2/NRPE2, NRPE5, AGO4, DMS3/IDN1, KTF1, IDP1, IDP2, SUVH9, SUVR2, LDL1, DDM1, RRP6L1, DCL4, SDE3, SDGS3
		CHH methylation	DDM1
		DNA demethylation	ROS1, DML2, IDM3
		Histone methylation:	SWN/SDG10, ASHR3/SDG4, ATX5/SDG29, SUVH9/SDG22, SUVR2/SDG18, PRMT4A, JMJ27, LDL1
Wild-type vs *Atnoa1-2* (NO-deficient mutant); Microarray analysis[66]	Up	DNA demethylation	DML2, APE1L
		RdDM	RDR6, NRPD4/NRPE4, NRPE5, HSP90-1
		CG methylation	MET1, VIM1
		Histone methylation	ATXR7/SDG2, PRMT1a, PRMT1b, PRMT3, PRMT10, PRMT5, JMJ22
	Down	RdDM	SUVR2/SDG18, SDGS3
		CHG/CHH methylation	CMT2
		Histone methylation	ASHH3/SDG7, SUVR2/SDG18, JMJ18
Wild-type vs *Atnia1nia2* (NO-deficient mutant); Microarray analysis[66]	Up	RdDM	RDM1
		DNA demethylation	NBP35
		Histone methylation	PRMT1b, PRMT3, PRMT4B
	Down	DNA demethylation	ROS1, DML2
		RdDM	DCL3, DRD1, IDN1, LDL1, UBP26, RRP6L1, RDM16

		CG/CHG/CHH methylation	MET1, CMT2
		Histone methylation	ASHH3/SDG7, ATXR6/SDG34, SUVH1/SDG32, JMJ11, JMJ18, JMJ28
Wild-type vs *Atnia1nia2noa1-2*[66] (NO-deficient mutant); Microarray analysis[66]	Up	DNA demethylation	APE1L, MBD7, NAR1, DRE2, NBP35, CIA1
		RdDM	RDM1, HSP90-1
		Histone methylation	PRMT1b, PRMT3, PRMT4B, PRMT10, PRMT5
	Down	DNA demethylation	ROS1, SSRP1
		RdDM	AGO4, SUVR2/SDG18, SDGS3
		CHG/CHH methylation	CMT2
		Histone methylation	ATX5/SDG29, ATXR6/SDG34, SUVH6/SDG23, SUVR2/SDG18, JMJ18
At35S::nNOS; Microarray analysis[152]	Down	Histone methylation	JMJ30
Atgsnor (Ws background); Microarray analysis[42]	Up	RdDM	AGO9
		CG methylation	VIM1, VIM3
		Histone methylation	ASHR3/SDG4, ATXR6/SDG34
	Down	Histone demethylation	JMJ30

For instance, proteins involved in *de novo* and maintenance DNA methylation as well as in demethylation are differentially expressed upon treatment with the NO-donor CysNO. Furthermore, genes encoding for HMTs and HDMs, which are involved in RdDM, are differentially regulated. For instance, CysNO treatment resulted in downregulation of *AtLDL1* histone demethylase[65], which function in the RdDM pathway by removing H3K4me2/3 to allow for *At*SHH1 binding and the synthesis of Pol IV-dependent siRNAs[91]. Additionally, *AtSUVH9* responsible for *At*Pol V recruitment in RdDM is downregulated[65]. Interestingly, CysNO revealed upregulation of *AtAGDP1*[65], which links H3K9me2 to DNA methylation in heterochromatin[153]. Hence, CysNO probably effects the establishment and maintenance of the DNA methylation pattern.

Transcriptomic analysis of NO-deficient *Atnoa1-2*, *Atnia1nia2*, and *Atnia1nia2noa1-2* mutants also revealed that enzymes involved in DNA methylation such as the DNA methyltransferases *AtMET1* and *AtCMT3* as well as the DNA demethylase *AtROS1* are differentially expressed[66]. Interestingly, several PRMTs are upregulated in NO-deficient plants[66]. For instance, *AtPRMT1b*, upregulated in all three NO-deficient mutants, methylates H4R3[154]. Another example is *At*PRMT5, which is upregulated in *Atnoa1-2* and *Atnia1nia2noa1-2*[66], is positively regulated by S-nitrosation during stress responses[155]. Regarding the late flowering phenotype of these NO-deficient mutants, it is worth mentioning that *AtJMJ18* (controls flowering) is downregulated in each mutant[156]. Summarized, the expression of DNA and histone methylation modifying enzymes are differentially controlled by NO. This implies an indirect effect of NO on epigenetic mechanisms in plants.

Furthermore, proteins involved in DNA and histone methylation are targets for NO-mediated PTMs. Indeed, S-nitrosation of *At*PRMT5[155], which catalyzes symmetric di-methylation of H4R3 *in vitro*[157], has been reported. Briefly, S-nitrosation of *At*PRMT5 promotes its methyltransferase activity, which enables methylation-dependent pre-RNA splicing associated with salt stress tolerance[155]. Further, *At*AGO4, a component of the canonical RdDM pathway[58,107], was identified as putative S-nitrosated in

15

a proteome-wide approach[44]. Based on the studies on human JHDM[63], Fe(II)-dependent plant JHDMs might be targets for metal nitrosylation by the formation of a nitrosyl-iron complex with the non-heme Fe(II) in their catalytic pocket. Hence, NO-induced changes of histone methylation levels by directly inhibiting the catalytic activity of plant JHDMs is suggested. In regard that iron-sulfur clusters of proteins are targeted by NO resulting in the disruption of the cofactor[158], the iron-sulfur containing *At*ROS1/*At*DME DNA demethylases[114] might be affected by NO in plants.

1.5.2 NO affects metaboloepigenetic processes interacting with DNA and histone methylation

Intriguingly, key enzymes of the methylation cycle providing the major methyl donor for transmethylation reactions such as DNA and histone methylation were identified as targets for S-nitrosation, namely MS, MAT, SAHH[44,69–72], and for tyrosine nitration, namely MS and SAHH[73–75]. This suggests that NO impairs the methylation cycle. In mammals, NO inhibits cobalamin-dependent MS due to its reaction with the cofactor cobalamin[159]. Unlike mammals, plants utilize solely cobalamin-independent MS, which are identified as targets for S-nitrosation[72,76] and nitration[73]. *At*MAT isoforms are differentially inhibited by protein S-nitrosylation. While *At*MAT1 is reversibly inhibited by GSNO, *At*MAT2 and *At*MAT3 are not affected[160]. A similar differential regulation of MAT activity was observed in mammals[161]. *At*SAHH1, a major component of epigenetic regulation in *A. thaliana*[162], is targeted by NO-mediated PTMs. Computational prediction and proteome-wide studies revealed *At*SAHH1 as target for S-nitrosation[44,69–72].
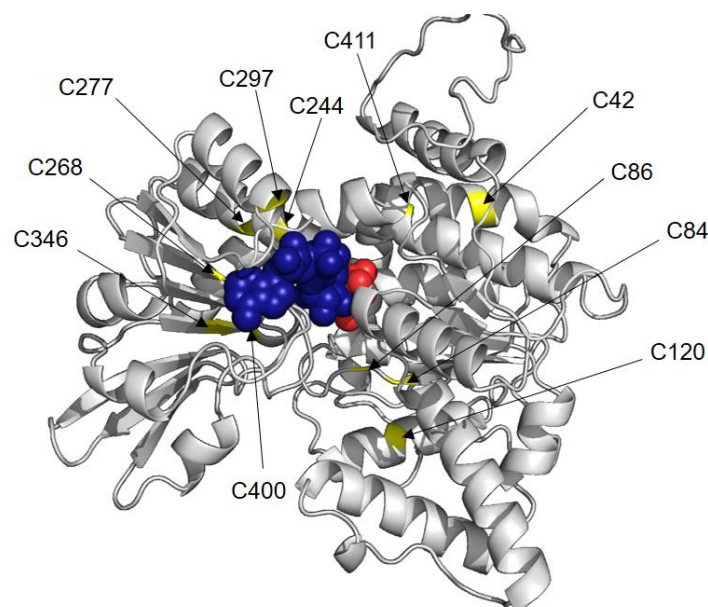
Figure 9. Three-dimensional model of *At*SAHH1. The *At*SAHH1 (UniProtKB O23255) was modelled using the protein structure homology-modelling server SWISS-MODEL[163] with SAHH from *Lupinus luteus* (PDB ID.: 3OND; Ref.[164]) as template. The sequence identity of query and template is 92%. PyMOL[165] was used for imaging. Cysteine resides are shown in yellow. The ligands NAD+ and adenosine are shown in blue and red, respectively.

Notably, *At*SAHH1 possesses a total of eleven cysteine residues (Figure 9) of which six cysteine residues (C86, C120, C244, C277, C346, C400) are highly conserved among invertebrates, vertebrates, yeast, and plants as demonstrated by multiple sequence alignment (Supplemental Figure 1). Computational prediction revealed that several of those cysteine residues of *At*SAHH1 are targets for S-nitrosation (Supplemental Table 1). Moreover, tyrosine nitration has been observed in SAHH of sunflower causing a decreased SAHH activity[74]. This suggests that *At*SAHH1 activity is affected by NO.

In addition to the identification of proteins, which are targets for NO-induced PTMs, the effect of NO on metabolic reprogramming using untargeted and targeted metabolomics together with transcriptomic profiling is an emerging field. In this regard, transcriptomic profiling upon NO-donor treatment and in mutants with altered NO homeostasis revealed that genes involved in the methylation cycle are regulated by NO (Table 2). For instance, treatment of *Arabidopsis* cell suspension with 0.5 mM NOR3 resulted in downregulation of *AtMS1*, *AtMAT3*, and *AtMAT4.* In contrast, exposure of 4-5-week-old *Arabidopsis* plants to gaseous NO resulted in an induction of *AtMAT4*[68]. Moreover, CysNO treatment induced expression of *AtMAT2*, *AtMAT3*, *AtMAT4*, *AtSAHH1*, and *AtSAHH2*[65]. Transcriptomic profiling of NO-deficient mutants *Atnoa1-2*, *Atnia1nia2*, and *Atnia1nia2noa1-2* revealed that genes coding for enzymes involved in the methylation cycle are also differentially regulated[66]. Since the methionine cycle depends on folate metabolism providing the key methyl donor CH$_3$-THF for methionine synthesis, it is noteworthily that NO modulate the folate cycle at the transcriptional level[42,65,66,68,151,152,166]. In addition, proteins involved in the folate metabolism were identified as targets for S-nitrosation[44,69,71,78].

Recently, an untargeted metabolomic analysis revealed that NO affect methionine metabolism in elm seeds[67]. In particular, SNP and GSNO modulate the methylation cycle at the transcriptional level by elevating *MAT* transcript levels and by increasing the levels of methionine and SAM[67]. In sum, these data demonstrate that NO affect the methyl-donor supply by NO-induced PTMs, altered transcription, and/or changed enzyme activities of genes/proteins involved in the methylation cycle.

Table 2. NO-induced transcriptional changes of genes involved in the methylation cycle. Previously reported transcriptomic analysis were screened for differentially expressed genes involved in the methylation cycle.

Treatment	Up/down	Gene
Fumigation of 4-5 week-old plants with 1,250 ppm gaseous NO; Microarray analysis[68]	Up	MAT4
Cell suspension culture treated with 0.5 mM NOR; Microarray analysis[68]	Down	MS1, MAT3, MAT4
Infiltration of 4-week-old leaves with 1 mM CysNO; RNA-seq analysis[65]	Up	MAT2, MAT3, MAT4, SAHH1, SAHH2
Wild-type vs *Atnoa1-2* (NO-deficient mutant); Microarray analysis[66]	Up	MS3
Wild-type vs *Atnia1nia2* (NO-deficient mutant); Microarray analysis[66]	Down	MAT2
Wild-type vs *Atnia1nia2noa1-2*[66] (NO-deficient mutant); Microarray analysis[66]	Up	MS3, MAT4, SAHH1, ADK2

Transcriptomic profiling and S-nitrosoproteomic studies revealed that numerous genes and proteins involved in the TCA cycle are differentially expressed[65,66] and targets for NO-mediated PTMs[44,69–72,78,79], respectively. For instance, *ACONITASE 2* and *3* were upregulated in NO-deficient mutants[66]. Furthermore, it was demonstrated NO inhibits ACONITASE by forming a metal-nitrosyl complex with its iron-sulfur cluster[77]. In addition, ACONITASE was found as target for S-nitrosation[44,72]. In addition, untargeted metabolic analysis revealed that plants exposed to NO for six hours undergo a transient metabolic reprogramming, including increased succinate (inhibit JHDMs) and decreased α-KG (substrate of JHDMs) levels[21]. Moreover, both NO-deficient mutants *Atnia1nia2* and *Atnia1,2noa1-2* display an impaired TCA cycle[44]. The *Atnia1,2noa1-2* plants display a significant increased level of succinate and a decreased level of fumarate (inhibit JHDMs), whereas the α-KG was not altered compared to wild-type[143]. In contrast, the succinate and fumarate level were decreased in the *Atnia1nia2* mutant[144]. Hence, it is suggested that NO may regulate histone methylation through effecting these metabolites.

Moreover, NO could reduce iron cofactor availability via DNIC formation affecting the functionality of JHDMs and probably TET enzymes in mammals[63,148]. Hence, a reduced availability of the cofactor iron could also affect the activity of JHMDs and DNA demethylases *At*ROS1/*At*DME1 in plants.

In addition, it is known that NO effects the cellular redox status[9], which potentially control epigenetic mechanisms[64]. Indeed, GSH a biological redox buffer was demonstrated to impact epigenetic mechanisms in the animal system[167]. Moreover, the degradation and recycling of ascorbate is largely controlled by the redox status, which can consequently impact histone demethylation as ascorbate functions as cofactor for JHDMs[57]. Further the redox state might influence the availability of FAD, and thus, the activity of LDL demethylases[168].

2 Aim of the thesis

Nitric oxide (NO) is an important signaling molecule during plant growth and development and during stress responses. As a free radical, NO has a very short lifetime that restricts its effect to the local microenvironment. However, S-nitrosothiols (RSNOs) represent a quite stable reservoir and transport form of NO in plants. The most abundant low molecular weight RSNO is S-nitrosoglutathione (GSNO). Its cellular level is mainly balanced by transnitrosation processes targeting proteins resulting in S-nitrosated proteins and by enzymatic degradation catalyzed by the GSNO REDUCTASE1 (GSNOR1) in *Arabidopsis thaliana*. Hence, *At*GSNOR1 indirectly influences the level of the total RSNO pool, including S-nitrosated proteins. A mutation in *AtGSNOR1 (Atgsnor1-3)* results in elevated RSNO/GSNO levels, which in turn allow the elucidation of RSNO/GSNO on cellular processes under physiological conditions.

I.   The aim of the thesis was to elucidate whether RSNO/GSNO affects the methylation cycle, DNA and histone methylation in *Arabidopsis thaliana*. This research approach was based on the identification of key enzymes involved in the methylation cycle as potential candidates for S-nitrosation in genome-wide S-nitrosoproteomic studies. Hence, the hypothesis was postulated that RSNO/GSNO may regulate the methylation cycle through protein S-nitrosation. The methylation cycle provides the main methyl group donor (S-adenosylmethionine, SAM) for transmethylation reactions, such as DNA and histone methylation, and recycles the by-product inhibitor S-adenosylhomocysteine (SAH). Since SAH removal by SAH hydrolase 1 (*At*SAHH1) is crucial for transmethylation reactions, the effect of GSNO on recombinant *At*SAHH1 was investigated. Further, the biotin switch assay was used to proof GSNO-induced S-nitrosation of *At*SAHH1.

II.   Next, the impact of impaired RSNO/GSNO homeostasis on the methylation cycle and on DNA and histone methylation using GSNO-treated seedlings and *Atgsnor1-3* plants were investigated. Additionally, *Atsahh1-ko* plants with an impaired methylation cycle were analyzed. First, the methylation capacity measured as the SAM/SAH ratio (MI, methylation index) was determined by targeted metabolomic analysis. Then, a LC-MS/MS based method for identification and quantification of histone lysine methylation marks, immunoblotting, and locus-specific DNA methylation analysis by chop-PCR was performed to elucidate the effect of an altered MI on DNA and histone methylation. Based on these results, the effects of *AtSAHH1* and *AtGSNOR1* mutations on genome-wide DNA methylation using whole genome bisulfite sequencing (WGBS) was investigated.

III. Further, the effect of the altered DNA methylome on the expression of transposable elements and genes were analyzed in an integrative analysis using WGBS and RNA sequencing data.

3 Materials and Methods

The practical work was carried out at the Institute of Biochemical Plant Pathology of Helmholtz Zentrum München German Research Center for Environmental Health and at the proteomics core facility at Ludwig-Maximilian-University of Munich. Reagents and resources are listed in Supplemental Table 2 and instruments in Supplemental Table 3. Oligonucleotides are listed in Supplemental Table 4 and Supplemental Table 5. Plasmids used and constructed in this study are summarized in Supplemental Table 6. General molecular and biochemical techniques were performed as described by Sambrook and Russel (Ref.[169]). All buffers and media were prepared with deionized water. All media were autoclaved at 121°C for 20 min. The media were cooled down to at least 50°C before adding filter-sterilized antibiotics. Solid media were cooled down to approximately 50°C before pouring into sterile petri dishes. Media plates were aseptically prepared in a sterile bench. The solid and liquid media were stored at 4°C until further use. All buffers used were autoclaved or sterile-filtered and degassed before usage.

3.1 Plant material and cultivation

A. thaliana ecotype Columbia-0 (Col-0) purchased from the Nottingham *Arabidopsis* Stock Center (NASC), *Atgsnor1-3* obtained from GABI-Kat (also named *hot5-2*, GABI-Kat 315D11), *Atsahh1* purchased from NASC (SALK 068487), *Athog1-7* and *A. thaliana* ecotype Zürich kindly provided by Ortrun Mittelsten Scheid, and *A. thaliana* Col-0 *TS-GUS* (possesses a transcriptionally silent (TS) highly repetitive β-glucuronidase (GUS) transgene; L5, 6b5) line kindly provided by Hervé Vaucheret were used in this study and were previously described (Ref.[45,46,120,121,124,170,171]). Transgenic *A. thaliana* plants overexpressing *AtSAHH1* under the control of the cauliflower mosaic virus (CaMV) 35S in the Col-0 background were generated as described in section 3.3.4. The *A. thaliana* Col-0 *TS-GUS* (L5, 6b5) line[171] was crossed with the mutants *Atsahh1* and *Atgsnor1-3*. The segregating F2 plants were genotyped and seeds from lines homozygous for the *TS-GUS* locus and the mutation were used for further analysis. Mutants and transgenic lines are listed in Supplemental Table 2.

Arabidopsis plants were grown on soil mixed with silica sand in a ratio of 4:1 in 4-well plant pots placed in a tray. Before sowing, soil was wetted with water supplemented with 0.15% (v/v) Neudorff Neudomück®. After stratification for two days at 4°C in the dark, plants were cultivated for four weeks in a climate chamber at 65-68% relative humidity under long-day conditions (14 h light/ 10 h dark cycle, 20°C day/ 18°C night regime, 70 µmol m^{-2} s^{-1} photon flux density). Plants were covered with clear plastic wrap during stratification and the first week of growing, followed by a propagator lid for seven days to ensure high humidity and proper growth. Plants were bottom-up watered three times a week. 4-week old rosette leaves were harvest 5 h after day-time start and flash frozen in liquid nitrogen.

For liquid culture experiments, *A. thaliana* seeds were surface sterilized by soaking in 70% (v/v) ethanol for 1 min and then in 50% (v/v) household bleach for 10 min followed by five washes with sterile ddH$_2$O. Seeds were suspended in sterile water and stratified for 2 days at 4°C in the dark. Seedlings were cultivated in a 250-mL Erlenmeyer flask or six-well plates containing 70 mL or 5 mL of 1x Murashige & Skoog (MS) medium[172] adjusted to pH 5.7 with potassium hydroxide and supplemented with 1% sucrose and 0.5 g L^{-1} MES, respectively. Liquid-cultured seedlings were grown under short-day conditions (10 h light/ 14 h dark cycle, 16°C day/ 20°C night regime, relative humidity 80% day/ 65% night, 100 µmol m^{-2} s^{-1} photon flux density) on a shaker (100 rpm). For treatments, GSNO, exGSNO (light-exposed, NO-exhausted GSNO), DHPA, and water (control) was added to 7-day-old liquid-cultured seedlings at night-time start and harvested after 16 h.

3.2 Molecular biology methods

3.2.1 Genomic DNA isolation using cetyltrimethylammonium bromide

For genotyping, one leave was squeezed in a 1.5 mL sterile tube in the presence of 250 µL of cetyltrimethylammonium bromide buffer (CTAB; 2% (w/v) CTAB, 100 mM Tris-HCl pH 8.0, 1.4 M NaCl, 1% (w/v) polyvinylpyrrolidone (PVP-40), 20 mM EDTA pH 8.0) or 250 µL of the CTAB buffer was added to 50-100 mg grinded plant material. After incubation at 65°C for 20 min under continuous shaking, 200 µL of chloroform:isoamyl alcohol (24:1) was added, vigorously vortexed for 1 min, and centrifuged (18,000*g*, 20 min, at 4°C). The upper aqueous phase was transferred into a fresh 1.5 mL tube containing 1 µL of 1% linear polyacrylamide used as co-precipitant for DNA, mixed with 600 µL of 100% ethanol, and the DNA was precipitated for 20 min at -20°C. The pellet was washed with 1 mL of ice-cold 70% (v/v) ethanol, air-dried, and then resuspended in 70 µL Tris-EDTA buffer (TE; 10 mM Tris-HCl pH 8.0; 1 mM EDTA pH 8.0). DNA was stored at -20°C until use.

3.2.2 Genomic DNA isolation using the DNeasy® Plant Mini Kit

Silica-based DNA extraction and purification was performed using the DNeasy® Plant Mini Kit from Qiagen according to manufacturer´s instructions with minor modifications. Approx. 1.5 g of rosette leaves were ground in liquid nitrogen and aliquoted. 400 µL of buffer AP1 supplemented with 1 mg mL^{-1} RNase A was added to 250 mg ground plant material, vortexed, and incubated in a thermoshaker at 300 rpm for 15 min at 65°C. After the addition of 130 µL of buffer P3, the sample was incubated for 5 min on ice. Then, the lysate was cleared (20,000*g*, 5 min) and transferred to the QIA®shredder spin column and centrifuged (20,000*g*, 2 min). The flow-through without the pellet was mixed with 1.5 volumes of buffer AW1 and loaded onto a DNeasy® Mini spin column. After centrifugation, the column was washed twice with 500 µL AW2 (6,000*g*, 1 min) with a final centrifugation step at 20,000*g* for 2 min. DNA was eluted twice with 50 µL of pre-warmed (65°C) AE buffer (incubation for 5 min at room temperature (RT) followed by centrifugation at 6,000*g* of 1 min).

All centrifugation steps were performed at 20°C. The DNA concentration was determined with Nanodrop ND-1000 (NanoDrop Technologies) and DNA was stored at -20°C until use.

3.2.3 RNA extraction and cDNA synthesis

Total RNA extraction was performed using an acid guanidinium-thiocyanate-phenol-chloroform protocol[173]. About 120 mg of ground plant material were homogenized in 1 mL of RNA extraction buffer (0.4 M ammonium thiocyanate, 0.8 M guanidinium thiocyanate, 5% (v/v) glycerol, 0.1 M sodium acetate pH 5.2, 38% (v/v) phenol) by brief vortexing and subsequent incubation on a thermoshaker at 1400 rpm for 10 min at 8°C. After the addition of 400 µL ice-cold chloroform, the sample was inverted several times before being incubated for 3 min on ice. Phases were separated by centrifugation. The upper aqueous phase was mixed with 500 µL chloroform by inverting before incubation for 3 min on ice and another centrifugation step. To precipitate RNA, the aqueous phase was mixed with 300 µL isopropanol by inversion. After incubation for 15 min on ice and centrifugation, the RNA pellet was washed twice with 70% (v/v) ethanol. The air-dried pellet was dissolved in 25 µL LiChrosolv® water and immediately frozen at -20°C. All centrifugation steps were carried out at 17,000g for 20 min at 4°C. RNA concentration was determined with Nanodrop ND-1000 (NanoDrop Technologies). For cDNA synthesis, 0.5-2.5 µg of total RNA were reverse transcribed using SuperScript™II Reverse Transcriptase (Thermo Fischer Scientific) according to the manufacturer´s instructions. A negative control without reverse transcriptase was prepared for each sample.

3.3 Generation and characterization of transgenic lines

3.3.1 Preparation of competent *Agrobacterium tumefaciens*

The *Agrobacterium tumefaciens* Ti plasmid helper strain GV3101::pMP90 (Ref.[174]) was used in this study. To generate electrocompetent cells, a 3-mL overnight culture in LB-Miller medium (1% (w/v) tryptone, 0.5% (w/v) yeast extract, 1% (w/v) NaCl adjusted to pH 7 with sodium hydroxide) supplemented with 100 µg mL^{-1} rifampicin and 25 µg mL^{-1} gentamycin was diluted 100-fold into a 1-L Erlenmeyer flask containing 300 mL fresh media and grown at 28°C until OD_{600} 0.5–0.7 was reached. Then, the bacteria suspension was cooled for 30 min on ice and cells were collected at 4,000g for 20 min at 4°C. The bacteria pellet was washed thrice by resuspending in 125 mL ice-cold, sterile ddH$_2$O, followed by an incubation step for 30 min on ice and centrifugation. The pellet was dissolved in one bacterial pellet volume of ice-cold 15% glycerol (v/v, in water), 50-µL aliquots were dispensed in pre-chilled 1.5 mL tubes, frozen in liquid nitrogen, and stored at -80°C.

3.3.2 Transformation of *Agrobacterium tumefaciens* by electroporation

Electrocompetent *A. tumefaciens* GV3101::pMP90 were transformed with a Bio-Rad Gene-Pulser™ linked to Bio-Rad Puls Controller and Bio-Rad Capacitance Extender with the following settings: 250 µF,

1.25 kV, and 400 Ω. For transformation, 1 μL plasmid DNA (approx. 100 ng) was added to 50 μL of electrocompetent cells on ice, gently mixed, and transferred into a pre-chilled 0.1 cm electroporation cuvette before an electric pulse was applied. The time constant was between 8.9 and 9.6 ms. Cells were immediately recovered by adding 500 μL of LB-Miller media, transferred to 2 mL of LB-Miller, and incubated for 2 h at 28°C with gentle shaking. Then, 20-200 μL were plated on LB medium supplemented with appropriate antibiotics. Transformation was verified with sequencing using plasmids isolated from *A. tumefaciens* with the QIAprep® Spin Miniprep Kit using a modified procedure as previously described[175].

3.3.3 Transformation of *Arabidopsis*

Transformation of *A. thaliana* was performed according to the protocol of Clough and Bent[176]. Plants were grown under long-day conditions and the first emerging bolts were cut to induce growth of multiple secondary bolts. Siliques and open flowers were eliminated before transformation. An overnight culture of the *A. tumefaciens* strain carrying the construct of interest (Supplemental Table 6) was diluted 300-fold in 300 mL LB-Miller media supplemented with 100 μg mL^{-1} rifampicin, 25 μg mL^{-1} gentamycin, and 50 μg mL^{-1} kanamycin. Bacteria suspension was grown overnight to and OD$_{600}$ of 1.5 and harvested by centrifugation (1,000g, 15 min, 4°C). The bacteria pellet was resuspended in infiltration medium (5% (w/v) sucrose supplemented with 0.05% (v/v) Silwet L-77) and diluted to an OD$_{600}$ of 0.8. Entire shoots were submerged into the bacterium suspension in a 50 mL tube for 10 s. Dipped plants were covered with a transparent plastic bag to maintain humidity and kept in a low light location for 24 h. Then plants were returned to the growth chamber, fertilized, and grown until seed harvest. The developing seed generation was subjected to selection process following the Mendelian rules. Therefore, transformed constructs contained a bialaphos resistance (*bar*) gene conferring resistance to the herbicide glufosinate-ammonium (BASTA®).

3.3.4 Generation of transgenic *35S::AtSAHH1*-tagged plants

Plasmids were constructed based on the Invitrogen™ Gateway™ recombination cloning technology, which is based on the site-specific recombination properties of bacteriophage lambda. Detailed manufacturer´s instructions for recombining target sequences into donor vectors generating entry vectors and subcloning them to destination vectors are available from Invitrogen´s website (http://www.invitrogen.com). General molecular biology techniques, such as restriction enzyme digestion and dephosphorylation of the vector, were performed according to Sambrook and Russel[169]. *AtSAHH1* (AT4G13940) coding sequence was amplified from cDNA either with or without stop codon and transferred into the pDONR221 vector in previous work (AG Lindermayr). The resulting pENTR221/*AtSAHH1-N-fusion* and pENTR221/*AtSAHH1-C-fusion* entry clones were linearized with the restriction enzyme *ApaL*I (Thermo Fisher Scientific) and dephosphorylated with calf intestine alkaline

phosphatase (New England Biolabs) to prevent subsequent transformation of the entry vector into *E. coli*. After preparative agarose gel electrophoresis using the innuPREP™ Gel Extraction Kit (Analytik Jena), *AtSAHH1* nucleotide sequence was subcloned by LR Clonase® mixture into the destination vector pEarlyGate 201 or 202 to generate an N-terminal FLAG or HA peptide tag, respectively[177]. Further, the *AtSAHH1* nucleotide sequence without a stop codon was subcloned into the pAUL 1 or 2 vector for C-terminal in frame fusion with HA or a HA-StrepIII-tag, respectively[178]. After recombination, the reaction mixture was treated with proteinase K to digest the clonase enzyme. The resulting recombined plasmids were transformed into *ccdB* -sensitive *E. coli* DH5α cells and positive clones were selected on LB plates supplemented with 50 μg mL^{-1} kanamycin. Plasmid DNA was isolated based upon a modified alkaline lysis method[179] employing the QIAprep® Spin Miniprep Kit (Qiagen) and sequenced by Eurofins Genomics. The pAUL2/*35S::AtSAHH1-HA-StrepIII* vector was transformed into electrocompetent *A. tumefaciens* Ti plasmid helper strain GV3101::pMP90 as described in Section 3.3.2, which was then used to transform wild-type ecotype Col-0 plants by floral dipping[176] as described in Section 3.3.3. Transgenic plants were selected on soil by glufosinate-ammonium (BASTA®; 0.25 g L^{-1}) resistance and selection process followed the Mendelian rules. Further, transgenic lines were confirmed by genomic PCR, semi-quantitative RT-PCR analysis, and immunoblotting against HA and *At*SAHH1. Homozygous T4 plants were used for further analysis.

3.3.5 PCR-based genotyping of mutants and transgenic lines

Homozygosity of T-DNA insertion lines (*Atgsnor1-3*, *Athog1-7*, and *Atsahh1*) were verified by PCR-based genotyping as previously described[180] using the primer design tool http://signal.salk.edu/tdnaprimers.2.htm or https://www.gabi-kat.de/db/primerdesign.php. Oligonucleotides for *Athog1-7* and *AtTS-GUS* verification were obtained from Ortrun Mittelsten Scheid. Genomic PCR to verify *35S::AtSAHH1-HA-StrepIII* insertion were performed with the CaMV35S_fw, Cterm_HA_rev, and Cterm_StrepIII_rev oligos (Supplemental Table 4). Briefly, PCR-based genotyping of T-DNA insertion lines was performed by using T-DNA border-specific primers in combination with gene-specific primers. A gene-specific primer pair spanning the T-DNA insertion (left border (LP) and right border (RP)) were used to amplify the wild-type allele in the absence of a T-DNA insertion. T-DNA insertion was confirmed by using a gene-specific (RP) and insertion-specific primer (T-DNA border primer (LB)). Hence, an amplicon pattern of wild-type negative and T-DNA positive indicated that the line is homozygous. Heterozygosity led to an amplicon pattern of wild-type and T-DNA positive, and a wild-type line was only wild-type amplicon positive. PCR reactions were performed in a total volume of 10 μL, containing 100-300 ng CTAB-extracted genomic DNA as template, 1x Mango*Taq*™ colored reaction buffer, 2.5 mM MgCl$_2$, 200 μM of each dNTP, 0.5 μM of each primer, and 0.5 U of Mango*Taq*™ polymerase. PCR was conducted in a T100™ Thermal Cycler from Bio-Rad. PCR conditions were as

follows: denaturation at 94°C for 2 min, then 30-37 cycles of 30 s at 94°C, 30 s at the required annealing temperature, and 1 min/kb at 72°C for extension, followed by a final extension at 72°C for 10 min. Cycle number, annealing temperature, and extension time are listed in Supplemental Table 4 for each reaction. The amplified products were separated by gel electrophorese in 1% or 2% (w/v) agarose in Tris Acetate-EDTA buffer (TAE; 40 mM Tris, 20 mM acetic acid, 1 mM EDTA) supplemented with 0.5 µg mL^{-1} ethidium bromide, illuminated with UV light, and documented using MegaCapt gel documentation system from Vilber Lourmat.

3.4 Epigenetic analysis and next generation sequencing

3.4.1 DNA methylation analysis by chop-PCR

Locus-specific DNA methylation analysis by chop-PCR was performed with the methylation-dependent restriction enzyme McrBC[181]. McrBC enzyme recognizes pairs of hemi- or fully methylated 5′-G/A^{m}C-3′ motifs separated by 40-3000 nucleotides with an optimal spacing of 55-103. Cleavage occurs in between those sites approximately 30 nucleotides from either side[182]. Hence, McrBC digestion allows the analysis of methylation of cytosines in each methylation context (CG, CHG, and CHH). Due to McrBC cleaves methylated DNA, higher levels of methylation result in increased McrBC digestion and consequently reduced amplification by PCR, and *vice versa*. For McrBC digestion, 1.2 µg of CTAB-extracted genomic DNA was digested with 12°U of McrBC enzyme in a total volume of 60 µL for 3 h at 37°C. After enzyme heat inactivation for 20 min at 65°C, PCR assays were performed in a final volume of 20 µl, containing 6 µL of digested or undigested control samples as template, 1x Mango*Taq*^{TM} colored reaction buffer, 2.5 mM MgCl$_2$, 200 µM of each dNTP, 0.5 µM of each primer, and 1 U of Mango*Taq*^{TM} polymerase. PCR was conducted in a T100™ Thermal Cycler from Bio-Rad. PCR conditions and oligonucleotides used are listed in Supplemental Table 5. Classification, short description, and accession numbers of selected loci are listed in Supplemental Table 7. The amplified products were separated by gel electrophorese in 1% or 2% (w/v) agarose in Tris Acetate-EDTA buffer (TAE; 40 mM Tris, 20 mM acetic acid, 1 mM EDTA) supplemented with 0.5 µg mL^{-1} ethidium bromide, illuminated with UV light, and documented using MegaCapt gel documentation system from Vilber Lourmat. Signal intensities were quantified by ImageJ software (National Institutes of Health) and normalized to actin.

3.4.2 Whole genome bisulfite sequencing and data analysis

WGBS was performed at the Gregor Mendel Institute in Vienna in Cooperation with Prof. Dr. Claude Becker and Patrick Hüther.

WGBS library preparation and sequencing. WGBS was performed from snap-frozen 4-week-old rosette leaves grown under long-day condition harvested 5 h after day-time start (total 1.5 g) for each genotype. Two biological replicates were analyzed for each genotype. gDNA was extracted from leaf samples (aliquot 150 mg, ground in liquid nitrogen) with DNeasy® Plant Mini Kit and sheared to

350 bps. WGBS DNA libraries were generated using the Illumina® TruSeq® Nano Kit and bisulfite treatment was conducted with the EpiTect® Plus Bisulfite Kit. Briefly, the fragmented DNAs were end-repaired, adenine bases were added to the 3´end (A-tailing) of the DNA fragments, and methylated adapters were ligated to the DNA fragment. Next, the DNA fragments were size-selected before sodium bisulfite treatment and PCR amplification (KAPA HiFi HS Uracil+ ReadyMix from Roche Cat.No:795905001). Libraries were sequenced with 125 bp paired-end reads on an Hiseq 2500 instrument. Library preparation (paired-end directional library) was performed by Katharina Jandrasits (Becker Lab, Gregor Mendel Institute Vienna).

Processing and alignment of bisulfite-converted reads. For read mapping and methylation calling, the pipeline available on https://github.com/phue/NGI-MethylSeq written by Phil Ewels and Rickard Hammarén at the National Genomics Infrastructure part of SciLifeLab Stockholm was used. In short, raw sequencing reads were quality controlled (FastQC) and sequencing adapters were trimmed off (Trim Galore). Reads were aligned to the TAIR9 Reference genome with Bismark (version v0.17.0)[183] and Bowtie2[184]. After deduplication (deduplicate_bismark), methylated Cs were extracted from aligned reads with the Bismark methylation extractor[185]. Bisulfite conversion efficiency was calculated from the proportion of unconverted Cs in the chloroplast genome.

Post-alignment Analysis. Aligned reads along with methylation calling information of each individual cytosine were tabulated in genome matrix and subjected to post-alignment analysis with the MethylScore pipeline. Briefly, identification of differentially methylated positions was performed according to Ref.[186]. Identification of methylated regions (MRs) and differentially methylated regions (DMRs) was conducted by an adaption of a Hidden-Markov-Model based approach as previously described[187], which identifies regions of dense methylation that are then tested for differential methylation[188]. The DMRs were identified by pairwise comparison of WGBS profiles (*Atgsnor1-3* vs Col-0; *Atsahh1* vs Col-0). WGBS data analysis was performed by Patrick Hüther (Becker Lab, Gregor Mendel Institute Vienna).

Annotation – Mapping to genomic elements. For annotation of genomic elements, the TAIR10 was used. MRs and DMRs were assigned to annotated elements (CDS, intron, 5' UTR, 3' UTR, transposon, 2kb upstream, 2kb downstream, as-lncRNA, lncRNA, miRNA, pri-miRNA, ncRNA, snoRNA, tRNA, pseudogene). Genes with at least one DMR in the gene body, 3kb up- or 3kb down-stream flanking regions were considered as differentially methylated genes (DMGs). Further, TEs with at least one DMR were identified.

EPIC-CoGe browser. DNA methylation data have been uploaded to the epigenome browser of EPIC (EPIC-CoGe) by Prof. Dr. Claude Becker (ID 2234 unpublished).

3.4.3 RNA-sequencing

RNA-sequencing (RNA-seq) was performed at the Gregor Mendel Institute in Vienna in cooperation with Prof. Dr. Claude Becker and Patrick Hüther. RNA-seq was performed from snap-frozen 4-week-old rosette leaves grown under long-day condition harvested 5 h after day-time start (total 1.5 g) for each genotype. Four replicates were analyzed for each genotype. RNA was extracted from 4-week-old rosette leaves using the innuPREP PLANT RNA Kit. Library preparation, sequencing, and data analyzing was performed by Patrick Hüthner. Data analyzing was performed with the RNA-seq quantification program kallisto[189] and DEseq2 package in R for differential expression analysis[190]. Gene annotation was performed using the following sources: UniProtKB, Swiss-Prot, TrEMBL, and TAIR.

3.4.4 Acid extraction of histones

Nuclei from 4-week-old rosette leaves were purified according to Ref.[191] with minor modifications. 2 g of plant tissue was grinded to a fine powder in liquid nitrogen, homogenized in two volumes of lysis buffer (20 mM Tris-HCl pH 7.4, 25% (v/v) glycerol, 20 mM KCl, 2 mM EDTA, 2.5 mM $MgCl_2$, 250 mM sucrose) supplemented with protease inhibitor, and incubated for 10 min on ice with intermittent vortexing. The homogenate was successively filtered through miracloth and a 160 µm nylon mesh. The flow-through was centrifuged at 1,500g for 10 min at 4°C and the pellet was washed four times with 4 mL of nuclear resuspension buffer (20 mM Tris-HCl pH 7.4, 25% (v/v) glycerol, 2.5 mM $MgCl_2$, 0.2% (v/v) Triton® X-100). The final pellet was resuspended in 700 µL of 0.2 M sulfuric acid to extract histones and other acid-soluble proteins overnight using an overhead shaker. The extract was then centrifuged at 16,000g for 20 min at 4°C. The supernatant containing core histones was transferred to a new tube and proteins were precipitated with 26% (v/v) trichloroacetic acid for 3 h on ice. After four washes with ice-cold acetone, the histone pellet was resuspended in 60 µL of 2x sample buffer (4% (w/v) SDS, 20% (v/v) glycerol, 10% (v/v) 2-mercaptoethanol, 0.004% (w/v) bromo-phenol blue and 0.125 M Tris-HCl, pH 6.8) by 1500 rpm for 20 min at RT using an thermoshaker and then stored at -20°C overnight. If necessary, pH was adjusted with 1 µL of 1 M Tris-HCl pH 8.0. Histones were separated by 12% SDS-PAGE (loading volume: 15-25 µL per lane) and stained with Coomassie® Blue for LC-MS/MS analysis or immunoblotted.

3.4.5 Quantification of histone methylation and acetylation by LC-MS/MS

Peptide processing. After electrophoreses, bands corresponding to histones H3 and H4 were excised from the gels. Calf histones were run as a size marker. Destaining, acylation, and acid extraction were performed following a slightly modified protocol[192] in cooperation with Protein Analysis Unit of the Ludwig Maximilian University under the supervision by Dr. Ignasi Forné. Briefly, gel pieces were suspended in 200 µL of water and then incubated in 200 µL of 50 mM ammonium bicarbonate (ABC) for 5 min at RT. For destaining the pieces were incubated in 50 mM ABC/50% acetonitrile (ACN) for

30 min at 37°C while shaking followed by two washes with water. Gel pieces were dehydrated by incubating three times with 200 µL of pure ACN for 5 min at RT. Next, the gel pieces were air-dried for 5 min to remove ACN. Histones were chemically acetylated with d6-deuterated acetic anhydride (99% D) for 1 h at 37°C by adding a master mix containing 10 µL acetic anhydride and 20 µL of 100 mM ABC per sample followed by the addition of 70 µL of 1 M ABC. Thereafter, gel pieces were washed thrice with water, three times with ACN, and air-dried. Trypsin digestion was started by the addition of 10 µL of trypsin (20 ng µl^{-1} in 50 mM ABC) and 5 min incubation on ice. Afterwards, 50 µL of 50 mM ABC were added and further incubated at 300 rpm overnight at 37°C using a thermoshaker. After digestion, the peptides had been released from the gel to the supernatant. Remaining tryptic peptides were extracted from the gel pieces twice with 50% acetonitrile/0.25% TFA and twice with acetonitrile. The pooled supernatants were vacuum concentrated and resuspended in 20 µL of 0.1% TFA by incubation for 20 min at 4°C. Histone peptides were desalted using C18-stage-tips assembled as previously described[193] by plugging two Empore™ extraction C18 disks (Agilent Technologies) of the appropriate diameter into the tip of a 200 µL pipette tip. The resin was wetted with 20 µL of methanol, 20 µl of 80% ACN/0.1% TFA, and then equilibrated with 20 µL of 0.1% TFA. After sample loading, the resin was washed thrice with 20 µL of 0.1% TFA and then peptides were eluted with 15 µL of 80% ACN/0.25% TFA for three times. The kept flow-through of the C18-stage purification after sample loading was applied to porous graphitic carbon top-tips (Glygen) and purification was performed as for C18-stage-tips. Desalted histones peptides were combined, vacuum concentrated, and reconstituted in 0.1% TFA for LC-MS.

LC-MS/MS. Desalted histone peptides in 0.1% TFA were injected in an RSLCnano system (Thermo Fisher Scientific) and separated in a 15-cm analytical column (75µm ID home-packed with ReproSil-Pur C18-AQ 2.4 µm from Dr. Maisch) with a 50-min gradient from 4 to 40% acetonitrile in 0.1% formic acid at 300 nL/min flowrate. The effluent from the HPLC was electrosprayed into Q Exactive HF mass spectrometer (Thermo Fisher Scientific). The MS instrument was programmed to target several ions as previously described[192] except for the MS3 fragmentation. Survey full scan MS spectra (from m/z 270-730) were acquired with resolution R=60,000 at m/z 400 (AGC target of 3x10^6). Targeted ions were isolated with an isolation window of 0.7 m/z to a target value of 2x10^5 and fragmented at 27% normalized collision energy. Typical mass spectrometric conditions were: spray voltage, 1.5 kV; no sheath and auxiliary gas flow; heated capillary temperature, 250°C.

Histone PTM identification. *In silico* preparation for the identification of histone H3 methylation and acetylation marks by MS1 and MS2 on these peptides was performed with the mass spectrometry software tool GPMAW[194] and is summarized in Supplemental Table 8. Histone peptides were separated on a C18 analytical column and electrosprayed into an Q Exactive HF mass spectrometer.

Chromatograms with typical retention times for *A. thaliana* histones are shown in Supplemental Figure 2. Motifs containing methylated lysines in addition to acetylation resulted in a characteristic shift in retention time: tri-methylated peptides elute shortly before di-methylated ones, followed by unmethylated and mono-methylated peptides as shown for peptide H3.3-8, H3.9-17, and H3.1.27-40 (Supplemental Figure 2A, B, E). Further, positional isomer peptides with identical mass but PTMs at different positions revealed characteristic retention time shifts: A di- or tri-methyl group close to the N-terminus of a peptide led to a lower hydrophobicity and hence earlier retention time as compared to when the methylation is closer to the C-terminus. For example, an H3 peptide bearing di-methylated lysine 27 (K27me2) eluted a few minutes before the positional isomer carrying di-methylated lysine 36 (K36me2), and an H3 peptide bearing tri-methylated lysine 27 (K27me3) eluted a few minutes before the positional isomer carrying tri-methylated lysine 36 (K36me3) (Supplemental Figure 2E). On the contrary, a more central mono-methyl group (K36me1) elutes before a more N-terminal mono-methyl group (K27me1). Due to mono-methylated lysines are still reactive to d6-acetic anhydride compared to di- and tri-methylated lysines, the endogenous mono-methyl/chemical d3-acetyl at the N-terminus in H3.1K27me1 is more hydrophobic and elutes after H3.1K36me1. Therefore, motifs containing methylated lysines only or in addition to a single acetylated lysine were quantified based on their MS1 values (Supplemental Table 8 and Supplemental Figure 3). Positional isomers containing a single or multiple acetylations as the only PTM are not separated during chromatography (Supplemental Figure 2C, D, F). Concerning chemically acetylated lysines (D3AA method; unmodified lysines are converted to d3-acetylated lysines) and endogenously acetylated lysines the following was observed. Chemically d3-acetylated histone peptides elute only slightly before endogenously acetylated histone peptides due to slightly decreased interaction of deuterated moieties with the C18 column[192]. Hence, acetylation motifs on histone H3 were identified and quantified with MS1 and MS2 (Supplemental Table 8 and Supplemental Figure 3).

Histone PTM quantification. For LC-MS data quantification, based on the area of the peak form the extracted ion chromatogram, the Xcalibur™ software (Thermo Fisher Scientific) was used. The theoretical mass to charge ratio was calculated with GPMAW 5.02 for each peptide (Supplemental Table 8). Further parameters were peak detection: Genesis; trace: mass range; mass tolerance 20 ppm; mass precision 4 decimals; S/N threshold 0.5. After peak integration, data were exported to Excel and the relative abundance was calculated. For detailed method and calculation of motif abundance see Feller et al. (Ref.[192]).

3.5 Protein analysis

3.5.1 Sodium dodecyl sulfate polyacrylamide gel electrophoresis

Sodium dodecyl sulfate polyacrylamide gel electrophoresis (SDS-PAGE) was performed according to Laemmli[195] as described by Sambrook and Russell[169]. Protein samples were diluted in 2x SDS sample buffer (4% (w/v) SDS, 20% (v/v) glycerol, 10% (v/v) 2-mercaptoethanol, 0.004% (w/v) bromophenol blue and 0.125 M Tris-HCl, pH 6.8.) and heated before electrophoresis for 5 min to 95°C. Proteins were separated by 10%, 12%, or 13.5% resolving gels and 5% SDS-PAGE stacking gels in SDS running buffer (25 mM Tris base, 192 mM glycine, 0.1% (w/v) SDS) on a Mini-PROTEAN® Tetra cell system (Bio-Rad). Running conditions were set to 200 V and 30 min. Proteins were visualized either by staining with Coomassie® Brilliant Blue G 250 or subjected to immunoblotting.

3.5.2 Coomassie® staining of SDS-PAGE gels

Gels were washed three times in deionized water for 2 min and then stained with Coomassie Brilliant Blue G 250 solution (0.1% Coomassie® G 250, 10% (v/v) glacial acetic acid, 45% (v/v) methanol) for 20 min while shaking. Destaining was allowed to proceed for several hours in deionized water or in destaining solution (10% (v/v) glacial acetic acid, 45% (v/v) methanol).

3.5.3 Immunoblotting

Electrophoretic separated proteins were blotted onto a Amersham™ Protran® 0.45 µM pore nitrocellulose membrane by semi-dry blotting using PerfectBlue™ Semi-Dry Electroblotter Sedec™ (VWR Peqlab) and Towbin buffer[196] (192 mM glycine, 25 mM Tris, 0.1% (w/v) SDS, 20% (v/v) methanol) at 2.5 mA cm^{-2} for 45 min at RT. Then blots were stained with Ponceau S to assess protein loading. After blocking in Tris-buffered saline buffer (TBS; 50 mM Tris-HCl pH 7.5, 150 mM NaCl) with 0.05% (v/v) Tween® (TBST) and 5% (v/v) BSA overnight, blots were incubated with primary antibody diluted in blocking buffer for 2 h at RT. Blots were washed thrice for 5 min in TBST. Then, the secondary antibodies in blocking buffer was added and the blot was further incubated for 1 h at RT. Thereafter, blots were washed thrice for 5 min in TBST and once with TBS. The bound secondary antibodies were detected by Western Lightning® Plus-ECL (PerkinElmer) chemiluminescence substrate and the luminograms were visualized using the Fusion FX7 imaging system (Vilber Lourmat). Signal intensities were measured using ImageJ software (National Institutes of Health) and normalized to Ponceau S staining. The antibodies and dilutions used were: mouse monoclonal to H3K9me2 (1:1,000; ab1220 from Abcam), rabbit polyclonal to histone H3 (1:5,000; AS10710 from Agrisera), mouse monoclonal to biotin (1:5,000; A6561 Sigma), rabbit polyclonal to HA (1:2,000; H6908 from Sigma), mouse monoclonal to anti-His (6x) (1:100; OB05 Calbiochem), anti-rabbit IgG (1:2,500; W4011, Promega) and anti-mouse IgG (1:2,500; W4021, Promega), rabbit polyclonal to *At*SAHH1 (1:10,000; Ref.[197]; kindly provided by Barbara Moffat).

3.5.4 Detection of S-nitrosated proteins

The biotin switch technique (BST; Ref.[198]) or the resin-assisted capture of S-nitrosothiols assay (RSNO-RAC; Ref.[199]) were used to analyze S-nitrosation of proteins. 10 µg of recombinant *At*SAHH1 in HEN buffer (100 mM Hepes-NaOH pH 7.7, 1 mM EDTA, 0.1 mM neocuproine) was treated with 50 µM, 250 µM, 500 µM GSNO or 500 µM GSH in a final volume of 100 µL for 30 min at RT in the dark with intermittent inverting of the tubes. Free thiols were blocked with 20 mM S-methylmethanethio-sulfonate (MMTS) in the presence of 2.5% (w/v) SDS at 300 rpm for 20 min at 50°C on a thermoshaker in the dark. After acetone precipitation to remove excess of GSNO and MMTS, the protein pellets were washed thrice with ice-cold acetone (10,000g for 10 min at 4°C), air-dried, and then resuspended in 32.5 µL of HENS buffer (HEN supplemented with 1% (w/v) SDS). The labeling reaction was started by the reduction of S-nitrosothiol groups with sodium ascorbate (1 mM final concentration) to generate thiols and O-nitrosoascorbates via a transnitrosation reactions. The nascent reduced thiols, which were originally S-nitrosated, were then biotinylated by adding 1 mM biotin-HPDP. The labeling reaction (50 µL final volume) was allowed to proceed at 300 rpm for 1 h at RT using a thermoshaker in the dark. After acetone precipitation, the biotin-labeled proteins were resuspended in 45 µL non-reducing sample buffer (0.06 M Tris-HCl, pH 6.8, 10% (v/v) glycerol, 0.008% (w/v) bromophenol blue) and separated on a 10% SDS-PAGE gel without boiling prior to loading. Biotinylated proteins were detected with an anti-biotin antibody conjugated with alkaline phosphatase and 5-Bromo-4-chloro-3-indolyl phosphate/Nitro blue tetrazolium (BCIP/NBT) chromogenic visualization. *In planta,* S-nitrosation of *At*SAHH1 was investigated in 4-week-old *Arabidopsis* rosette leaves homogenized in HEN-T buffer (HEN supplemented with 0.2% (v/v) Triton® X-100 and protease inhibitor cocktail) in a ratio of 1:2. The extract was centrifuged twice at 18,000g for 20 min at 4°C. After desalting using Zeba™ Spin columns equilibrated with HEN buffer, the protein content was assayed by Bradford[200] using the Bio-Rad Protein Assay according to the manufacturer´s microplate protocol with BSA as standard. For *in vitro* S-nitrosation, extracts (1.5 mg; 1.13 µg µl^{-1}) were incubated with 0.5 mM GSNO or water as mock for 30 min at RT in the dark with frequent inverting. Next, free cysteine thiols were blocked by S-methylthiolation with 20 mM MMTS in the presence of 2.5% SDS at 300 rpm for 20 min at 50°C on a thermoshaker in the dark in a final volume of 1.5 mL. Excess of GSNO and MMTS was removed by precipitation with two volumes of ice-cold acetone for 20 min at -20°C. After centrifugation (10,000g for 10 min at 4°C), the protein pellet was washed three times with 70% (v/v) acetone, air-dried, and resuspended in HENS buffer (1 mL per mg protein). Afterwards 30 µL of the protein suspension were taken for analysis of total protein input. Next, 16 mg thiopropyl sepharose 6B per sample (equal to 50 µL bed volume) was equilibrated in excess HEN buffer for 15 min, washed thrice with HEN buffer by centrifugation (1,000g for 1 min) and resuspended by the addition of 150 µL HEN buffer. The protein

suspension was added to 200 µL slurry (equal to 50 µL bed volume) in the presence of 50 mM ascorbate (prepared in HEN buffer) to a final volume of 2.3 mL. Thus, nascent SNO-proteins bind after their reduction to thiols with ascorbate to the thiol-reactive resin. Ascorbate was omitted for negative controls. Protein capture was allowed to proceed for 3 h at RT in the dark using an overhead shaker. To remove non-bond proteins, the resin was washed four times with 3 mL of HENS buffer and two times with 2 mL of HENS/10 buffer (HENS diluted 1:10). Centrifugation steps to collect beads were performed at 500g for 1 min. Originally S-nitrosated proteins were eluted with one bed volume of HENS/10 supplemented with 100 mM β-mercaptoethanol for 20 min at 22°C on a thermo-shaker (1500 rpm), separated on a 13.5% SDS-PAGE, and analyzed by immunoblotting with an anti-*At*SAHH1 antibody.

3.6 Heterologous protein production and enzymatic activity assays

3.6.1 Heterologous production of *At*SAHH1

*At*SAHH1 was produced as N-terminal His$_6$-tagged fusion protein in *E. coli* BL21 (DE3) carrying the pDEST17/*T7::His$_6$-AtSAHH1* plasmid, which encodes the full-length cDNA of *AtSAHH1* (AT4G13940). An overnight pre-culture was 100-fold diluted in 500 mL of LB-Lennox media (1% tryptone (w/v), 0.5% (w/v) yeast extract, 0.5% (w/v) NaCl adjusted to pH 7 with NaOH) supplemented with 100 µg mL^{-1} ampicillin in a 2-L Erlenmeyer baffled flask. The culture was incubated to an OD$_{600}$ of 0.6 (37°C, 180 rpm shaking rate), induced with 1 mM isopropyl β-D-1-thiogalactopyranoside (IPTG), and further cultivated at 16°C overnight. Cells were harvested by centrifugation (4,000g, 4°C, 15 min), flash frozen, and stored at -80°C until purification. For lysis, the bacteria pellet was resuspended in ice-cold lysis buffer (50 mM Tris-HCl pH 8.0, 300 mM NaCl, 20 mM imidazole, 0.5% (v/v) Triton® X-100, 1 mM β-mercaptoethanol; about 2.5 mL x g cell weight) and cells were lysed by three freeze-thaw cycles (-80°C freezer and 30°C water bath). Then, the lysate was supplemented with 1 mg mL^{-1} lysozyme and incubated on ice with gentle shaking for 30 min. After sonication, cellular debris were removed by centrifugation (18,000g, 20 min, 4°C) and the soluble faction was subjected to affinity chromatography using Ni-NTA agarose (Qiagen) and Econo-Pac® columns (Bio-Rad). The lysate was applied onto the column, equilibrated with lysis buffer, and washed with 10 CV of buffer A (50 mM Tris-HCl pH 8.0, 300 mM NaCl, 20 mM imidazole, 1 mM β-mercaptoethanol), 10 CV with buffer A supplemented with 1 M NaCl, and again with 10 CV of buffer A. Adsorbed proteins were eluted with buffer B (50 mM Tris-HCl pH 8.0, 300 mM NaCl, 300 mM imidazole, 20% (v/v) glycerol, 1 mM β-mercaptoethanol). The eluates were frozen in liquid nitrogen and stored at -80°C. Based on SDS-PAGE gels, fractions containing recombinant *At*SAHH1 protein were pooled together and rebuffered using Zeba™ Spin columns (Thermo Scientific) equilibrated with 50 mM Tris-HCl pH 8.0 before use. The protein content was determined by

Bradford[200] using the Bio-Rad Protein Assay according to the manufacturer´s microplate protocol with BSA as standard.

3.6.2 SAHH activity assay

The activity of SAHH was determined in the SAH hydrolytic direction in the presence of excess adenosine deaminase (Ado). SAH is hydrolyzed to Hcys and adenine, which is subsequently converted into inosine and ammonia by Ado. This deamination is associated with the decrease in absorbance at 265 nm[201]. The reaction mixture contained 50 mM potassium-phosphate buffer pH 7.2, 1 mM EDTA, 0.75 U adenosine deaminase, and 2 µg purified recombinant protein in a final volume of 500 µl. After the addition of SAH to a final concentration of 100 µM, the decrease of absorbance at 265 nm at 10 s intervals for 300 s at RT in a *Ultrospec™ 3100 pro* UV/Visible spectrophotometer (Amersham Biosciences) using quartz suprasil® Hellma® Precission cells cuvettes (Hellma Analytics) was monitored. The reference sample contained water instead of SAH. The product concentrations were calculated from the slope of ΔA and $\varepsilon = 8.1$ mM^{-1} cm^{-1} (Ref.[202]). The effect of GSNO or N-ethylmaleimide (NEM) on SAHH activity was analyzed by incubation of recombinant *At*SAHH1 (in 50 mM Tris-HCl pH 8) with these compounds for 30 min at RT in the dark. Thereafter, samples were desalted using Zeba™ Spin columns equilibrated with 50 mM Tris-HCl pH 8. To assess reversibility of GSNO-dependent inhibition of recombinant *At*SAHH1, 10 mM of the reducing agent dithiothreitol (DTT) was added 30 min following addition of GSNO, after which samples were incubated for 10 min prior to buffer exchange.

3.6.3 GSNOR activity assay

GSNOR activity in 4-week-old rosette leaves were determined as previously described[203]. Briefly, 0.5 g grinded plant material was extracted with 1 mL of extraction buffer (100 mM Tris–HCl pH 7.5, 0.1 mM EDTA, 0.2% (v/v) Triton® X-100, 10% (v/v) glycerol) on ice for 10 min with intermittent vortexing. The extracts were clarified by two centrifugation steps at 14,000g for 15 min at 4°C, and then, the protein concentration was determined according to Bradford[200] with BSA as standard. The reaction mixture contained 20 mM Tris-HCl pH 8.0, 0.5 mM EDTA, 0.2 mM NADH, and 100 µg protein extract in a final volume of 1 mL. After the addition of GSNO to a final concentration of 500 µM, the oxidation of NADH was monitored by the decrease of absorbance at 340 nm ($\varepsilon = 6.22$ mM^{-1} cm^{-1}) at 10 s intervals for 300 s at RT in a *Ultrospec™ 3100 pro* UV/Visible spectrophotometer (Amersham Biosciences) using quartz suprasil® Hellma® Precission cells cuvettes (Hellma Analytics). The reference sample contained water instead of GSNO. The activity was expressed as consumption of nmol NADH min^{-1} mg^{-1}.

3.6.4 GUS activity staining

GUS activity was detected by histochemical staining according to Ref.[204] with modifications. *A. thaliana* line L5 harboring multiple copies of a 35Spro::*GUS* marker gene (*TS–GUS*; Morel et al. 2000) plantlets

were immersed in fixing solution (50 mM sodium phosphate buffer pH 7.0, 0.05% (v/v) Triton® X-100, 0.5% (v/v) formaldehyde), vacuum infiltrated, and washed thrice with 50 mM sodium phosphate buffer pH 7.0. Then the plantlets were immersed into GUS staining solution (50 mM sodium phosphate buffer pH 7.0, 0.1% Triton® X-100, 1 mM potassium ferrocyanide, 1 mM potassium ferricyanide, 1 mM 5-bromo-4-chloro-3-indolyl-D-glucuronic acid) and incubated at 37°C overnight. Plantlets were washed once with 70% (v/v) ethanol and incubated in 70% (v/v) ethanol at 80°C to remove chlorophyll for 10 min.

3.7 Metabolic analysis

3.7.1 Quantification of chlorophyll contents

Chlorophyll was extracted from plant tissue with 80% (v/v) acetone and the content was determined spectrophotometrically according to Ref.[205]. In detail, pigments of 50 mg of 4-week-old rosette leaves frozen and ground in pools of two plants per genotype were extracted with 2 mL of 80% (v/v) acetone for 30 min in the dark at RT with vigorous vortexing every 10 min. Samples were centrifuged at $15,000g$ for 15 min to pellet cellular debris. The absorbance of the supernatant was measured using a DU® 640 Spectrophotometer (Beckman) and quartz suprasil® Hellma® Precission cells cuvettes (Hellma Analytics) at 646 nm and 663 nm to measure chlorophyll a and b, respectively. Chlorophyll a and b were determined with the following formulae and normalized to fresh weigh: $(12.21*A_{663} - 2.81*A_{646})$ x Volume/Weight = Chl a µg/g FW and $(20.13*A_{646} - 5.03*A_{663})$ x Volume/Weight = Chl b µg/g FW.

3.7.2 Quantification of S-nitrosothiols

The S-nitrosothiol level in 4-week-old rosette leaves were determined by triiodide-dependent ozone-based chemiluminescence using the Nitric Oxide Analyzer Sievers® 280i from GE Healthcare. This method is based on the reduction of nitrite and RSNO by triiodide to NO, which reacts with ozone to form the excited state of nitrogen dioxide (NO_2) and O_2. Upon decay to its ground state, NO_2* emits a photon which is detected by a photomultiplier[206]. The intensity of emitted light is directly proportional to the amount of NO. In short, rosette leave extracts were prepared by homogenization of 500 mg ground plant material in two volumes of 1x phosphate buffered saline (PBS; 137 mM NaCl, 2.7 mM KCl, 4.3 mM Na_2HPO_4, 1.47 mM KH_2PO_4, pH 7.4) and incubation on ice for 10 min with intermittent vortexing. After centrifugation at $18,000g$ for 15 min at 4°C, the supernatant was used for further analysis. For RSNO measurements, extracts were pre-treated with 5% sulfanilamide (w/v, in 1 M HCl) at a ratio of 9:1 (extract : sulfanilamide) to scavenge nitrite and 200 µL were injected into the reaction vessel containing acidic triiodide as reducing agent (28.5 mM I_2, 66.9 mM KI, 77.7% glacial acetic acid; 30°C). The peak area integration and quantification of RSNO content were performed with Sievers® NOA Analysis™ software (GE Healthcare) using nitrite standards and normalized to the protein content assayed according to Bradford[200].

3.7.3 Quantification of polyamines

The levels of free putrescine, spermidine, and spermine in 4-week-old leaves were quantified after pre-column derivatization with 9-Fluorenylmethoxycarbonyl chloride (FMOC-Cl)[207]. 100 mg plant material was ground in liquid nitrogen and extracted with 1 mL of 5% (v/v) perchloric acid for 1 h at RT with intermittent vortexing. After centrifugation (18,000g, 10 min, 20°C), 15 μL of the supernatant was neutralized with 360 μL of 0.1 M NaHCO$_3$ supplemented with 1,7-diaminoheptane as internal standard. After the addition of 100 μL acetone and 200 μL 6 mM FMOC in acetone, the reaction was allowed to proceed for 5 min at RT and for 10 min at 50 °C. The reaction was stopped at -20°C for 5 min and then 300 μL methanol was added. The derivatized polyamines were separated by reverse phase chromatography on a Luna® C18 column (5 μ 100 Å C18(2) 250 x 4.6 mm column, Phenomenex) connected to a Beckman System Gold HPLC equipped with a Shimadzu RF 10AxL fluorescence detector (excitation: 260 nm, emission: 313 nm). The flow rate and the column temperature were set at 1 mL/min and 20°C. Elution was performed with water as Eluent A and methanol as eluent B. Elution conditions were (min/B%): 0/80; 30/100, 36/100, 42/80, and 45/80. Quantification was based on the external standard method using calibration curves fitted by linear regression analysis in combination with internal standard method, where the response factor of each derivative was corrected with respect to that of internal standard[207].

3.7.4 Quantifications of thiols

Quantification of SAM, SAH, MTA, Hcy, Cys, and GSH was performed at the Centre for Organismal Studies at the University of Heidelberg by Dr. Markus Wirtz, Dr. Gernot Poschet, and Michael Schulz.

3.8 Statistical data analysis

Statistical data analyses and graphic representation of data were performed using GraphPad Prism version 7.05 for Windows software. Data were subjected to the Grubb´s outlier-test (α = 0.05). Data were tested for normality using the Shapiro-Wilk test (α = 0.05) and for equal variances using the Brown-Forsythe test (α = 0.05). Normally distributed data and data with equal variance were subjected to ANOVA, Dunnett´s multiple comparisons test. Non-normally distributed data and/or heteroskedastic data were subjected to Kruskal-Wallis test, Dunn´s multiple comparison test.

DMG and DEGs were assigned to GO terms. Statistical significance of GO term enrichment was determined using Fisher´s exact test with FDR correction. GO-term enrichment analysis was performed in R version 3.6.0 using the following R packages org.At.tair.db (version 3.8.2) and package Go.db (version 3.8.2). GO term analysis was performed by Dr. Elisabeth Georgii (Institute of Biochemical Plant Pathology Munich).

4 Results

4.1 S-Nitrosation of *At*SAHH1

SAHH plays an important role in regulating methyl homeostasis in all biological systems[121] by removing the by-product inhibitor SAH of methyltransferases. In *Arabidopsis*, SAHH1 regulates TGS through DNA methylation at numerous targets[120,123] by removing the competitive inhibitor SAH of MTs[121]. Computational prediction and proteome-wide studies revealed *At*SAHH1 as target for S-nitrosation (see Chapter 1.5.2). Hence, the biotin switch technique[198] using His-tagged *At*SAHH1 fusion protein recombinantly produced in *E. coli* (Supplemental Figure 4) and resin-assisted capture of SNO-proteins[199] with plant extracts were performed to confirm whether *At*SAHH1 undergoes S-nitrosation (Figure 10).
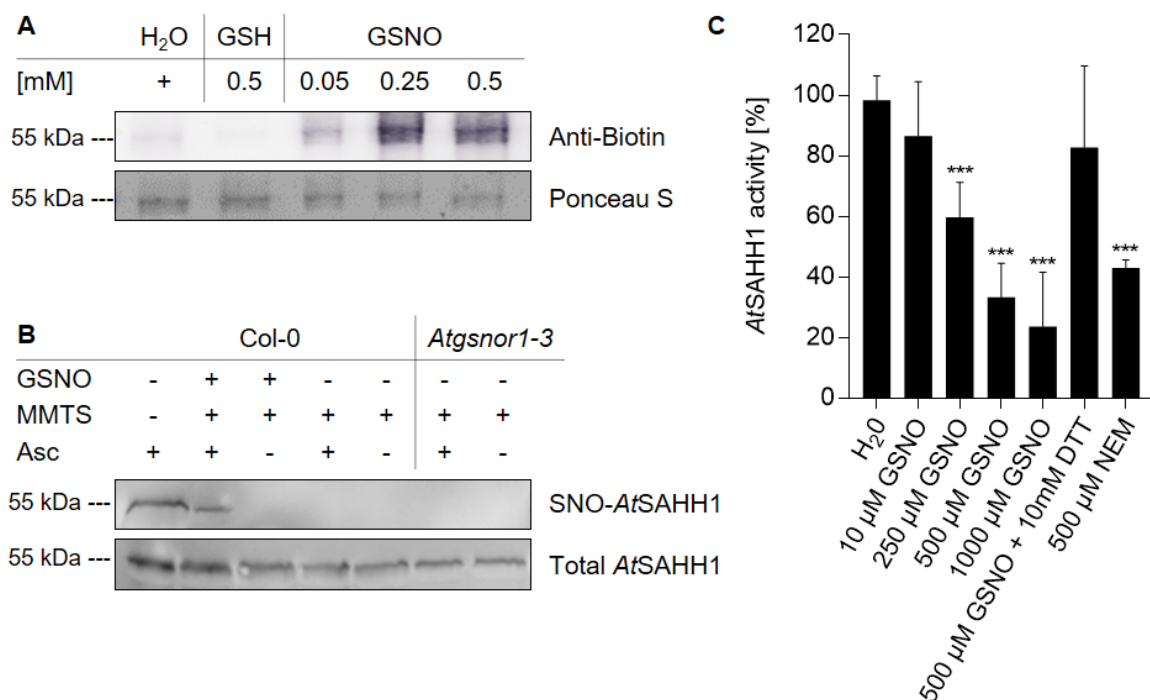
Figure 10. *At*SAHH1 is S-nitrosated and inhibited by exogenous GSNO. (A) *In vitro* S-nitrosation of *At*SAHH1. 10 µg of purified recombinant His-tagged *At*SAHH1 (56 kDa) was treated with water, GSH, and increasing concentrations of GSNO. Free thiols were blocked with MMTS, excessive GSNO and MMTS were removed by acetone precipitation, and then proteins were subjected to the biotin switch assay using ascorbate (Asc) as reducing agent. Electrophoretically separated proteins were transferred onto a nitrocellulose membrane. Ponceau S staining of blotted proteins demonstrate sample loading. Biotinylated *At*SAHH1 was detected by an alkaline phosphatase-conjugated anti-Biotin IgG followed by BCIP/NBT chromogenic visualization. **(B)** *In vivo* S-nitrosation of *At*SAHH1 (54 kDa) using wild-type and *Atgsnor1-3* plants. GSNO induced S-nitrosation of *At*SAHH1 *in vitro*. Leaf extracts from Col-0 plants were exposed to GSNO and subjected to the RSNO-RAC. *In vivo* S-nitrosation was not detected. Total *At*SAHH1 protein ensures equal protein loading. The positions of 55 kDa markers are indicated. The assay was repeated thrice with similar results. **(C)** Concentration dependent inhibition of *At*SAHH1 by GSNO *in vitro*. *At*SAHH1 produced in *E. coli* was treated with water (control), GSNO, and NEM with indicated concentration. After desalting, *At*SAHH1 activity was measured. For restoring of *At*SAHH1 activity, 10 mM DTT was added to the GSNO inhibited enzyme and then desalted. Statistics: Values are expressed as percentage of the control activity (at 0 mM: 0.44-0.89 nmol SAH min^{-1} µg^{-1} varied among independent purification) and represent the mean ± SD of at least three independent preparations of recombinant *At*SAHH1 (n = 3-7). Grubb´s outlier-test (α = 0.05) was performed. ***(p<0.001) represents significant differences between non-treated and treated *At*SAHH1 enzyme (ANOVA, Dunnett´s multiple comparisons test). Note that enzymatic assay data are from PD. Dr. Christian Lindermayr and Eva Rudolf.

The biotin switch assay is based upon the labeling of SNO-cysteine residues with a biotin moiety in a three-step procedure. First, free protein thiols are blocked with thiol-specific methylthiolating agent MMTS under denaturing conditions using SDS to ensure reagent access to buried thiol groups[208]. After ascorbate-based denitrosation of SNO-cysteines, nascent thiols are labeled with biotin-HPDP. The degree of biotinylation (and hence S-nitrosation) of recombinant *At*SAHH1 was directly visualized by anti-biotin immunoblotting (Figure 10A). In the RSNO-RAC assay, the thiol-reactive biotinylating agent is substituted by a thiol-reactive resin allowing the enrichment of SNO-proteins by covalent chromatography. After methylthiolation of free protein thiols, SNO-proteins were captured due to formation of a disulfide linkage between the RSNO site (reduced to a sulfhydryl group by ascorbate) and the resin. To detect S-nitrosation of the target protein, enriched SNO-proteins were subjected to anti-*At*SAHH1 immunoblotting (Figure 10B). The biotin switch assay (Figure 10A) with recombinant *At*SAHH1 protein confirms that *At*SAHH1 is S-nitrosated by GSNO, but not by GSH regarded as inactive donor control[198]. Similarly, *At*SAHH1 was S-nitrosated when plant extracts were treated with GSNO. However, *in vivo* S-nitrosated *At*SAHH1 was neither detected in wild-type nor in *Atgsnor1-3* (Figure 10B). Next, the effect of GSNO on the catalytic activity of *At*SAHH1 was determined. Recombinantly produced *At*SAHH1 was incubated with increasing concentration of GSNO and a dose-dependent reduction of *At*SAHH1 activity was observed (Figure 10C). Treatment with 10 µM GSNO caused 12% inhibition and the activity significantly decreased to 60%, 34%, and 28% in the presence of 250 µM, 500 µM, and 1 mM GSNO, respectively. Reduction of recombinant GSNO-treated *At*SAHH1 with DTT restored the enzymatic activity to 84%. This reversible inhibition suggests inactivation by S-nitrosation of cysteine thiols[43]. *At*SAHH1 was also inhibited by the sulfhydryl-modifying agent NEM to 44% confirming that cysteine residues are important for its activity (Figure 10C). Taken together, these results demonstrate that the activity of *At*SAHH1 is inhibited by GSNO and *At*SAHH1 is S-nitrosatable.

4.2 The effect of exogenous GSNO and DHPA on methylation

The main function of the methylation cycle is to produce SAM for transmethylation reactions and recycle the by-product SAH. Both SAM and SAH levels are well known to regulate DNA and histone methylation (Ref.[129,133] and references therein). Due to S-nitrosoproteomic studies identified key enzymes of the methylation cycle as target proteins for S-nitrosation, the hypothesis was postulated that RSNO/GSNO may regulate the methylation cycle through S-nitrosation. Further, the differential inhibition of *At*MAT by S-nitrosation has been previously reported[160]. In this study, it was demonstrated that GSNO S-nitrosates *At*SAHH1 and impairs its activity *in vitro* (Chapter 4.1). Hence, the effect of exogenous GSNO application to 7-day-old liquid-cultured seedlings on the methylation cycle, H3K9me2, and DNA methylation was investigated. As control, light-exposed, and hence NO-exhausted, GSNO (exGSNO) was used. Noteworthy, the enhancement of total cellular RSNO levels in 7-day-old liquid-cultured seedlings treated with exogenous GSNO was previously demonstrated[40]. Further, the specific inhibitor of SAHH, the adenosine homologue DHPA, was used. DHPA was previously shown to induce hypomethylation *in planta*[120,127]. Next, the effects of these pharmacological compounds on the methylation cycle, H3K9me2, DNA methylation, and on the transcriptionally silenced GUS transgene in the *TS-GUS* (6b5, L5) line are presented.

4.2.1 Impairment of the methylation cycle by exogenous GSNO and DHPA

The functional effect of exogenous GSNO, exGSNO, and DHPA on SAM, SAH, Hcy, and on the methylation ratio (SAM/SAH) was determined in 7-day-old liquid-cultured seedlings (Figure 11A-D). Exogenous application of GSNO resulted in a 2.3-fold and 3.8-fold increase in the level of SAM and SAH compared to non-treated seedlings (Figure 11A, B), respectively. However, the stronger increase in SAH levels led to a diminished SAM/SAH ratio upon GSNO treatment, albeit not significant (Figure 11C). The SAM and SAH level, and hence, the SAM/SAH ratio were unaffected by exGSNO treatment (Figure 11A-C). The inhibition of SAH hydrolase by DHPA resulted in an accumulation of SAH, whereas the SAM level remained unchanged compared to wild-type (Figure 11A, B). As a result, the overall SAM/SAH ratio was declined by a factor of 35 upon DHPA treatment indicating hypomethylation (Figure 11C). GSNO treatment led to accumulation of Hcys (Figure 11D), a hallmark of an impaired methylation cycle[133].

Next, levels of MTA a downstream metabolite of SAM and inhibitor of HMTs were determined (Figure 11E). Exogenous application of GSNO, exGSNO, and DHPA led to increased MTA levels by 3-fold, 1.4-fold, and 1.6-fold, respectively. In addition, the cysteine and GSH levels were determined (Figure 11F, G). Cysteine is essential for the synthesis of Hcys, an intermediate in the methylation cycle. Further, it is postulated that GSH metabolism is linked to the control of epigenetic mechanisms[167]. Besides, GSH is a precursor of GSNO. The analysis of these thiols revealed that GSNO-treated seedlings

displayed a 5-fold and 2-fold increased level of cysteine and total GSH (Figure 11F, G), respectively. Interestingly, exGSNO treatment resulted in a significant increased cysteine content, but did not alter GSH levels (Figure 11F, G). Both cysteine and GSH levels remained unchanged upon DHPA treatment. In sum, target metabolic analysis in 7-day-old seedlings upon GSNO treatment revealed that the MI is reduced, albeit not significant. Moreover, the cysteine and glutathione metabolism are impaired in GSNO-treated seedlings. These results suggest impairment of DNA and histone methylation due to metaboloepigenetic effects.
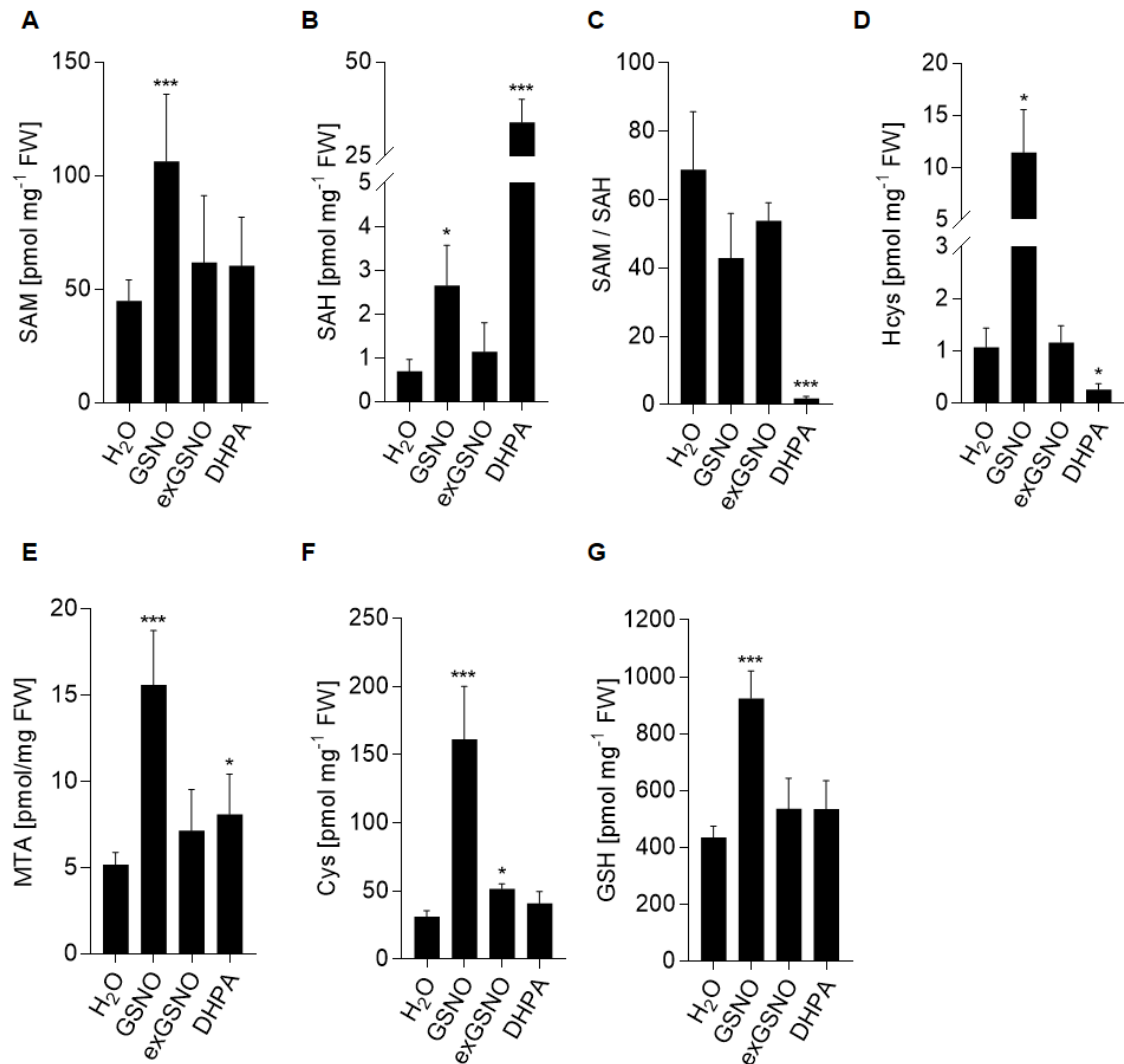
Figure 11. The methylation cycle in GSNO- and DHPA-treated seedlings is impaired. Analysis of steady-state levels of **(A)** SAM, **(B)** SAH, **(C)** Hcys **(D)** SAM/SAH, **(E)** MTA, and **(F, G)** selected thiols in 7-day-old Col-0 seedlings grown under short day conditions, treated with water (control), 1 mM GSNO, 1 mM exGSNO, or 200 µM DHPA for 16 h. Pharmacological compounds were added to liquid media at night-time start. <u>Statistics:</u> Values are normalized against total fresh weight and represent the mean ± SD of two independent experiments (n = 7-11). *($p<0.05$) and ***($p<0.001$) represents significant differences between wild-type and mutant lines. Grubb´s outlier-test ($\alpha = 0.05$) was performed. Normally distributed data and data with equal variance were subjected to ANOVA, Dunnett´s multiple comparisons test. Non-normally distributed data and/or heteroskedastic data were subjected to Kruskal-Wallis test, Dunn´s multiple comparison test. Targeted metabolomic analysis was performed at the Centre for Organismal Studies in Heidelberg by Dr. Markus Wirtz, Dr. Gernot Poschet, and Michael Schulz.

4.2.2 H3K9me2 methylation levels are not altered by exogenous GSNO and DHPA

In order to elucidate whether an impaired MI affects histone methylation upon exogenous application of GSNO, exGSNO, or DHPA, the H3K9me2 methylation level in 7-day-old seedlings was analyzed. GSNO treatment resulted in a slightly increased H3K9me2 level, whereas exGSNO, and DHPA treatments yielded to a marginally decreased H3K9me2 level, albeit these alterations are not significant (Figure 12). Similarly, the DHPA-induced alleviation of the H3K9me2 level was reported previously in a Chip-qPCR approach[120].
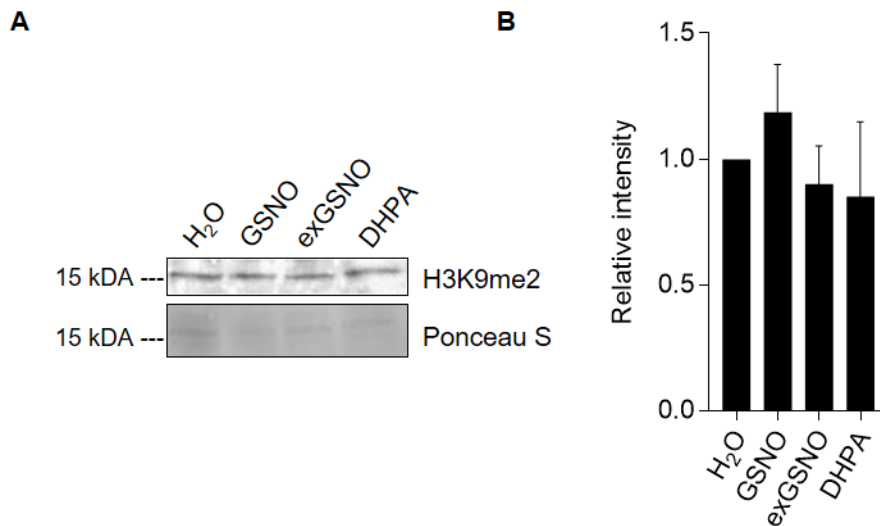
Figure 12. H3K9me2 methylation levels are not altered in GSNO- and DHPA-treated seedlings. (A) H3K9me2 levels in seedlings analyzed by immunoblotting. Histones were acid-extracted from 7-day-old Col-0 seedlings grown under short day conditions, treated with water (control), 1 mM GSNO, 1 mM exGSNO, or 200 µM DHPA for 16 h and probed against H3K9me2 marks by western blot. Pharmacological compounds were added to liquid media at night-time start. As loading control, the Ponceau S stained membrane is shown. One representative immunoblot is shown. **(B)** Quantification of western blot results. Signal intensities were measured using ImageJ software and normalized to the amount of loaded H3. Statistics: Values are expressed as fold change over control seedlings at 16h post treatment and represent the mean ± SD of at least three independent experiments (n = 4-5). Grubb´s outlier-test (α = 0.05) was performed. No significant differences were observed between non-treated and treated seedlings (Kruskal-Wallis, Dunn´s multiple comparisons test).

4.2.3 DNA methylation levels are not altered by exogenous GSNO and DHPA

To assess whether GSNO, exGSNO, or DHPA treatments alter DNA methylation at selected loci, a semiquantitative PCR following methylation-dependent restriction digestion using McrBC[181] was performed in 7-day-old liquid-cultured seedlings (treatment: 16 h; 1 mM GSNO, 1 mM exGSNO; 200 µM DHPA). The endonuclease McrBC cleaves DNA containing 5-methylcytosines, but not unmethylated DNA. Hence, methylated DNA has decreased amounts of PCR product after McrBC digestion. As shown in Figure 13, the lack of any PCR amplicon after McrBC digestion indicates that the retrotransposon *AtCopia4* and the DNA-transposon *AtMu1* are highly methylated in 7-day-old seedlings and treatments with GSNO, exGSNO, and DHPA did not reduce DNA methylation at these loci. Further, the DNA methylation level at analyzed retrotransposons (*AtGP1, AtTA2, AtLine1-4, AtSN1)* and transcriptionally silent information (*TSI*) repeats were not significantly altered upon

indicated treatments. Although, a tendency for decreased DNA methylation in DHPA-treated seedlings is obvious. This tendency is in accordance with previous studies[120] demonstrating that *AtLine1-4* was hypomethylated after DHPA treatment. In sum, treatments of GSNO, exGSNO, and DHPA for 16 h did not significantly change DNA methylation levels in 7-day-old liquid-cultured seedlings.
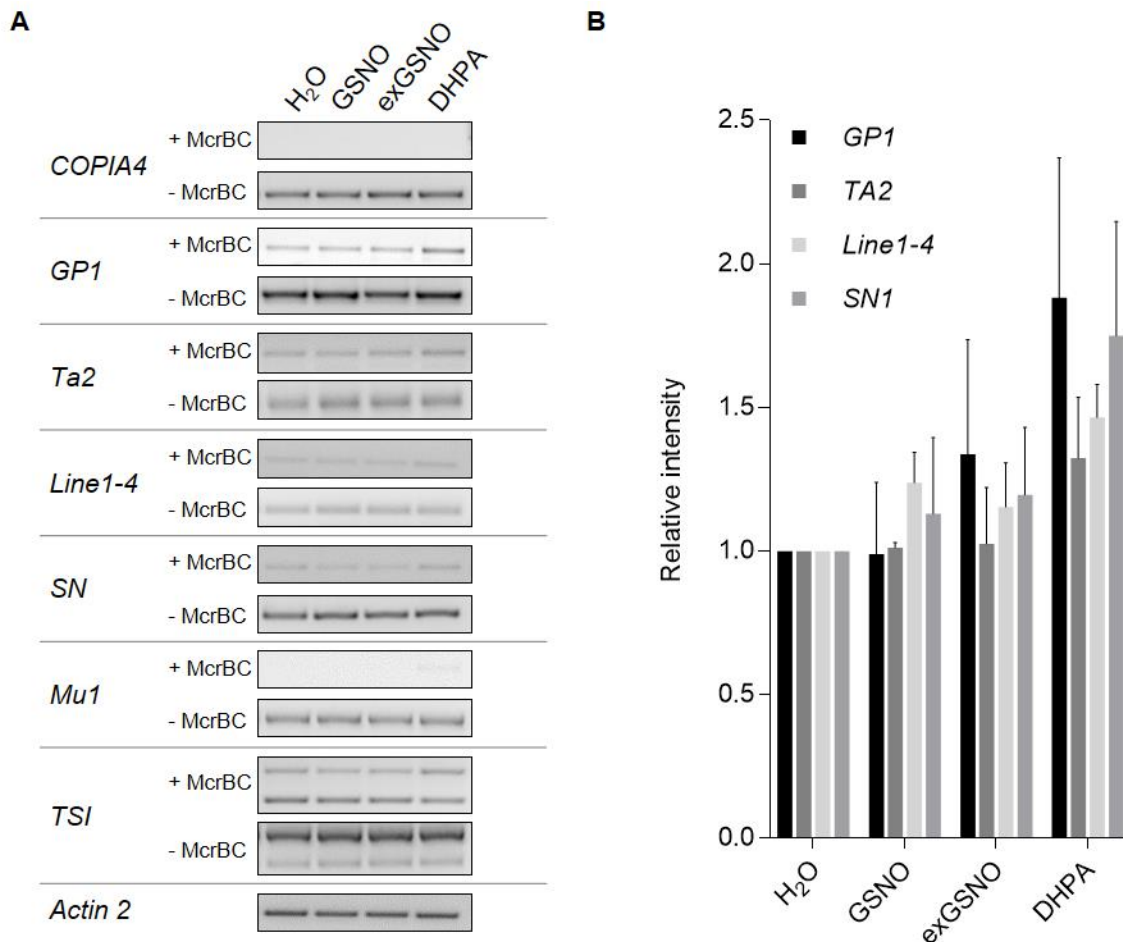
Figure 13. DNA methylation levels are not altered in GSNO- and DHPA-treated seedlings. (A) DNA methylation analysis by McrBC PCR. DNA methylation of indicated loci were determined by chop-PCR in 7-day-old Col-0 seedlings grown under short day conditions, treated with water (control), 1 mM GSNO, 1 mM exGSNO, and 200 μM DHPA for 16 h. Pharmacological compounds were added to liquid media at night-time start. Genomic DNAs were digested by McrBC followed by PCR and agarose gel electrophoresis. McrBC specifically cleaves methylated DNA sequences. Representative gel analysis of PCR produces of McrBC digested and undigested DNA is shown. **(B)** Quantification of McrBC-PCR results. Signal intensities were measured using Image J software and normalized to Actin 2 (undigested DNA). Statistics: Values are expressed as fold change over control seedlings and represent the mean ± SEM of at least three independent experiments (n = 5). Grubb´s outlier-test (α = 0.05) was performed. Normally distributed data (Shapiro-Wilk test α = 0.05) and data with equal variance (Brown-Forsythe test α = 0.05) were subjected to ANOVA, Dunnett´s multiple comparisons test. Non-normally distributed data and/or heteroskedastic data were subjected to Kruskal-Wallis test, Dunn´s multiple comparison test. No significant differences were observed. *AtCopia4*, *AtGP1*, *AtTa2*, and *AtLine1-4* are retrotransposons; *AtMu1* is a DNA transposon; *AtSN1*, short interspersed retroelement 1; *AtTSI*, transcriptionally silent information. Note that *AtCopia* and *AtMu1* were highly methylated, and hence, fully digested. The amplification of *TSI* in Col-0 background results in two products of 598 bps (*TSI*) and 318 bps (AT3G32980) according to BLASTN. Hence, quantification of *TSI* amplification is not shown.

4.2.4 Inhibition of *At*SAHH by DHPA releases *TS-GUS* silencing

The release of TGS associated with DNA methylation and heterochromatic marks by pharmacological approaches[120] has previously been demonstrated using the *AtTS-GUS* (L5, 6b5) line harboring multiple copies of a transcriptionally silenced *35Spro::GUS* marker gene[171]. Reactivation of *AtTS-GUS* was shown by exogenous application of DNA methylation inhibitors[209] or DHPA[120]. In this study, we evaluated the effect of exogenous GSNO and DHPA on the release of transcriptional silenced *TS-GUS* transgene by germinating and growing seeds in their presence for twelve days in liquid-culture (Figure 14). DHPA induced reactivation of the GUS transgene verifying the presence and availability to reactivate the *TS-GUS* insert. However, exogenous GSNO treatment was not effective. Taken together, these results indicate that GSNO does not reactivate the silent *TS-GUS* transgene. In contrast, the inhibition of *At*SAHH with DHPA release TS-GUS silencing.
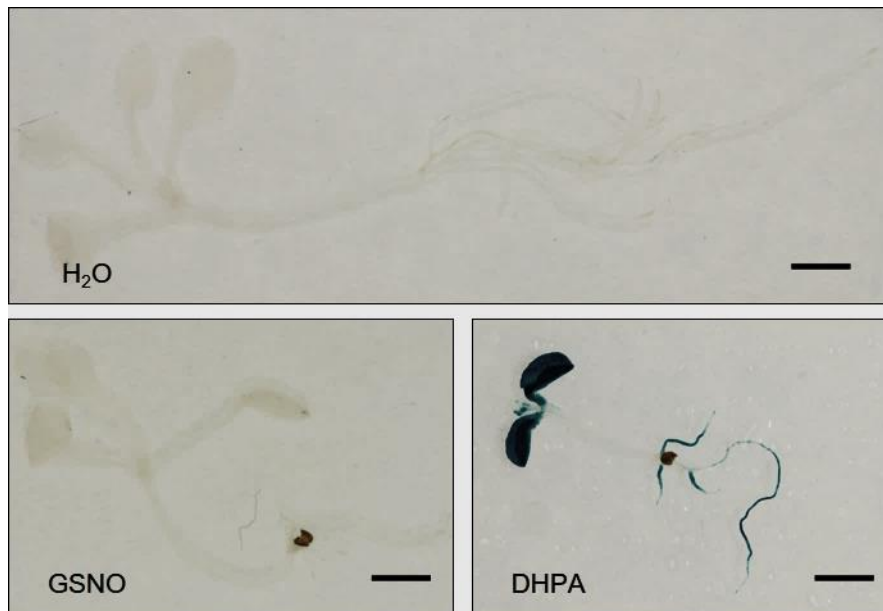
Figure 14. Inhibition of *At*SAHH by DHPA releases *TS-GUS*. Histochemical GUS staining of 12-day-old seedlings grown in the presence of DHPA or GSNO (water-control, 500 µM GSNO, or 200 µM DHPA). Seeds were surface sterilized, suspended in sterile water, and stratified for two days at 4°C in the dark. Then, plantlets were germinated and grown for twelve days in liquid media supplemented with indicated chemicals under short day conditions. Due to the instability of GSNO in light, media including drugs were exchanged every day. Blue areas indicate reactivation of *TS-GU*S silencing, which is very pronounced in response to DHPA treatment. Scale bar = 2 mm.

4.3 The effect of enhanced endogenous RSNOs and SAH levels on methylation

Both pharmacological and genetic approaches has been performed to elucidate NO-mediated physiological processes in plants[7] using either the exogenous application of NO-donors such as GSNO or mutants with impaired NO/GSNO homeostasis. In this study, the GSNOR-deficient line, namely *Atgsnor1-3*[45,46], was used to investigate the effect of RSNO/GSNO bioactivity on methylation processes. Further, the *Atsahh1* mutant[121,124,170] was used to study the effect of an impaired methylation cycle on histone methylation and genome wide DNA methylation.

4.3.1 Characterization of mutants and transgenic lines

Mutants used in this study were verified by genomic PCR analysis. Homogeneity for *Atgsnor1-3*, *Atsahh1*, and *Athog1-7* mutant lines was confirmed (Supplemental Figure 5 and Supplemental Figure 6). *A. thaliana* lines expressing *At*SAHH1 tagged with an epitope (HA-StrepIII double tag; Figure 15A), which is recognized by commercially available antibodies, were generated. Transgenic *35S::AtSAHH1-HA-StrepIII* lines were confirmed by genomic PCR (Figure 15B). Further, RT-PCR analysis confirmed the expression of *AtSAHH1* in wild-type and *35S::AtSAHH1-HA-StrepIII* transgenic plants, which is distinctly diminished in the *Atsahh1* mutant (Figure 15C). Moreover, immunoblotting using an anti-HA and an anti-*At*SAHH1 antibody confirmed the expression of *the At*SAHH1-HA-StrepIII fusion protein in the generated transgenic lines (Figure 15D, E). Of note, *At*SAHH1 levels were reduced in *Atsahh1* mutant (Figure 15E). These results indicate that *35S::AtSAHH1-HA-StrepIII* coding region is inserted in the genome and expressed in T4 generation of Line 2 and Line 3. To note, the predicted molecular mass from *At*SAHH1 is 54 kDa and from *At*SAHH1-HA-StrepIII is 61 kDa.
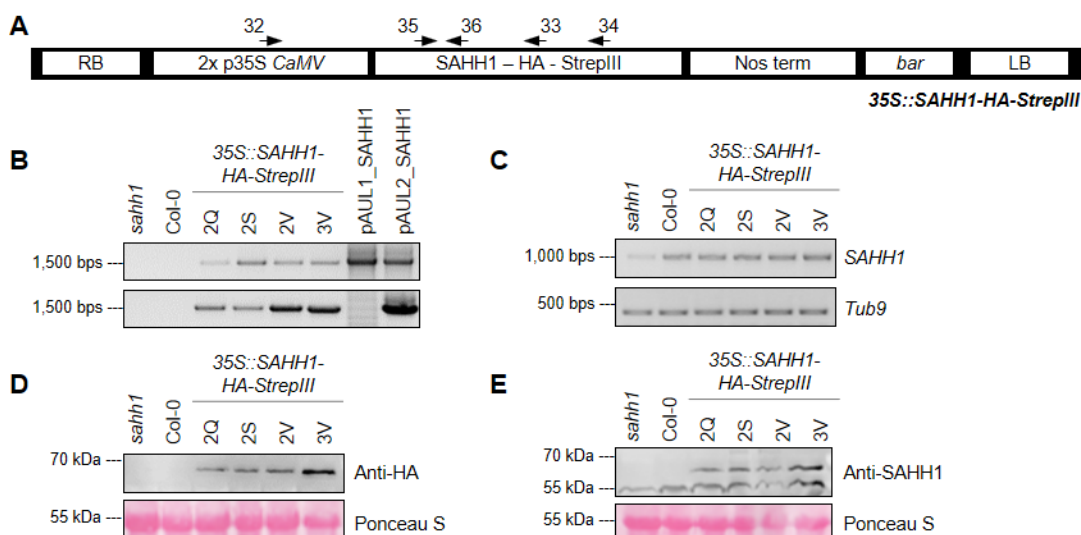
Figure 15. Molecular characterization of *35S::AtSAHH1-HA-StrepIII* transgenic lines. (A) Schematic illustration of the 35S::SAHH1-HA-StrepIII insertion and primes (indicated with black arrows) used for **(B)** genomic PCR **(C)** and RT-PCR. The plant expression vectors pAUL1_*At*SAHH1 and pAUL2_*At*SAHH1 encodes for *At*SAHH1-HA or *At*SAHH1-HA-StrepIII, respectively. Amplicon length, primers, and PCR conditions are listed in Supplemental Table 4. **(D)** Immunoblots probed either with primary anti-HA or **(E)** primary anti-*At*SAHH1 antibody. Total proteins were extracted from 4-week-old rosette leaves of

transgenic lines 2 and 3 in two volumes of HEN buffer and 15 µg of each protein extract was electrophoretically separated by 13.5% SDS-PAGE gel and transferred onto a nitrocellulose membrane. The immunoblots were labeled with anti-rabbit IgG and Western Lightning® Plus-ECL substrate. The amount of loaded RuBisCo-LSU (53 kDa) is shown as loading control using Ponceau S staining. Note 2Q, 2S, 2V and 3V are progenies of transformants (T1) plant 2 and plant 3 in T4 generation, respectively. Transgenic lines harboring the *At*SAHH1-HA-StrepIII insertion in Col-0 background are verified. Abbreviations: LB, left border; RB, right border; *bar*, Basta resistance gene; p35S *CaMV*, 35S promoter of cauliflower mosaic virus; NOS term, nopaline synthase terminator; HA-StrepIII, epitope tag.

4.3.2 Loss of *At*GSNOR1 function results in increased RSNO levels

*At*GSNOR1 catalyze the NADPH-dependent reduction of GSNO to GSSG and ammonia. Hence, *At*GSNOR1 controls the cellular levels of the NO reservoir and nitrosating species GSNO, and in turn the level of S-nitrosated proteins[14,38,39]. Both the GSNOR activity and total RSNO content were analyzed to investigate their correlation in *Atgsnor1-3* and *Atsahh1* mutants under basal conditions. Phenotypes of 4-week-old plants are shown in Figure 16A. Leaf extracts from *Atsahh1* exhibit 118% of the GSNOR activity detected in wild-type, even though not statistically significant. Whereas GSNOR activity significantly decreased to 10% in *Atgsnor1-3* relative to wild-type plants (Figure 16B).
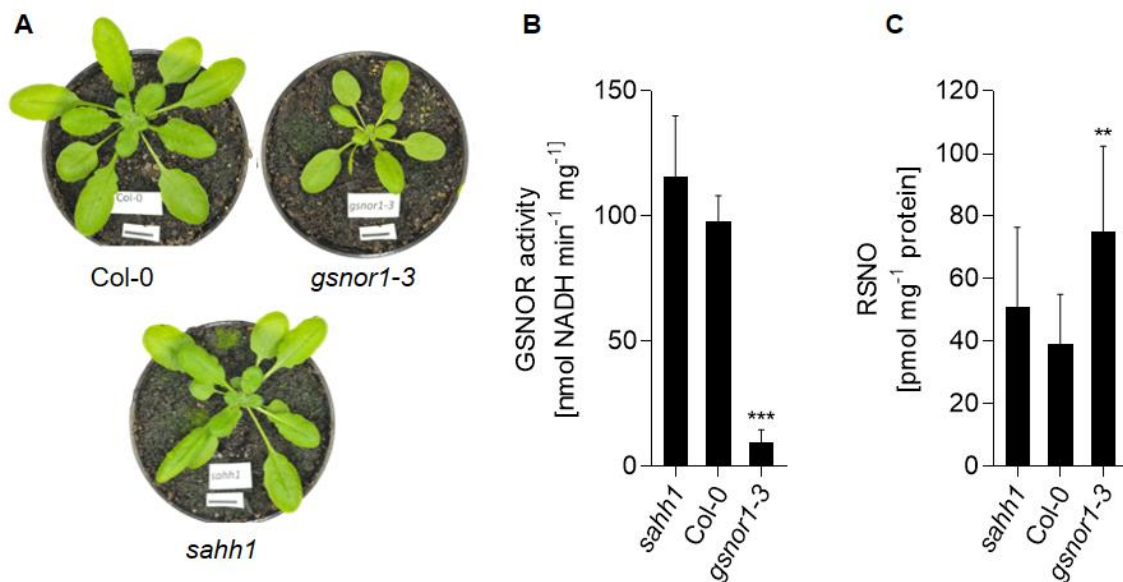
Figure 16. Loss of *At*GSNOR1 function results in an increased RSNO content under basal conditions. (A) Phenotype of 4-week-old *Arabidopsis* mutants. **(B)** GSNOR activity was determined by NADPH consumption in the presence of GSNO (n = 3-5). **(C)** RSNO content was determined by triiodide-dependent ozone-based chemiluminescence (n ≥ 5). Both analyses were measured in 4-week-old rosette leaves grown under long-day condition harvested 5 h after day-time start. Statistics: Values represent the mean ± SD of at least three independent experiments. Grubb´s outlier-test (α = 0.05) was performed. **(p<0.01) and ***(p<0.001) represents significant differences between wild-type and mutants (ANOVA with Dunnett´s multiple comparisons test).

The determination of the GSNO content in plant samples is still demanding in analytical terms[210], and hence, a robust method remains to be developed. Though, it is commonly received that GSNO levels are in registry with total RSNO levels in biological systems[49]. Total RSNO levels were measured by ozone-based chemiluminescence and tended to increase in *Atsahh1*, albeit not statistically significant (Figure 16C). These results indicate a positive correlation between GSNOR activity and RSNO levels for

Atsahh1 mutant. Of note, most previous studies described a negative correlation between RSNO and GSNOR activity[42,49], however, positive correlations were examined in Medicago roots overexpressing GSNOR[211] and pea seedlings exposed to different abiotic stresses[212]. The decreased GSNOR activity in *Atgsnor1-3* mutant compared to wild-type was accompanied by an almost 2-fold increase in RSNO levels. These results are in accordance with previous studies[42,45,46]. Most important, *Atgsnor-ko* resulted in an increased total RSNO level allowing a direct functional analysis of enhanced RSNO/GSNO levels under physiological conditions in *Arabidopsis*.

4.3.3   Mutations in *AtGSNOR1* and *AtSAHH1* results in an impaired methylation cycle

To investigate the effect of *At*GSNOR1- and *At*SAHH1-deficiency on the methylation capacity, steady-state levels of SAM and SAH were determined in wild-type*, Atsahh1*, and *Atgsnor1-3* (Figure 17A, B). Further, the SAM/SAH ratio, also named MI, which is regarded as an indicator of the cellular methylation state was calculated (Figure 17C). The major methyl group donor SAM was significantly elevated in *Atsahh1* and *Atgsnor1-3* plants by 61% and 43%, respectively. The *Atsahh1* mutant also had a two-fold increase in the SAH level resulting in an overall decrease of the MI by 14% compared to wild-type. This result is concordant with previous studies[123,124] and the decreased *At*SAHH1 protein level in *Atsahh1* mutant line as determined by immunoblotting (Supplemental Figure 7). As the SAH level of *Atgsnor1-3* was similar compared to wild-type, the resulting SAM/SAH ratio was significantly increased by 47%. Taken together, the metabolic phenotypes of *Atsahh1* and *Atgsnor1-3* plants indicate hypo- and hyper-methylation, respectively.

In addition, SAM is required in a late step of chlorophyll biosynthesis, and its decreased availability may result in a bottleneck in chlorophyll formation[213]. *Atsahh1* plants had a slightly increased chlorophyll content compared to wild-type (Supplemental Figure 8) as previously demonstrated[124]. In contrast, the level of total chlorophyll was decreased in *Atgsnor1-3* plants (Supplemental Figure 8) as previously shown[46], despite the SAM level was increased. MTA is produced from SAM as a by-product of ethylene, polyamines, and nicotinamide synthesis and it is further recycled to methionine in the methionine salvage cycle[117]. In *Atgsnor1-3* and *Atsahh1* the MTA levels were significantly enhanced by 33% and 57% relative to wild-type, respectively (Figure 17D). However, only *Atgsnor1-3* plants displayed an MTA-accompanied significant rise in spermidine and spermine, respectively (Supplemental Figure 9). Besides, MTA affect histone methylation as a HMTase inhibitor[214] suggesting alteration in histone methylation in *Atsahh1* and *Atgsnor1-3*.

In addition, cysteine and total GSH levels were determined. Cysteine is a sulfur-containing amino acid and a central precursor of all reduced sulfur containing organic molecules including amino acid methionine, which is metabolized to SAM in the methylation cycle[117,215]. *Atgsnor1-3* plants showed an almost two-fold increase in cysteine levels, whereas *Atsahh1* had a slightly increased cysteine level.

Additionally, the antioxidant GSH is synthesized from cysteine. In regard to metaboloepigenetics, growing evidence support the hypothesis that GSH metabolism is linked to the control of epigenetic mechanisms[167]. The amount of total GSH in *Atgsnor1-3* and in *Atsahh1* plants were significantly enhanced compared to wild-type plants. Elevated GSH levels in GSNOR-deficient plants were also previously observed[42].
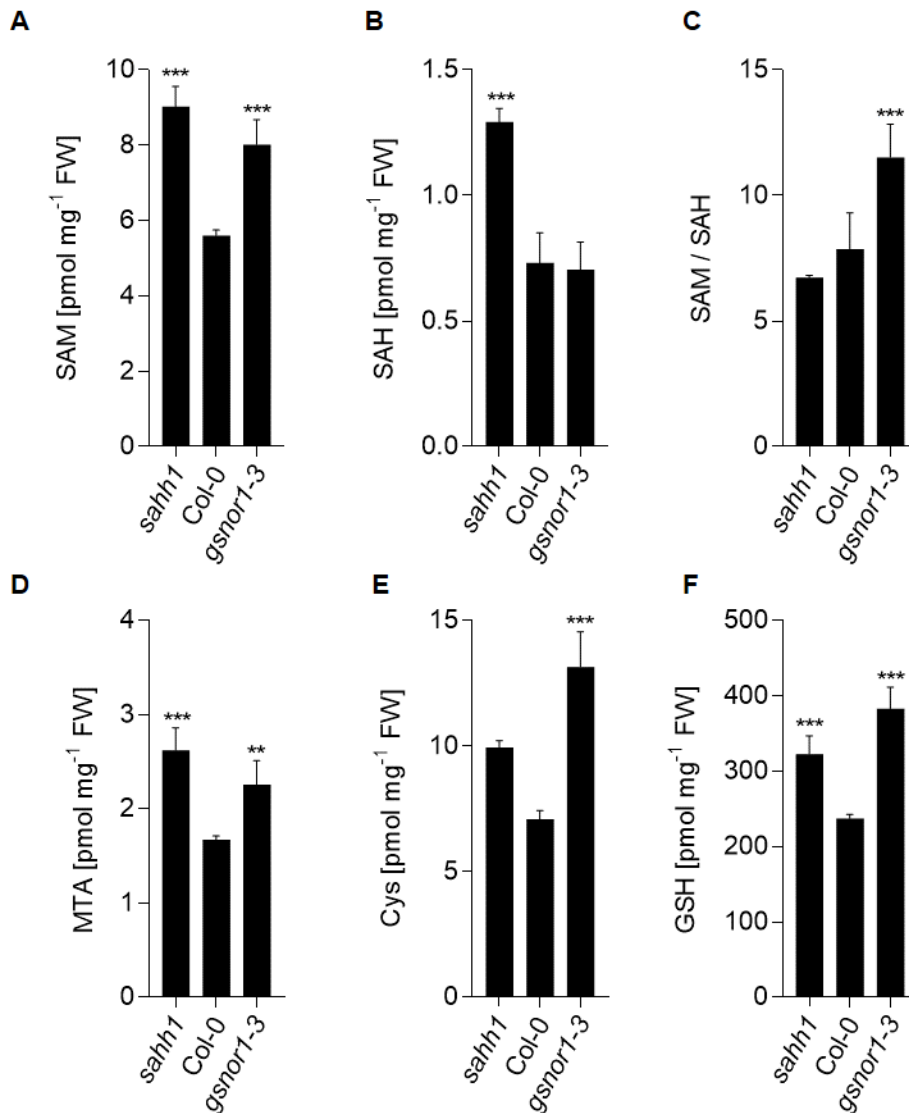
Figure 17. Mutations in *AtGSNOR1* and *AtSAHH1* result in an impaired methylation cycle. Analysis of steady-state levels of **(A)** SAM, **(B)** SAH, **(C)** SAM/SAH, **(D)** and **(E, F)** selected thiols in 4-week-old rosette leaves grown under long-day condition harvested 5 h after day-time start (n = 5). The Hcys levels were under limit of quantification. <u>Statistics:</u> Values are normalized against total fresh weight and represent the mean ± SD. Grubb´s outlier-test (α = 0.05) was performed. ****(p<0.01)** and *****(p<0.001)** represents significant differences between wild-type and mutants (ANOVA with Dunnett´s multiple comparisons test). Targeted metabolomic analysis was performed at the Centre for Organismal Studies in Heidelberg by Dr. Markus Wirtz, Dr. Gernot Poschet, and Michael Schulz. The impairment of the methylation cycle in GSNO- and DHPA-treated seedlings is shown in Figure 11.

Worth mentioning, total metabolite levels in leaves (Figure 17; comparable to previous studies[123,124]) are lower compared to seedling (Figure 11). This is in agreement with the fact that actual levels depend on tissue type, developmental stage, and age[216]. Notably, distinct metabolic reprogramming was found in GSNO-treated seedlings compared to *Atgsnor1-3* plants. Loss of *At*GSNOR1 function resulted in an unaltered level of SAH and an increased MI in leaves (Figure 17B, C), whereas exogenously applied GSNO to seedlings resulted in an increased level of SAH and a decreased MI (Figure 11B, C). Levels of SAM, MTA, Cys, and GSH were significantly increased in both approaches (GSNO-treated seedlings Figure 11A, E, F, G; genetic approach using *Atgsnor1-3* Figure 17A, D, E, F). Inhibition of *At*SAHH with DHPA or *Atsahh1-kd* resulted in an increased SAH level, and concomitantly, in a decreased SAM/SAH ratio (Figure 11B, C; Figure 17B, C; Ref.[123,124,127]). Levels of SAM and GSH were accumulated in *Atsahh1* plants (Figure 17A, F), but not in DHPA-treated seedlings(A, G). Levels of MTA were enhanced in both approaches (DHPA-treated seedlings Figure 11E; genetic approach using *Atsahh1* Figure 17D).

It is generally accepted that metaboloepigenetics is an intricate interaction between metabolites and chromatin modifications. Target metabolomic analysis in wild-type, *Atsahh1,* and *Atgsnor1-3* revealed alterations in levels of SAM, SAH, MTA, cysteine, and GSH acting as precursor of substrates or cofactors in epigenetic processes. In sum, these results suggest alteration in chromatin modifications in *Atsahh1* and *Atgsnor1-3* plants.

4.3.4 Loss of *At*GSNOR1 and *At*SAHH1 function results in altered histone methylation and/or acetylation levels

4.3.4.1 Proteomic strategy to investigate combinatorial histone acetylation and methylation motifs on histone H3

To investigate the effect *Atsahh1* and *Atgsnor1-3* on histone acetylation and methylation marks in 4-week-old rosette leaves a bottom up LC-MS/MS approach was used as previously described[192]. Briefly, histones were extracted from nuclei by acid extraction and separated on SDS-PAGE (Figure 18A, B). Histones were then chemically acetylated with d6-deuterated acetic anhydride. Thus all unmodified and mono-methylated lysines are converted to d3-acetylated lysines, but not di-, tri-methylated or endogenous acetylated lysine residues (D3AA method[217]). The deuterated acetyl group contains deuteron instead of hydrogen resulting in a mass shift of +3 Da allowing the distinction of endogenous from chemical acetylation. Due to the derivatization step, lysine residues are blocked and trypsin only cleaves C-terminal to arginine residues. As a result, peptides of an intermediate size required for bottom-up analysis of PTM motifs are generated containing the following residues: T3-R8, K9-R17, K18-R26, and K27-R40 (Figure 18C).

Noteworthy, this method was established for investigation of acetylation and methylation motifs on histone H3.1 and H4 in *Drosophila*[192]. Due to conservation in the amino acid sequence of Histone H3 (Figure 18C), this LC-MS/MS approach was applied to investigate histone methylation and acetylation

marks on histone H3 in *Arabidopsis*. However, the sequence of *At*H3.1/*Dm*3.1 differ from *At*H3.3 at amino acid 31 (Figure 18C), and hence, only fragment K27-R40 of the *At*H3.1 was analyzed. Summarized, K4, K9, K14, K18, and K23 methylation and acetylation marks on *At*H3.1 and *At*H3.3 as well as K27, K36, and K37 methylation and acetylation marks on *At*H3.1 were quantified in this study using a bottom-up LC-MS/MS approach.
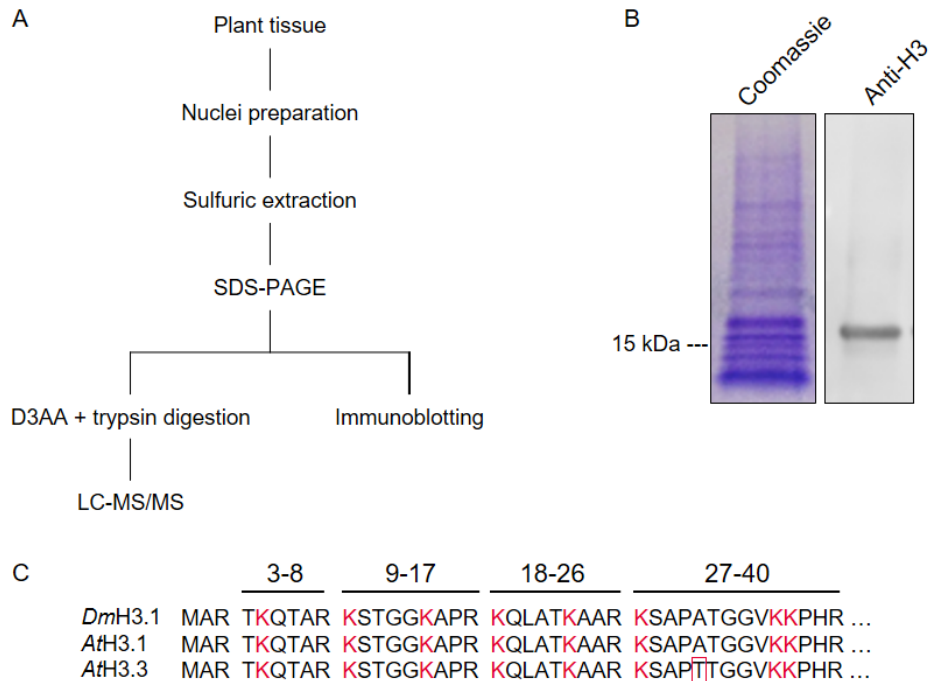
Figure 18. LC-MS/MS quantification of histone H3 methylation and acetylation marks. (A) Flowchart of the LC-MS workflow. **(B)** 12% SDS-PAGE analysis of histones from *A. thaliana* leaves extracted with sulfuric acid from nuclei. The western blot was probed with primary anti-H3 and labeled with anti-rabbit IgG conjugated to HRP and Western Lightning® Plus-ECL substrate. **(C)** Amino acid sequence alignment of the N-termini of histone H3 variants of *Drosophila melanogaster* (*Dm*) and of *A. thaliana* (*At*). The protein abbreviation and UniProt identification number are as follows: *Dm*H3.1 (P02299), *At*H3.1 (P59226), *At*H3.3 (P59169). The multiple sequence alignment was performed using ClustalW[218] in BioEdit Software[219]. Lysine (K) residues are highlighted in red. The sequence of *At*H3.1/*Dm*3.1 differ from *At*H3.3 at aa31 (boxed). Peptides resulting from tryptic digest are indicated: T3-R8, K9-R17, K18-R26, and K27-R4. Note methionine is not counted.

4.3.4.2 Alteration of the SAM/SAH ratio results in impaired histone marks

Quantitative analysis of the histone methylation and acetylation pattern of histone H3 of revealed that the H3K9me2 level significantly increased by 23% and significantly decreased by 34% in *Atgsnor1-3* and *Atsahh1*, respectively, relative to wild-type (Table 3). In addition, the H3.1K27me2 mark was significantly increased in *Atgsnor1-3* plants by 23%. Concerning acetylation marks, only a significantly increased H3K18ac level was observed in *Atsahh1*. Further, the altered H3K9me2 levels were confirmed by immunoblotting using an anti-H3K9me2 antibody. Immunoblotting revealed that the H3K9me2 level was significantly increased by 40% in *Atgsnor1-3* and significantly decreased by 54% in *Atsahh1* (Figure 19). Accordingly, decreased H3K9me2 methylation was demonstrated in the *Athog1-7*

(*Atsahh1* in Zürich background), as shown in Supplemental Figure 10. In summary, *Atsahh1* and *Atgsnor1-3* plants are hypo- and hyper-methylated at H3K9me2, respectively.

Table 3. Histone H3K9me2 methylation level is altered in *Atgsnor1-3* and *Atsahh1*. Abundance of histone methylation and acetylation marks on histone H3 in 4-week-old *Arabidopsis* plants as determined by LC-MS/MS. Abundance for 31 PTMs involving lysine acetylation and methylation marks on histone H3 in 4-week-old rosette leaves grown under long-day condition harvested 5 h after day-time start from wild-type, *Atsahh1*, and *Atgsnor1-3* plants are listed. <u>Statistics:</u> Values are relative abundance of each histone motif at each peptide and represent the mean ± SD (n=3). *(p<0.05), **(p<0.01), and ***(p<0.001) represents significant differences between wild-type and mutant lines (ANOVA, Dunnett´s multiple comparisons test). For calculation of motif abundance refer to Feller et. al. (Ref.[192]). The motif identifier name contains, PTM type and position. H3.K4me1: Abundance of mono-methylation on K4 relative to H3.K4me2, H3.K4me3, and H3.K4noPTM. Kac, lysine acetylation; Kme1, lysine mono-methylation; Kme2, lysine di-methylation; Kme3, lysine tri-methylation; noPTM, peptide without PTM. LC-MS/MS was performed at the Protein Analysis Unit of the Ludwig-Maximilians-University of Munich, in cooperation with Dr. Ignasi Forné.

Motif	Sequence of peptide	Mean % abundance ± SD		
		sahh1	Col-0	*gsnor1-3*
H3.K4_noPTM	TKQTAR	42.81 ± 1.81	43.64 ± 3.12	42.70 ± 3.94
H3.K4me1	TKme1QTAR	56.71 ± 1.75	55.71 ± 2.56	56.43 ± 3.63
H3.K4me2	TKme2QTAR	0.21 ± 0.05	0.29 ± 0.24	0.40 ± 0.16
H3.K4me3	TKme3QTAR	0.27 ± 0.08	0.36 ± 0.3	0.47 ± 0.19
H3.K9_K14_noPTM	KSTGGKAPR	42.62 ± 0.65 **	39.68 ± 0.26	37.09 ± 0.78 **
H3.K9ac	KacSTGGKAPR	1.97 ± 0.31	1.55 ± 0.18	1.58 ± 0.10
H3.K14ac	KSTGGKacAPR	27.07 ± 0.79	27.02 ± 0.19	27.46 ± 0.56
H3.K9ac_K14ac	KacSTGGKacAPR	3.02 ± 0.12	3.13 ± 0.13	2.85 ± 0.20
H3.K9me1_K14ac	Kme1STGGKacAPR	1.17 ± 0.06	1.13 ± 0.08	1.24 ± 0.14
H3.K9me2_K14ac	Kme2STGGKacAPR	0.16 ± 0.03	0.16 ± 0.06	0.22 ± 0.06
H3.K9me3_K14ac	Kme3STGGKacAPR	0.02 ± 0.00	0.03 ± 0.02	0.03 ± 0.01
H3.K9me1	Kme1STGGKAPR	20.01 ± 0.34	21.31 ± 0.61	22.14 ± 0.50
H3.K9me2	Kme2STGGKAPR	3.88 ± 0.09 ***	5.83 ± 0.38	7.17 ± 0.41 **
H3.K9me3	Kme3STGGKAPR	0.10 ± 0.02	0.17 ± 0.03	0.22 ± 0.02
H3.K18_K23_noPTM	KQLATKAAR	60.62 ± 0.93 *	62.46 ± 0.11	62.72 ± 0.83
H3.K18ac	KacQLATKAAR	24.33 ± 0.30 **	22.82 ± 0.25	22.17 ± 0.57
H3.K23ac	KQLATKacAAR	6.90 ± 0.35	6.82 ± 0.08	7.14 ± 0.22
H3.K18ac_K23ac	KacQLATKacAAR	8.15 ± 0.40	7.90 ± 0.09	7.97 ± 0.25
H3.1.K27_K36_K37_noPTM	KSAPATGGVKKPHR	10.19 ± 1.33	9.55 ± 1.09	9.22 ± 0.83
H3.1.K27ac	KacSAPATGGVKKPHR	0.18 ± 0.01	0.17 ± 0.02	0.17 ± 0.01
H3.1.K36ac	KSAPATGGVKacKPHR	0.15 ± 0.01	0.14 ± 0.01	0.13 ± 0.01
H3.1.K27ac_K36me2	KacSAPATGGVKme2KPHR	0.08 ± 0.01	0.07 ± 0.01	0.09 ± 0.03
H3.1.K27ac_K36me3	KacSAPATGGVKme3KPHR	0.78 ± 0.14	0.76 ± 0.09	0.63 ± 0.03
H3.1.K27me2_K36ac	Kme2SAPATGGVKacKPHR	0.16 ± 0.02	0.16 ± 0.02	0.14 ± 0.02
H3.1.K27me3_K36ac	Kme3SAPATGGVKacKPHR	0.08 ± 0.04	0.07 ± 0.01	0.08 ± 0.04
H3.1.K27me1	Kme1SAPATGGVKKPHR	49.45 ± 3.87	49.40 ± 3.38	43.24 ± 0.26
H3.1.K27me2	Kme2SAPATGGVKKPHR	18.68 ± 1.87	19.48 ± 1.46	24.08 ± 0.77 *
H3.1.K27me3	Kme3SAPATGGVKKPHR	6.53 ± 1.63	6.68 ± 1.28	7.74 ± 0.24
H3.1.K36me1	KSAPATGGVKme1KPHR	2.27 ± 0.36	2.32 ± 0.29	2.85 ± 0.78
H3.1.K36me2	KSAPATGGVKme2KPHR	1.49 ± 0.05	1.41 ± 0.08	1.63 ± 0.26
H3.1.K36me3	KSAPATGGVKme3KPHR	9.97 ± 1.76	9.78 ± 1.43	10.22 ± 0.59
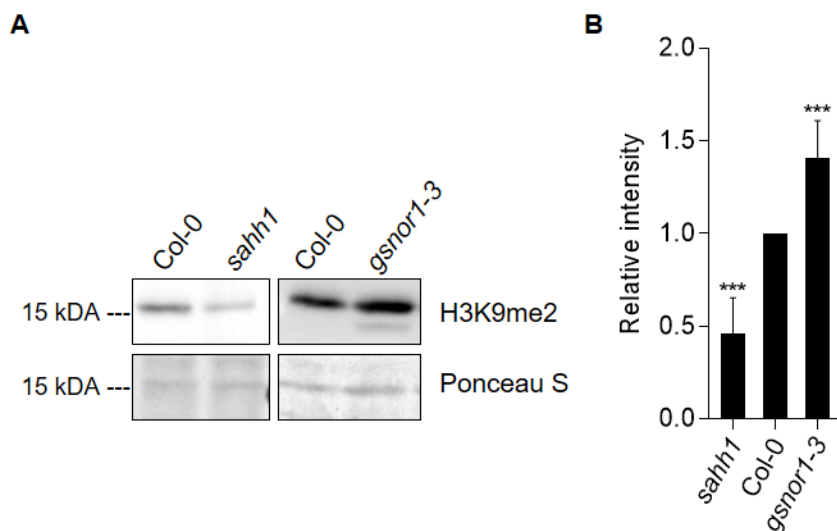
Figure 19. Histone H3K9me2 methylation level is altered in *Atgsnor1-3* and *Atsahh1*. (A) <u>H3K9me2 immunoblot.</u> Histones were acid-extracted from 4-week-old rosette leaves grown under long-day condition harvested 5 h after day-time start and probed against H3K9me2 marks by western blotting. As loading control, the Ponceau S stained membrane is shown. One representative experiment is shown. **(B)** <u>Quantification of western blot results.</u> Signal intensities were measured using ImageJ software and normalized to the amount of loaded H3. <u>Statistics:</u> Values are expressed as fold change over wild-type and represent the mean ± SD of at least three independent experiments (n = 4-7). Grubb´s outlier-test (α = 0.05) was performed. ***(p<0.001) represents significant differences between wild-type and mutant lines (ANOVA, Dunnett´s multiple comparisons test).

4.3.5 Loss of *At*SAHH1 and *At*GSNOR1 function results in impaired DNA methylation pattern

As H3K9me2 is functionally liked to DNA methylation[58,91,108], the question arose if an altered global H3K9me2 level might be associated with changes in DNA methylation levels in *Atsahh1* and *Atgsnor1-3* plants. Hence, DNA methylation was investigated by using chop-PCR (methylation-sensitive enzyme digestion followed by PCR) and WGBS. Since TGS is generally concomitant with high levels of DNA methylation and inactive chromatin marks such as H3K9me2, the function of *At*SAHH1 and *At*GSNOR1 in epigenetically regulated transcription was investigated. Therefore, both lines were crossed with *A. thaliana* Col-0 *TS-GUS* (L5, 6b5) line carrying a single insertion of a highly GUS transgene suppressed by TGS[171].

4.3.5.1 Knock-down of *At*SAHH1 causes reactivation of *TS-GUS*

TGS associated with DNA methylation and heterochromatic marks can be released by different means, including specific inhibitors or loss of function of epigenetic regulators[120]. The *A. thaliana* Col-0 *TS-GUS* (L5, 6b5) line possesses a transcriptionally silent highly repetitive GUS transgene on chromosome III (Figure 20A)[171]. The *TS-GUS* transgene was previously reactivated in the background of various epigenetic mutations, including *Athog1-7* (allele of *sahh1* in Zürich background)[120,220]. To investigate whether the *TS-GUS* transgene is reactivated in the *Atsahh1* and *Atgsnor1-3* background, the *TS-GUS* (L5) line was crossed with *Atsahh1* and *Atgsnor1-3* mutant lines, respectively. Homogeneity for *TS-GUS* locus and the T-DNA insertion in *AtSAHH1* and *AtGSNOR1* were verified (Figure 20B).
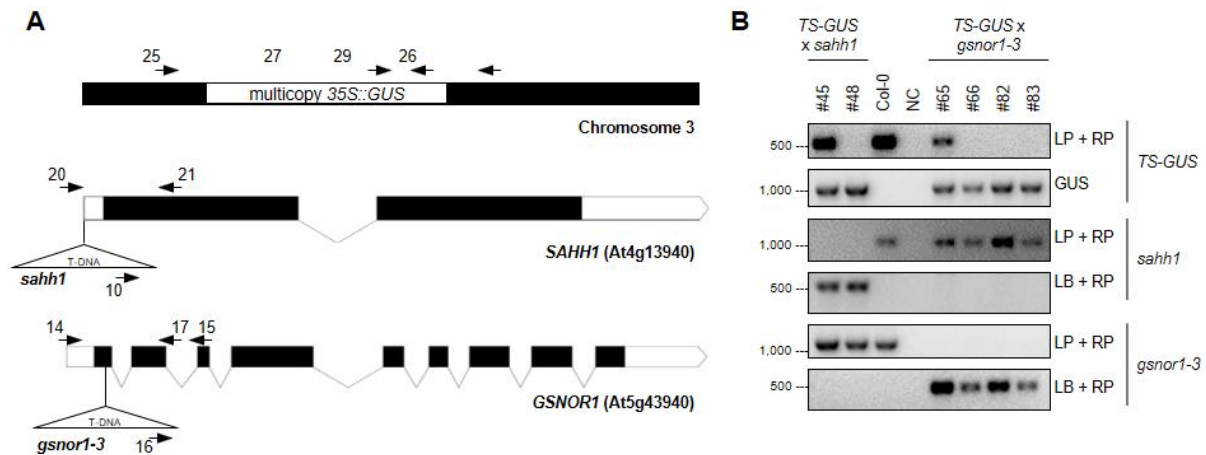
Figure 20. PCR-based genotyping of transgenic lines harboring *TS-GUS* insertion and *Atsahh1* or *Atgsnor1-3* mutation. **(A)** The diagram illustrates the positions of the single insert of a multicopy *35S::GUS* transgene[171]. Black box, Chromosome 3; white box, *GUS* locus. Below the position of the T-DNA insertion sites for *Atsahh1* and *Atgsnor1-3* are shown. Black box, coding region; open box, untranslated region; solid black line, intron. The T-DNA insertion of the mutant line *Atsahh1*[124] are located in the 5´UTR. The position of the T-DNA insertion in *Atgsnor1-3*[45,46] is located in the first exon. **(B)** PCR-based genotyping resulted in homogeneity for *TS-GUS* x *Atsahh1* and *TS-GUS* x *Atgsnor1-3* for #48, and #66, #82, #83, respectively. Amplicon length, primers, and PCR conditions are listed in Supplemental Table 4. DNA ladder (bps) is indicated. Abbreviation: *TS-GUS*, multicopy *35S::GUS* insertion; LP/RP, left/right border genomic primer; LB T-DNA border primer.

Reactivation of TS-GUS was examined in 10-day-old seedlings (Figure 21). As control, seedlings were grown in the presence of DHPA, a SAHH specific inhibitor previously demonstrated to reactivate *TS-GUS*[120]. DHPA induced reactivation of the GUS transgene, verifying the presence and availability to reactivate the L5 insert in each mutant background. However, resilencing of the GUS transgene in the absence of DHPA was only observed in *Atsahh1* background and not in the *Atgsnor1-3* background. Taken together, these results indicate that *Atsahh1* is TGS deficient presumably due to hypomethylation at the repetitive *35S::GUS* insert.
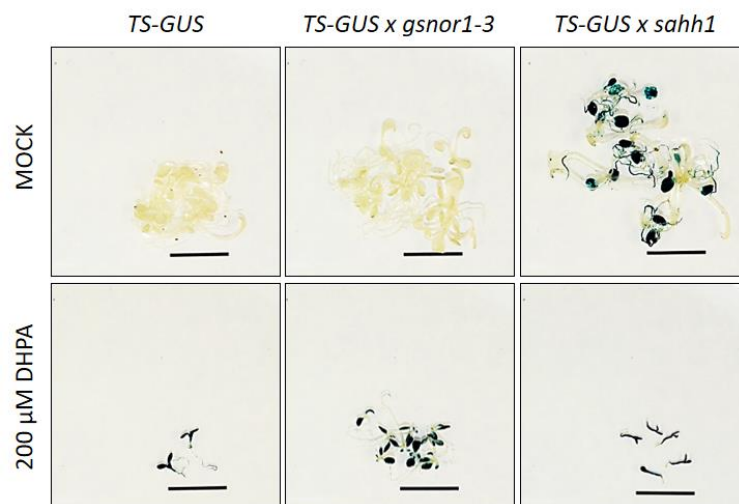
Figure 21. Knock-down of *At*SAHH1 results in reactivation of *TS-GUS*. Blue staining indicates release of gene silencing. Plantlets were grown in liquid 1x MS under short day conditions. As control, seedlings were grown in the presence of 200 μM DHPA. Hence, reduced growth is observed as previously demonstrated[120]. In the *Atsahh1* background GUS reactivation is observed and in the *Atgsnor1-3* background not. Treatments with the SAHH inhibitor DHPA releases TS-GUS silencing in all mutant backgrounds. Scale bar = 1 cm.

4.3.5.2 Transposons are differentially methylated in *Atsahh1* as analyzed by chop-PCR

DNA methylation levels in wild-type, *Atsahh1*, and *Atgsnor1-3* plants were examined with locus-specific DNA methylation analysis by chop-PCR using the methylation-dependent restriction enzyme McrBC[181]. McrBC is an endonuclease, which cleaves DNA containing 5-methylcytosines on one or both DNA strands, but not unmethylated DNA. Hence, higher levels of methylation results in increased McrBC digestion and consequently reduced amplification by PCR[221]. To assess DNA methylation, four class I retrotransposons (*AtCOPIA4*, *AtGP1*, *AtTA2*, *AtLine1-4, AtSN1*), one class II DNA transposon (*AtMu1*) and the transcriptionally silent information (*AtTSI*) repeats were selected. Those transposable elements and *AtTSI* are annotated in the pericentromeric regions of chromosomes, except *AtSN1*, which is located outside the chromocenters within euchromatin environment[222].
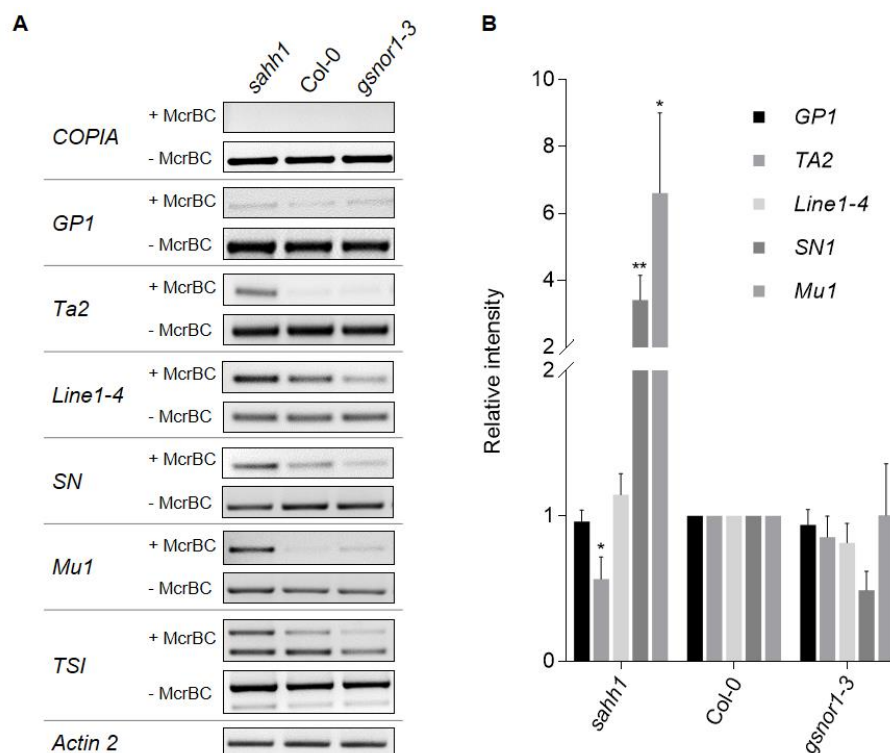
Figure 22. DNA methylation is altered in *Atsahh1* but not in *Atgsnor1-3* as analyzed by chop-PCR. DNA methylation analysis by McrBC PCR in 4-week-old *Arabidopsis* plants. **(A)** <u>DNA methylation level</u> of indicated loci were determined by chop-PCR in 4-week-old rosette leaves grown under long-day condition harvested 5 h after day-time start from wild-type, *Atsahh1*, and *Atgsnor1-3.* Genomic DNAs were digested by McrBC followed by PCR and agarose gel electrophoreses. McrBC specifically cleaves methylated DNA sequences. Representative gel analysis of PCR products of McrBC digested and undigested DNA is shown. Length of the amplicons is given in Supplemental Table 5. **(B)** <u>Quantification of McrBC-PCR results.</u> Signal intensities were measured using Image J software and normalized to Actin 2 (undigested DNA). <u>Statistics:</u> Values are expressed as fold change over wild-type and represent the mean ± SEM of at least three independent experiments (n = 5-7). Normally distributed data and data with equal variance were subjected to ANOVA, Dunnett´s multiple comparisons test. Non-normally distributed data and/or heteroskedastic data were subjected to Kruskal-Wallis test, Dunn´s multiple comparison test. Grubb´s outlier-test (α = 0.05) was performed. *($p<0.05$) and **($p<0.01$) represents significant differences between wild-type and mutant lines at each locus. *AtCopia4, AtGP1, AtTa2*, and *AtLine1-4* are retrotransposons; *AtMu1* is a DNA transposon; *AtSN1*, short interspersed retroelement 1; *AtTSI*, transcriptionally silent information. Note that the amplification of *AtTSI in* Col-0 wild-type results in two products of 598 bps (*AtTSI*) and 318 bps (AT3G32980) according to BLASTN, compared to Zürich wild-type (Supplemental Figure 11B). Hence, quantification of TSI amplification is not shown.

As shown in Figure 22 the lack of any PCR amplicon after McrBC digestion indicates that the retrotransposon *AtCopia4* is highly methylated in all analyzed genotypes. Concerning *AtGP1* and *AtLine1-4*, no obvious changes of DNA methylation in *Atsahh1* compared to wild-type were detected. However, methylation levels at *AtTA2*, *AtSN1*, and *AtMu1* are significantly decreased in the *Atsahh1* mutant. Accordingly, *AtMu1* hypomethylation was previously demonstrated in the *sah1L459F* mutant (allele of *Atsahh1* in the background of accession Wassilewskija; Ref.[223]). In contrast to the *Athog1-7* mutant (allele of *sahh1* Zürich background; Supplemental Figure 11A) reduced DNA methylation at *AtLine1-4* was not observed in the *Atsahh1* mutant. The locus-specific DNA methylation analysis did not reveal significant differences between wild-type and *Atgsnor1-3*, although a tendency for enriched DNA methylation was observed in *Atgsnor1-3*, particularly at *AtSN1* locus. Taken together, these results suggest an hypomethylated *Atsahh1* phenotype and a weak hypermethylated *Atgsnor1-3* phenotype. Based on these results, genome wide DNA methylation analysis in *Atsahh1* and *Atgsnor1-3* was performed using WGBS.

4.3.5.3   Genome wide DNA methylation status is altered in *Atgsnor1-3* and *Atsahh1*

WGBS was performed to study the genome wide DNA methylation at single-nucleotide resolution in Col-0, *Atgsnor1-3*, and *Atsahh1* plants. Chemical treatment of genomic DNA with sodium bisulfite converted unmethylated cytosines into uracils, whereas methylcytosines remained unmodified. In a subsequent PCR, uracils were read as thymines, and hence, unmethylated cytosines appear as thymines in the resulting amplicons[224]. Taken together, observed cytosines in sequencing reads indicates that the cytosines were methylated. After sequencing, the obtained sequencing reads were mapped against the TAIR10 reference genome to enable the identification of the methylated loci in each sample. To assess bisulfite conversion efficiency, reads were mapped to the non-methylated chloroplast genome resulting in an average conversion rate of more than 98%. The DNA methylation levels as percent cytosines methylated in mCG, mCHG, or mCHH context (H = A, C, or T) are listed in Table 4. These data are in accordance with average methylation levels of 24% CG, 7% CHG, and 2% CHH found in *Arabidopsis*[225].

Table 4. Global cytosine methylation levels as analyzed by WGBS. Average genome wide DNA methylation given as percentage methylated cytosines in CG, CHG, or CHH context (H = A, C, or T) in Col-0, *Atsahh1*, and *Atgsnor1-3* as analyzed by WGBS.

	CG	CHG	CHH
Col-0	22.75%	6.35%	1.65%
Atgsnor1-3	19.8%	5.95%	1.55%
Atsahh1	20.2%	3.4%	1.05%

Regarding DNA methylation levels as percent cytosines methylated in *Atgsnor1-3*, the strongest effect was observed in CG context, which lost 13% DNA methylation relative to wild-type, followed by 6%

decrease in both CHG and CHH context (Table 4). However, chromosomal distribution of DNA methylation shows that DNA methylation in *Atgsnor1-3* was particulately increased most pronounced in CHG context over the highly methylated TE-rich pericentromeric regions (Figure 23). Metaplot analyses of average DNA methylation over all protein coding genes (PCGs) and TEs indicated that CG methylation and particulately CHG methylation is lost over TEs in *Atgsnor1-3* (Figure 24A).
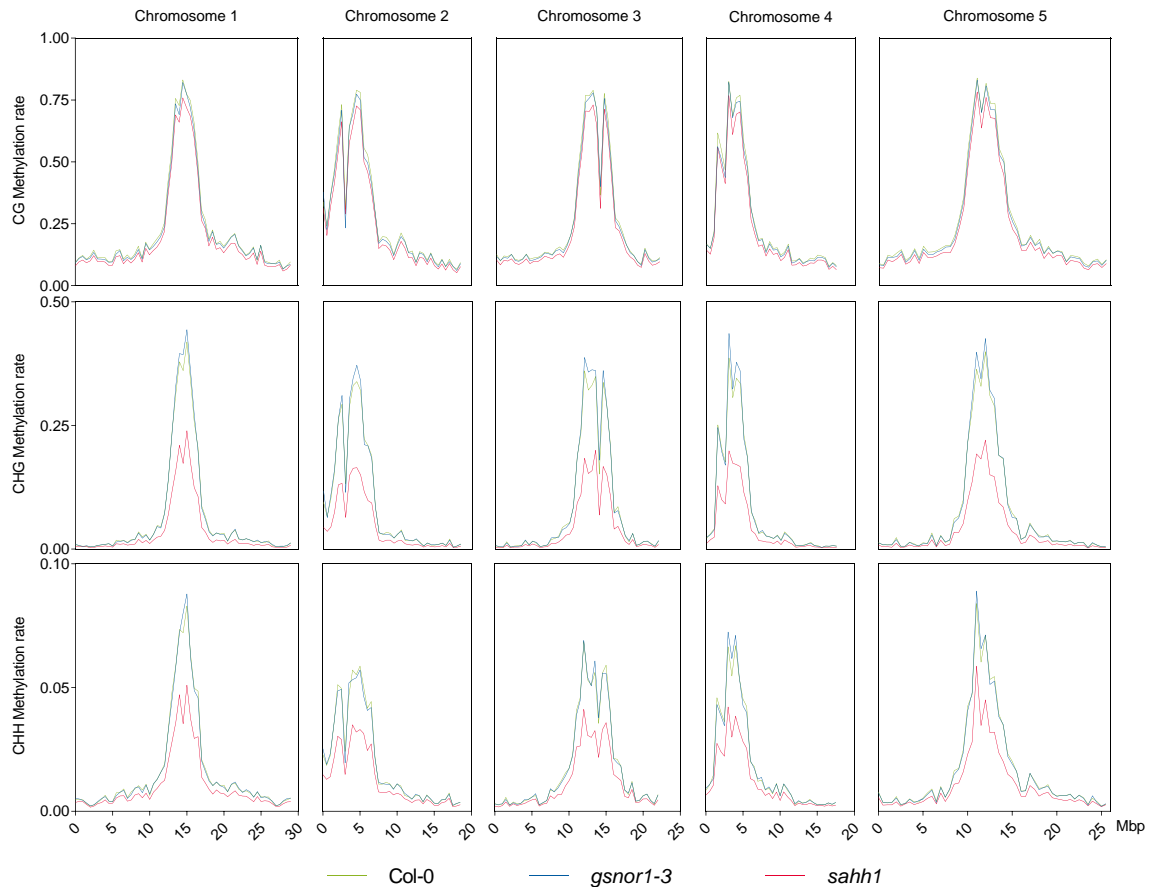
Figure 23. Chromosomal distribution of DNA methylation is altered in *Atgsnor1-3* and *Atsahh1*. The methylation levels across the chromosomes in each sequence context were calculated with MethGeno (Huang et al., 2018b) for each replicate by Dr. Elisabeth Georgii (Institute of Biochemical Plant Pathology Munich). Then replicates were merged and graphs were made with GraphPad Prism. Average methylation of all cytosines within an 0.5 Mbp interval was plotted.

In case of DNA methylation levels as percent cytosines methylated in *Atsahh1*, the strongest effect was observed in the CHG context, which lost 46% DNA methylation relative to wild-type, followed by CHH and CG with 36% and 11% decreases, respectively (Table 4). Accordingly, chromosomal distribution of DNA methylation plots show decreased DNA methylation in each sequence context, particularly in CHG and CHH context over the highly methylated TE-rich pericentromeric regions (Figure 23). Likewise, the methylome over all PCGs and over all TEs CG was decreased in *Atsahh1*, as illustrated in metaplots (Figure 24B). In addition, TEs lost CHG and CHH methylation and reduced CHG methylation was observed 3kb up- and 3kb down-stream of PCGs in *Atsahh1*. Taken together, DNA methylation over all PCGs and especially over all TEs in both mutants is changed compared to wild-type.

54
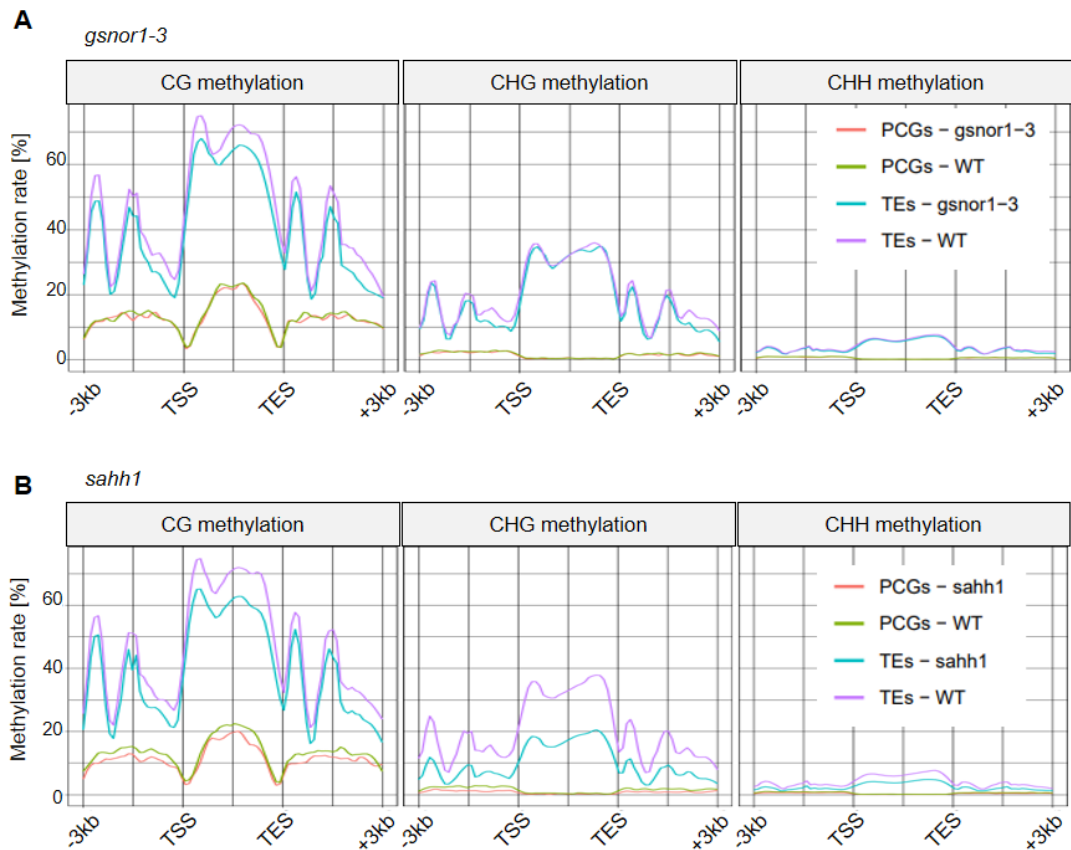
Figure 24. Global DNA methylation pattern over all PCGs and TEs are changed in *Atgsnor1-3* and *Atsahh1*. Average levels of CG, CHG, and CHH methylation along all protein coding genes (PCGs) and TEs in *Atgsnor1-3* **(A)** and *Atsahh1* **(B)**. PCGS and TEs were aligned and average methylation levels for all cytosines are plotted from 3kb up- to 3kb down-stream. <u>Abbreviations:</u> TSS, transcriptional start site; TES, transcriptional end site. Metaplot analysis was performed by Patrick Hüther (Becker Lab, Gregor Mendel Institute Vienna).

4.3.5.4   Identification of DMRs in *Atgsnor1-3* and *Atsahh1*

To further investigate a potential effect of *Atgsnor-ko* and *Atsahh1-kd* on the DNA methylome, methylated regions (MRs) and differentially methylated regions (DMRs) were identified by the adaption of a two-state Hidden-Markov-Model based approach[187]. MR calling identified 39,790 and 44,442 MRs in *Atgsnor1-3* and *Atsahh1*, respectively. In pairwise comparison (mutant versus wild-type) DMRs with a minimum methylation difference of 20% were identified. In detail, 752 and 292 DMRs were identified for *Atsahh1* and *Atgsnor1-3* mutant lines, respectively. In *Atsahh1* a DNA methylation status of 35 hypermethylated and 717 hypomethylated DMRs was identified. In case of *Atgsnor1-3*, 61 DMRs were classified as hypomethylated and 231 DMRs as hypermethylated. Accordingly, heatmaps of hierarchically clustered DMRs illustrate that DNA methylation was decreased in *Atsahh1* and increased in *Atgsnor1-3* compared to wild-type (Figure 25).

Further, heatmaps of hierarchically clustered CG, CHG, and CHH DMRs illustrates that DNA methylation was decreased in *Atsahh1* compared to wild-type plants in each sequence context (Supplemental Figure 12). In case of *Atgsnor1-3* mutant line, DNA methylation levels on identified DMRs were increased compared to wild-type mainly in CG and CHG context (Supplemental Figure 13). In addition,

55

hierarchical clustering as depicted in heatmaps demonstrates that biological replicates (for each genotyped analyzed and each sequence context) clustered together indicating reproducibility. In summary, DNA methylation analysis in terms of DMRs revealed hypo- and hyper-methylation in *Atsahh1* and *Atgsnor1-3*, respectively.
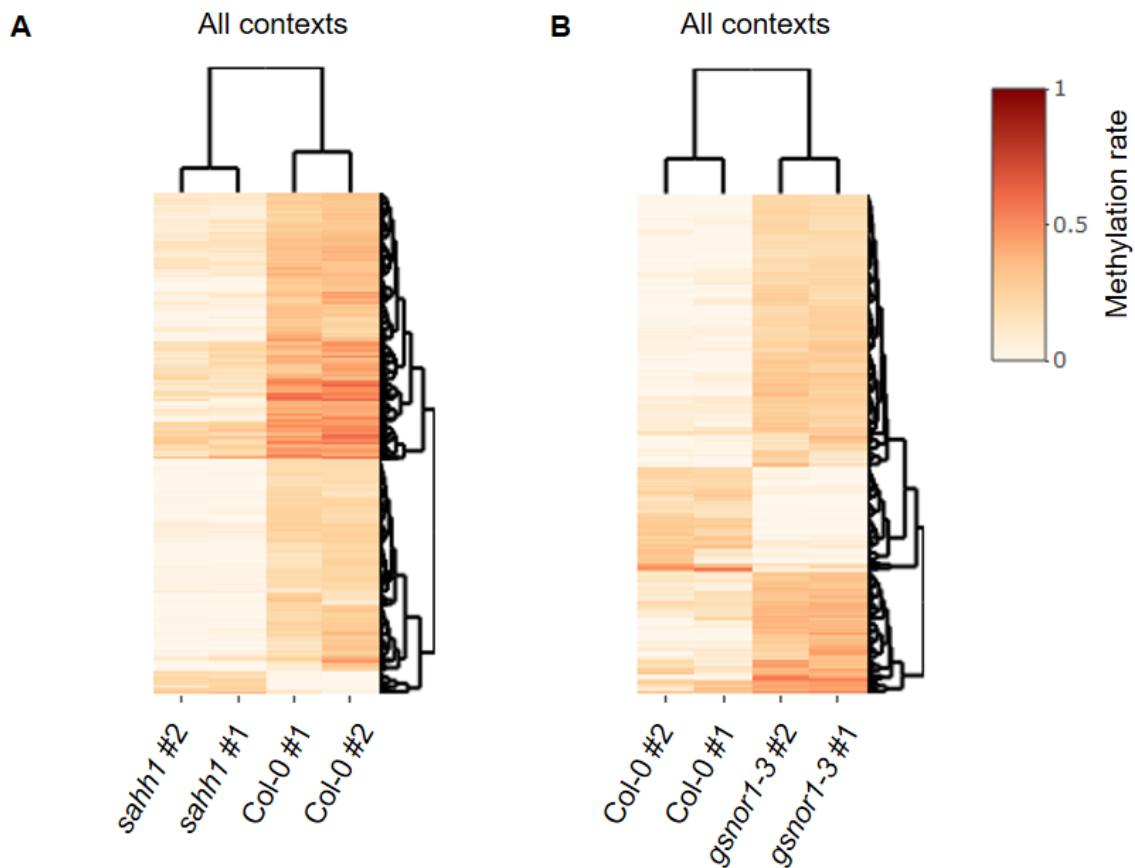
Figure 25. WGBS analysis revealed enrichment of hypo- and hyper-DMRs in *Atsahh1* and *Atgsnor1-3*, respectively. Heatmaps showing the methylation rates in all sequence contexts for pairwise comparison of *Atsahh1* versus wild-type **(A)** and *Atgsnor1-3* versus wild-type **(B)**. DNA was extracted from 4-week-old rosette leaves grown under long-day condition harvested 5 h after day-time start and subjected to WGBS. Heatmaps represent the methylation level across DMRs: Red = 100% methylated, white = 0% methylated. Two biological replicates were analyzed for each genotype. R was used for imaging.

4.3.5.5 Annotation of identified DMRs to annotated genomic elements

Next, assignment of MRs and DMRs to annotated genomic elements was performed (Supplemental Figure 14). Genomic feature annotation showed that MRs and DMRs are mainly mapped to the genic, 3kb up- or 3kb down-stream flanking regions of genes (hereafter differentially methylated genes DMGs), and TEs. Loss of *At*GSNOR1 results in an enrichment of hypermethylated DMGs and TEs (Figure 26A). In detail, 587 DMGs were identified in *Atgsnor1-3.* Among those identified DMGs, 449 are hyper- and 138 are hypo-methylated. DMGs possessing DMRs in multiple genomic elements were identified as illustrated in the Venn diagram (Figure 26B). For instance, AT5G46295 encoding a transmembrane protein is hypermethylated in its 3kb upstream flanking and genic region (Figure 26C). Loss of

*At*GSNOR1 function resulted in an enrichment of hypermethylated TEs (Figure 26D). In detail, 55 and 12 TEs with hyper- and hypo-methylated DMRs were identified, respectively. TEs classified as retrotransposons in the superfamily LTR/Gypsy and LINE/L1, as well TEs classified as DNA transposon belonging to the superfamily MuDR and RC/Helitron were mainly hypermethylated in *Atgsnor1-3* (Figure 26D). A snapshot in the EPIC-CoGE browser of a representative hypermethylated TE (AT3TE65465, LTR/Gypsy) is shown in Figure 26E.
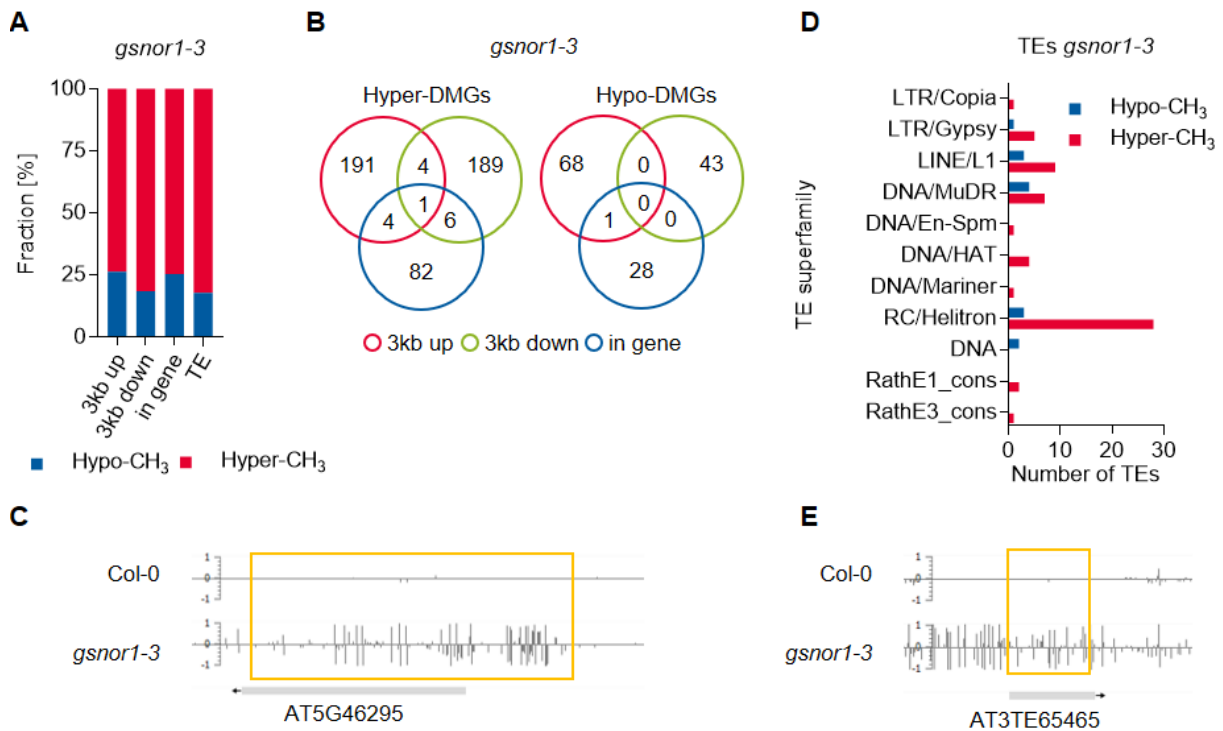
Figure 26. Loss of *At*GSNOR1 function results in an enrichment of hypermethylated DMGs and TEs. (A) Stacked bar blot showing the fraction of hyper- and hypo-DMGs and TEs with respected to DMRs found in their genic, 3kb up- or 3kb-downstream region or TE coding region. **(B)** Venn diagram summarizing DMGs with DMRs in multiple genomic features (genic, 3kb up and/or 3kb down-stream flanking regions). **(C)** Snapshot of AT5G46295 in the EPIC-CoGE browser. **(D)** Distribution of differentially methylated TEs over TE superfamilies. **(E)** Snapshot of AT3TE65465 in the EPIC-CoGE browser. DNA methylation data have been uploaded to the epigenome browser of EPIC (EPIC-CoGE) by Prof. Dr. Claude Becker (ID 2234 unpublished). DNA methylation analysis were performed in duplicates and average methylation ratios calculated in the CoGE browser are shown. TE classification according to www.arabidopsis.org.

Atsahh1-ko results mainly in an enrichment of hypomethylated DMGs and TEs (Figure 27A). In *Atsahh1* plants, 1299 DMGs were identified. Among those, 72 are hypermethylated and 1227 are hypomethylated. Of note, three of those DMGs in *Atsahh1* possess hyper- and hypo-DMRs. (AT1g65220, AT3g54730, AT4g13440). As illustrate in Venn diagrams, DMGs with DMRs in multiple genomic elements were identified (Figure 27B). For instance, AT3G50250 encoding a transmembrane protein is hypermethylated in its 3kb upstream flanking and genic region (Figure 27C). TEs were mainly hypomethylated in *Atsahh1*. In detail, 3 TEs and 271 TEs with hyper- and hypo-methylated DMRs were identified, respectively. Hypomethylation was mainly found in members of the retrotransposon superfamily LTR/Copia and LINE/L1 and in members of the DNA transposon superfamily MuDR and

RC/Helitron (Figure 27D). A snapshot in the EPIC-CoGE browser of a representative hypomethylated TE (AT1TE93270, DNA/HAT) is shown in Figure 27E. Of note, loci identified as hypomethylated with McrBC-PCR in *Atsahh1* namely, *AtTa2*, *AtSN1*, and *AtMu1* (Figure 22), were not identified as differentially methylated TEs by WGBS with the chosen parameters. However, snapshots showing DNA methylation levels of those loci in the epigenome browser EPIC-CoGE show a tendency towards hypomethylation (Supplemental Figure 15).
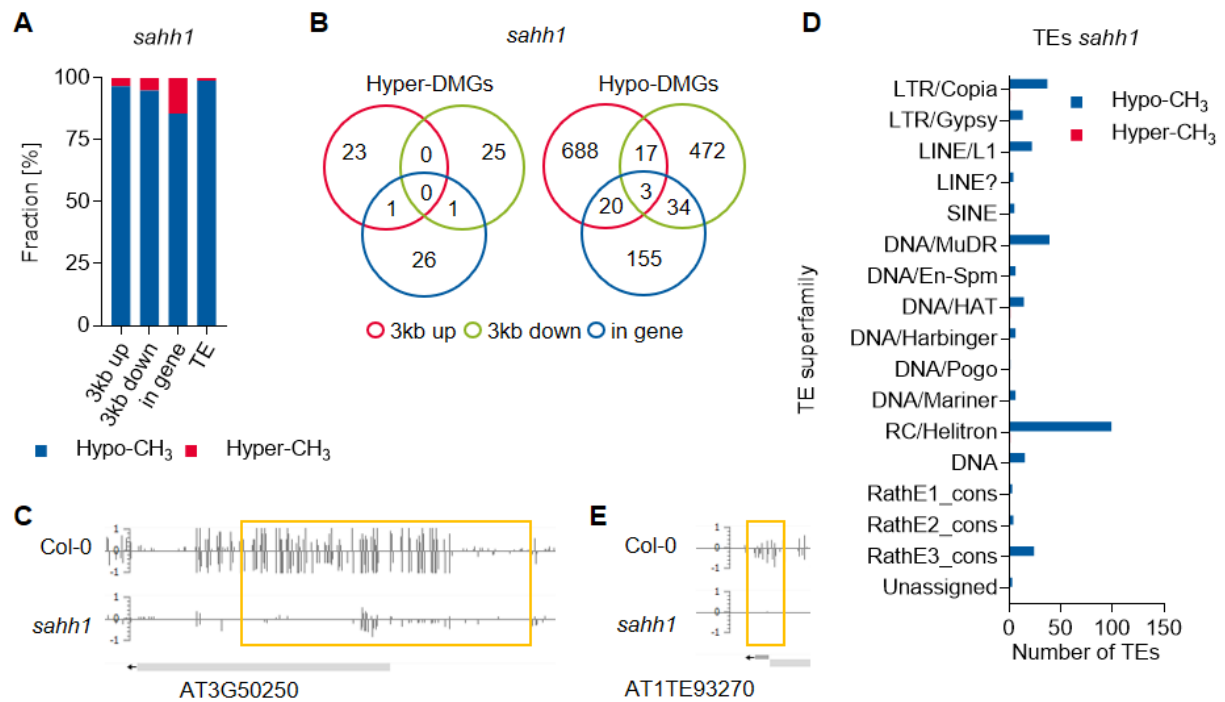
Figure 27. Knock-down of *At*SAHH1 function results in an enrichment of hypomethylated DMGs and TEs. (A) Stacked bar blot showing the fraction of hyper- and hypo-DMGs and TEs with respected to DMRs found in their genic, 3kb up- or 3kb-down-stream region or TE coding region. **(B)** Venn diagram summarizing DMGs with DMRs in multiple genomic features (genic, 3kb up and/or 3kb down-stream flanking regions). **(C)** Snapshot of AT3G50250 in the EPIC-CoGE browser. **(D)** Distribution of differentially methylated TEs over TE superfamilies. **(E)** Snapshot of AT1TE93270 in the EPIC-CoGE browser. DNA methylation data have been uploaded to the epigenome browser of EPIC (EPIC-CoGE) by Prof. Dr. Claude Becker (ID 2234 unpublished). DNA methylation analysis were performed in duplicates and average methylation ratios calculated in the CoGE browser are shown. TE classification according to www.arabidopsis.org.

Gene ontology enrichment analysis of DMGs identified in *Atgsnor1-3* and *Atsahh1* did not result in significantly enriched terms. In regard of the pre-induced antioxidant system under normal growth conditions in *Atgsnor* (Ws background)[42], it is noteworthily that genes encoding peroxidases, thioredoxins, and glutathione-S transferases were identified as DMGs (Table 5). Moreover, genes related to DNA and histone methylation and metaboloepigenetic processes interacting with DNA and histone methylation were identified (Table 5). Interestingly, two genes encoding components of the canonical RdDM pathway[58,107], namely *AtAGO4* and *AtDMS3* were identified as hyper-DMGs in *Atgsnor1-3*. Whereas, the *AtLDL3* gene encoding a histone demethylase acting on H3K4me2[96] was identified as hypo-DMG.

Table 5. List of selected DMGs identified in *Atgsnor1-3*. DMGs related to DNA and histone methylation and related to metaboloepigenetic processes interacting with DNA and histone methylation identified in *Atgsnor1-3*. Query list is given in Chapter 7.3. The methylation status in *Atgsnor1-3* compared to wild-type is given as (-) and (+) referring to hypo- and hyper-methylation, respectively. DMRs are annotated with genomic features (3kb up- or down-stream, and in gene). For example, "3kb up" and "AT2G27040" means that the DMR overlaps with the 3kb upstream region of AT2G27040. Annotation was performed using TAIR10. <u>Abbreviations:</u> Chr, Chromosome; start, DMR start position; bp, length of overlapping DMR with genomic feature.

Chr	Start	bp	CH$_3$	Feature	Gene ID	Description
RdDM pathway						
Chr2	11544522	56	+	3kb up	AT2G27040	Protein Argonaute 4 (AGO4)
Chr3	18254606	137	+	3kb down	AT3G49250	DEFECTIVE IN MERISTEM SILENCING 3 (DMS3), INVOLVED in de novo (IDN1)
Histone demethylation						
Chr5	113792	113	+	3kb up	AT5G01270	POL II carboxy- terminal domain phosphatase CARBOXY-TERMINAL PHOSPHATASE- LIKE 2 (CPL2)
Chr4	9228874	61	-	3kb down	AT4G16310	Lysine-specific histone demethylase 1 homolog 3 (LDL3)
DNA methylation						
Chr5	4989732	205	+	3kb up	AT5G15380	Domains rearranged methylase 1 (DRM1; non-function)
Folate biosynthesis						
Chr1	22459754	86	+	3kb down	AT1G60990	Glycine decarboxylase T-protein
Chr1	22460005	91	+	3kb down	AT1G60990	Glycine decarboxylase T-protein
Ethylene biosynthesis						
Chr3	18431449	61	-	3kb down	AT3G49700	1-aminocyclopropane-1-carboxylate synthase 9 (ACS9)
TCA cycle						
Chr5	20057539	47	+	in gene	AT5G49460	ATP-citrate lyase (ACLB -2)
Antioxidant system						
Chr1	18637357	72	+	3kb down	AT1G50320	Thioredoxin X, cp
Chr1	18458119	155	-	3kb up	AT1G49860	Glutathione S-transferase F14 (GSTF14)
Chr1	29468110	61	+	in gene	AT1G78320	Glutathione S-transferase U23 (GSTFU23)
Chr2	14386660	66	+	in gene	AT2G34060	Peroxidase 19 (PER19)
Chr2	14386726	249	+	3kb down	AT2G34060	Peroxidase 19 (PER19)

In *Atsahh1*, genes involved in active DNA demethylation were identified as hypo-DMGs (Table 6), for example *AtDML3* encoding a DNA demethylase[58,114]. Another hypo-DMG encoding *At*VIM3, which is involved in maintenance of CG methylation[58,91,108], was identified in *Atsahh1*. Further, *AtSUVH4* and *AtSUVH5*, both encoding H3K9me2 methyltransferases, which are functionally linked to DNA methylation[58,91,108] are hypo-DMGs. In addition, *AtSUVR4* encoding a histone lysine methylase trimethylating H3K9 on transposon chromatin[226] possess a hypo-methylated DMR. Two genes encoding members of the KDM3/JHDM2 group are identified as hypomethylated DEGs in *Atsahh1*, namely *AtJMJ27* and *AtJMJ28*. *At*JMJ27 displays H3K9me1/2 demethylase activity[227]. Whereas *At*JMJ28 lack the conserved Fe(II) and α-KG binding amino acids within the cofactor binding site of JHDM proteins suggesting that *At*JMJ28 is inactive[228]. Further, *AtJMJ12/REF6* encoding a histone demethylase acting on H3K27me[229] is identified as hyper-DMG. The gene encoding *At*MAT4, which catalyzes synthesis of SAM and mediate DNA and histone methylation[129] is also identified as hypo-DMG in *Atsahh1*. In regard that SAM also acts as precursor for polyamines, it is noteworthily, that *SAM DECARBOXYLASE* (*SAMDC*) involved in polyamine biosynthesis[117] is hypo-methylated in *Atsahh1*.

Table 6. List of selected DMGs identified in *Atsahh1*. DMGs related to DNA and histone methylation and related to metaboloepigenetic processes interacting with DNA and histone methylation identified in *Atsahh1*. Query list is given in Chapter 7.3. The methylation status in *Atsahh1* compared to wild-type is given as (-) and (+) referring to hypo- and hyper-methylation, respectively. DMRs are annotated with genomic features (3kb up- or down-stream, and in gene). For example, "3kb down" and "AT4G34060" means that the DMR overlaps with the 3kb downstream region of AT4G34060. Annotation was performed using TAIR10. Chr, Chromosome; start, DMR start position; bp, length of overlapping DMR with genomic feature.

Chr	start	bp	CH₃	Feature	Gene ID	Description
DNA demethylation						
Chr4	16320816	124	-	3kb down	AT4G34060	DEMETER-LIKE PROTEIN 3 (DML3)
Chr4	9266255	216	-	3kb down	AT4G16440	NAR1
Canonical RdDM pathway						
Chr2	16713747	100	-	3kb up	AT2G40030	DNA-directed RNA polymerase V subunit 1 (NRPE1)
Chr3	8574593	138	-	3kb up	AT3G23780	DNA-directed RNA polymerase subunit beta (NRPD2/NRPE2)
Chr5	4508148	289	-	3kb down	AT5G13960	Histone-lysine N-methyltransferase, H3 lysine-9 specific SUVH4
Chr5	22675179	115	-	3kb down	AT5G56000	HSP90-4
CG methylation						
Chr5	15840971	394	-	3kb up	AT5G39550	VARIANT IN METHYLATION 3 (VIM3)
CHG methylation						
Chr5	4508148	289	-	3kb down	AT5G13960	Histone-lysine N-methyltransferase, H3 lysine-9 specific SUVH4
Chr2	14820902	46	-	3kb up	AT2G35160	Histone-lysine N-methyltransferase, H3 lysine-9 specific SUVH5
Histone methylation						
Chr5	4508148	289	-	3kb down	AT5G13960	Histone-lysine N-methyltransferase, H3 lysine-9 specific SUVH4
Chr2	14820902	46	-	3kb up	AT2G35160	Histone-lysine N-methyltransferase, H3 lysine-9 specific SUVH5
Chr3	1165940	160	-	3kb down	AT3G04380	Histone-lysine N-methyltransferase SUVR4
Histone demethylation						
Chr3	17938844	64	+	in gene	AT3G48430	JmjC domain-containing histone demethylase 12 (JMJ12/REF6)
Chr4	434259	249	-	3kb down	AT4G00990	JmjC domain-containing histone demethylase 27 (JMJ27)
Chr4	11414129	110	-	3kb up	AT4G21430	JmjC domain-containing histone demethylase 28 (JMJ28)
Folate biosynthesis						
Chr5	16601046	44	-	3kb down	AT5G41480	Dihydrofolate synthetase (DHFS)
Chr1	13699281	197	-	3kb up	AT1G36370	Serine hydroxymethyltransferase 7 (SHMT7; MSA1)
Chr1	13699565	94	-	3kb up	AT1G36370	Serine hydroxymethyltransferase 7 (SHMT7; MSA1)
Chr1	11737276	147	-	3kb down	AT1G32470	Glycine decarboxylase - H Protein 3 (GDH3)
Cysteine and methionine biosynthesis						
Chr5	10035685	160	-	3kb up	AT5G28030	O-acetylserine(thiol)lyase (DES1)
Methylation cycle						
Chr3	5955123	246	-	3kb up	AT3G17390	methionine S-adenosyltransferase 4 (MAT4)
Polyamine/ ethylene biosynthesis						
Chr3	9287734	37	-	in gene	AT3G25570	S-adenosyl-L-methionine decarboxylase 3 (SAMDC3)
Chr3	18431449	61	-	3kb down	AT3G49700	1-aminocyclopropane-1-carboxylate synthase 9 (ACS9)
TCA cycle						
Chr2	2148301	215	-	3kb down	AT2G05710	Aconitase 3 (ACO3)
Chr5	7829116	527	-	3kb up	AT5G23250	succinyl-CoA synthetase alpha 2 subunit (SCS-A-2)
Chr5	26037435	449	-	3kb up	AT5G65165	Succinate dehydrogenase (SDH2-3)

Further, the overlap of DMGs of *Atgsnor1-3* and *Atsahh1* was analyzed. Of note, WGBS analysis was performed in pairwise comparison (mutant vs. wild-type). 110 DMGs were identified in both mutants (Supplemental Table 9). Of note, all hyper-methylated DMGs found in *Atsahh1*, were also hyper-methylated in *Atgsnor1-3*. Because of the enhanced SAM and MTA levels (intermediates in ethylene biosynthesis) determined in both mutants (Figure 17), it is worth mentioning that genes encoding the *ETHYLENE-RESPONSIVE TRANSCRIPTION FACTOR ERF37*, the *ETHYLENE INSENSITIVE 3-LIKE 1 PROTEIN*, and *1-AMINOCYCLOPROPANE-1-CARBOXYLATE SYNTHASE-LIKE PROTEIN 9* are hypo-DMGs.

Interestingly, two Myb family transcription factor are also identified as hypo-DMRs in both mutants analyzed. In regard, that iron is an essential co-factor for DNA demethylases[113] and histone demethylases[63], it is of noteworthy that the *VACUOLAR IRON TRANSPORTER HOMOLOG 2.1* is hypomethylated in both mutants.

Analyzing the overlap of differentially methylated TEs in *Atgsnor1-3* and *Atsahh1* identified six TEs (Supplemental Table 9). For instance, AT4TE34260 (RC/Helitron superfamily) was found to be hypermethylated in both mutants, whereas both AT1TE37390 (RC/Helitron superfamily) and AT1TE61180 (DNA superfamily) were hypomethylated in each mutant analyzed.

4.3.6 Transcriptomic profiling of *Atgsnor1-3* and *Atsahh1* plants

RNA sequencing was performed to characterize the effects of *Atsahh1-kd* and *Atgsnor1-3-ko* on transcription. Three quarters of identified differentially expressed genes (DEGs; |log2FC| >1, adjusted p-value less than 0.1) were downregulated in *Atgsnor1-3* (Figure 28A). Whereas mutation in *AtSAHH1* resulted in an almost equal number of up- and down-regulated DEGs (Figure 28B). Volcano plot representations of differential expression analysis of genes in *Atgsnor1-3* and *Atsahh1* are shown (Figure 28C, D). Blue and red points mark significantly decreased or increased expressed genes, respectively.

In detail, the *Atgsnor1-3* mutation caused 1129 DEGs, among those 180 were upregulated, whereas 949 were downregulated. Out of 394 genes, which were differentially regulated, 211 genes were significantly upregulated and 183 genes were significantly downregulated in *Atsahh1*.

Expression levels of *AtGSNOR1* and *AtSAHH1* were significantly decreased in their corresponding mutants indicating the reliable quality of the RNA-seq data (Table 7). *A. thaliana* encodes two genes in the *SAHH* gene family, namely *AtSAHH1* and *AtSAHH2*. In the *Atsahh1* mutant *AtSAHH1* expression is significantly reduced, but not of *AtSAHH2*. Hence, *SAHH2* is not upregulated to compensate for the loss of *SAHH1*.

The expression levels of genes encoding proteins related to DNA and histone methylation and metaboloepigenetic processes interacting with DNA and histone methylation were analyzed (Table 7). For instance, upregulation of the molecular chaperon *AtHSP90* (*AtHSP90-2*, *AtHSP90-3*) facilitating the loading of 24-nt siRNAs onto *At*AGO4 in the RdDM pathway[230] was observed in *Atgsnor1-3*. Further, a histone arginine demethylase, namely *AtJMJ22*[231], was found to be upregulated. Also a histone arginine methyltransferase, *AtPRMT3*, which methylates H3 and H4 *in vitro*[232], is upregulated. In regard that SAM is a precursor in the biosynthesis of ethylene, polyamines, and nicotianamines, two *NICOTIANAMINE SYNTHASE* genes (*AtNAS1* and *AtNAS3*) are upregulated, whereas two *AMINO-CYCLOPROPANE-1-CARBOXYLATE SYNTHASE* genes (*AtACS7* and *AtACS8)* catalyzing the conversion of SAM into ACC, a precursor of ethylene, are downregulated. In accordance with previous transcriptomic

studies[121], large scale regulation of genes encoding proteins related to DNA and histone methyltransferases were not observed in *Atsahh1* (Table 7).
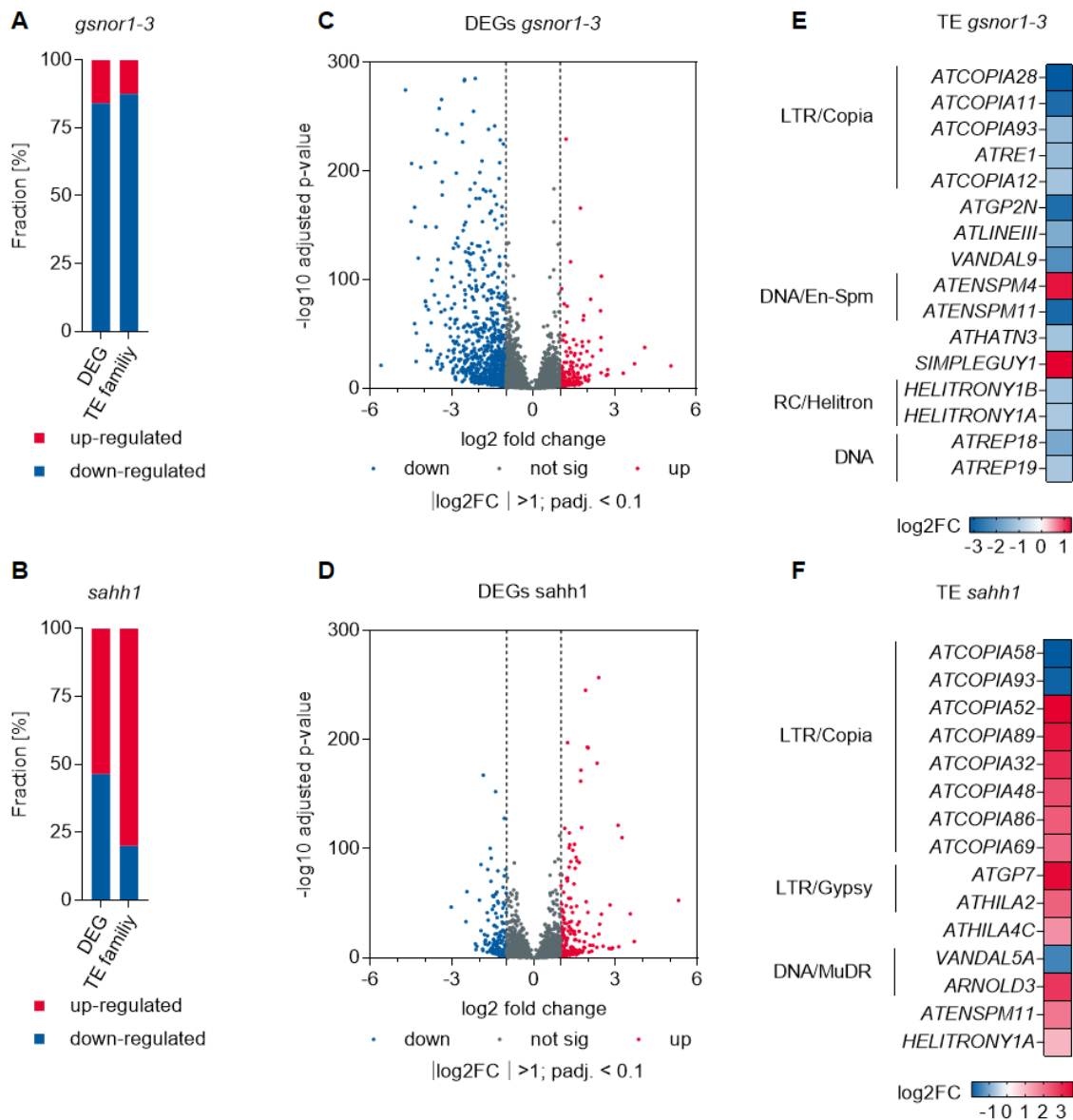
Figure 28. Mutations in *AtGSNOR1* and *AtSAHH1* result in transcriptional reprogramming. (A, B) Stacked bar blots showing the fraction of significant differentially expressed genes (DEGs) and transposable element (TE) families in *Atgsnor1-3* and *Atsahh1*. **(C, D)** Volcano plot highlighting significant DEGs in *Atgsnor1-3* and *Atsahh1*. **(E, F)** Heat map showing differential expression of TE families in *Atgsnor1-3* and *Atsahh1*. If more than one family within a superfamily is differentially methylated, superfamilies are indicated. TEs are classified according to www.arabidopsis.org. RNA was extracted from 4-week-old rosette leaves grown under long-day conditions (n =4). Significant criteria: |log2FC| >1, adjusted p-value less than 0.1.

Table 7. List of selected DEGs in *Atgsnor1-3* and *Atsahh1*. DEGs related to DNA and histone methylation and to metaboloepigenetic processes interacting with DNA and histone methylation identified in *Atgsnor1-3*. Query list is given in Chapter 7.3. Significant criteria: |log2FC| >1, adjusted p-value less than 0.1.

Gene ID	Description	log2FC	padj.
	Differentially expressed genes in *Atgsnor1-3*		
Components of the canonical RdDM pathway			
AT5G56030	HSP90-2	1,05	2,07E-92
AT5G56010	HSP90-3	1,21	3,25E-230
Histone methylation			

AT3G12270	Protein arginine methyltransferase 3 (PRMT3)	1,01	4,59E-20
AT5G06550	JmjC domain-containing histone demethylase 22 (JMJ22)	1,17	3,77E-11
Folate biosynthesis			
AT4G13890	Serine hydroxy methyltransferase 5 (SHMT5)	-1,57	7,13E-06
Nicotianamine/ ethylene biosynthesis			
AT5G04950	Nicotianamine synthase 1 (NAS1)	1,85	1,09E-63
AT1G56430	Nicotianamine synthase 4 (NAS4)	1,03	7,19E-15
AT4G26200	1-Aminocyclopropane-1-carboxylate synthase-like protein 7 (ACS7)	-1,14	4,75E-17
AT4G37770	1-Aminocyclopropane-1-carboxylate synthase-like protein 8 (ACS8)	-1,62	2,88E-15
Methionine salvage cycle			
AT2G26400	Acireductone dioxygenase 3 (ARD3)	-2,94	4,08E-17
Other selected genes			
AT5G43940	GSNO reductase (GSNOR)	-3,17	0,00E+00
AT2G14610	Pathogenesis-related protein 1 (PR1)	-3,73	0,00E+00
AT3G22840	Early light-induced protein 1 (ELIP1)	1,36	4,52E-08
Differentially expressed genes in *Atsahh1*			
Folate biosynthesis			
AT4G13930	Serine hydroxymethyltransferase 4 (SHMT4, cyt)	1,19	0,00E+00
Methylation cycle			
AT4G13940	S-Adenosylhomocysteine hydrolase 1 (SAHH1)	-1,86	3,73E-168
Methionine Salvage cycle			
AT2G26400	Acireductone dioxygenase 3 (ARD3)	-1,05	1,37E-02
Other selected genes			
AT1G72520	Lipoxygenase 4 (LOX4)	-1,12	1,9E-65

Gene Ontology term enrichment analysis was applied to assess molecular functions and biological processes underlying the observed transcriptional changes in *Atgsnor1-3* and *Atsahh1*. Among the most significantly enriched molecular functional categories of the upregulated genes in *Atgsnor1-3* were the catalytic-, glutathione transferase-, and oxidoreductase activity (Supplemental Table 10). In this regard, biological process categories such as cellular response to reactive oxygen species and cellular response to oxidative stress were significantly enriched. According to that, the transcript profile analysis of *Atgsnor1-3* plants suggest a pre-induced antioxidant system under normal growth conditions as previously reported for *Atgsnor* (Ws background)[42]. Further, in the GO enrichment analysis for upregulated genes the biological process category response to nitric oxide was found. This is in agreement with the enhanced RSNO/NO level in *Atgsnor1-3*[45,46]. The majority of GO terms in the biological process aspect of the downregulated genes were related to defense response and response to stress. For instance, the *PATOGENESIS-RELATED GENE 1* (*PR1*) is downregulated in *Atgsnor1-3* (Table 7), as previously reported[233]. This is in line with the impaired resistance to pathogens of *Atgsnor1-3* plants[45,234].

Concerning *Atsahh1*, the terms DNA-binding transcription factor activity and metal ion binding were the dominant categories among the molecular function aspect of downregulated genes (Supplemental Table 11). Among biological processes, terms related to hormones and response to chemical were over-represented. For instance, *LIPOXYGENASE 4* involved in the biosynthesis of the plant hormone jasmonic acid was downregulated as previously reported[121]. Further, the term anthocyanin containing

compound biosynthesis was found analyzing upregulated DEGs in *Atsahh1,* which is in line with previous studies[121].

4.3.7   Integrative analysis of WGBS and RNA-seq data

In general, DNA methylation defines chromatin structure and accessibility. Therefore, DNA methylation helps to regulate gene expression and transposon silencing[58]. To investigate the correlation of DNA methylation and transcription, DEGs (here differentially expressed protein coding genes, PCGs) and TE families differentially expressed in *Atgsnor1-3* were aligned, and their average methylation levels in CG, CHG, and CHH sequence context were plotted from 3kb up- to 3kb down-stream (Figure 29). Metaplot analysis revealed that DNA methylation levels of up- and down-regulated PCGs in *Atgsnor1-3* are similar to wild-type (Figure 29). To investigate the relationship between DMGs and DEGs on gene level, an integrative analysis of those was performed. This analysis revealed that about 4% of DMGs were differentially expressed (percentage are relative to DMGs). Hypo- and hyper-methylation were positively and negatively correlated with transcription (Table 8).
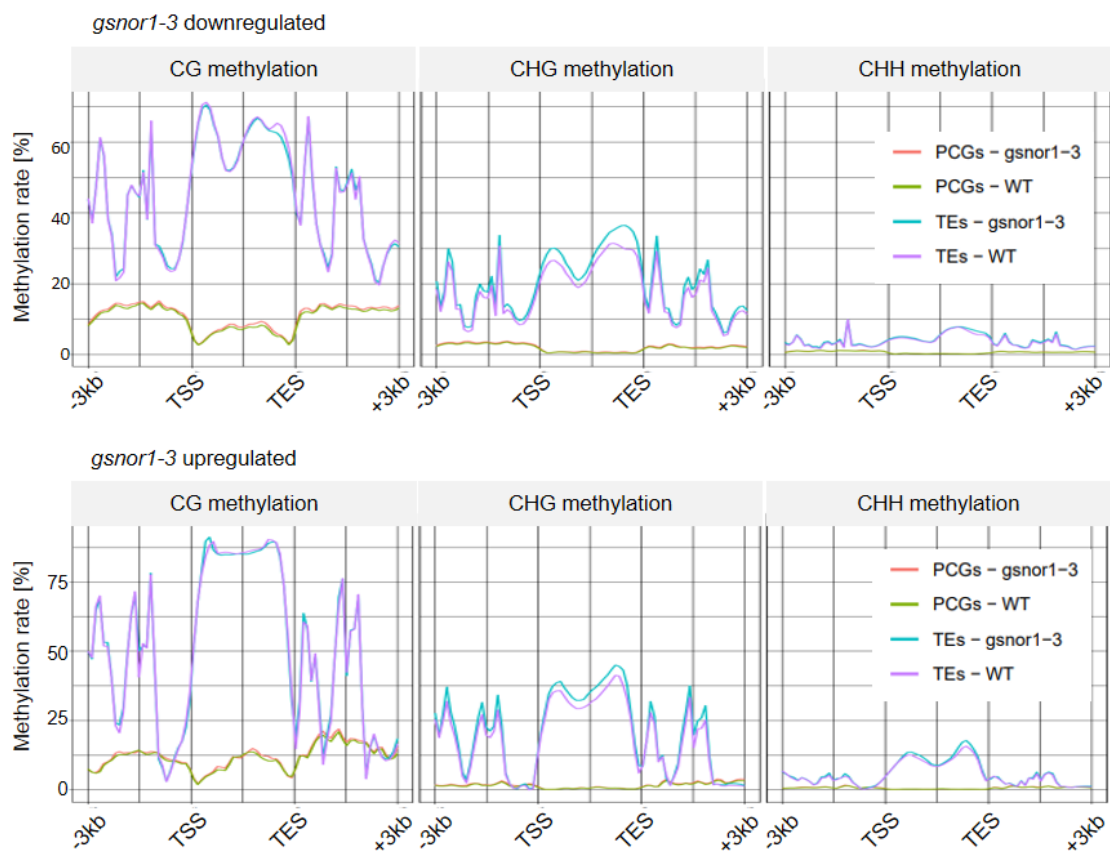
Figure 29. DNA methylation is poorly correlated with gene expression differences in *Atgsnor1-3*. Average levels of CG, CHG, and CHH methylation over DEGs (here protein coding genes; up- or down-regulated) and differentially expressed TE families are plotted from 3kb up- to 3kb down-stream. Abbreviations: TSS, transcriptional start site; TES, transcriptional end site; PCGs, protein coding genes. Metaplot analysis was performed by Patrick Hüther (Becker Lab, Gregor Mendel Institute Vienna).

Atgsnor1-3-ko resulted in hypermethylation of up- and down-regulated TEs in the CHG context (Figure 29). Integrative analysis of differentially methylated TEs and differentially expressed TE families revealed that DNA methylation is negatively associated with TE expression. In detail, TE families ATLINEIII, ATHATN3, and HELITRONY1A are downregulated (expression analysis on family level performed) and members of those TE families possess hyper-DMRs (Supplemental Table 12).

Table 8. Integrative analysis of DMGs and DEGs in *Atgsnor1-3*. The methylation status in *Atgsnor1-3* compared to wild-type is given as (-) and (+) referring to hypo- and hyper-methylation, respectively. DMRs are annotated with genomic features (3kb up- or down-stream, and in gene). Abbreviations: Chr, Chromosome; start, DMR start position; bp, length of overlapping DMR with genomic feature. Statistics RNA-seq: |log2FC| >1, adjusted p-value less than 0.1.

Chr	Start	bp	CH$_3$	Feature	Gene ID	log2FC	padj.	Description
Overlap of significantly downregulated genes with DMGs								
Chr5	8751681	42	+	3kb down	AT5G25250	-3,37	2,0E-266	Flotillin-like protein 1
Chr5	9309455	206	-	3kb up	AT5G26690	-3,35	2,3E-23	Heavy metal-associated isoprenylated plant protein 2
Chr2	11812888	185	+	3kb down	AT2G27690	-2,94	7,6E-36	Cytochrome P450 94C1
Chr5	8751681	42	+	3kb up	AT5G25260	-2,80	2,0E-64	Flotillin-like protein 2
Chr2	9741371	43	+	in gene	AT2G22880	-2,24	3,8E-12	At2g22880
Chr2	15110344	63	+	3kb up	AT2G35980	-2,07	1,7E-08	NDR1/HIN1-like protein 10
Chr2	18325130	77	+	3kb up	AT2G44380	-2,05	1,8E-08	At2g44380
Chr1	24395763	100	+	3kb up	AT1G65610	-1,82	4,4E-06	Endoglucanase 7
Chr5	5767502	32	-	3kb up	AT5G17490	-1,56	6,8E-10	DELLA protein RGL3
Chr3	22556563	37	+	3kb down	AT3G60966	-1,45	1,8E-04	RING/U-box superfamily protein
Chr2	18325130	77	+	3kb up	AT2G44400	-1,39	1,1E-03	Cysteine/Histidine-rich C1 domain family protein
Chr1	27068879	85	+	3kb down	AT1G71910	-1,34	7,2E-06	At1g71910
Chr2	3304271	210	-	in gene	AT2G07774	-1,31	4,1E-05	unknown protein
Chr5	18136940	44	+	3kb up	AT5G44920	-1,21	2,5E-03	TIR domain-containing protein
Chr5	18136984	64	+	3kb up	AT5G44920	-1,21	2,5E-03	TIR domain-containing protein
Chr3	3063382	181	-	in gene	AT3G09960	-1,21	4,7E-03	Calcineurin-like metallo-phosphoesterase superfamily protein
Chr5	18779966	240	+	in gene	AT5G46295	-1,19	2,3E-04	Transmembrane protein
Chr5	18780206	180	+	3kb up	AT5G46295	-1,19	2,3E-04	Transmembrane protein
Chr2	12426536	39	-	3kb down	AT2G28940	-1,17	1,7E-17	At2g28940
Chr1	4123656	44	-	3kb up	AT1G12160	-1,13	2,0E-04	Flavin-containing monooxygenase FMO GS-OX-like 1
Chr1	21823145	288	-	3kb down	AT1G59124	-1,08	2,9E-19	Probable disease resistance protein RF45
Overlap of significantly upregulated genes with DMGs								
Chr	Start	bp	CH$_3$	Feature	Gene Id	log2FC	padj.	Description
Chr5	7376314	54	-	3kb up	AT5G22300	1,82	1,3E-39	Bifunctional nitrilase/nitrile hydratase NIT4
Chr3	9173846	95	-	3kb up	AT3G25190	1,30	2,7E-04	Vacuolar iron transporter homolog 2.1
Chr5	17145940	99	+	3kb up	AT5G42760	1,29	1,8E-08	Leucine carboxyl methyltransferase
Chr4	13766210	58	+	3kb up	AT4G27570	1,02	1,1E-02	UDP-glycosyltransferase 79B3
Chr5	9637396	186	+	3kb up	AT5G27330	1,02	2,3E-11	Prefoldin chaperone subunit family protein

Metaplot analysis revealed that DNA methylation levels of up- and down-regulated PCGs in *Atsahh1* incline to be decreased compared to wild-type (Figure 30). To investigate the relationship between DMGs and DEGs on gene level, an integrative analysis of those genes was performed. This analysis revealed that about 1.7% of DMGs were differentially expressed (percentage are relative to DMGs). Upregulated genes were mostly correlated with decreased methylation in their 3kb upstream and

genic region (Table 9). Interestingly, downregulated genes were associated with reduced DNA methylation levels in their 3kb up- and 3kb down-stream region in *Atsahh1* (Table 9).
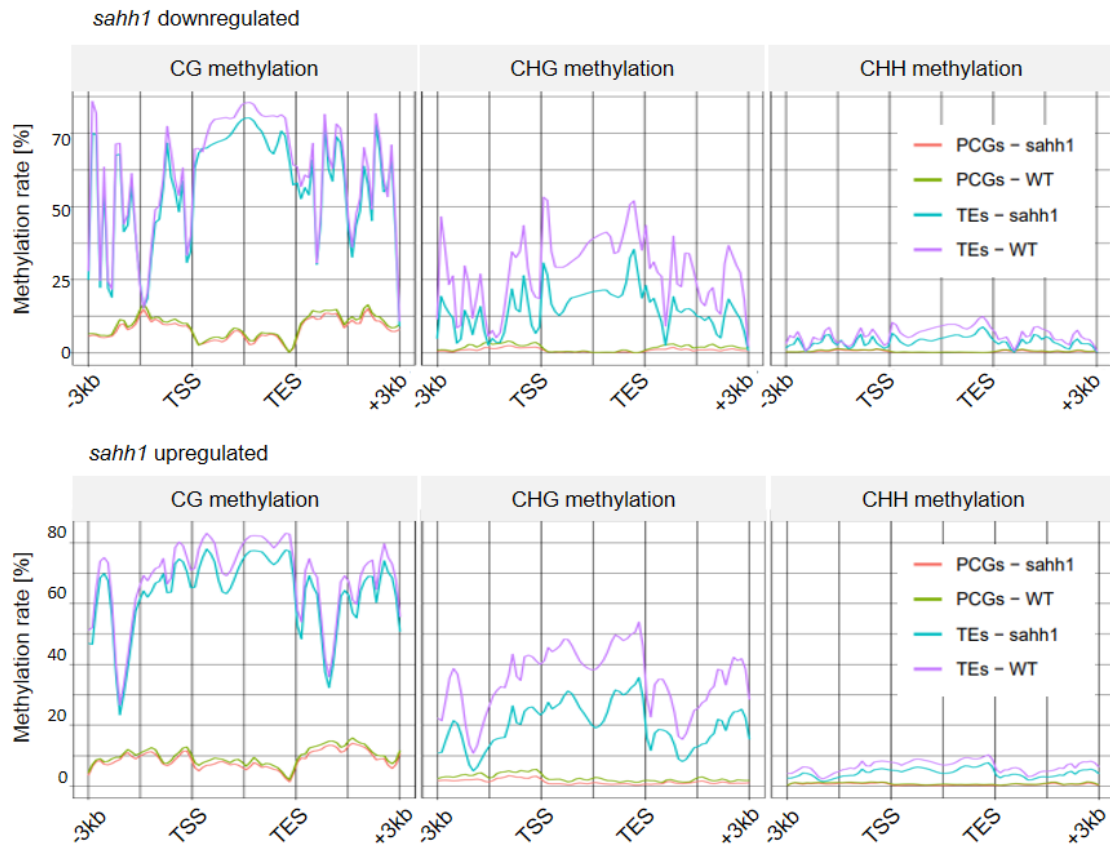
Figure 30. DNA methylation is poorly correlated with gene expression differences in *Atsahh1*. Average levels of CG, CHG, and CHH methylation over DEGs (here protein coding genes; up- or down-regulated) and differentially expressed TE families are plotted from 3kb up- to 3kb down-stream. <u>Abbreviations:</u> TSS, transcriptional start site; TES, transcriptional end site; PCGs, protein coding genes. Metaplot analysis was performed by Patrick Hüther (Becker Lab, Gregor Mendel Institute Vienna).

Hypomethylation in each sequence context was observed in up- and down-regulated TEs in *Atsahh1* (Figure 30). Integrative analysis of differentially methylated TEs and differentially expressed TE families revealed that DNA hypomethylation caused TE activation. In detail, TE families ATCOPIA89, ATHILA2, and HELITRONY1A were upregulated (expression analysis on family level performed) and members of those TE families possess hypo-DMRs (Supplemental Table 12). Taken together, alteration in DNA methylation of protein coding genes is poorly correlated with gene expression differences. Whereas DNA methylation is principally negatively associated with TE expression.

Table 9. Integrative analysis of DMGs and DEGs *Atsahh1*. The methylation status in *Atsahh1* compared to wild-type is given as (-) and (+) referring to hypo- and hyper-methylation, respectively. DMRs are annotated with genomic features (3kb up- or down-stream, and in gene). <u>Abbreviations:</u> Chr, Chromosome; start, DMR start position; bp, length of overlapping DMR with genomic feature. <u>Statistics RNA-seq:</u> │log2FC│ >1, adjusted p-value less than 0.1.

Overlap of significantly downregulated genes with DMGs

Chr	Start	bp	CH₃	Feature	Gene ID	log2FC	padj.	Description
Chr5	19178939	108	-	3kb up	AT5G47230	-1,94	1,3E-25	Ethylene responsive element binding factor 5 ERF5
Chr5	5907343	107	-	3kb up	AT5G17860	-1,88	1,3E-08	Cation/calcium exchanger 1
Chr2	18497356	377	-	3kb down	AT2G44840	-1,79	9,7E-16	Ethylene-responsive transcription factor 13 ERF13
Chr1	13837861	133	-	3kb up	AT1G36622	-1,51	4,6E-05	Transmembrane protein
Chr1	13837994	23	-	3kb up	AT1G36622	-1,51	4,6E-05	Transmembrane protein
Chr5	7261113	306	-	3kb up	AT5G21960	-1,26	2,2E-03	Ethylene-responsive transcription factor ERF016
Chr5	16023667	82	-	3kb up	AT5G40010	-1,24	8,2E-04	AAA-ATPase ASD, mt
Chr1	26140005	248	-	3kb up	AT1G69530	-1,08	1,7E-128	Expansin
Chr4	14031509	89	-	3kb down	AT4G28350	-1,07	8,3E-10	Probable L-type lectin-domain containing receptor kinase VII.2

Overlap of significantly upregulated genes with DMGs

Chr	start	bp	CH₃	Feature	Gene ID	log2FC	padj.	Description
Chr5	9206475	54	-	in gene	AT5G26270	5,31	3,0E-53	unknown protein
Chr3	20260251	114	-	in gene	AT3G54730	3,69	1,3E-15	Putative transmembrane protein At3g54730
Chr3	20260365	94	-	in gene	AT3G54730	3,69	1,3E-15	Putative transmembrane protein At3g54730
Chr3	20260459	7	+	3kb down	AT3G54730	3,69	1,3E-15	Putative transmembrane protein At3g54730
Chr5	18208166	230	-	in gene	AT5G45095	3,12	7,8E-11	Putative uncharacterized protein
Chr1	12851246	141	-	3kb up	AT1G35140	2,38	1,2E-257	Protein EXORDIUM-like 1
Chr4	6431517	56	+	in gene	AT4G10380	1,44	6,9E-10	At4g10380
Chr2	12887310	93	-	3kb down	AT2G30210	1,44	9,8E-04	Laccase-3
Chr2	13160854	47	-	3kb up	AT2G30930	1,43	2,3E-99	Expressed protein
Chr1	3980123	55	-	in gene	AT1G11785	1,31	2,6E-03	Putative uncharacterized protein
Chr3	9173846	95	-	3kb up	AT3G25190	1,29	6,6E-04	Vacuolar iron transporter homolog 2.1
Chr3	21509510	77	-	3kb up	AT3G58070	1,14	2,0E-03	GIS
Chr3	20206910	10	-	3kb up	AT3G54580	1,01	4,4E-02	Proline-rich extensin-like family protein

5 Discussion

5.1 *At*SAHH1 as target of S-nitrosation

NO synthesized in plants provide directly or indirectly the nitroso moiety of S-nitrosothiols under both physiological and stress conditions[10,34]. Biosynthesis, chemical properties/reactivity, and turnover mechanisms of NO/RNS determine the NO-based signaling including the rate of protein-SNO formation[34]. The latter compete with denitrosation reactions in setting the levels of S-nitrosated proteins[34]. *At*SAHH1 possess a total of eleven cysteine residues (Figure 9) and several of those are computationally predicted as targets for S-nitrosation (Supplemental Table 1). In particular, *At*SAHH1 possess consensus motifs of protein-SNO sites with GSNO reactive and non-reactive cysteine residues[235]. Accordingly, *At*SAHH1 was identified as target for S-nitrosation in protein extracts exposed to GSNO and in *Atgsnor1-3* seedlings (enhanced levels of GSNO/RSNO[45,46]). Furthermore, *At*SAHH1 was identified as putatively S-nitrosated under both basal and stress conditions in proteome-wide studies[44,69–72].

In this study, *in vitro* S-nitrosation of *At*SAHH1 by GSNO was confirmed using purified recombinant *At*SAHH1 and plant protein extracts (Figure 10A, B). Furthermore, it was previously reported that S-nitrosation strongly inhibits *At*SAHH1 activity *in vitro*[236]. Concordantly, GSNO-induced inhibition of recombinant *At*SAHH1 was demonstrated (Figure 10C). The inhibition was reversed when the reducing agent DTT was added to the GSNO-treated samples (Figure 10C). This reversible effect is characteristic for protein S-nitrosation[160]. Even though *At*SAHH1 was S-nitrosatable and inhibited by GSNO *in vitro*, S-nitrosated *At*SAHH1 could neither be detected in wild-type nor in *Atgsnor1-3* plants (Figure 10B). This is in contrast to proteome-wide studies using switch techniques and mass spectrometric analysis under basal conditions[44,69,71]. Reasons why *in vivo* S-nitrosated *At*SAHH1 could not be detected are most likely distinct developmental stages, plant materials, and experimental conditions used in those studies. Additional reasons are most likely low RSNO/GSNO concentrations and/or the activation of protein denitrosation processes. *In vitro* approximately 500 pmol GSNO mg^{-1} protein was used to investigate whether *At*SAHH1 undergoes S-nitrosation. Of note, only 75 pmol total RSNO mg^{-1} protein were detected in *Atgsnor1-3* (Figure 16). Hence, the excess of exogenous GSNO might result in "over-S-nitrosation" of proteins. Nevertheless, those concentrations are considered as physiological relevant and used for *in vitro* S-nitrosation studies. In this regard, it is noteworthily that up to 300 pmol total RSNO mg^{-1} protein were detected in *Atgsnor1-3* challenged with *Pseudomonas syringae pv. tomato* (*Pst*) strain DC3000[45]. In general, protein denitrosation is conducted via enzymatic mechanism involving GSNOR (indirect) or the thioredoxin (TRX)/ NADPH-thioredoxin reductase (NTR) system. The latter is not activated in *Atgsnor1-3* on transcript level[237]. Of note, *At*SAHH1 is one of the TRX targets[238] suggesting that it is actively denitrosated by TRX. Further, GSH can act as direct protein denitrosylating

agent in a non-enzymatic mechanism leading to a denitrosylated protein and GSNO, which is then decomposed by GSNOR to prevent renitrosation[34]. Although levels of GSH were elevated in *Atgsnor1-3* (Figure 17F), GSH-mediated denitrosation is not likely to occur due to the lack of the GSNO degrading enzyme. On the other hand, GSNO can be decomposed in the presence of reductants, such as glutathione or ascorbate[8,239]. In this regard, both GSH and ascorbate concentrations are altered in *Wsgsnor* compared to wild-type plants[42].

Taken together, depending on experimental conditions, *At*SAHH1 is S-nitrosatable. Nevertheless, a key technical bottleneck is the lack of methods that are highly sensitive for the analysis of protein-SNOs. In this regard, the formation of *At*SAHH1-SNO under the detection limit of the biotin switch technique and RSNO-RAC cannot be excluded and requires further investigations. Moreover, functionally important heterogeneity among different cell types could be masked, because S-nitrosoproteomic studies assess the formation of protein-SNOs in plant tissues (or extracted organelles). Despite these technical limitations, it is a relevant finding that *At*SAHH1 is S-nitrosatable and inhibited by GSNO *in vitro*. This raises the intriguing possibility that the formation of *At*SAHH1-SNO play a key role in fine-tuning the *At*SAHH1 enzyme activity in respect to epigenetic methylation marks.

5.2 S-Nitrosothiols are crucial for methylation homeostasis

5.2.1 The methylation cycle is affected in GSNO-treated seedlings

The main function of the methylation cycle is to produce SAM for transmethylation reactions and recycle the by-product inhibitor SAH[116,117], and hence, the SAM/SAH ratio reflects the methylation status. Both SAM and SAH are significantly increased in GSNO-treated seedlings, but the stronger increase in SAH levels results in a slightly decreased SAM/SAH ratio indicating a hypomethylated phenotype (Figure 11A, B, C). Since GSNO treatment did not alter the expression of genes involved in the methylation cycle[82], the impairment of the methylation cycle most likely results from metabolic effects and/or NO-mediated PTMs rather than from transcriptional changes upon GSNO treatment. Indeed, the accumulation of SAH is attributable to Hcys accumulation, because increased levels of Hcys cause decreased SAH hydrolase activity and accumulation of SAH (Ref.[133] and references therein). Further, *At*SAHH1 inhibition by exogenous GSNO could contribute to enhanced levels of SAH. Previous studies demonstrated that Hcys accumulation and a decreased MI, as observed in GSNO-treated seedlings (Figure 11C, D), are hallmarks of impaired Hcys remethylation due to impaired folate metabolism[133]. In this context, accumulation of Hcys, and consequently SAH accumulation, might be caused by an activated SMM cycle during CH_3-THF limitation (CH_3-THF serves as cosubstrate for Hcys remethylation[117]). Decreased remethylation of Hcys to methionine would intuitively lead to decreased levels of SAM, however, an increased cellular level of SAM in GSNO-treated seedlings was observed. Of note, the accompanied feedback accumulation of SAM in plants with increased levels of SAH and a

decreased SAM/SAH ratio was previously observed[118,133]. It is likely that enhanced levels of SAM result from an activated methionine salvage cycle indicated by an enhanced level of MTA[117]. Moreover, downregulation of *METHIONINE GAMMA-LYASE* (catalyzes the degradation of methionine) as observed in GSNO-treated *Arabidopsis* leaves[82] may contribute to enhanced levels of methionine, and hence enhanced levels of SAM. Remarkably, *At*MAT1 is inhibited by GSNO *in vitro*[160], and hence, SAM synthesis could be affected by exogenous GSNO treatment. However, only *At*MAT4 plays a predominant role in SAM synthesis *in vivo* compared to *At*MAT1/2/3[129]. Regarding the enhanced levels of Hcys, another aspect beside impaired remethylation has to be considered. GSNO-treated seedlings show enhanced levels of cysteine, which is a precursor for Hcys and GSH[117,215]. Further, the level of GSH, a key player in epigenetic processes (reviewed by Ref.[167]), is enhanced. Taken together, exogenously applied GSNO to 7-day-old liquid-cultured seedlings resulted in elevation of total RSNOs[40] and in an impaired methylation cycle (Figure 11).

Although the reduced MI indicated hypomethylation (Figure 11C), DNA and H3K9me2 methylation levels were not significantly changed as analyzed by chop-PCR and immunoblotting (Figure 12 and Figure 13), respectively. Similarly, DHPA treatment resulted in a decreased SAM/SAH ratio but DNA and H3K9me2 were not significantly changed (Figure 11C, Figure 12, and Figure 13). However, long-time treatment with DHPA resulted in altered epigenetic methylation marks (three weeks; Ref.[120]) indicating an exposure time-dependent effect. Consequently, plants harboring a model silenced locus of tandem-repeats of a *GUS* transgene similar to heterochromatic repeats and TEs[171] were grown in the presence of GSNO and DHPA for a longer period (12 days; Figure 14). *GUS* reactivation is likely to occur because of reduced DNA methylation at the *TS-GUS* transgenic locus[171]. Interestingly, the release of *TS-GUS* silencing was observed in plants grown in the presence of DHPA, whereas it was not observed in GSNO-treated plants. In this regard, a concentration-dependent effect is suggested. For instance, exposure of rice to 50 µM SNP resulted in hypermethylation, whereas hypomethylation occurred in rice plants treated with 0.1 mM – 1 mM SNP[62]. Of note, the use of SNP in NO research is debatable, because it simultaneously release NO, cyanide, and iron[240].

Notably, GSNO-treated seedlings showed global H3K9ac hyperacetylation[40]. Even though H3K9 can either be acetylated or methylated, these epigenetic modifications are differentially distributed in the chromatin[241]. In general, H3K9me2 serves as the major repressive heterochromatic mark in both pericentromeric regions and patches of heterochromatin in the chromosome arms and is a signal for transcription silencing[58], whereas H3K9ac is characteristic for transcriptionally active euchromatic regions[6]. Hence, alteration in H3K9ac levels may not affect H3K9me2 on a global level.

5.2.2 Loss of *At*GSNOR1 function results in an increased methylation index

The ratio of SAM to SAH (MI) is considered as a metabolic indicator of the organismal methylation status[119], because SAM is used as methyl-donor by methyltransferases and SAH competitively inhibits most known SAM-dependent methyltransferases[242]. Loss of *At*GSNOR1 triggered a metabolic reprogramming affecting the methylation cycle (Figure 31). Indeed, increased levels of SAM and a significantly increased SAM/SAH ratio were determined (Figure 17A, B, C). Interestingly, transcriptomic changes of genes involved in the methylation cycle were not observed in *Atgsnor1-3* by RNA-seq. Whereas proteins involved in the methylation cycle were identified as targets for S-nitrosation in *Atgsnor1-3* seedlings[44]. In particular, *At*MAT1/2/3 were identified as protein-SNO targets in *Atgsnor1-3* seedlings[44] and are differentially inhibited by S-nitrosation[160], however, *At*MAT4 is the key player in SAM synthesis *in vivo*[129]. *At*MS1 was also identified as protein-SNO target[44], albeit, *At*MS isoforms are not inhibited by GSNO *in vitro* (AG Lindermayr unpublished). Of note, *At*SAHH1-SNO was identified in *Atgsnor1-3* seedlings[44], but not in *Atgsnor1-3* leaves (Figure 10B). In sum, these findings suggest that protein S-nitrosation plays a regulatory role in controlling enzymatic reactions of the methylation cycle.
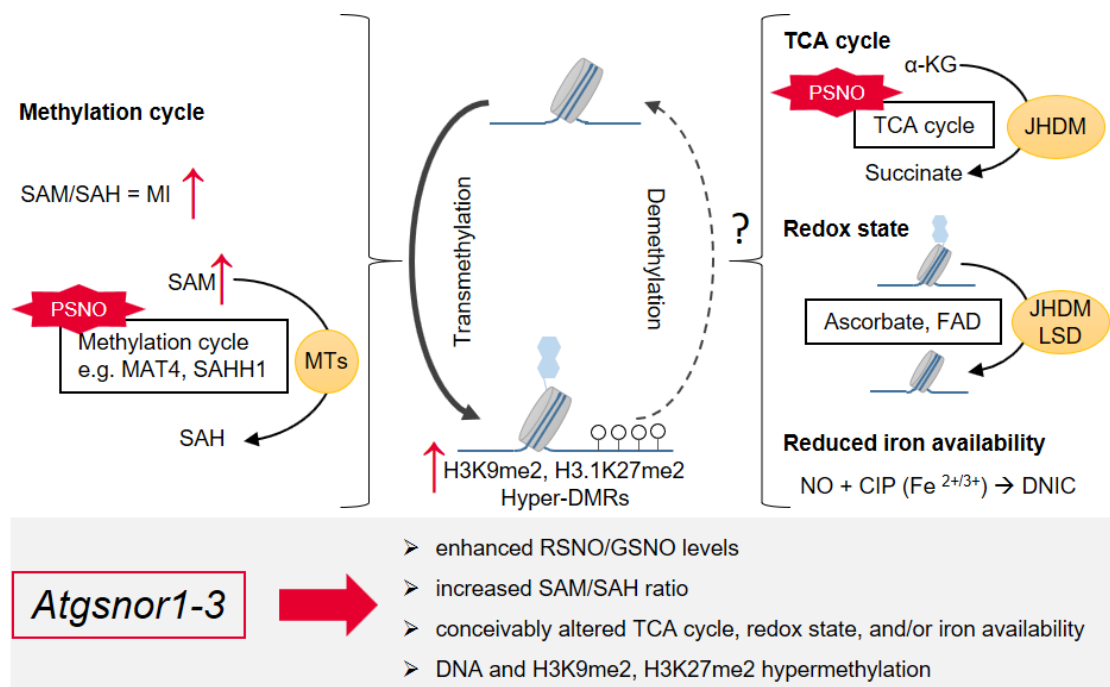
Figure 31. Loss of *At*GSNOR1 function induces metabolic reprogramming leading to hypermethylation. Loss of *At*GSNOR1 resulted in a significantly increased MI accompanied by hypermethylation. Based on studies in the human/animal field, other metaboloepigenetic effects may contribute to changes in the epigenetic landscape. Indeed, the TCA cycle[87,138], the cellular redox status[38] and/or iron cofactor bioavailibilty[63,148] could be affected. However, those metaboloepigenetic effects are uninvestigated in plants. For details see text. <u>Abbreviations:</u> CIP, chelatable iron pool; DMR, differentially methylated region; DNIC, dinitrosyl-iron complex; FAD, flavin adenine dinucleotide; H3K9/27me2, histone H3 lysine 9/27 di-methylation; JHDM/LSD, Jumonji C domain-containing/ lysine specific demethylase-like histone demethylase; MAT4, METHIONINE S-ADENOSYLTRANSFERASE 4; MI, methylation index; MTs, methyltransferases; NO, nitric oxide; PSNO, protein S-nitrosothiol; SAH, S-adenosylhomocysteine; SAHH, SAHH HYDROLASE 1; SAM, S-adenosylmethionine; TCA, tricarboxylic acid cycle; α-KG, α-ketoglutaric acid.

The altered methylation cycle could also result from metabolic effects. For instance, elevated levels of cysteine (Figure 17E; Ref.[42]) were measured in *Atgsnor1-3*. As precursor of methionine its enhanced level may contribute to elevated methionine *de novo* synthesis, and hence, elevated levels of SAM[117]. Furthermore, an activated methionine salvage cycle, as indicated by the enhanced level of MTA (Figure 17D), could contribute to increased levels of SAM.

Notably, depending on the source of GSNO, distinct metabolic reprogramming was found. Loss of *At*GSNOR1 function resulted in an unaltered level of SAH and an increased MI in leaves (Figure 17B, C), whereas exogenously applied GSNO to seedlings resulted in an increased level of SAH and a decreased MI (Figure 11B, C). Similar distinct findings have been observed (Ref.[14]). In particular, the use of plant material with different physiology, such as seedlings and whole leaves, could cause controversy. In addition, the differences could be a consequence of the different GSNO sources, exogenous (GSNO treatment) versus endogenous (in *Atgsnor1-3*)[14]. Taken together, loss of *At*GSNOR1 function resulted in an increased MI indicating hypermethylation of DNA and histones in a modification specific manner as discussed beyond.

Besides the altered MI, loss of *At*GSNOR1 function could affect other metabolic pathways interacting with histone and DNA methylation (Figure 31). For instance, enzymes of the TCA cycle are identified as targets for S-nitrosation in *Atgsnor1-3*[44]. The TCA cycle is essential to produce metabolites involved in histone demethylation. In particular, the TCA cycle intermediates α-KG promotes demethylation catalyzed by JHDMs[87], whereas succinate and fumarate act as competitive inhibitors of those enzymes[138]. To date, metabolic reprogramming affecting the TCA cycle are reported in NO-deficient mutants[143,144] and in plants exposed to NO for six hours[21]. However, whether the depletion of *At*GSNOR1 function impacts the TCA cycle remains elusive.

Further, *At*GSNOR1 is involved in the control of cellular redox status[38], which potentially control epigenetic mechanisms (reviewed by Ref.[64]). Indeed, depletion of *At*GSNOR1 affects cellular levels of metabolites functioning as redox buffer such as GSH (Figure 17F; Ref.[42]) and ascorbate[42]. In terms of epigenetics, GSH was demonstrated to impact epigenetic mechanisms in the animal system[167]. For instance, the activity of the liver isoform MAT1 depends on the GSH/GSSG ratio[167], indicating a crosstalk between GSH/GSSG levels and SAM synthesis. However, the GSH/GSSG ratio was unchanged in *Wsgsnor* mutant plants compared to wild-type[42]. Moreover, histone demethylation could be affected by altered levels of ascorbate[42], because ascorbate functions as cofactor for JHDMs[57]. Furthermore, the availability of the redox cofactor FAD for LSD histone demethylases[168] could be influence by the redox status, and hence, changed in *Atgsnor1-3*. In sum, it is likely that an altered redox status impacts epigenetic methylation processes in *Atgsnor1-3.*

Moreover, loss of *At*GSNOR1 function could result in sequestration of iron via DNIC formation (DNICs are formed by the interaction between NO, iron, and thiol-containing ligands such as GSH[15]; Figure 31). In this context, the elevated level of GSNO/NO[49] and GSH (Figure 17F; Ref.[42]) in *Atgsnor1-3* under basal conditions could result in enhanced DNIC formation. A reduced availability of the cofactor iron could affect the activity of JHMDs and DNA demethylases *At*ROS1/*At*DME1. In plants, the detection of DNIC by electron paramagnetic resonance techniques faces the problems of the high detection limit of this method and the high manganese levels in plant tissues, which has paramagnetic properties appear at the same magnetic field[243,244]. Only when NO production is stimulated to a sufficient amount (e.g. in *Hibiscus rosa-sinensiss* exposed to 10 mM nitrite[243]) or NO is exogenously applied (e.g. exposure of sorghum embryos to 1 mM SNP or GSNO[245]) the formation of DNICs is measurable.

Besides, iron bioavailability could be impaired by elevated levels of nicotianamines being high-affinity metal chelator molecules[246]. This is indicated by upregulation of genes encoding NICOTINAMINE SYNTHASES 1 and 4 in *Atgsnor1-3* (Table 7). It is worth mentioning that the chlorophyll content, a hallmark for iron deficiency[247], is decreased in *Atgsnor1-3* (Supplemental Figure 8). However, the decreased chlorophyll content may also result from the upregulation of EARLY LIGHT-INDUCED PROTEIN 1 (Table 7) preventing excess accumulation of free chlorophyll by inhibiting the entire chlorophyll biosynthesis pathway[248]. Moreover, proteins associated with chlorophyll metabolism are targets for S-nitrosation[44] indicating impairment of chlorophyll biosynthesis by elevated RSNO/GSNO levels.

In sum, it is likely that vicious combination of such metabolic dysregulations might have synergistic effects on induction of aberrant epigenetic landscapes. To date, the regulatory function of *At*GSNOR1 on metaboloepigenetic processes is unraveled. The scope of this study was to investigate the regulatory role of *At*GSNOR1 on the methylation cycle and on DNA and histone methylation pattern.

5.2.3 Alteration of the methylation index affects DNA and histone methylation in a modification specific manner

Several lines of evidence have demonstrated that an altered MI affect DNA and histone methylation in plants and animals (Ref.[57,118,119] and references therein). To date, the interconnection between an increased MI and hypermethylation is hardly reported[249,250], whereas a decreased MI concomitant by a hypomethylated phenotype, as observed in the *Atsahh1* plants, are well described (Ref.[118,119] and references therein). Interestingly, the alteration of the MI has a biased effect on DNA and histone methylation marks (Figure 32)[118,129]. Indeed, a decreased MI predominantly results in loss of non-CG and loss of H3K9me2, whereas CG methylation and other histone methylation marks are less affected, including H3K27me1 and H3K9me1 in *Arabidopsis* (Ref.[118,119] and references therein). Loss of

*At*GSNOR1 function resulted in an increased MI (Figure 17C) accompanied by enhanced levels of H3K9me2 and H3.1.K27me2 (Table 3), and enrichment of hyper-DMRs (Figure 25).
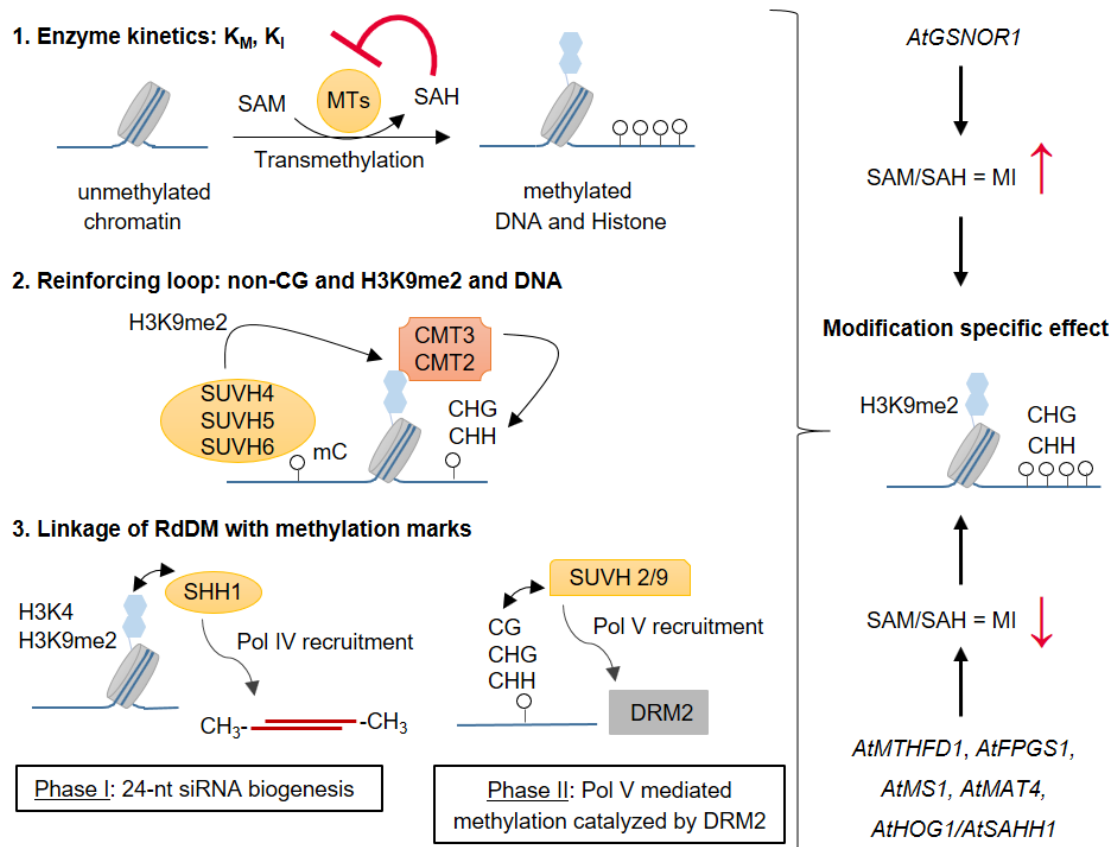
Figure 32. Changes of the methylation index affects DNA and histone methylation in a modification specific manner. For details see text. Methylation pathways modified from Ref.[58]. Simplified schema of the RdDM pathway is depicted, for details refer to Ref.[58,107]. The effect of the MI was previously demonstrated for *AtFPGS1* [131], *Athog1-1/AtSAHH1*[123,124], *AtMAT4*[129], *AtMS1*[118], *AtMTHFD1*[133]. For details see text. <u>Abbreviations:</u> CG, CHG, CHH, DNA methylation in sequence context; CMT2/3, CHROMOMETHYLASE 2/3; DRM2, DOMAIN REARRANGED METHYLASE 2;H3K4, histone H3 lysine 4 unmodified; H3K9me2, histone H3 lysine 9 di-methylation; mC, 5-methylcytosine; MTs, methyltransferases; SAHH, S-adenosylhomocysteine; SAM, S-adenosylmethionine; SHH1, SAWADEE HOMEODOMAIN HOMOLOGUE 1; SUVH4/5/6, SU(VAR)3-9 HOMOLOG 4/5/6.

The modification specific effect can be explained by the following factors (Figure 32). First, the K_M and the K_I of each enzyme for its substrate or inhibitor, respectively, can vary even between closely related members of a protein family. Hence, methyltransferases are sensitive to a greater or lesser extent towards fluctuations in the availability of SAM or the presence of SAH[57].

Second, DNA methylation is functionally linked to histone methylation. Indeed, non-CG methylation and H3K9me2 are linked together by a reinforcing loop, which perpetuates both epigenetic marks catalyzed by *At*CMT2/3 and *At*SUVH4/5/6, respectively[91].

Third, the RdDM pathway is interwoven with previous established methylation marks. Briefly, the canonical RdDM pathway involves two main phases; an upstream *At*Pol IV-dependent siRNA biogenesis phase and a downstream *At*Pol V-mediated methylation phase[58,107]. In both phases the recruitment of the plant specific *At*Pol IV and *At*Pol V depends on interaction of proteins with previous

established methylation marks. *At*Pol IV is recruited to RdDM loci by *At*SHH1, which specifically binds to H3K9me2 and to unmodified H3K4[91]. Whereas *At*Pol V is recruited by the non-catalytic *At*SUVH2 and *At*SUVH9 proteins, which binds to pre-existing methylated DNA[58]. In particular, CHH maintenance methylation is prone to changes in the RdDM pathway, because it depends on the activity of *At*CMT2 and *At*DRM2/RdDM[58].

5.2.4 *At*GSNOR1 function is crucial for DNA methylation processes

Analysis of DNA methylation levels at selected heterochromatin repeats and TEs using chop-PCR showed that loss of *At*GSNOR1 function did not induce significant changes in DNA methylation (Figure 22). Further, transcriptional gene silencing associated with DNA methylation and heterochromatic marks was not released by loss of *At*GSNOR1 function. Indeed, a model silenced locus of tandem-repeats of a *GUS* transgene similar to heterochromatic repeats and TEs[171], was not reactivated in the background of *Atgsnor1-3* (Figure 21). In contrast, it was reactivated in the background of *Atsahh1* (Figure 21) and other epigenetic mutations[120,220]. This result indicates that loss of *At*GSNOR1 function does not negatively regulate DNA methylation at the *TS-GUS* transgenic locus.

However, profiling of cytosine methylation pattern with high resolution by WGBS demonstrated that *At*GSNOR1 play a regulatory role in DNA methylation. Indeed, reduced DNA methylation calculated as percentage methylated cytosines was observed in *Atgsnor1-3* (Table 4). However, comparison of DNA methylation levels along chromosomes revealed differences in the TE-rich pericentromeric region compared to wild-type (Figure 23). Indeed, parts are hyper- and hypomethylated. Whereas comparison of methylation levels along all TEs and PCGs resulted in reduction of CG and CHG methylation in TEs and partial reduction of CG methylation in PCGs (Figure 24A). Nevertheless, in relation to the genome-wide position of methylated cytosines rather hyper-DMRs than hypo-DMRs were identified (Figure 25). In fact, the number of hyper-DMRs was more than 3.8 times that of hypo-DMRs (61 hypo-DMRs; 231 hyper-DMRs). This finding indicates that loss of *At*GSNOR1 function predominantly causes hypermethylation in a region-specific manner. In particular, genomic feature annotation showed that the identified DMRs are mainly mapped to protein coding genes (PCGs in their genic, 3kb up- or 3kb down-stream flanking region; hereafter differentially methylated genes DMGs) and TEs (Supplemental Figure 14A). Overall, loss of *At*GSNOR1 function caused enrichment of hyper-DMGs and hyper-TEs (Figure 26A).

This altered DNA methylation phenotype of *Atgsnor1-3* is attributable to metabolic alteration rather than to changes in the expression of genes and/or GSNO/NO-mediated PTMs of proteins involved in DNA methylation. This is based upon that the RNA-seq analyses revealed only upregulation of the molecular chaperon *At*HSP90 (HSP90-2, HSP90-3) in *Atgsnor1-3* (Table 7), which facilitates the loading of 24-nt siRNAs onto *At*AGO4 in the RdDM pathway[58,107]. Further, to date solely *At*AGO4 (targeting 24-

nt to RdDM loci) was identified as target for S-nitrosation in a proteome-wide study using *Atgsnor1-3* plants[44]. Indeed, loss of *At*GSNOR1 function caused a significantly increased MI (Figure 17C) accompanied by the enrichment of hyper-DMRs. This result is congruent with the observation that an enhanced MI results in enhanced DNA methylation in mice[249,250]. Further, overexpression of *AtMETS1* (here abbreviated as *AtMS1*) is accompanied by a genome-wide global increase in DNA methylation[130]. Of note, the MI and histone methylation levels were not analyzed in *35S::AtMS1* plants.
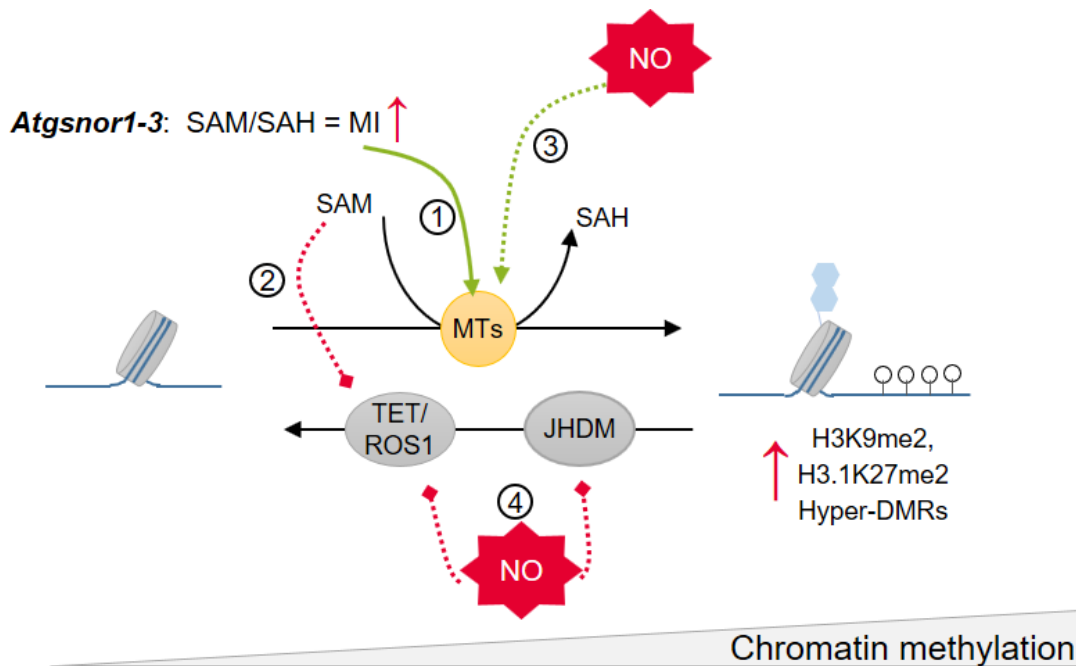
Figure 33. The equilibrium of methylation processes towards methylation in *Atgsnor1-3*. (1) An increased methylation index causes hypermethylation in *Atgsnor1-3* and in mice[249,250]. Proposed mechanisms based on studies in mammalian are **(2)** SAM inhibit DNA demethylation[214,251], **(3)** NO enhances DMTs activity[146], and **(4)** direct inhibition of JHDM and TET by nitrosyl-iron complex formation[63,148]. Of note, loss of *At*GSNOR1 function results in enhanced RSNO/GSNO and NO levels. Metaboloepigenetic effects are discussed above. Green and red arrows indicate positive and negative effects, respectively. Dashed lines represent mechanisms demonstrated in the animal research field. For details see text. Abbreviations: DMR, differentially methylated region; H3K9me2, histone H3 lysine 9 di-methylation; JHDM, Jumonji C domain-containing histone demethylase; mC, 5-methylcytosine; MI, methylation index; MTs, methyltransferases; NO, nitric oxide; ROS1, REPRESSOR OF SILENCING 1; SAH, S-adenosylhomocysteine; SAM, S-adenosylmethionine; TET, TEN-ELEVEN TRANSLOCATION.

Based on studies in the human/animal field, other effects could contribute to the altered DNA methylation pattern in *Atgsnor1-3* (Figure 33). Indeed, declined active DNA demethylation could tile the equilibrium of methylation processes toward methylation in *Atgsnor1-3*. In this context, elevated levels of SAM, as observed in *Atgsnor1-3* (Figure 17A), inhibit active DNA demethylation in human cells[214,251]. Further, mammalian TET enzymes involved in DNA demethylation are inhibited by NO due to the formation of a nitrosyl-iron complex with their catalytic iron[148]. Similarly, the iron-sulfur containing *At*ROS1/*At*DME DNA demethylases[114] could be affected by NO in *Atgsnor1-3*. The vulnerability of iron-sulfur clusters to attack by NO[252] has been previously shown. For instance, NO inhibits aconitase by forming a metal-nitrosyl complex with its iron-sulfur cluster[77]. Further, iron

sequestration via DNIC formation (see Chapter 5.2.2) may yield to reduced iron bioavailability for iron-sulfur cluster assembly. In this context, *Arabidopsis* mutants impaired in the iron-sulfur cluster assembly pathway reveal DNA hypermethylation[113]. Moreover, hypermethylation could be a result of enhanced DMT activity. In this context, increased DMT activity was observed in nuclear protein extracts treated with NO[146].

5.2.5 *At*GSNOR1 function is crucial for the maintenance of histone methylation

Loss of *At*GSNOR1 function results in global hypermethylation of H3K9me2 and H3.1.K27me2 (Table 3). This modification specific alteration of histone methylation marks is most likely caused by metabolic alteration rather than changes in the expression of genes and/or GSNO/NO-mediated PTMs of proteins involved in histone methylation. Indeed, RNA-seq analysis revealed only upregulation of *At*JMJ22, a histone arginine demethylase[231]. Further, only regulation of the histone arginine demethylase *At*PRMT5 by S-nitrosation was reported[155]. Indeed, loss of *At*GSNOR1 function caused a significantly increased MI (Figure 17C) indicating hypermethylation in a modification specific manner.

Nevertheless, other effects could contribute to altered histone lysine methylation pattern in *Atgsnor1-3* and need to be unraveled in future work (Figure 33)*.* For instance*,* the level of MTA, which is known to inhibit HMTs targeting H3K4 in human cells[214,253], is elevated in *Atgsnor1-3*. However, significant global changes in H3K4 methylation levels were not observed (Table 3). Additionally, based on studies on the human JHDM KDM3A, plant JHMDs might be targets for metal nitrosylation by the formation of a nitrosyl-iron complex with their non-heme Fe(II) coordinated by a 2-histidine-1-carboxylate facial triad in their catalytic pocket[63]. Moreover, metaboloepigenetic effects such as iron sequestration, impairment of the TCA cycle providing α-KG (substrate for JHMDs[87]), and an altered cellular redox status[38] could impair the activity of JHMDs as discussed above.

Biochemical evidence from a number of studies indicates that JHDMs confer substrate specificity[228]. Among the JHDM groups, JHDM2/KDM3 group is required for demethylation of H3K9me1/2. For instance, mutations in *At*JMJ25 (also named *At*IBM1, *INCREASE IN BONSAI METHYLATION 1*) leads to induced ectopic H3K9me2 methylation, and concomitantly, to enhanced gene body methylation in CHG context[101,105]. In *Atgsnor1-3* plants, enrichment of hyper-DMRs in the CHG context (Supplemental Figure 13) and increased global levels of H3K9me2 are observed (Table 3; Figure 19). However, further investigations are needed to test whether the function of *At*JMJ25 is impaired in this mutant. Moreover, *At*JMJ27 and *At*JMJ24 functions could be impaired. Whereas *At*JMJ27 has H3K9 demethylase activity[227], *At*JMJ24 is considered as inactive due to the lack of conserved amino acid residues within the Fe(II) binding site in its catalytic pocket[228]. However, *At*JMJ24 was shown to have a role in transposon silencing by antagonizing H3K9me2 through locus-specific interactions[101,103]. Demethylation of H3K27me2/3 is catalyzed by members of the KDM4/JHDM3 and Jumonji C-domain-

only group of JHMD proteins. The two major erasers of the H3K27me2 methylation mark are *At*JMJ11/ELF6 and *At*JMJ12/REF6 (KDM4/JHDM3 family)[254,255]. Moreover, *At*JMJ30 and *At*JMJ32 (Jumonji C -domain-only group) target H3K27me2/3[256]. Together, it seems reasonable to investigate whether loss of *At*GSNOR1 function impairs the activity of JHDMs responsible for demethylation of H3K9me2 and H3.1K27me2.

5.2.6 Alteration of DNA methylation modestly effects gene transcription in *Atgsnor1-3*

Several recent studies indicate little association between differential DNA methylation and gene expression changes[257]. For instance, in mutants impaired in the methylation cycle (*Atmat4*[129] and *Atms1*[118]) differential DNA methylation was not associated with the expression of genes. Consistent with these findings, protein coding genes transcriptionally up- and down-regulated displayed similar DNA methylation profiles in *Atgsnor1-3* and wild-type (Figure 29). Hence, these results indicate that transcriptional changes occur largely independently of detectable variation in the DNA methylation pattern. In this regard, only 4% of DMGs (genes overlapping with identified DMRs in their genic, 3kb up- and/or 3kb down-stream region) were differentially expressed (Figure 34A). This finding is comparable to previous studies. For instance, about 5% of DMGs were differentially expressed in *Arabidopsis* roots challenged with beet cyst nematode *Heterodera schachtii*[257]. In detail, promotor methylation (3kb upstream region) was typically associated with gene repression, however, it partly enhanced gene transcription in *Atgsnor1-3* (Table 8). This is in agreement with general observations[58]. Gene body methylation (between start and stop codon) seems to have a modest effect on gene expression in *Arabidopsis*[258,259] and its function remains enigmatic (reviewed by Ref.[106]). In this study, reduction and enrichment of genic DNA methylation caused downregulation of genes in (Table 8). Furthermore, hyper- and hypo-DMRs in the 3kb downstream flanking region of genes resulted in downregulation of genes. Another remarkable observation was that only one DMG out of sixteen harboring DMRs in multiple genomic features was differentially expressed (Figure 26B; Table 8). This gene, namely At5G46295, is associated with hyper-DMRs in its genic and 3kb upstream flanking region (Table 8).

Nevertheless, constitutive misregulation of genes, which are not directly targeted by DNA methylation, may result from methylation-dependent alteration in the transcriptional networks(Figure 34B)[260]. The linkage between DEGs not targeted by DNA methylation and methylation-dependent alteration in the transcriptional network[130,260] is exemplified at the *AtPR1* gene. *AtPR1* transcript is upregulated in mutants globally defective in maintenance of CG (*Atmet1*) or non-CG methylation (*Atddc*)[260], whereas *AtPR1* is downregulated in hypermethylated *35S::AtMS1* plants[130]. Likewise, *AtPR1* expression is reduced (Table 7) and delayed[45] in *Atgsnor1-3*. Notably, mutants globally defective in DNA methylation

were markedly resistant to *Pst*[260], whereas plants with increased DNA methylation level (*35S::AtMETS1*; overexpressing *AtMS1*) and *Atgsnor1-3* showed attenuated resistance to *Pst*[45,130].
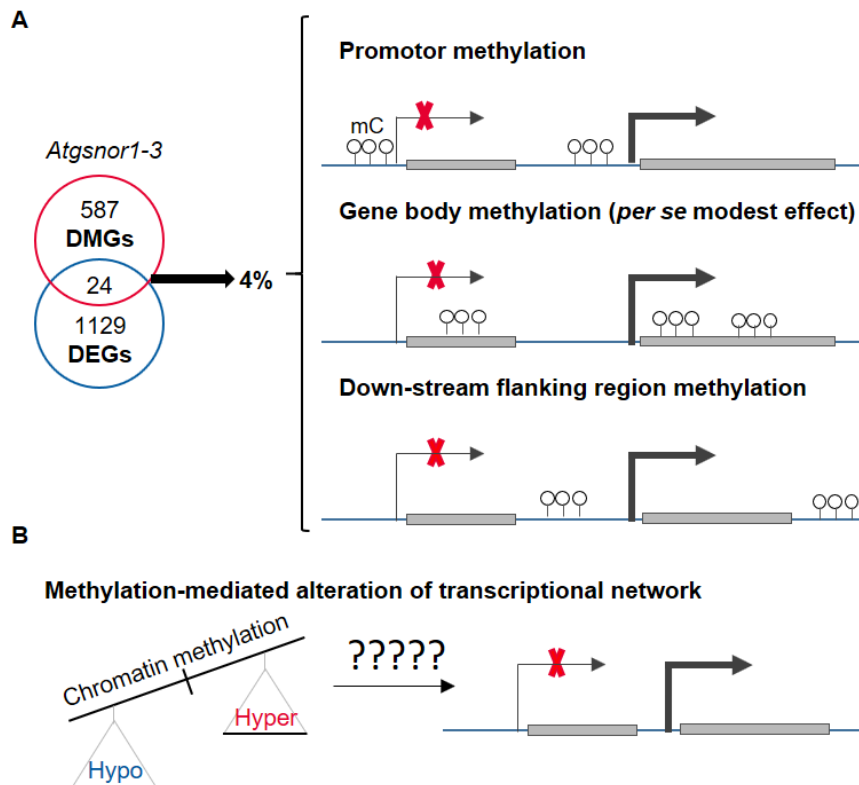
Figure 34. Control of gene expression by DNA methylation in *Atgsnor1-3*. (A) Integrative analysis of DMGs harboring DMRs in their 3kb up- (promotor), 3kb down-stream or genic (gene body methylation) regions resulted in an overlap of 4%. This demonstrate a modest effect of DNA methylation on transcription. **(B)** However, methylation-mediated alteration of transcriptional network could cause transcriptional changes. DMGs differentially expressed are listed in Table 8. <u>Abbreviations:</u> DMGs, differentially methylated genes; DEGs, differentially expressed genes.

Besides altered DNA methylation levels, transcriptional changes are probably caused by pleiotropic effects of impaired *At*GSNOR1 function, rather than by altered DNA methylation levels. For instance, loss of *At*GSNOR1 function caused differential expression of several transcription factors (Supplemental Table 13). Further, proteins involved in transcriptional regulation were identified as targets for S-nitrosation[44]. Moreover, loss of *At*GSNOR1 function caused enhanced global levels of H3K27me2 (Table 3), which is usually highly enriched at the promoter of inactive genes[89]. Other reasons why loss of *At*GSNOR1 function induces transcriptional changes could be the modulation of chromatin structure by other epigenetic mechanisms. For instance, non-coding miscelleanous RNAs are differentially expressed in response to GSNO[82]. In general, non-coding RNAs are regulators of gene expression by a variety of mechanisms such as chromatin remodeling or regulate gene expression at transcriptional or post-transcriptional level. Furthermore, transcriptional changes could be linked to the proximity of differentially methylated TEs to DEGs[257]. Moreover, mRNA stabilization could be affected by enhanced GSNO/NO levels in *Atgsnor1-3*[56].

In detail, the integrative analysis of DMGs and DEGs in *Atgsnor1-3* (Table 8) revealed upregulation of *UDP-GLYCOSYLTRANSFERASE 79B3* contributing to salt stress tolerance[261]. Hence, this enzyme might also be involved in the salt resistant phenotype of *Atgsnor1-3*[155]. Interestingly, a hypo-DMG encoding the *At*VTL5 was found to be upregulated in *Atgsnor1-3* as well as in *Atsahh1*. *At*VTL5 is involved in the regulation of cellular iron homeostasis conceivably by the transfer of iron ions from the cytosol to the vacuole for intracellular iron storage[262]. In this regard, it is worth mentioning that the chlorophyll content, a hallmark for iron deficiency[247], is decreased in *Atgsnor1-3* and increased in *Atsahh1* (Supplemental Figure 8). Hence, a complex interrelationship between iron homeostasis, altered DNA methylation, and expression of *At*VTL5 is suggested.

Taken together, DNA methylation modestly effects gene transcription in *Atgsnor1-3.* However, further work is needed to reveal possible hidden mechanisms and/or functions that will help to explain the role of DNA methylation in gene expression regulation[263].

5.2.7 *At*GSNOR1 function is crucial for TE repression

Repression of TEs is required to guarantee genome stability. Therefore, TEs are generally located in transcriptionally silenced heterochromatic regions marked by DNA methylation and repressive histone modifications, such as H3K9me2[58]. In *Atgsnor1-3*, DNA methylation differs in the TE-rich pericentromeric region from wild-type (Figure 23). Indeed, parts are hyper- and hypomethylated. However, the genomic annotation of identified DMRs resulted in mainly hypermethylated TEs (Figure 26A, D). Among them, LTR/Copia and Line/L1 type TE, predominantly regulated through H3K9me2 and non-CG DNA methylation pathways[264], but also LTR/Gypsy type TEs, predominantly regulated by H3K27me1 methylation[264], were found. Interestingly, H3K27me1 is slightly diminished in *Atgsnor1-3* (Table 3), albeit not significant. Consistent with the enhanced DNA methylation, RNA-seq data indicated that TEs (expression analysis on family level performed) were mainly repressed in the *Atgsnor1-3* mutant (Figure 28A, E).

In general, TE responsiveness to stress is considered as major compound cost to the deleterious impact of stress on an organism. Although TE activation under stress is widely shared across eukaryotes, stress can also result in repression of TEs as shown for different ecotypes of *A. thaliana* exposed to cold stress. TE activation/repression likely depend on the type of stress and the TE type. In this context, TE activation may generate adaptive genetic variation and accelerate host stress adaption (Ref.[265] and references therein). Given that *At*GSNOR1 deficiency caused impaired plant disease responses[45,234], heat sensitivity[46], and resistance to paraquat-induced cell death[42,47], an effect of hypermethylated TEs might be linked to those responses. However, further research is needed to understand how activated and/or repressed TEs influence stress responses in plants, particularly, in *Atgsnor1-3*.

5.3 *At*SAHH1 a key enzyme in the maintenance of methylation homeostasis

*At*SAHH1 is a key enzyme in the maintenance of methylation homeostasis because it is needed to metabolize SAH, which competitively inhibits SAM-dependent methyltransferases, including DMTs and HMTs. Hence, SAH removal is the key metabolic determinant of methyltransferase reactions[168]. Accordingly, inhibition of *At*SAHH with DHPA or *Atsahh1-kd* resulted in an increased SAH level, and concomitantly, in a decreased SAM/SAH ratio (Figure 11B, C; Figure 17B, C; Ref.[123,124,127]). It is well known, that a decreased MI yield to decreased DNA and H3K9me2 methylation (Ref.[118,119] and references therein). According to that, DHPA treatment resulted in slightly decreased H3K9me2 and DNA levels as determined by immunoblotting and chop-PCR, respectively (Figure 12 and Figure 13), albeit not significant. Inherently, the effect of DHPA on DNA and histone methylation is more pronounced upon long-time treatment (three weeks; Ref.[120]). Whereas *Atsahh1-kd* caused significant reduced levels of H3K9me2 and DNA methylation at selected heterochromatin repeats, as analyzed by immunoblotting and chop-PCR, respectively (Figure 19 and Figure 22). In addition, both DHPA treatment (12days) and *Atsahh1-kd* induced loss of silencing at the L5 locus (Figure 14 and Figure 21; Ref.[120,220]), a model silenced locus of tandem-repeats of a *GUS* transgene similar to heterochromatic repeats and TEs[171].
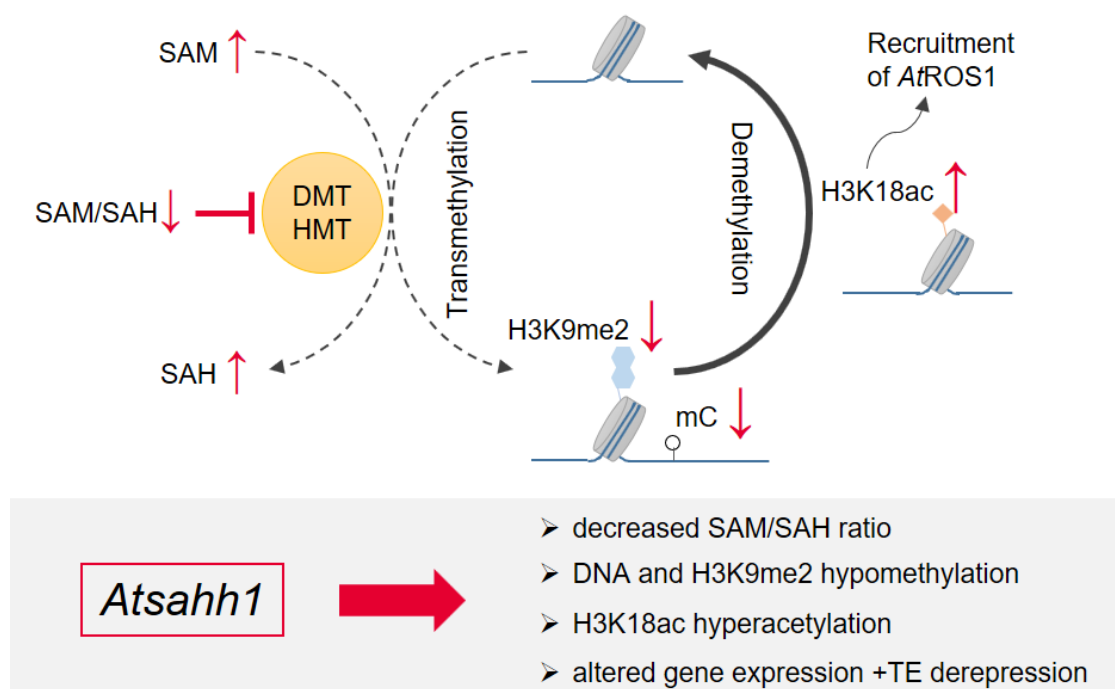
Figure 35. Mutation in *AtSAHH1* causes hypomethylation. Downregulation of *AtSAHH1* resulted in a decreased MI and hypomethylation (dashed arrow). Further, the hypomethylated phenotype can be caused by enhanced DNA demethylation activity indicated by elevated H3K18ac levels[58,111] (solid arrow). See text for details. <u>Abbreviations:</u> DMT, DNA methyltransferase; HMT, histone methyltransferases; mC, cytosine methylation; MI (SAM/SAH ratio), methylation index; ROS1, REPRESSOR OF SILENCING 1; SAH, S-adenosylhomocysteine; SAHH1, SAH HYDROLASE 1; SAM, S-adenosylmethionine; TE, transposable element.

In sum, this findings together with previous studies[120,121,123] confirms the function of *At*SAHH1 as a central factor for DNA and H3K9me2 methylation (Figure 35).

To date, an integrative analysis using next generation sequencing methods such as WGBS and RNA-seq as well as an epigenetic histone modification analysis by LC-MS/MS to delineate the regulatory role of *At*SAHH1 in DNA and histone methylation and transcription have been elusive. Briefly, *Atsahh1-ko* caused decreased levels of H3K9me2, whereas other histone lysine methylation marks were not significantly altered as analyzed by LC-MS/MS (Table 3). WGBS analysis of *Atsahh1-kd* plants revealed extensive hypomethylation in CHG and CHH sequence context (Table 4; Figure 23 and Figure 24). Whereas loss of CG methylation was comparatively low. This is in agreement with previous results demonstrating that changes in the methylation cycle mainly affect CHG/CHH and H3K9me2 methylation (Ref.[118,119] and references therein) reflecting the mechanistic interdependence of non-CG and H3K9me2 methylation[91]. For instance, *Atmthfd1-ko* resulted in a diminished SAM/SAH ratio and hypomethylation most pronounced in H3K9me2 and CHG/CHH DNA methylation marks[133]. However, the histone methylation independent DNA methylation in CG context[91] is also reduced in *Atsahh1* indicating a general inhibition of SAM-dependent methyltransferases, including *At*MET1. In turn, *At*MET1 disfunction may further reinforce loss of CHH methylation because *At*SUVH2 and *At*SUVH9 bind to pre-existing methylated DNA in each sequence context to recruit Pol V for RdDM[58].

Besides the decreased MI resulting in hypomethylation, the enhanced levels of H3K18ac (Table 3) may also contribute to DNA hypomethylation in *Atsahh1* (Figure 35). Indeed, the DNA demethylase *At*ROS1 is recruited to a subset of demethylation target loci by the IDM complex, in which *At*IDM1 catalysis acetylation of H3K18 to create a permissive chromatin environment for *At*ROS1 function[58,111]. Hence, the enhanced H3K18ac level may result in enhanced *At*ROS1 activity in *Atsahh1*. Of note, RNA-seq analysis of *Atsahh1* plants did not reveal any differentially regulated genes involved in DNA and histone methylation. In sum, these data suggest that DNA and H3K9me2 hypomethylation in *Atsahh1* are caused by metaboloepigenetic effects and enhanced H3K18ac levels rather than on transcriptional changes of enzymes involved in DNA and histone methylation (Figure 35).

5.3.1 Knock-down of *At*SAHH1 causes activation of TEs

In *Arabidopsis*, silenced TEs and repeats are enriched in pericentromeric heterochromatin marked with dense DNA methylation in all three sequence contexts and have high levels of the repressive chromatin mark H3K9me2[58,91]. In *Atsahh1*, DNA methylation is reduced in the TE-rich pericentromeric region (Figure 23) particularly in non-CG context. Further, metaplot analysis showed that the DNA methylation pattern over all TEs in the genome is diminished in *Atsahh1* (Figure 24B). In general, removal of those repressing epigenetic marks leads to transcriptional activation of TEs and repeated elements[266]. In this regard, a correlation between DNA hypomethylation and derepression of TEs in

Atsahh1 mutant was observed (Figure 27A, D and Figure 28B, F; note TE expression analysis on family level performed). In general, TEs can be divided into different classes[267]. Among them LTR/Copia and Line/L1 type TEs are predominantly regulated through H3K9me2 and non-CG DNA methylation pathways[264]. WGBS analysis revealed that a large portion of hypomethylated TEs in *Atsahh1* belong to those types of TEs (Figure 27D). These results support the hypothesis that *Atsahh1-kd* mainly effect the intertwined mechanisms maintaining non-CG and H3K9me2 methylation resulting in derepression of TEs.

5.3.2 Knock-down of *At*SAHH1 induced reduction of DNA methylation modestly effects gene transcription

To correlate the hypomethylated *Atsahh1* phenotype with gene expression an integrative analysis of WGBS and RNA-seq data was performed (Table 9). Metaplot analyses revealed that both up- and down-regulated genes show hypomethylation in their genic, 3kb up-, and 3kb down-stream flanking regions (Figure 30). This indicates that transcriptional changes occur largely independently of variation in DNA methylation. Accordingly, only 1.7% of DMGs (genes overlapping with DMRs in their genic, 3kb up- and 3kb-down-stream region) were differentially expressed in *Atsahh1* (Table 9).

In general, methylation of gene promoters is associated with silencing, but can also promote expression through poorly understood mechanisms[58]. In *Atsahh1* hypomethylation of the promoter region (3kb upstream) resulted in both down- and up-regulation of genes. In plants, gene body methylation is associated with intermediate expression level. However, some plants lack gene body methylation, and thus its role in transcriptional regulation is controversially discussed[106,268]. This integrative analysis revealed that both hyper- and hypo-methylation in the genic region of identified DMGs caused enhanced expression of those genes. Another remarkable observation was that DMGs harboring DMRs in their gene body, 3kb up- and 3kb down-stream flanking region (Figure 27B) were not differentially expressed. These results are in agreement with previous studies demonstrating that DNA methylation has only minor effects on gene expression[257]. Hence, the majority of differentially expressed genes is probably caused by pleiotropic effects of impaired *At*SAHH1 function, rather than on altered DNA methylation levels. For instance, GO term analysis of downregulated genes in *Atsahh1* revealed a significant enrichment of genes belonging to the term "DNA-binding transcription factor" (Supplemental Table 11). Further, methylation-dependent alteration in the transcriptional networks may contribute to alteration in gene expression[260].

It is noteworthily, that the integrative analysis identified three ethylene responsive transcription factors *AtERF5*, *AtERF13*, and *AtERF016* in *Atsahh1* (Table 9). Those genes are associated with hypo-DMR and downregulation. The ethylene biosynthesis relies on a continuous SAM supply, which is enhanced in *Atsahh1* (Figure 17). ERF proteins are involved in mediating responses to ethylene. For

instance, *At*ERF5 expression has a major repressive effect on genes related to ethylene synthesis[269]. Hence, its downregulation could result in enhanced ethylene synthesis to counteract the accumulation of SAM. Further, a hypo-DMG encoding the *At*VTL5 was found to be upregulated. *At*VTL5 is involved in the regulation of cellular iron homeostasis, conceivably by the transfer of iron ions from the cytosol to the vacuole for intracellular iron storage[262]. This suggests a nexus between the methylation cycle and iron homeostasis. Of note, the chlorophyll content, a hallmark for iron deficiency[247], is increased in *Atsahh1* (Supplemental Figure 8). Another interesting candidate uncovered in the integrative analysis is the At3g54730 locus encoding a putative transmembrane protein. The At3g54730 encoded gene is upregulated and associated with hypo-DMRs in its genic and a hyper-DMR in its 3kb downstream region. Interestingly, this gene is also upregulated in mutants with severe DNA hypomethylation such as *Atmet1-3*[270], *At*vim[270,271], and *Atdrm1drm2cmt2cmt3*[272].

6 Outlook

This study established that GSNO, the main source of bioavailable NO, functions as an epigenetic regulator in plants by impairing metaboloepigenetic processes. Indeed, exogenous and endogenous GSNO resulted in an impaired methylation cycle resulting in an altered methylation index, which is an important measure of the organismal methylation status. In this regard, enhanced endogenous RSNO/GSNO levels (*Atgsnor1-3*[45]) resulted in altered DNA and histone methylation levels in a modification specific manner. Although metaboloepigenetics is an emerging research field, the approaches that specifically address the interconnection between metabolism and epigenetics in plants are still sparse compared to animal models.

- In particular, the impact of GSNO/NO as well as ROS on epigenetic/metaboloepigenetics processes are of interest, as they fulfill integral stress signaling function and regulate cellular redox homeostasis[273]. Both are hallmarks of stress responses, and hence, they may also play a pivotal role in mediating chromatin dynamics during environmental stress responses. Hence, further research may focus on environmentally induced epigenetic and metaboloepigenetic changes and how these alterations might contribute to stress resistance in plants.

- Another aspect is to understand the molecular mechanisms of GSNO/NO induced alteration in chromatin marks. First, the effect of GSNO/NO on DNA and histone modifying enzymes may be investigated. In the animal field it was demonstrated, that NO affect histone methylation directly by inhibiting histone demethylases KDM3A through iron-nitrosyl formation in their catalytic center[63]. In plants, direct effects of GSNO/NOS on DNA and histone modifying enzymes remain elusive. Second the impact of GSNO/NO on cofactor/substrate availability of chromatin-modifying enzymes is worth investigating in plants using global metabolomic approaches in combination with techniques for epigenetic analysis.

- Further investigations may focus on the regulator function of *At*GSNOR1 on epigenetic methylation processes and metaboloepigenetic effects under environmental stress and developmental processes. Besides the usage of *Atgsnor1-3* plants, pharmacological approaches using the GSNOR specific inhibitor N6022[274] could be useful to understand the role of *At*GSNOR1 in epigenetic processes.

7 Supplement

7.1 Supplemental Figures

```
AtSAHH1  MALLVEKTSSGREYKVKDMSQADFGRLELELAEVEMPGLMACRTEFGPSQPFKGARITGSLHMTIQTAVLIETLTALGAEVRWCSCNIFS 90
AtSAHH2  MALLVEKTSSGREYKVKDMSQADFGRLEIELAEVEMPGLVSCVTEFGPSQPLKGARITGSLHMTIQTAVLIETLTALGAEVRWCSCNIFS 90
CeSAHH   ------MAQSKPAYKVADIKLADFGRKEIILAENEMPGLMARSKYGPSQPLKGARIAGCLHMTIQTAVLIETLTALGAEVQWSSCNIFS 84
DmSAHH   -------MS-KPSYKVADISLAEWGRKAIIIAENEMPGLMACRKKYGPSKPLKGARITGCLHMTVQTAVLIETLVELGAQVQWSSCNIFS 82
HsSAHH   -------MSDKLPYKVADIGLAAWGRKALDIAENEMPGLMRMRERYSASKPLKGARIAGCLHMTVETAVLIETLVTLGAEVQWSSCNIFS 83
LlSAHH   MALLVEKTTSGREYKVKDMSQADFGRLEIELAEVEMPGLMASRSEFGPSQPFKGAKITGSLHMTIQTAVLIETLTALGAEVRWCSCNIFS 90
MmSAHH   ------MSDKLPYKVADIGLAAWGRKALDIAENEMPGLMRMREMYSASKPLKGARIAGCLHMTVETAVLIETLVALGAEVRWSSCNIFS 83
NtSAHH   MALLVEKTTSGREYKVKDMSQADFGRLEIELAEVEMPGLMACRTEFGPSQPFKGAKITGSLHMTIQTAVLIETLTALGAEVRWCSCNIFS 90
ScSAHH   ------MSAPAQNYKIADISLAAFGRKEIELAEHEMPGLMAIRKAYGDVQPLKGARIAGCLHMTIQTAVLIETLVALGAEVTWSSCNIYS 84
TaSAHH   MALSVEKTSSGREYKVKDLFQADFGRLELELAEVEMPGLMACRTEFGPSQPFKGARISGSLHMTIQTAVLIETLTALGAEVRWCSCNIFS 90
                  **: *:   *  :**    :  :**  *****:       :.   :*:***:*:*.****::********. ***:*  *.****:*


AtSAHH1  TQDHAAAAIARDSAAVFAWKGETLQEYWWCTERALD-WGPGGGPDLIVDDGGDATLLIHEGVKAEEIFEKTGQVPDPTSTDNPEFQIVLS 179
AtSAHH2  TQDHAAAAIARDSAAVFAWKGETLQEYWWCTERALD-WGPGGGPDLIVDDGGDATLLIHEGVKAEEIFAKNGTFPDPTSTDNPEFQIVLS 179
CeSAHH   TQDHAAAAIAQTGVPVYAWKGETDEEYEWCIEQTIV-FKDGQPLNMILDDGGDLTNLVHA----------------------------- 143
DmSAHH   TQDNAAAAIAATGVPVYAWKGETDEEYMWCIEQTLV-FPDGQPLNMILDDGGDLTNLVHE----------------------------- 141
HsSAHH   TQDHAAAAIAKAGIPVYAWKGETDEEYLWCIEQTLY-FKDG-PLNMILDDGGDLTNLIHT----------------------------- 141
LlSAHH   TQDHAAAAIARDSAAVFAWKGETLQEYWWCTERALD-WGPGGGPDLIVDDGGDTTLLIHEGVKAEEIYEKSGQFPDPDSTDNAEFKIVLS 179
MmSAHH   TQDHAAAAIAKAGIPVFAWKGETDEEYLWCIEQTLH-FKDG-PLNMILDDGGDLTNLIHT----------------------------- 141
NtSAHH   TQDHAAAAIARDSAAVFAWKGETLQEYWWCTERALD-WGPGGGPDLIVDDGGDATLLIHEGVKAEEEFAKNGTIPDPNSTDNAEFQLVLT 179
ScSAHH   TQDHAAAAIAASGVPVFAWKGETEEEYLWCIEQQLFAFKDNKKLNLILDDGGDLTTLVHE----------------------------- 144
TaSAHH   SQDHAAAAIARDSAAVFAWKGETLEEYWWCTERCLD-WGVGGGPDLIVDDGGDATLLIHEGVKAEEEFEKSGKVPDPESTDNPEFKIVLT 179
              :**:****** . .*:****** :** ** *::  :   :    ::*.***** *  *:*                         96


AtSAHH1  IIKEGLQVDPKKYHKMKERLVGVSEETTTGVKRLYQMQQNGTLLFPAINVNDSVTKSKFDNLYGCRHSLPDGLMRATDVMIAGKVAVICG 269
AtSAHH2  IIKDGLQVDPKKYHKMKERLVGVSEETTTGVKRLYQMQETGALLFPAINVNDSVTKSKFDNLYGCRHSLPDGLMRATDVMIAGKVAVICG 269
CeSAHH   -----------KYPQYLAGIRGLSEETTTGVHNLAKMLAKGDLKVPAINVNDSVTKSKFDNLYGIRESLPDGIKRATDVMLAGKVAVVAG 222
DmSAHH   -----------KFPQYLKNIKGLSEETTTGVHNLYKMFKEGRLGVPAINVNDSVTKSKFDNLYGCRESLIDGIKRATDVMIAGKVCCVAG 220
HsSAHH   -----------KYPQLLPGIRGISEETTTGVHNLYKMMANGILKVPAINVNDSVTKSKFDNLYGCRESLIDGIKRATDVMIAGKVAVVAG 220
LlSAHH   IIKEGLKTDPKRYHKMKDRVVGVSEETTTGVKRLYQMQANGTLLFPAINVNDSVTKSKFDNLYGCRHSLPDGLMRATDVMIAGKVAVVAG 269
MmSAHH   -----------KYPQLLSGIRGISEETTTGVHNLYKMMSNGILKVPAINVNDSVTKSKFDNLYGCRESLIDGIKRATDVMIAGKVAVVAG 220
NtSAHH   IIKESLKTDPLKYTKMKERLVGVSEETTTGVKRLYQMQANGTLLFPAINVNDSVTKSKFDNLYGCRHSLPDGLMRATDVMIAGKVALVAG 269
ScSAHH   -----------KHPEMLEDCFGLSEETTTGVHHLYRMVKEGKLKVPAINVNDSVTKSKFDNLYGCRESLVDGIKRATDVMLAGKVAVVAG 223
TaSAHH   IIRDGLKTDASKYRKMKERLVGVSEETTTGVKRLYQMQESGTLLFPAINVNDSVTKSKFDNLYGCRHSLPDGLMRATDVMIAGKVAVVCG 269
                     *:*********:.* :*   * * .***************** *.** **: *****:****. ::.*


AtSAHH1  YGDVGKGCAAAMKTAGARVIVTEIDPICALQALMEGLQVLTLEDVVSEADIFVTTTGNKDIIMVDHMRKMKNNAIVCNIGHFDNEIDMLG 359
AtSAHH2  YGDVGKGCAAAMKTAGARVIVTEIDPICALQALMEGLQVLTLEDVVSEADIFCTTTGNKDIIMVDHMRKMKNNAIVCNIGHFDNEIDMLG 359
CeSAHH   YGDVGKGSAASLKAFGSRVIVTEIDPINALQAAMEGYEVTTLEEAAPKANIIVTTTGCKDIVTGKHFELLPNDAIVCNVGHFDCEIDVKW 312
DmSAHH   YGDVGKGCAQALKGFGGRVIVTEVDPINALQAAMEGYEVTTMEEASKEASIFVTTTGCRDIITSVHLQQMPDDAIVCNIGHFDIEIDVDW 310
HsSAHH   YGDVGKGCAQALRGFGARVIITEIDPINALQAAMEGYEVTTMDEACQEGNIFVTTTGCIDIILGRHFEQMKDDAIVCNIGHFDVEIDVKW 310
LlSAHH   YGDVGKGCAAALKQAGARVIVTEIDPICALQATMEGLQVTLEDVVSEADIFVTTTGNKDIIMLDHMKKMKNNAIVCNIGHFDNEIDMLG 359
MmSAHH   YGDVGKGCAQALRGFGARVIITEIDPINALQAAMEGYEVTTMDEACKEGNIFVTTTGCVDIILGRHFEQMKDDAIVCNIGHFDVEIDVKW 310
NtSAHH   YGDVGKGCAAALKQAGARVIVTEIDPICALQATMEGLQVLTLEDVVSDVDIFVTTTGNKDIIMVDHMRKMKNNAIVCNIGHFDNEIDMLG 359
ScSAHH   YGDVGKGCAAALRGMGARVLVTEIDPINALQAAMEGYQVVTMEDASHIGQVFVTTTGCRDIINGEHFINMPEDAIVCNIGHFDIEIDVAW 313
TaSAHH   YGDVGKGCAAALKQAGARVIVTEIDPICALQALMEGIQILTLEDVVSEADIFVTTTGNKDIIMVDHMRKMKNNAIVCNIGHFDNEIDMNG 359
         *******.* :::  *.**::**:*** **** *** :: *:::.   .:: ****  **:   *:    : ::****:**** ***:    215


AtSAHH1  LETYPGVKRITIKPQTDRWVFPETKAGIIVLAEGRLMNLGCATGHPSFVMSCSFTNQVIAQLELWNEKA------------SGKYEKKVY 437
AtSAHH2  LETYPGVKRITIKPQTDRWVFPDTNSGIIVLAEGRLMNLGCATGHPSFVMSCSFTNQVIAQLELWNEKS-----------SGKYEKKVY 437
CeSAHH   LNTN-ATKKDTIKPQVDRYTLKNGRH-VILLAEGRLVNLGCATGHPSFVMSNSFTNQVLAQVELWTKFGT-----------PQEYKLGLY 389
DmSAHH   LNAN-AKEKVNVKPQVDRYTMQSGKH-IILLAEGRLVNLGCAHGHPSFVMSNSFTNQVLAQIELWTK-------------SDKYAVGVH 384
HsSAHH   LNEN-AVEKVNIKPQVDRYRLKNGRH-IILLAEGRLVNLGCAMGHPSFVMSNSFTNQVMAQLELWTH-------------PDKYPVGVH 384
LlSAHH   LETHPGVKRITIKPQTDRWVFPETNTGIIILAEGRLMNLGCATGHPSFVMSCSFTNQVIAQLELWNEKS-----------SGKYEKKVY 437
MmSAHH   LNEN-AVEKVNIKPQVDRYWLKNGRH-IILLAEGRLVNLGCAMGHPSFVMSNSFTNQVMAQIELWTH-------------PDKYPVGVH 384
NtSAHH   LETYPGVKRITIKPQTDRWVFPDTNSGIIVLAEGRLMNLGCATGHPSFVMSCSFTNQVIAQLELWNEKS-----------SGKYEKKVY 437
ScSAHH   LKAN-AKECINIKPQVDRYLLSSGRH-VILLANGRLVNLGCATGHSSFVMSCSFSNQVLAQIALFKSNDKSFREKHIEFQKTGPFEVGVH 401
TaSAHH   LETYPGVKRITIKPQTDRWVFPETKTGIIVLAEGRLMNLGCATGHPSFVMSCSFTNQVIAQLELWNEKA------------SGKYEKKVY 437
         *:    . :  .:***.**: :  .  :*:**:***:***** **.***** **:***:**: *:.              . :   :: 263


AtSAHH1  VLPKHLDEKVALLHLGKLGARLTKLSKDQSDYVSIPIEGPYKPPHYRY 485
AtSAHH2  VLPKTLDEKVAALHLGKLGARLTKLTKDQSDYVSIPVEGPYKPVHYRY 485
CeSAHH   VLPKTLDEEVAYLHLAQLGVKLTKLSDEQASYLGVPVAGPYKPDHYRY 437
DmSAHH   VLPKILDEEVASLHLEKLGVKLTKLTEKQATYLGVSQTGPFKPDHYRY 432
HsSAHH   FLPKKLDEAVAEAHLGKLNVKLTKLTEKQAQYLGMSCDGPFKPDHYRY 432
LlSAHH   VLPKHLDEKVAALHLEKLGAKLTKLSKDQADYISVPVEGPYKPFHYRY 485
MmSAHH   FLPKKLDEAVAEAHLGKLNVKLTKLTEKQAQYLGMPINGPFKPDHYRY 432
NtSAHH   VLPKHLDEKVAALHLGKLGAKLTKLSKDQADYISVPVEGPYKPAHYRY 485
ScSAHH   VLPKILDEAVAKFHLGNLGVRLTKLSKVQSEYLGIPEEGPFKADHYRY 449
TaSAHH   VLPKHLDEKVAALHLGKLGARLTKLTKSQSDYISIPIEGPYKLRLYRY 485
         .*** *** **  ** :*..:****:. *: *:.:.  **:*   *** 293
```

Supplemental Figure 1. Multiple sequence alignment of SAHH. Amino acid sequence alignment of SAHH of *Arabidopsis thaliana* (*At*), *Caenorhabditis elegans* (*Ce*), *Drosophila melanogaster* (*Dm*), *Homo sapiens* (*Hs*), *Lupinus luteus* (*Ll*), *Mus musculus* (*Mm*), *Nicotiana tabacum* (*Nt*), *Saccharomyces cerevisiae* (*Sc*), and *Triticum aestivum* (*Ta*). The protein abbreviation and UniProt identification number are as follows: *At*SAHH1 (O23255), *At*SAHH2 (Q9LK36), *Ce*SAHH (P27604), *Dm*SAHH (Q27580), *Hs*SAHH1 (P23526), *Ll*SAHH (Q9SP37), *Mm*SAHH (P50247), *Nt*SAHH (P68173), *Sc*SAHH (P39954), *Ta*SAHH (P32112). The multiple sequence alignment was performed using ClustalW[218] in   Edit Software[219]. Cysteine residues are highlighted in orange. The asterisks at the bottom line of the alignment indicate fully conserved residues in each sequence position, while single and double dots refer to highly and moderately conserved (chemically similar) residues, respectively.
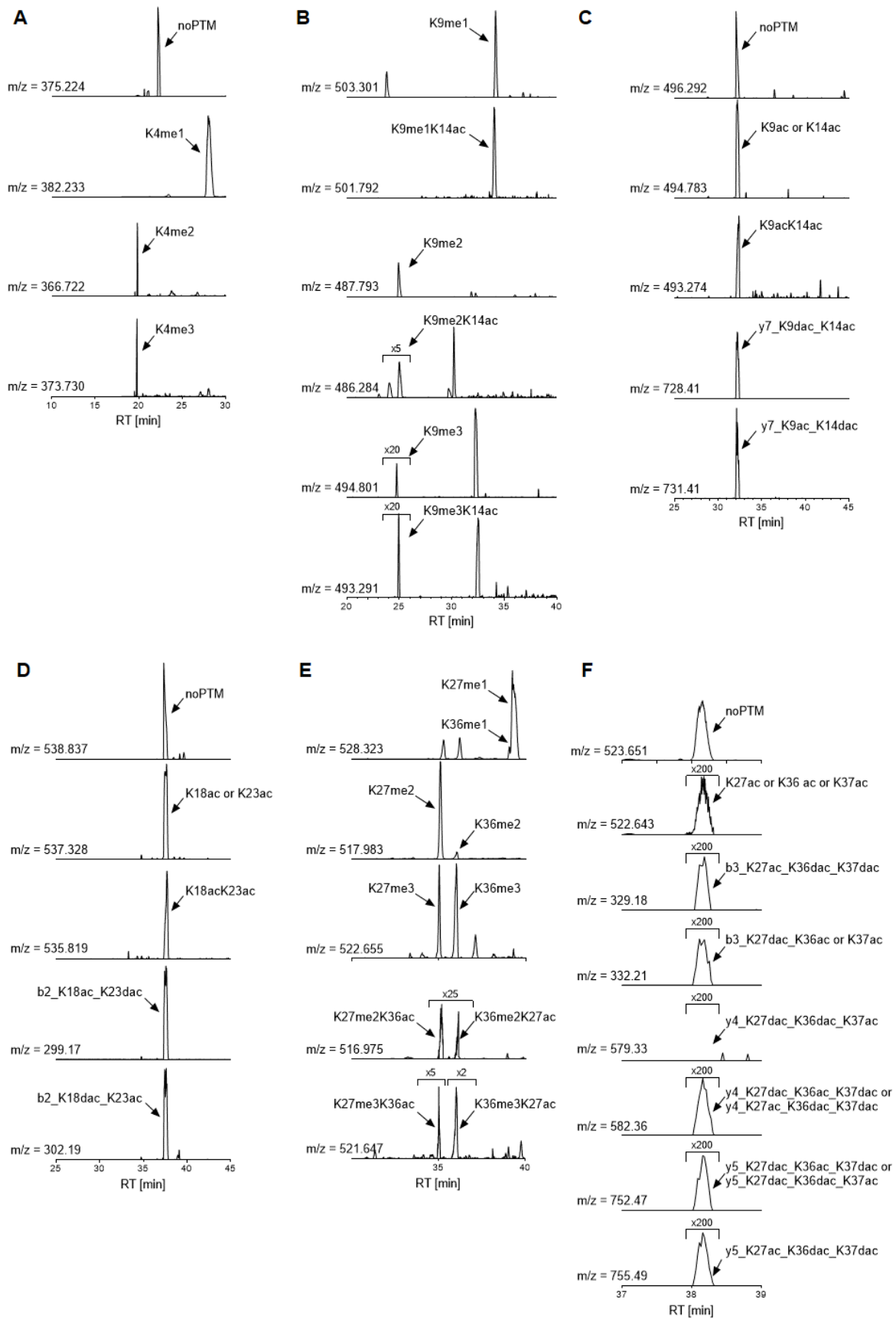
Supplemental Figure 2. Chromatographic separation of histone PTM motifs. Chromatograms for the H3.3-8 peptides **(A)**, H3.9-17 methylated peptides **(B)**, H3.9-18 acetylated peptides **(C)**, H3.18-26 **(D)**, H3.1.27-40 methylated peptides and methylated/acetylated peptides **(E)**, and H3.1.27-40 acetylated peptides **(F)**. Lysine methylation results in characteristic shifts

in retention: tri-methylated peptides elute shortly before di-methylated ones, followed by unmethylated and mono-methylated peptides. Note that unmodified lysines and mono-methylated lysines are reactive to d6-acetic anhydride, but di- and tri-methylated lysines are not. Masses corresponding to mono-methylation (528.323) belong to H3K27me1 and H3K36me1. Due to the endogenous mono-methyl/chemical d3-acetyl at the N-terminus in H3K27me1, it is more hydrophobic and elutes after H3K36me1. A more N-terminal methyl group (K27me) elutes before a more central methyl group (K36me). Endogenously acetylated and chemically acetylated lysines co-elute during chromatography. Note that peptide H3.27-40 is only analyzed for histone variant H3.1. Acetylation on H3.1K37ac was not detected. Figure modified from Ref.[192].
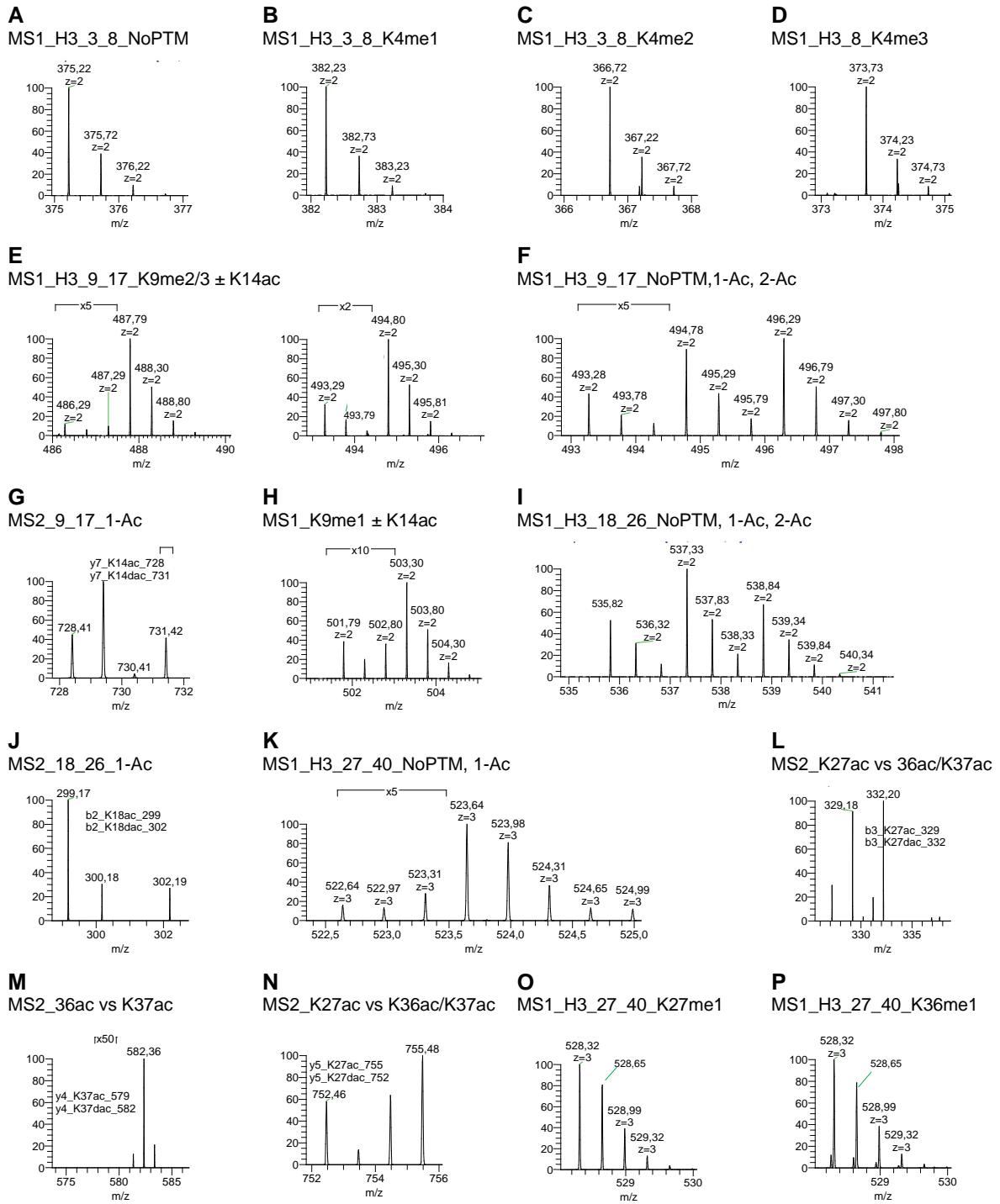
Q

MS1_27_40_K27me2 ± 1-Ac and K27me3 ± 1-Ac
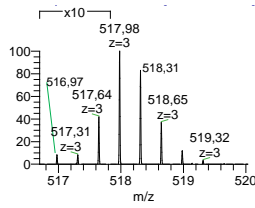
R

MS1_27_40_K36me2 ± 1-Ac and K36me3 ± 1-Ac
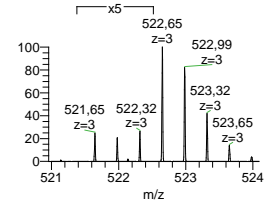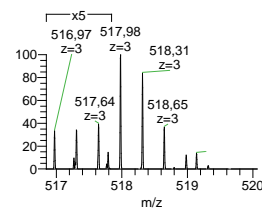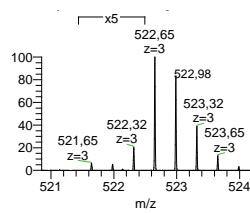
Supplemental Figure 3. MS1 and MS2 spectra for quantification of H3 motifs. MS spectra are related to Supplemental Figure 2 and Supplemental Table 8. **(A-D)** MS1 spectra of H3.3-8 peptide, with no modification, H3.K4me1, H3.K4me2, and H3.K4me3. **(E, F, H)** MS1 spectra of H3.9-17 peptide, with H3.K9me2/3 ± K14ac, unmodified-, mono- and di-acetylated H3.9-17 peptides, and H3.K9me1 ± K14ac. **(G)** MS2 on mono-acetylated H3.9-17 to differentiate between H3.K9ac and H3.K14ac. Only diagnostic y7 ion pair is shown. **(I)** MS1 spectrum of H3.18-26 peptide with unmodified-, mono- and di-acetylated isoforms. **(J)** MS2 on mono-acetylated H3.18-26 to differentiate between H3.K18ac and H3.K23ac. Only diagnostic b2 ion pair is shown. **(K, O, P, Q, R)** MS1 spectra of H3.27-40 peptide, with unmodified- and mono-acetylated isoforms of the non-methylated peptide, H3.K27me1, H3.K36me1, H3.K27me2/3 ± K36ac, and H3.K36me2/3 ± K27ac. **(L-M)** MS2 on mono-acetylated H3.27-R40 is required to distinguish H3.K27ac, H3.K36ac, and H3.K37ac. Only diagnostic b3, y4, and y5 ions pairs are shown. Note that peptide H3.27-40 is only analyzed for histone variant H3.1. For quantification details refer to Ref.[192].
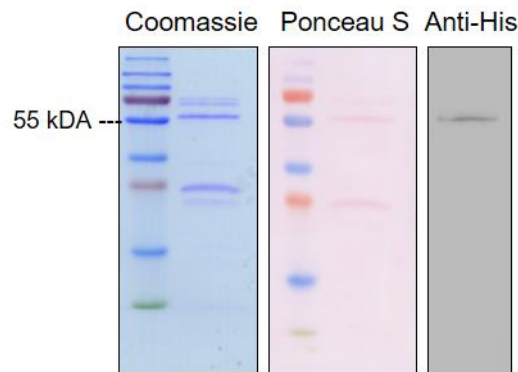
Supplemental Figure 4. Recombinant production of *At*SAHH1 in *E. coli* BL21 (DE3). 12% SDS-PAGE and western blot analysis of recombinant N-terminal His-tagged *At*SAHH1 produced in *E. coli* (56 kDa). The western blot was probed with primary Anti-His (6x) and then labeled with Anti-Mouse IgG and Western Lightning® Plus-ECL substrate. Ponceau S is shown as loading control. The positions of 55 kDa marker is indicated.
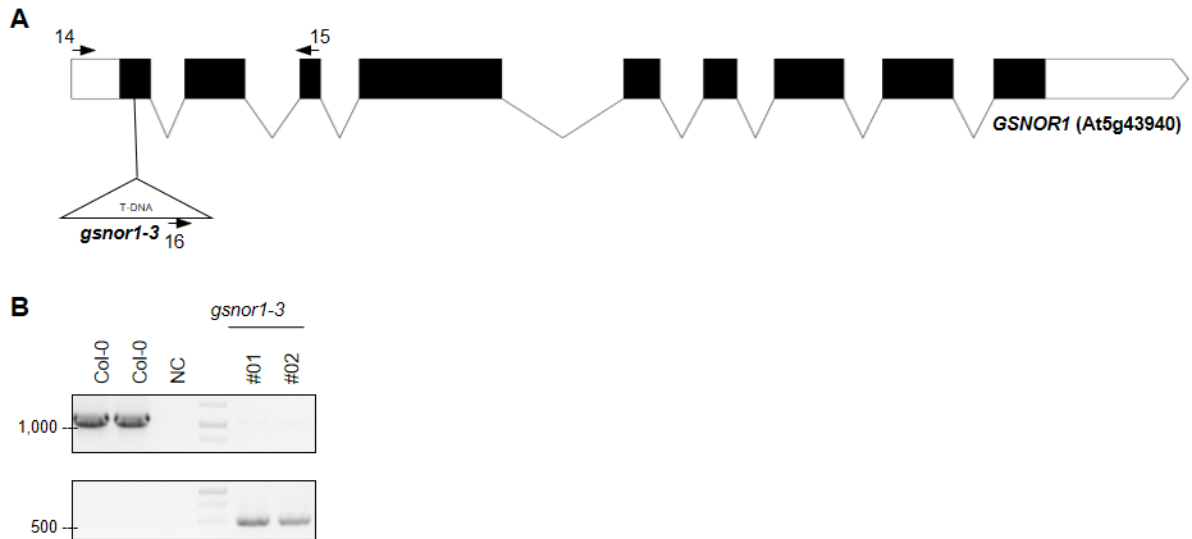
Supplemental Figure 5. PCR-based genotyping of *Atgsnor1-3*. Homogeneity for *Atgsnor1-3* (GABI-Kat 315D11; also named *hot5-2*) mutant lines were confirmed. **(A)** The diagram shows the position of the T-DNA insertion and primer (indicated with arrows) used for genotyping. Black box, coding region; open box, untranslated region; solid black line, intron. Amplicon length, primers, and PCR conditions are listed in Supplemental Table 4. The position of the T-DNA insertion in *Atgsnor1-3* is in the 5´UTR and in the first exon, respectively. **(B)** PCR-based genotyping of *Atgsnor1-3*. DNA ladder (bps) is indicated.
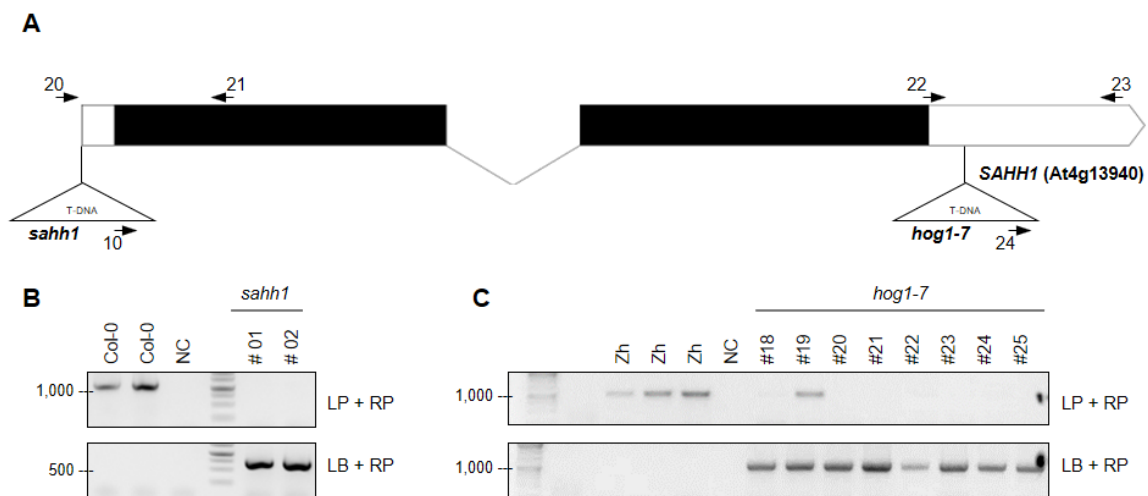
Supplemental Figure 6. PCR-based genotyping of mutants of *AtSAHH1*. (A) The diagram shows the position of the T-DNA insertion sites and primers (indicated with arrows) used for genotyping. Black box, coding region; open box, untranslated region; solid black line, intron. Amplicon length, primers, and PCR conditions are listed in Supplemental Table 4. *AtSAHH1* encodes a SAH hydrolase and is also named *AtHOG1* (homology-dependent gene silencing 1). The T-DNA insertion of the mutant lines *Atsahh1*[121,124,170] and *Athog1-7*[120] are located in the 5´UTR and 3´UTR, respectively. The mutants *Atsahh1* and *Athog1-7* are in the background of accession Columbia and Zürich, respectively. Homogeneity for **(B)** *Atsahh1* and **(C)** *Athog1-7* (except line 19) was confirmed. DNA ladder (bps) is indicated.
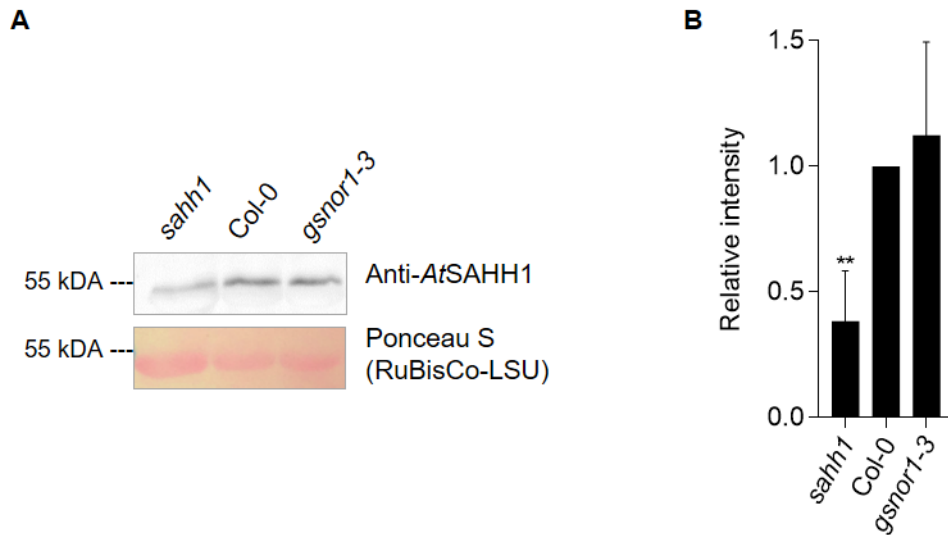
Supplemental Figure 7. *At*SAHH1 protein level is decreased in *Atsahh1*. (A) <u>Western blot analysis</u> of *At*SAHH1 (54 kDa). Total proteins were extracted from in 4-week-old rosette leaves grown under long-day condition harvested 5 h after day-time start in two volumes of HEN buffer and 15 µg of each protein extract was electrophoretically separated by 13.5% SDS-PAGE gel and transferred onto a nitrocellulose membrane. The western blot was probed with primary anti-*At*SAHH1 antibody[197] and then labeled with anti-rabbit IgG and Western Lightning® Plus-ECL substrate. One representative immunoblot is shown. **(B)** <u>Quantification of western blot results</u> in A. Signal intensities were measured using ImageJ software and normalized to the amount of loaded RuBisCo-LSU (53 kDa). <u>Statistics:</u> Values are expressed as fold change over wild-type and represent the mean ± SD of three independent experiments (n = 5-6). **(p<0.01) represent significant differences between wild-type and mutant lines (ANOVA, Dunnett´s multiple comparisons test).
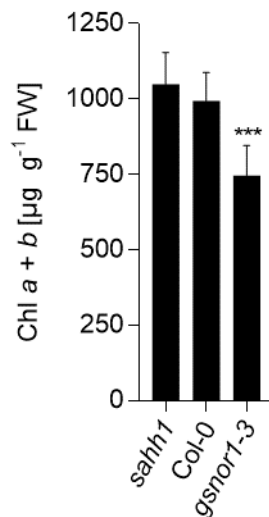
Supplemental Figure 8. Chlorophyll content is decreased in *Atgsnor1-3*. Analysis of chlorophyll *a* and *b* content in 4-week-old rosette leaves grown under long-day condition harvested 5 h after day-time start from wild-type, *Atsahh1*, and *Atgsnor1-3* lines. <u>Statistics:</u> Values are normalized against total fresh weight and represent the mean ± SD (n ≤ 19) of three independent experiments. ***(p<0.001) represents significant differences between wild-type and mutant lines (Kruskal-Wallis test, Dunn´s multiple comparison test).
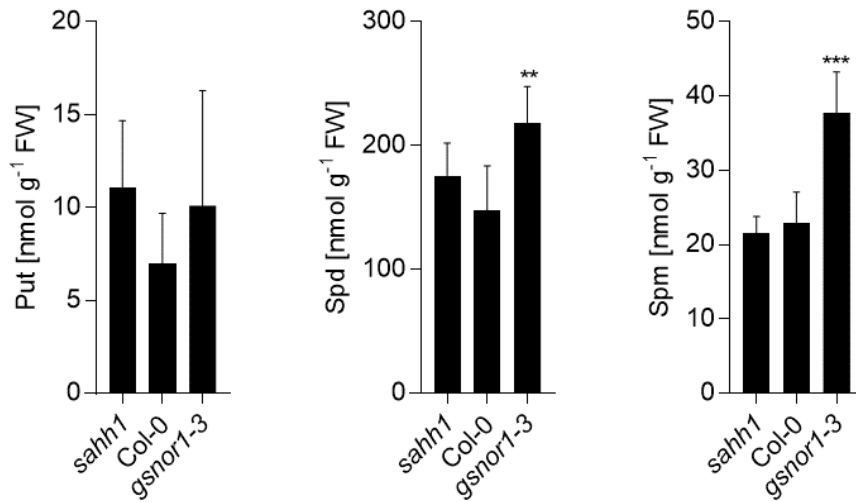
Supplemental Figure 9. Polyamine levels are altered in *Atgsnor1-3*. The levels of free putrescine (put), spermidine (spm), and spermine (spd) were quantified with HPCL after pre-column derivatization with FMOC-Cl in perchloric acid extracts of 4-week-old rosette leaves grown under long-day condition harvested 5 h after day-time start from wild-type, *Atsahh1*, and *Atgsnor1-3* lines. Statistics: Values are normalized against total fresh weight and represent the mean ± SD (n = 4-5) of two independent experiments. **(p<0.01) and ***(p<0.001) represents significant differences between wild-type and mutant (ANOVA, Dunnett´s multiple comparison test).
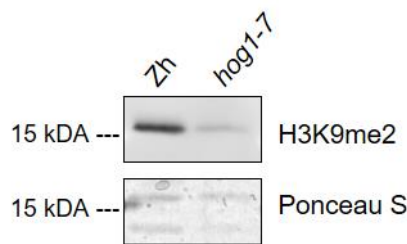
Supplemental Figure 10. Histone H3K9me2 methylation is decreased in *Athog1-7*. Histones were acid-extracted from leaves of 4-week-old plants grown under LD condition harvested 5 h after day-time start from *Athog1-7* (allele of *Atsahh1*) and the corresponding Zh wild-type and probed against H3K9me2 marks by western blot. As loading control, the Ponceau S stained membrane is shown. One representative experiment is shown. The experiment was repeated twice with similar results and is in accordance with previous studies[120].

Supplemental Figure 11. DNA methylation analysis by chop-PCR in the accession Zürich and Col-0 and in *Athog1-7*. DNA methylation of indicated loci were determined by chop-PCR in 4-week-old rosette leaves grown under LD condition harvested 5 h after day-time start from Zürich wild-type (Zh), *Athog1-7*, and Col-0 wild-type. **(A)** McrBC analysis of *Line1-4* in *Athog1-7* and the corresponding background of accession Zürich. *AtLine1-4* is hypo-methylated in *Athog1-7* as previously demonstrated[120]. **(B)** The amplification of *AtTSI* in Col-0 wild-type results in two products of 598 bps (TSI) and 318 bps (AT3G32980) according to BLASTN, compared to Zürich wild-type, as previously demonstrated[275]. *AtLine1-4* is a retrotransposon; *TSI*, transcriptionally silent information.
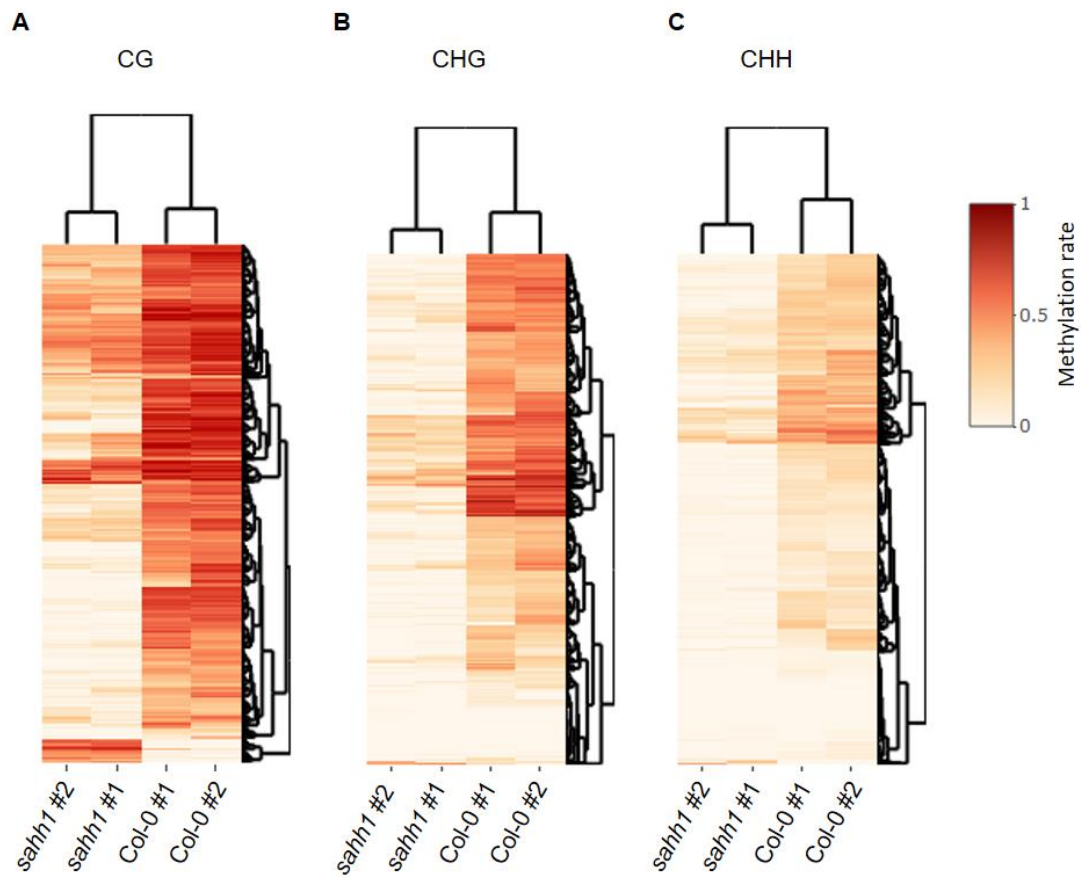
Supplemental Figure 12. WGBS analysis revealed enrichment of hypo-DMRs in each sequence context in *Atsahh1*. Heatmaps of hierarchically clustered CG **(A)**, CGH **(B)**, and CHH **(C)** DMRs identified in pairwise comparison of wild-type versus *Atsahh1* methylome. DNA was extracted from 4-week-old rosette leaves grown under long-day condition harvested 5 h after day-time start and subjected to WGBS. Heatmaps represent the methylation level across DMRs per sequence context: Red = 100% methylated, white = 0% methylated. Two biological replicates were analyzed for each genotype. R was used for imaging.
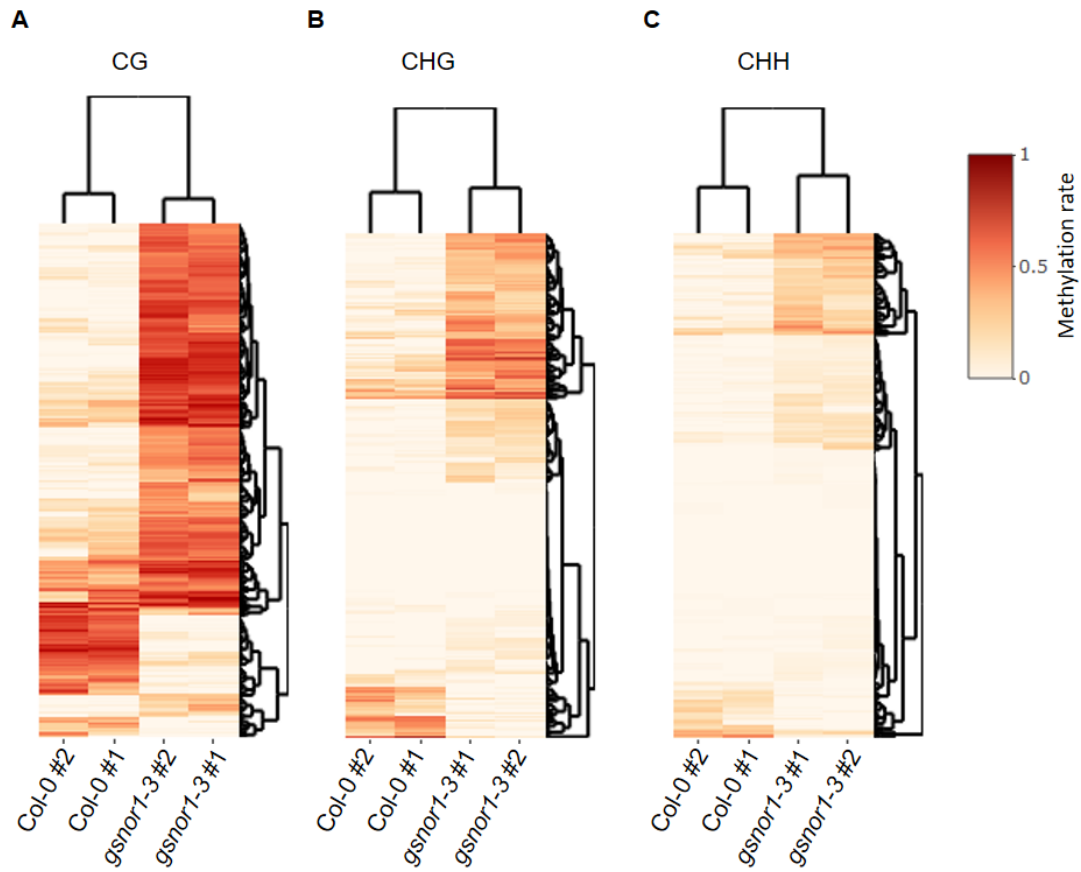
Supplemental Figure 13. WGBS analysis revealed enrichment of hyper-DMRs in each sequence context in *Atgsnor1.3*.
Heatmaps of hierarchically clustered CG **(A)**, CGH **(B)**, and CHH **(C)** DMRs identified in pairwise comparison of wild-type versus *Atgsnor1-3* methylome. DNA was extracted from 4-week-old rosette leaves grown under long-day condition harvested 5 h after day-time start and subjected to WGBS. Heatmaps represent the methylation level across DMRs per sequence context: Red = 100% methylated, white = 0% methylated. Two biological replicates were analyzed for each genotype. R was used for imaging.
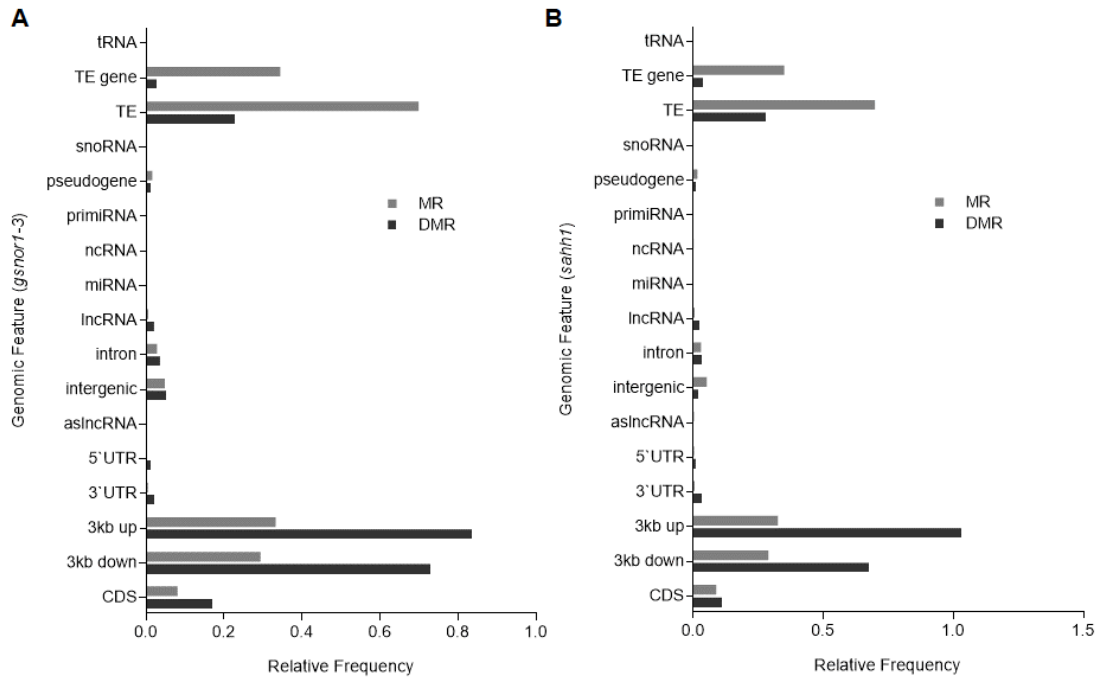
Supplemental Figure 14. Annotation of DMRs to genomic features. Genomic context of MRS and DMRs identified in *Atgsnor1-3* **(A)** and *Atsahh1* **(B)**. TAIR 10 was used for annotation of genomic elements. MRs and DMRs were assigned to the following annotated elements: coding sequence (CDS), 3kb up- and 3kb down-stream of protein coding genes, 5' UTR, 3' UTR, as-lncRNA, intergenic, intron, lncRNA, miRNA, ncRNA, pri-miRNA, pseudogene, snoRNA, transposable element (TE), TE gene, and tRNA. Genomic feature annotation performed by Patrick Hüther (Becker Lab, Gregor Mendel Institute Vienna).
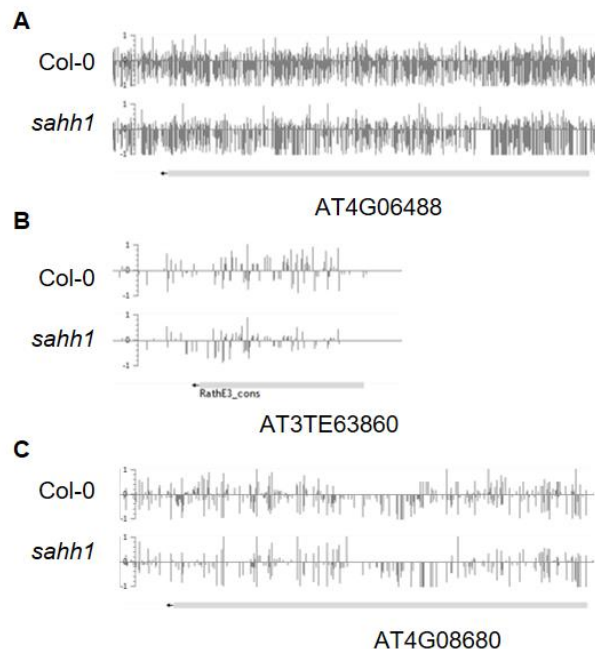
Supplemental Figure 15. Snapshots in the EPIC-CoGE browser. Snapshots showing DNA methylation levels of loci identified as hypomethylated by chop-PCR (methylation rate in all three sequence contexts are shown). DNA methylation data have been uploaded to the epigenome browser of EPIC (EPIC-CoGe) by Prof. Dr. Claude Becker (ID 2234 unpublished). DNA methylation analysis were performed in duplicates and average methylation ratios calculated in the CoGE browser are shown. DNA methylation of **(A)** At4g06488 (*AtTa2*), **(B)** At3TE63860 (*AtSN1*) is also annotated as RATHE3_cons (www.arabiodopsis.com), and **(C)** At4g08680 (*AtMu1*) in wild-type and *Atsahh1* plants is shown.

7.2 Supplemental Tables

Supplemental Table 1. Computational prediction of *At*SAHH1 S-nitrosation sites. The following S-nitrosation site-prediction programs were used: GPS-SNO 1.0[276], SNOSite[277], iSNO-AAPair[278], and iSNO-PseAAC[279].

	Program	Predicted Cys-NO sites
GPS-SNO 1.0	Low threshold	C42, C277, C411
	Medium threshold	C42
	High threshold	C42
SNOSite	Specificity level low	C84, C86, C244, C277, C297, C400
	Specificity level medium	C42, C84, C86, C244, C268, C277, C297, C346, C400
	Specificity level high	C42, C84, C86, C244, C268, C277, C297, C346, C400, C411
iSNO-AAPair		C268, C297, C346
iSNO-PseAAC		C86, C120, C244, C268, C277, C346

Supplemental Table 2. List of reagents and resources used.

Resources	Source, Reference	Identification number
Antibodies		
Anti-AtSAHH1 antibody (rabbit pAb)	Barbara Moffat; Ref.[197]	
Anti-Biotin (mouse, mAb), Alkaline phosphatase Conjugate	Sigma-Aldrich (Steinheim, Germany)	A6561
Anti-HA antibody (rabbit pAb)	Sigma-Aldrich (Steinheim, Germany)	H6908
Anti-Histidine-Tagged Protein (mouse mAb)	Merck (Darmstadt, Germany)	OB05
Anti-Histone H3 antibody (rabbit pAb)	Agrisera AB (Vännäs, Sweden)	AS10 710
Anti-Histone H3 di methyl K9 (H3K9me2; mouse mAb)	Abcam (Cambridge, UK)	Ab1220
Anti-Mouse IgG (H+L), HRP Conjugate	Promega (Madison, WI, USA)	W4021
Anti-Rabbit IgG (H+L), HRP Conjugate	Promega (Madison, WI, USA)	W4011
Antibiotics		
Ampicillin sodium (Amp; 100 mg ml-1 stock in ddH2O)	Duchefa Biochemie (Haarlem, The Netherlands)	A0104
Gentamycin sulphate solution (Gent; 50 mg ml-1 stock in ddH2O)	Carl Roth (Karlsruhe, Germany)	HN09
Kanamycin sulphate monohydrate (Kan; 50 mg ml-1 stock in ddH2O)	Duchefa Biochemie (Haarlem, The Netherlands)	K0126
Rifampicin (Rif; 10 mg ml-1 stock in methanol)	Duchefa Biochemie (Haarlem, The Netherlands)	R0146
***Arabidopsis* lines**		
Arabidopsis thaliana ecotype Columbia (Col-0)	AG Lindermayr; Lehle Seeds	
Arabidopsis thaliana ecotype Zürich (Zh)	Ortrun Mittelsten Scheid	
Atgsnor1-3 (also named *hot5-2*)	Gabi-Kat; [45,46]	GABI-Kat 315D11
Athog1-7	Ortrun Mittelsten Scheid; [120]	
Atsahh1	NASC; [121,124,170]	SALK_068487
AtTS-GUS (L5, former 6b5)	Hervé Vaucheret; [171]	
AtTS-GUS x *gsnor1-3*		This study.
AtTS-GUS x *sahh1*		This study.
35S: AtSAHH1-HA-StrepIII		This study.
***Arabidopsis* cultivation**		
2-(N-Morpholino)-ethane sulfonic acid monohydrate PUFFERAN® ≥99,5 % (MES)	Carl Roth (Karlsruhe, Germany)	6066
Amblyseius cucumeris	Sautter & Stepper (Ammerbuch, Germany)	952
Cell culture 6 well plates Cellstar®	Greiner Bio-One (Kremsmünster, Austria)	657160
D(+)-Saccharose ≥99,5 %, p.a.	Carl Roth (Karlsruhe, Germany)	4621
DanKlorix hygiene cleaners (bleach)	CP GABA (Hamburg, Germany)	N-11648

Ethanol absolute for analysis EMSURE® ACS, ISO, Reag. Ph Eur.	Merck (Darmstadt, Germany)	100983
Floradur® B Seed Propagation Substrate	Floragard (Oldenburg, Germany)	10220
Glufosinate-ammonium (BASTA®)	Hoechst Landwirtschaft (Frankfurt, Germany)	
Hypoaspis miles	Sautter & Stepper (Ammerbuch, Germany)	hyp0
Murashige & Skoog medium including vitamins	Duchefa Biochemie (Haarlem, The Netherlands)	M0222
Neudomück®	W. Neudorff (Emmerthal, Germany)	N14294
Potassium hydroxide pellets for analysis EMSURE®	Merck (Darmstadt, Germany)	105033
Propagator lid	Romberg (Ellerau, Germany)	74062K
Seeding tray TEKU®	Pöppelmann (Lohne, Germany)	PL 2838/24
Silica sand Dorsilit® 7 FG 0,6 - 1,2 mm	Dorfner Kaolin- und Kristallquarzsand-Werke (Hirschau, Germany)	

Bacterial strains		
E. coli DH5α F– Φ80lacZΔM15 Δ(lacZYA-argF) U169 recA1 endA1 hsdR17 (rK–, mK+) phoA supE44 λ– thi-1 gyrA96 relA1	Invitrogen (Carlsbad, CA, USA)	
E. coli BL21 (DE3) fhuA2 [lon] ompT gal (λ DE3) [dcm] ΔhsdS λ DE3 = λ sBamHIo ΔEcoRI-B int::(lacI::PlacUV5::T7 gene1) i21 Δnin5	Invitrogen (Carlsbad, CA, USA)	
E. coli DB3.1 F- gyrA462 endA1 glnV44 Δ(sr1-recA) mcrB mrr hsdS20(rB-, mB-) ara14 galK2 lacY1 proA2 rpsL20(Smr) xyl5 Δleu mtl1	Invitrogen (Carlsbad, CA, USA)	
Agrobacterium tumefaciens GV3101::pMP90	provided by AG Erwin Grill; [174]	

Reagents and Chemicals		
1,4-Dithiothreitol ≥99 %, p.a. (DTT)	Carl Roth (Karlsruhe, Germany)	6908
1,7-Diaminoheptane 98% (DIA)	Sigma-Aldrich (Steinheim, Germany)	D17408
2-(4-Carboxyphenyl)-4,4,5,5-tetramethylimidazoline-1-oxyl-3-oxide potassium salt (cPTIO)	Santa Cruz Biotechnology (Dallas, Texas, USA)	sc-202985
2-Mercaptoethanol ≥99.0%	Sigma-Aldrich (Steinheim, Germany)	M6250
5-Bromo-4-chloro-3-indolyl β-D-glucuronide sodium salt ≥99 %, for microbiology (X-Gluc)	Carl Roth (Karlsruhe, Germany)	0018
9-(2',3'-Dioxypropyl)-adenine (DHPA)	Sigma-Aldrich (Steinheim, Germany)	T341754
Acetic acid (glacial) 100 %, Ph.Eur., extra pure	Carl Roth (Karlsruhe, Germany)	6755
Acetic acid (glacial) 100% anhydrous for analysis EMSURE® ACS, ISO, Reag. Ph Eur.	Merck (Darmstadt, Germany)	100063
Acetic anhydride-d6 99 atom % D	Sigma-Aldrich (Steinheim, Germany)	175641
Acetone for analysis EMSURE® ACS, ISO, Reag. Ph Eur.	Merck (Darmstadt, Germany)	100014
Acetonitrile ROTISOLV® ≥99,98%, Ultra LC-MS (ACN)	Carl Roth (Karlsruhe, Germany)	HN40.1
Acrylamide, 2x cryst. ≥98 % (LPA)	Carl Roth (Karlsruhe, Germany)	7871
Ammonium hydrogen carbonate ≥99%, p.a. (ABC)	Carl Roth (Karlsruhe, Germany)	T871
Ammonium persulfate for electrophoresis, ≥98% (APS)	Sigma-Aldrich (Steinheim, Germany)	A3678
ATX Ponceau S red staining solution	Sigma-Aldrich (Steinheim, Germany)	9189
Bio-Rad Protein Assay Dye Reagent	Bio-Rad Laboratories (Hercules, CA, USA)	5000006
Bovine serum albumin cryst. lyophil. (BSA)	SERVA Electrophoresis (Heidelberg, Germany)	11930
Bromophenol blue indicator ACS, Reag. Ph Eur	Merck (Darmstadt, Germany)	108122
Chloroform for analysis EMSURE® ACS, ISO, Reag. Ph Eur	Sigma-Aldrich (Steinheim, Germany)	1.02445
Chloroform: Isoamyl alcohol 24:1	AppliChem (Darmstadt, Germany)	A1935
Coomassie® Brilliant blue G250	Merck (Darmstadt, Germany)	15444
D(+)-Saccharose ≥99,5 %, p.a.	Carl Roth (Karlsruhe, Germany)	4621
Dimethyl sulfoxide ACS spectrophotometric grade, ≥99.9% (DMSO)	Sigma-Aldrich (Steinheim, Germany)	154938

Di-Potassium hydrogen phosphate ≥99 %, p.a., anhydrous (K2HPO4)	Carl Roth (Karlsruhe, Germany)	P749
Di-Sodium hydrogen phosphate dihydrate ≥99,5 %, p.a. (Na2HPO4 x 2 H2O)	Carl Roth (Karlsruhe, Germany)	4984
DNA Agarose	Biozym Scientific (Hessisch Oldendorf, Germany)	870055
dNTP Set 100 mM Solutions	Thermo Fischer Scientific (Waltham, MA, USA)	R0181
Ethanol absolute for analysis EMSURE® ACS, ISO, Reag. Ph Eur.	Merck (Darmstadt, Germany)	100983
Ethidium bromide solution 1% (EtBr)	Carl Roth (Karlsruhe, Germany)	2218
Ethylenediamine tetraacetic acid ≥99 %, p.a., ACS (EDTA)	Carl Roth (Karlsruhe, Germany)	8040
Ethylenediamine tetraacetic acid disodium salt dihydrate ≥99 %, p.a., ACS (EDTA)	Carl Roth (Karlsruhe, Germany)	8043
EZ-Link™ HPDP-Biotin	Thermo Fischer Scientific (Waltham, MA, USA)	21341
Fmoc chloride BioReagent, ≥99.0% (HPLC)	Sigma-Aldrich (Steinheim, Germany)	23184
Formaldehyde solution for molecular biology, 36.5-38% in H2O	Sigma-Aldrich (Steinheim, Germany)	F8775
Gene Ruler 1kB DNA Ladder	Thermo Fischer Scientific (Waltham, MA, USA)	SM0241
GeneRuler 100 bp DNA Ladder	Thermo Fischer Scientific (Waltham, MA, USA)	SM0321
Glycerol ROTIPURAN® ≥99,5 %, p.a., anhydrous	Carl Roth (Karlsruhe, Germany)	3783
Glycine ≥99 %, Blotting-Grade	Carl Roth (Karlsruhe, Germany)	0079
Glycine CELLPURE® ≥99 % For cell culture and biochemistry	Carl Roth (Karlsruhe, Germany)	HN07
Guanidinium thiocyanate for synthesis	Merck (Darmstadt, Germany)	820613
Hepes PUFFERAN® ≥99,5 %, p.a.	Carl Roth (Karlsruhe, Germany)	9105
Hexadecyltrimethylammonium bromide ≥98% (CTAB)	Sigma-Aldrich (Steinheim, Germany)	H-5882
Histone from calf thymus Type II-A, lyophilized powder	Sigma-Aldrich (Steinheim, Germany)	H9250
Hydrochloric acid ROTIPURAN® 37 %, p.a., ACS, ISO (HCl)	Carl Roth (Karlsruhe, Germany)	4625
Imidazol ≥99.9 %	Carl Roth (Karlsruhe, Germany)	3899
Iodine ACS reagent, ≥99.8%, solid (I2)	Sigma-Aldrich (Steinheim, Germany)	20777-2
Isopropanol GR for Analysis, ACS, ISO, Reagent Ph Eur	Sigma-Aldrich (Steinheim, Germany)	1.09634
Isopropyl-β-D-thiogalactopyranoside ≥99 %, for biochemistry (IPTG)	Carl Roth (Karlsruhe, Germany)	CN08
L(+)-Ascorbic acid sodium salt BioXtra, ≥99.0% (NT) (Asc)	Sigma-Aldrich (Steinheim, Germany)	11140
LB Broth High salt; LB-Miller	Duchefa Biochemie (Haarlem, The Netherlands)	L1704
L-Glutathione reduced ≥98.0% (GSH)	Sigma-Aldrich (Steinheim, Germany)	G4251
Magnesium chloride hexahydrate ≥99 %, p.a. (MgCl2 x 6 H2O)	Carl Roth (Karlsruhe, Germany)	2189
Methanol for analysis EMSURE® ACS, ISO, Reag. Ph Eur. (MeOH)	Merck (Darmstadt, Germany)	106009
Methanol ROTISOLV® ≥99,95%, LC-MS-Grade (MeOH)	Carl Roth (Karlsruhe, Germany)	AE71.1
N,N,N',N'-Tetramethylethylendiamin (Temed)	Merck (Darmstadt, Germany)	110732
N,N-Dimethylformamide (DMF)	Fluka (Buchs, Switzerland)	40255
Neocuproine ≥98%	Sigma-Aldrich (Steinheim, Germany)	N1501
N-Ethylmaleimide BioXtra, ≥98% (NEM)	Sigma-Aldrich (Steinheim, Germany)	E1271
Oligonucleotides	Eurofins Genomics (Ebersberg, Germany)	
PageRuler Prestained Protein Ladder	Thermo Fischer Scientific (Waltham, MA, USA)	26616, 26619, 26628
Perchloric acid puriss. p.a. (PCA)	Sigma-Aldrich (Steinheim, Germany)	30755
Polyvinylpyrrolidone (PVP-40)	Sigma-Aldrich (Steinheim, Germany)	PVP40
Potassium chloride ≥99,5 %, p.a. (KCl)	Carl Roth (Karlsruhe, Germany)	6781

Potassium dihydrogen phosphate ≥99 %, p.a., ACS (KH2PO4)	Carl Roth (Karlsruhe, Germany)	3904
Potassium hexacyanoferrate(II) trihydrate	Merck (Darmstadt, Germany)	4982
Potassium hexacyanoferrate(III)	Merck (Darmstadt, Germany)	4973
Potassium iodide for analysis EMSURE® ISO, Reag. Ph Eur (KI)	Merck (Darmstadt, Germany)	105043
Protease Inhibitor Cocktail tablets cOmplete™, EDTA-free (PI)	Roche (Mannheim, Germany)	04693132001
Protease Inhibitor Cocktail cOmplete™, Mini, EDTA-free (PI)	Roche (Mannheim, Germany)	4693159001
Putrescine dihydrochloride ≥98% (Put)	Sigma-Aldrich (Steinheim, Germany)	P7505
Roti®-Aqua-Phenol for RNA extraction	Carl Roth (Karlsruhe, Germany)	A980
Rotiphorese® Gel 30 (37.5:1)	Carl Roth (Karlsruhe, Germany)	3029
S-(5'-Adenosyl)-L-homocysteine crystalline (SAH)	Sigma-Aldrich (Steinheim, Germany)	A9384
Sample Buffer, Laemmli 2x Concentrate	Sigma-Aldrich (Steinheim, Germany)	S3401
Silwet L-77	Lehle seeds (Round Rock, TX, USA)	
S-Methyl methanethiosulfonate 97% (MMTS)	Sigma-Aldrich (Steinheim, Germany)	208795
S-Nitroso-L-glutathione (GSNO)	Enzo Life Sciences (Lörrach, Germany)	ALX-420-002
Sodium acetate anhydrous	Merck (Darmstadt, Germany)	106236
Sodium chloride ≥99,5 %, p.a., ACS, ISO (NaCl)	Carl Roth (Karlsruhe, Germany)	3957
Sodium dihydrogen phosphate monohydrate p.a. EMSURE® ACS (NaH$_2$PO$_4$ x H$_2$O)	Merck (Darmstadt, Germany)	106346
Sodium dodecyl sulfate ≥99 %, for biochemistry (SDS)	Carl Roth (Karlsruhe, Germany)	CN30
Sodium dodecyl sulphate ultra-pure ≥99,5 % (SDS)	Carl Roth (Karlsruhe, Germany)	2326
Sodium hydrogen carbonate (NaHCO3)	Merck (Darmstadt, Germany)	6329
Sodium hydroxide ≥98 %, Ph.Eur., USP, BP, in pellets (NaOH)	Carl Roth (Karlsruhe, Germany)	P031
Sodium nitrite puriss. p.a., ACS reagent, Reag. Ph. Eur., ≥99% (NaNO2)	Sigma-Aldrich (Steinheim, Germany)	31443
Spermidine ≥99% (GC) (Spm)	Sigma-Aldrich (Steinheim, Germany)	S2626
Spermidine trihydrochloride ≥99.0% (Spd)	Sigma-Aldrich (Steinheim, Germany)	85580
Sulfanilamide ≥99%	Sigma-Aldrich (Steinheim, Germany)	S9251
Sulfuric acid 95-97% or analysis EMSURE® ISO (H2SO4)	Merck (Darmstadt, Germany)	100731
Trichloroacetic acid ACS reagent, ≥99.0% (TCA)	Sigma-Aldrich (Steinheim, Germany)	T6399
Trifluoroacetic acid for spectroscopy Uvasol® (TFA)	Merck (Darmstadt, Germany)	108262
Tris(hydroxymethyl)-aminomethane PUFFERANE® ≥99.9 %, p.a. (Tris)	Carl Roth (Karlsruhe, Germany)	4855
Triton® X 100 extra pure	Carl Roth (Karlsruhe, Germany)	3051
Tryptone/Peptone ex casein pancreatic digest, for microbiology	Carl Roth (Karlsruhe, Germany)	8952
Tween® 20 Ph.Eur. Non-ionic detergent	Carl Roth (Karlsruhe, Germany)	9127
Water for chromatography (LC-MS Grade) LiChrosolv®	Merck (Darmstadt, Germany)	115333
Yeast extract for bacteriology	Carl Roth (Karlsruhe, Germany)	2363
β-Nicotinamide adenine dinucleotide disodium salt ≥98 %, for biochemistry (NADH)	Carl Roth (Karlsruhe, Germany)	AE12

Kits		
BCIP NBT ready to use tablets	Roche (Mannheim, Germany)	11697471001
DNeasy® Plant Mini Kit	Qiagen (Venlo, the Netherlands)	69104
EpiTect® Plus Bisulfite Kit	Qiagen (Venlo, the Netherlands)	59124
Illumina® TruSeq® Nano kit	Illumina (San Diego, CA, USA)	FC-121-4001
innuPREP Gel Extraction Kit	Analytic Jena (Jena, Germany)	845-KS-5030050
innuPREP PLANT RNA Kit	Analytic Jena (Jena, Germany)	845-KS-2060050
Oligo(dT)12-18 Primer	Thermo Fischer Scientific (Waltham, MA, USA)	18418012
QIAprep® Spin Miniprep Kit	Qiagen (Venlo, the Netherlands)	27104
Western Lightning® Plus-ECL, Enhanced Chemiluminescence Substrate	PerkinElmer (Waltham, MA, USA)	NEL103001EA

Enzymes

Adenosine deaminase (Ado)	Sigma-Aldrich (Steinheim, Germany)	A6648; A5043
Alkaline Phosphatase, Calf Intestinal (CIP)	New England Biolabs (Ipswich, MA, USA)	M0290S
*Apa*LI	Thermo Fischer Scientific (Waltham, MA, USA)	ER0041
Gateway™ LR Clonase® Enzyme Mix	Invitrogen (Carlsbad, CA, USA)	11791-019
KAPA HiFi Uracil + R	Roche (Mannheim, Germany)	795905001
Lysozyme from chicken egg white lyophilized powder, protein ≥90 %,	Sigma-Aldrich (Steinheim, Germany)	L-6876
Mango*Taq*™ DNA Polymerase	Bioline (Luckenwalde, Germany)	BIO-21082
McrBC	New England Biolabs (Ipswich, MA, USA)	M0272S
Proteinase K	Invitrogen (Carlsbad, CA, USA)	25530049
RNAseOUT™ Recombinant Ribonuclease Inhibitor	Thermo Fischer Scientific (Waltham, MA, USA)	10777-019
Sequencing Grade Modified Trypsin	Promega (Madison, WI, USA)	V5111
SuperScript™ II Reverse Transcriptase	Thermo Fischer Scientific (Waltham, MA, USA)	18064014

Columns, membranes, resins

Amersham™ Protran® Western blotting membranes, Nitrocellulose, 0.45µm pore size	GE Healthcare Europe (Freiburg, Germany)	10600007
Econo-Pac® Chromatography Columns	Bio-Rad Laboratories (Hercules, CA, USA)	7321010
Empore™ disk-C18, 47MM	Agilent Technologies (Santa Clara, CA, USA)	12145004
Luna® C18 column (5 µ 100 Å C18(2) 250 x 4.6 mm column	Phenomenex (Aschaffenburg, Germany)	00G-4252-E0
Miracloth	Merck (Darmstadt, Germany)	475855
Ni-NTA Agarose	Qiagen (Venlo, the Netherlands)	30210
Nylon Net Filter, Hydrophilic, 160 µm, 90 mm	Merck (Darmstadt, Germany)	NY6H09000
PD-10 Desalting Columns	GE Healthcare Europe (Freiburg, Germany)	17-0851-01
Thiolpropyl sepharose 6B	GE Healthcare Europe (Freiburg, Germany)	71-7105-00 AE
TopTip Carbon (Hypercarb)	Glygen Corporation (Columbia, MD, USA)	TT1CAR
Whatman 3MM CHR Blotting Paper	Merck (Darmstadt, Germany)	3030-917
Zeba™ Spin Desalting Columns, 7K MWCO, 0.5 mL	Thermo Fischer Scientific (Waltham, MA, USA)	89882
Zeba™ Spin Desalting Columns, 7K MWCO, 2 mL	Thermo Fischer Scientific (Waltham, MA, USA)	89889
Zeba™ Spin Desalting Columns, 7K MWCO, 5 mL	Thermo Fischer Scientific (Waltham, MA, USA)	89891

Webpages

http://signal.salk.edu/tdnaprimers.2.htm
https://www.gabi-kat.de/db/primerdesign.php
http://wormweb.org/exonintron
http://www.graphpad.com
https://apps.araport.org/thalemine/

Software

ImageJ	National Institutes of Health, (Bethesda, Maryland)
SnapGene® and SnapGene® Viewer	GSL Biotech LLC (Chicago, IL, USA)
32 Karat™ 8.0	Beckman Coulter (Brea, CA, USA)
Xcalibur™ 2.2 SP1	Thermo Fischer Scientific (Waltham, MA, USA)
Sievers® NOA Analysis™ software version 3.2	GE Healthcare (Chicago, IL, USA)
GPMAW 5.02	Lighthouse data (Odense, Denmark)
Graphpad Prism version 7.05 for Windows	GraphPad Software (La Jolla, CA, USA)

Supplemental Table 3. List of instruments used.

Instrument	Source
Beckman System Gold® HPLC	Beckman Coulter (Brea, CA, USA)
Fluorescence detector RF 10AxL	Shimadzu (Kyōto, Japan)
Autoclave Evo®150 vertical	MediTech Service (Norderstedt, Germany)
Balances (Sartorius® CPA2250, L2200P)	Sartorius (Göttingen, Germany)
Camera Powershot G2	Canon (Tokyo, Japan)
Centrifuge 5430R (FA-45-45-16, FA-45-16-17, FA-45-48-11 rotors)	Eppendorf (Hamburg, Germany)
Centrifuge MiniSpin®	Eppendorf (Hamburg, Germany)
Centrifuge Rotanta 460R (swing out rotor 5699, adapter 6338-B and 6337-B)	Hettich (Bäch, Switzerland)
DNA Electrophoresis Units	VWR Peqlab (Erlangen, Germany)
Electrophoresis Power Supply EPS 601	GE Healthcare (Chicago, IL, USA)
Fusion FX-7 Imaging System	Vilber Lourmat (Eberhardzell, Germany)
Gel Documentation – MegaCapt	Vilber Lourmat (Eberhardzell, Germany)
Gene Pulser®/MicroPulser™ Electroporation Cuvettes, 0.1 cm gap	Bio-Rad Laboratories (Hercules, CA, USA)
Gene-Pulser™, Puls Controller, Capacitance Extender for electroporation	Bio-Rad Laboratories (Hercules, CA, USA)
Heraeus™ Fresco™ 17 Microcentrifuge	Thermo Fisher Scientific (Waltham, MA, USA)
Innova™ 4340 Refrigerated Incubator Shaker	New Brunswick Scientific (Edison, NJ, USA)
Microplate 96-well, Polystyrene, F-bottom, clear	Greiner Bio-One (Kremsmünster, Austria)
Mixing Block MB-102	Bioer Technology (Hangzhou, China)
Nanodrop ND-1000 spectrophotometer	NanoDrop Technologies (Wilmington, DE, USA)
NO-Analyzer NOA™ Sievers® 280 i	GE Healthcare (Chicago, IL, USA)
Overhead shaker Reax 2 and adapter 1	Heidolph Instruments (Schwabach, Germany)
PerfectBlue™ Semi-Dry Elektroblotter Sedec™	VWR Peqlab (Erlangen, Germany)
pH electrode InLab Routin	Mettler-Toledo (Zurich, Switzerland)
pH meter pH 523	WTW (Weilheim, Germany)
Platform Shaker Polymax 1040	Heidolph Instruments (Schwabach, Germany)
Quartz suprasil® Hellma® Precission cells cuvettes	Hellma Analytics (Müllheim, Germany)
SDS-PAGE Unit Mini-PROTEAN® Tetra cell system	Bio-Rad Laboratories (Hercules, CA, USA)
Sonifier® cell disrupter B15	Branson (Danbury, CT, USA)
Centrifuge Sorvall™ Evolution RC (Rotor SS-34 and SLA-1500)	Thermo Fisher Scientific (Waltham, MA, USA)
Spectrophotometer Beckmann Coulter DU®640	Beckman Coulter (Brea, CA, USA)
SpeedVac	Christ (Osterode am Harz, Germany)
T100™ Thermal Cycler	Bio-Rad Laboratories (Hercules, CA, USA)
Tecan Infinite® M1000 PRO	Tecan Austria (Gröding, Austria)
ThermoMixer® F1.5	Eppendorf (Hamburg, Germany)
Ultra-Clear™ UV UF	Siemens (Munich, Germany)
Spectrophotometer Ultrospec™ 3100 pro UV/Visible	Amersham Biosciences (Buckinghamshire, UK)
Vacuum Desiccator Kartell	Kartell S.p.A. (Noviglio, Italy)
Vacuum pump Trivac® E2 D 2.5 E	Leybold Vakuum (Cologne, Germany)

Supplemental Table 4. Oligonucleotides used for the characterization of transgenic lines. All PCR reactions were performed using Mango*Taq*™ DNA Polymerase and the following PCR conditions: denaturation at 94°C for 2 min, then x cycles of 30 s at 94°C, 30 s at the required annealing temperature, and 1 min/kb at 72°C for extension, followed by a final extension at 72°C for 10 min.

Primer name	Sequence	Uses	PCR	Reference
GABI_315D11_LP #14	ATGGTTCGACGCATATTTTTC	Atgsnor1-3 genotyping. Wt allele 1108 bps.	37 cyc., 59°C ann., 1´ 30´´ ext.	This work.
GABI_315D11_RP #15	GGAAAGAGACCTTCAGGATCC			
GABI8474_LB #16	ATAATAACGCTGCGGACATCTACATTTT	Atgsnor1-3 genotyping. T-DNA allele 513 bps.	37 cyc., 59°C ann., 1´ 30´´ ext.	
GABI315D11_AF01 #17	CACAGCCTCAAATTGATTCACTAA			

SALK068487_LP #20	TTTCTCGTGGTCCAATCAGAC	Atsahh1 genotyping. Wt allele 1114 bps. T-DNA allele (RP + LBb1.3) approx. 610 pbs.	35 cyc., 60°C ann., 1´ 30´´ ext.	This work.
SALK068487_RP #21	AGTAGCGTCACCACCATCATC			
HOGex2F2 (LP) #22	CAGTTCGACAACTTGTATGGTTG	Athog1-7 genotyping. Wt allele 1123 bps. Mutant allele approx. 950 bps.	33 cyc., 60°C ann., 1´ 15´´ ext.	Ortrun Mittelsten-Scheid
HOGex2R2 (RP) #23	TTGTTCGTGTCCTAACACACATT			
barbG (LB) #24	GGTTCTTATAGGGTTTCGCTC			
TsGUS1F (LB) #25	TGGATTTTGGCTCGAGATTC	Amplicon in wt and hemizygous alleles (572 bps).	33 cyc., 58°C ann., 50´´ ext.	Ortrun Mittelsten-Scheid
TsGUS1R (RP) #26	CAATCATGGCAGATCGAGAA			
qPCR-GUS-F #27	TTAACTATGCCGGAATCCATCGC	Amplicon of TS-GUS insert (128 bps).	33 cyc., 58°C ann., 10´´ ext.	Ortrun Mittelsten-Scheid
qPCR-GUS-R #28	CACCACCTGCCAGTCAACAGACGC			
GUS_R_short #29	CCCGGCTAACGTATCCACGCCGTA	Amplicon of TS-GUS insert with #27 (1043 bps).	33 cyc., 58°C ann., 1´ 20´´ ext.	Ortrun Mittelsten-Scheid
FLAG_pEARLY202_fw #30	ACTACAAAGACGATGACGAC	Amplicon of 35S::FLAG-GSNOR1 insertion (approx.. 1250 bps).	35 cyc., 58°C ann., 2´ ext.	This work.
GSNOR1_rev # 31	TCATTTGCTGGTATCGAGGAC			
CaMV35S_fw #32	CTATCCTTCGCAAGACCCTTC	Amplicon of 35S::SAHH1-HA-Strep insertion in pAUL1/2 vector (#32 + #33 = 1637 bps; #32 + # 34 = 1742 bps). #32 sequencing of pEarly gate and pAUL.	35 cyc., 58°C ann., 2´ ext.	This work.
Cterm_HA_rev #33	GATACGCGTAGTCTGGAACGTC			
Cterm_StrepIII_rev #34	CTATCCTTCGCAAGACCCTTC			
sahh1 RT-PCR fw #35	CGTGACTCCGCCGCTGTTTT	Amplicon of CDS of AtSAHH1 (992 bps).	35 cyc., 56°C ann., 1´ ext.	Ref.[170]
sahh1 RT-PCR rev #36	TTTCCGCTTGCTTTCTCGTTCC			
AtTUB9 f #37	GTACCTTGAAGCTTGCTAATCCTA	Amplicon of AtTub9 (At4g20890; 368 bps).	35 cyc., 56°C ann., 1´ ext.	AG Schäffner
AtTUB9 r #38	GTTCTGGACGTTCATCATCTGTTC			
M13fw #39	GTAAAACGACGGCCAG	Sequencing of pENTR221.		
M13rev #40	CAGGAAACAGCTATGAC	Sequencing of pENTR221.		
NOS term #41	ATGACACCGCGCGCGATA	Sequencing of pAUL1/2 vectors.		This work.
OCS term #42	GAGCTACACATGCTCAGG	Sequencing of pEarly 201/202.		This work.
pAUL_fw #43	TCATTTGGAGAGGGGCGCGCC	Sequencing of pAUL1/2 vectors.		This work.
NOS begin #44	GCAACAGGATTCAATCTTAAG	Sequencing of pAUL1/2 vectors.		This work.

Supplemental Table 5. Oligonucleotides used for DNA methylation analysis. All PCR reactions were performed using Mango*Taq*™ DNA Polymerase and the following conditions: denaturation at 94°C for 2 min, then 35 cycles of denaturation for 30 s at 94°C, annealing for 30 s at 56°C, and extension for 40 s at 72°C, followed by a final extension at 72°C for 10 min.

Primer name	Sequence	Target; amplicon length	Reference
COPIA4 f	CTCACTCAAGCTTCGGTTCC	At4g16870; 473 bps	Ref.[280–282]
COPIA4 r	TGTTGGTGAAGGACCGTACA		
GP1 f	ACAGTGCCACAGTTGAGCAG	At4g03650; 381 bps	Ref.[280–284]
GP1 r	CAGAAAAATACTCGGTGCCAAT		
TA2 f	AAACGATGCGTTGGGATAGGTC	At4g06488; 303 bps	Ref.[222,284]
TA2 r	ATACTCTCCACTTCCCGTTTTTCTTTTTA		
Line1-4 f	CCGATGGTGACCAAGAGTTT	At2g01840, 163 bps	Ref.[280,282,284,285]
Line1-4 r	TCAATGTCGGAGACCTCCTC		
Mu1 f	GTGGATATACCAAAAACACAA	At4g08680; 564 bps	Ref.[280–284]
Mu1r	CTTAGCCTTCTTTTCAATCTGA		
SN1 f	TGTCTTGGAAAGGATATTGGAAG	At3TE63860; 325 bps	Ref.[285]
SN1 r	AAGTGGTGGTTGTACAAGCC		
TSI f	GAACTCATGGATACCCTAAAATAC	BD298459.1; 598 bps	Ref.[131,222]
TSI r	CTCTACCCTTTGCATTCATGAATC		
Actin2 f	AAACCTCAAAGACCAGCTCTT	At3g18780; 514 bps	Ref.[281]
Actin 2 r	AACGATTCCTGGACCTGCC		

Supplemental Table 6. Plasmids used and generated in this study.

Plasmid	Resistance	Description	Reference
pEARLYGATE201	KanR	pEarleyGate 201 allows for rapid recombination cloning of cDNAs from Gateway™ entry vectors to be epitope tagged with Ha tag at the N-terminus of the encoded protein. This vector makes use of a CaMV 35S promoter to drive expression.	Ref.[177]
pEARLYGATE202	KanR	pEarleyGate 202 allows for rapid recombination cloning of cDNAs from Gateway™ entry vectors to be epitope tagged with FLAG tag at the N-terminus of the encoded protein. This vector makes use of a CaMV 35S promoter to drive expression.	Ref.[177]
pAUL1	KanR	pAUL1 allows for rapid recombination cloning of cDNA from Gateway entry vectors to be epitope tagged with HA tag at the C-terminus of the encoded protein. CaMV 35S driven.	Ref.[178]
pAUL2	KanR	pAUL1 allows for rapid recombination cloning of cDNA from Gateway entry vectors to be epitope tagged with HA tag and StrepIII tag at the C-terminus of the encoded protein. CaMV 35S driven.	Ref.[178]
pENTR221/*AtSAHH1-C-fusion*	KanR	Full length CDS of *AtSAHH1* for C-terminal fusion (without stop codon).	AG Lindermayr unpublished.
pENTR221/*AtSAHH1-N-fusion*	KanR	Full length CDS of *AtSAHH1* for N-terminal fusion (with stop codon).	AG Lindermayr unpublished.
pDEST17/*T7::His6-AtSAHH1*	AmpR	Expression plasmid (*E. coli*) encoding CDS of *AtSAHH1* with N- terminal His6-tag fusion.	AG Lindermayr unpublished.
pEARLYGATE201/*35S::HA-AtSAHH1*	KanR	Encodes CDS of *AtSAHH1* AT4G13940 with N-terminal HA-tag fusion.	This work.
pEARLYGATE202/*35S::FLAG-AtSAHH1*	KanR	Encodes CDS of *AtSAHH1* AT4G13940 with N-terminal FLAG-tag fusion	This work.
pAUL1/*35S:: AtSAHH1-HA*	KanR	Encodes CDS of *AtSAHH1* AT4G13940 with a C-terminal HA-tag fusion.	This work.
pAUL2/*35S::AtSAHH1-HA-StrepIII*	KanR	Encodes CDS of *AtSAHH1* AT4G13940 with a C-terminal HA-StrepIII-tag fusion.	This work.

Supplemental Table 7. Selected loci for chop-PCR analysis. TEs can be divided into retrotransposons (Class I) and DNA transposons (Class II). Retrotransposons can be further split into those that are flanked by long terminal repeats (LTR retrotransposons) and non-LTR retrotransposons. In *Arabidopsis*, the *GYPSY* and *COPIA* families are the main LTR retrotransposons, and LINE elements are predominant non-LTR retrotransposons. DNA transposons can be broadly divided into six classes: *MuDR, EnSpm/CACTA, hAT, PIF/HARBINGER*, the related *POGO, Tc1* and *MARINER* elements, and rolling circle replicating *HELITRON* elements (Ref.[267] and references therein) .

Loci	Accession number	Description
COPIA4	At4g16870	The GC-rich LTR retrotransposon *AtCOPIA4*[221] is hypermethylated in the *A. thaliana* genome, mainly due to maintenance methylation involving *At*MET1 and *At*SUVH4 [286]. *AtCOPIA4* methylation is hardly affected in mutants of RdDM components[287].
GP1	At4g03650	*AtGP1* is a gypsy-class LTR retrotransposon. *AtGP1* is a canonical target of RdDM[131,282].
Ta2	At4g06488	*AtTa2* belongs to the gypsy-like LTR retrotransposon family and is located in the pericentromeric region[222].
Line1-4	At2g01840	Non-LTR retrotransposon. DNA and histone methylation is reduced in the *Athog1-7* mutation[120].
SN1	At3TE63860	Short interspersed element 1 (*AtSN1*) non-LTR retrotransposon resides outside of chromocenters within a euchromatin environment (located between At3g44000 and At3g44005)[222]. It is methylated in all sequence contexts (Ref.[288] and references therein).
Mu1	At4g08680	The *AtMu1* DNA transposon is a transcriptionally silent element that carries CG and non-CG methylation and H3K9me in wild-type[221].
TSI	BD298459.1	Transcriptionally Silent Information (*AtTSI*) repeats are in the pericentromeric region of chromosomes. *AtTSI* is regulated by TGS[289] as demonstrated by increased TSI transcript levels in TGS mutants such as *hog1*[289]. *TSI* is targeted by DNA replication and repair proteins but not by RdDM components[290].

Supplemental Table 8. Identification list for LC-MS/MS analysis of histone PTMs. The MS identifier name contains MS scan type (MS1, MS2), target peptide, and PTM type and position. MS1_H3_9_17_K9me2: Quantification based on MS1 peak area to determine di-methylation on K9. MS2_9_17_y7_K14ac_728: MS2 on peptide H3.9-17-1-Ac that reports on y7 fragment ion (m/z of 728) necessary to determine acetylation on K14. Theoretical m/z, theoretical mono-isotopic mass/charge; charge state, charge state of MS identifier; sequence, target peptide sequence; RT [min], typical retention time; XIC range min/max, mass/charge range used for chromatographic peak integration according to the method previously established[192]. Mass spectrometry software tool GPMAW[194] was used to calculate theoretical monoisotopic m/z and fragments. Kac, lysine acetylation; Kme1, lysine mono-methylation; Kme2, lysine di-methylation; Kme3, lysine tri-methylation; noPTM, peptide without PTM, hence all lysines are chemically (d3)-acetylated (dac). Note that mono-methylated lysines are still reactive to d6—acetic anhydride. Chemical acetylation with d6-deuterated acetic anhydride, D3AA method[217], results in lysine D3-acetylation (+45.0294 Da), lysine mono-methylation (masses of D3-acetylation (+45.0294) plus mass of mono-methylation (+14.016 Da)), lysine di-methylation (+28.031 Da), lysine tri-methylation (42.046 Da), and endogenous lysine acetylation (+42.010 Da)[291]. Table adapted from Ref.[192].

MS identifier	theoretical m/z	charge state	Sequence of peptide	RT [min]	XIC range (min)	XIC range (max)
MS1_3_8_NoPTM	375.224	2	TKQTAR	22.20	375.074	375.374
MS1_3_8_K4me1	382.233	2	TKme1QTAR	27.97	382.083	382.383
MS1_3_8_K4me2	366.722	2	TKme2QTAR	19.83	366.572	366.872
MS1_3_8_K4me3	373.73	2	TKme3QTAR	19.80	373.58	373.88
MS1_9_17_noPTM	496.292	2	KSTGGKAPR	32.03	496.142	496.442
MS1_9_17_1Ac	494.783	2	K(ac?)STGGK(ac?)APR	32.19	494.633	494.933
MS1_9_17_2Ac	493.274	2	KacSTGGKacAPR	32.37	493.124	493.424
MS1_9_17_K9me1	503.301	2	Kme1STGGKAPR	34.04	503.151	503.451
MS1_9_17_K9me1_K14ac	501.792	2	Kme1STGGKacAPR	34.05	501.642	501.942
MS1_9_17_K9me2	487.793	2	Kme2STGGKAPR	24.97	487.643	487.943
MS1_9_17_K9me2_K14ac	486.284	2	Kme2STGGKacAPR	25.14	486.134	486.434
MS1_9_17_K9me3	494.801	2	Kme3STGGKAPR	24.77	494.651	494.951
MS1_9_17_K9me3_K14ac	493.291	2	Kme3STGGKacAPR	24.79	493.141	493.441
MS2_9_17_y7_K14ac_728	728.41	1	TGGK14acAPR	32.18	727.91	728.91
MS2_9_17_y7_K14noAc_731	731.43	1	TGGK14dacAPR	32.1	730.93	731.93
MS1_18_26_noPTM	538.837	2	KQLATKAAR	37.34	538.687	538.987
MS1_18_26_1Ac	537.328	2	K(ac?)QLATK(ac?)AAR	37.67	537.178	537.478
MS1_18_26_2Ac	535.819	2	KacQLATKacAAR	37.71	535.669	535.969
MS2_18_26_b2_K18ac_299	299.17	1	K18acQ	37.58	298.67	299.67
MS2_18_26_b2_K18noAc_302	302.19	1	K18dacQ	37.62	301.69	302.69
MS1_27_40_noPTM	523.651	3	KSAPATGGVKKPHR	38.16	523.55	523.75
MS1_27_40_1Ac	522.643	3	K(ac?)SAPATGGVK(ac?)K(ac?)PHR	38.18	522.54	522.74
MS1_27_40_K27me1	528.323	3	Kme1SAPATGGVKKPHR	39.22	528.173	528.473
MS1_27_40_K27me2	517.983	3	Kme2SAPATGGVKKPHR	35.07	517.833	518.133
MS1_27_40_K27me2_K36ac	516.975	3	Kme2SAPATGGVKacKPHR	35.10	516.825	517.125
MS1_27_40_K27me3	522.655	3	Kme3SAPATGGVKKPHR	35.02	522.505	522.805
MS1_27_40_K27me3_K36ac	521.647	3	Kme3SAPATGGVKacKdacPHR	35.02	521.497	521.797
MS1_27_40_K36me1	528,323	3	KSAPATGGVKme1KPHR	39.02	528.173	528.473
MS1_27_40_K36me2	517,983	3	KSAPATGGVKme2KPHR	36.02	517.833	518.133
MS1_27_40_K36me2_K27ac	516,975	3	KacSAPATGGVKme2KPHR	36.03	516.825	517.125
MS1_27_40_K36me3	522,655	3	KSAPATGGVKme3KPHR	36.01	522.505	522.805
MS1_27_40_K36me3_K27ac	521,647	3	KacSAPATGGVKme3KPHR	36.03	521.497	521.797
MS2_27_40_b3_K27ac_329	329,18	1	K27acSA	38.18	328.68	329.68
MS2_27_40_b3_K27NoAc_332	332,21	1	K27dacSA	38.11	331.71	332.71
MS2_27_40_y4_K37ac_579	579,33	1	K37acPHR	n.d.	578.83	579.83
MS2_27_40_y4_K37NoAc_582	582,36	1	K37dacPHR	38.16	581.86	582.86
MS2_27_40_y5_K27NoAc_752	752,47	1	K36(ac?)K37(ac?)PHR	38.16	751.97	752.97
MS2_27_40_y5_K27ac_755	755,49	1	K36dacK37dacPHR	38.16	754.99	755.99

Supplemental Table 9. List of DMGs and differentially methylated TEs identified in *Atgsnor1-3* and *Atsahh1*. In total 110 DMGs were found in both mutants. The methylation status in each mutant compared to wild-type is given as (-) and (+) referring to hypo- and hyper-methylation, respectively. DMRs are annotated with genomic features (3´kb up- or down-stream, and in gene). Annotation was performed using TAIR10.

Gene ID	*Atsahh1* CH₃	Feature	*Atgsnor1-3* CH₃	Feature	Description
AT1G29560	-	3kb up	-	3kb up	Zinc finger C-x8-C-x5-C-x3-H type family protein
AT1G29550	-	3kb up	-	3kb up	Eukaryotic translation initiation factor 4E-3
AT1G29535	-	3kb up	-	3kb up	Uncharacterized protein (Fragment)
AT1G29540	-	3kb down	-	3kb down	LOW protein: protein BOBBER-like protein
AT1G32100	-	3kb up	-	3kb up	Pinoresinol reductase 1
AT1G32120	-	3kb up	-	3kb up	
AT1G49870	-	3kb up	-	3kb up	Myosin-2 heavy chain-like protein
AT1G49860	-	3kb up	-	3kb up	Glutathione S-transferase F14
AT1G49850	-	3kb up	-	3kb up	Probable E3 ubiquitin-protein ligase RHY1A
AT1G52920	-	3kb up	+	3kb up	LanC-like protein GCR2
AT1G52940	-	3kb up	+	3kb up	purple acid phosphatase 5
AT1G52930	-	3kb down	+	3kb down	Ribosome biogenesis protein BRX1 homolog 2
AT1G63610	-	3kb up	+	3kb up	At1g6361
AT1G63630	-	3kb up	+	3kb up	Tetratricopeptide repeat (TPR)-like superfamily protein
AT1G63640	-	3kb down	+	3kb down	P-loop nucleoside triphosphate hydrolases superfamily protein with CH (Calponin Homology) domain
AT1G63615	-	3kb down	+	3kb down	
AT1G67623	+	3kb down	+	3kb down	Putative F-box protein At1g67623
AT1G67620	+	3kb down	+	3kb down	Protein Iojap-related, mt
AT1G67630	+	3kb down, in gene	+	3kb down	DNA polymerase alpha subunit B
AT1G75950	-	3kb up	+	3kb up	SKP1-like protein 1A
AT1G75960	-	3kb up	+	3kb up	Probable acyl-activating enzyme 8
AT1G75945	-	3kb down	+	3kb down, in gene	
AT1G75940	-	3kb down	+	3kb down	Beta-glucosidase 2
AT1G77180	-	3kb up	-	3kb up	SNW/SKI-interacting protein
AT1G77170	-	3kb up	-	3kb up	Pentatricopeptide repeat-containing protein At1g7717, mt
AT1G77200	-	3kb down	-	3kb down	Ethylene-responsive transcription factor ERF37
AT2G03680	-	3kb up	-	3kb up	Protein SPIRAL1
AT2G03670	-	in gene	-	in gene	Cell division control protein 48 homolog B
AT2G03667	-	3kb down	-	3kb down	Asparagine synthase family protein
AT2G03690	-	3kb down	-	3kb down	Ubiquinone biosynthesis protein COQ4 homolog, mt
AT2G03821	-	3kb up, in gene	+	3kb up	Putative uncharacterized protein
AT2G03820	-	3kb up	+	3kb up	6S ribosomal export protein NMD3
AT2G03830	-	3kb up	+	3kb up	Probable root meristem growth factor 8
AT2G03822	-	3kb up	+	3kb down	unknown protein
AT2G03823	-	3kb down, in gene	+	3kb down	
AT2G24520	-	3kb up	+	in gene	H(+)-ATPase 5
AT2G27050	-	3kb down	+	3kb up	ETHYLENE INSENSITIVE 3-like 1 protein
AT2G28470	-	3kb up	+	3kb up	Beta-galactosidase 8
AT2G28480	-	3kb down	+	3kb down	At2g2848
AT2G35990	-	3kb up	+	3kb up	Cytokinin riboside 5'-monophosphate phosphoribohydrolase LOG2
AT2G35965	-	3kb up	+	3kb up	
AT2G35980	-	3kb up	+	3kb up	NDR1/HIN1-like protein 1
AT2G35970	-	3kb down	+	3kb down	Late embryogenesis abundant (LEA) hydroxyproline-rich glycoprotein family
AT2G35960	-	3kb down	+	3kb down	NDR1/HIN1-like protein 12
AT2G40340	-	3kb up	-	3kb up	Integrase-type DNA-binding superfamily protein
AT2G40350	-	3kb down	-	3kb down	Integrase-type DNA-binding superfamily protein

AT2G40360	-	3kb down	-	3kb down	Ribosome biogenesis protein BOP1 homolog
AT3G06160	-	3kb up	-	3kb up	AP2/B3-like transcriptional factor family protein
AT3G06145	-	3kb up	-	3kb up	Putative RING zinc finger protein
AT3G06150	-	in gene	-	in gene	Cytochrome P45 family protein
AT3G14210	-	3kb up	+	3kb up	GDSL esterase/lipase ESM1
AT3G24310	-	3kb up	-	3kb up	MYB35
AT3G24350	-	3kb up	+	3kb down	Syntaxin of plants 32
AT3G25190	-	3kb up	-	3kb up	Vacuolar iron transporter homolog 2.1
AT3G25200	-	3kb up, 3kb down	-	3kb up	unknown protein; BEST Arabidopsis thaliana protein match is: Protein of unknown function (DUF295) (TAIR:AT5G5432.1)
AT3G29810	-	in gene	+	3kb up	COBRA-like protein 2
AT3G30160	-	in gene	-	in gene	Transmembrane protein
AT3G45170	-	in gene	+	in gene	GATA transcription factor 14
AT3G45180	-	3kb down	+	3kb down	Ubiquitin-like superfamily protein
AT3G45780	-	in gene	+	3kb up	RPT1
AT3G49690	-	3kb down	-	3kb down	RAX3
AT3G49700	-	3kb down	-	3kb down	1-aminocyclopropane-1-carboxylate synthase 9
AT3G55430	+	in gene	+	in gene	Beta-1, 3-glucanase-like protein
AT3G55420	+	3kb down	+	3kb down	Uncharacterized protein At3g5542
AT3G62530	-	3kb up	-	3kb up	ARM repeat superfamily protein
AT3G62528	-	3kb down	-	3kb down	unknown protein
AT3G62540	-	3kb down	-	3kb down	Pentatricopeptide repeat-containing protein At3g6254, mt
AT4G10050	-	3kb up	+	3kb down	Protein phosphatase methylesterase 1
AT4G13260	-	3kb up, 3kb down	+	3kb down	Indole-3-pyruvate monooxygenase YUCCA2
AT4G13430	+	3kb up	+	3kb up, 3kb down	3-isopropylmalate dehydratase large subunit, cp
AT4G13440	+/-	in gene, 3kb down	+	in gene	Calcium-binding EF-hand family protein
AT4G13790	+	3kb up	+	3kb up	At4g1379
AT4G13800	+	in gene	+	in gene	Probable magnesium transporter NIPA2
AT4G13810	+	3kb down	+	3kb down	
AT4G15050	-	3kb up	-	3kb up	NEP-interacting protein, putative (DUF239)
AT4G15053	-	3kb down	-	3kb down	Protein of Unknown Function (DUF239)
AT4G17460	-	3kb up	+	3kb up	Homeobox-leucine zipper protein HAT1
AT4G20070	-	3kb up	+	3kb up	Allantoate deiminase
AT4G20060	-	3kb up	+	3kb up	ARM repeat superfamily protein
AT4G26480	-	3kb up	-	3kb up	KH domain-containing protein At4g2648
AT4G26483	-	3kb up	-	3kb up	Nicotianamine synthase
AT4G26485	-	3kb down	-	3kb down	Uncharacterized protein At4g26485
AT4G26490	-	3kb up	-	3kb up	Late embryogenesis abundant (LEA) hydroxyproline-rich glycoprotein family
AT4G29090	-	3kb up, in gene	+	3kb down	Putative reverse transcriptase/RNA-dependent DNA polymerase
AT5G11360	-	3kb up	-	3kb up	Interleukin-1 receptor-associated kinase 4 protein
AT5G11380	-	3kb up	-	3kb up	1-D-deoxyxylulose 5-phosphate synthase-like protein
AT5G11370	-	in gene	-	in gene	FBD / Leucine Rich Repeat domains containing protein
AT5G12970	-	3kb up	-	3kb up	Anthranilate phosphoribosyltransferase-like protein
AT5G12960	-	in gene	-	in gene	Proline-tRNA ligase (DUF168)
AT5G12950	-	3kb down	-	3kb down	Proline-tRNA ligase (DUF168)
AT5G17490	-	3kb up	-	3kb up	DELLA protein RGL3
AT5G17500	-	in gene		in gene	Glycosyl hydrolase superfamily protein
AT5G17510	-	3kb down	-	3kb down	Glutamine-rich protein
AT5G23110	-	3kb down	+	3kb up	Zinc finger, C3HC4 type (RING finger) family protein
AT5G23100	-	3kb up	+	3kb down	At5g23100
AT5G28288	-	3kb down	-	3kb down	Putative defensin-like protein 11
AT5G35940	-	3kb up	+	in gene	Jacalin-related lectin 41
AT5G39471	-	3kb up	+	3kb up	Cysteine/Histidine-rich C1 domain family protein
AT5G43560	+	3kb up	+	3kb up	TNF receptor-associated factor homolog 1a

AT5G43550	+	3kb down	+	3kb down	F-box associated ubiquitination effector family protein
AT5G43540	+	3kb down	+	3kb down	C2H2 and C2HC zinc fingers superfamily protein
AT5G46660	-	3kb up	+	3kb up	CHP-rich zinc finger protein
AT5G46650	-	3kb up	+	3kb down	RING-H2 finger protein ATL3
AT5G47290	-	3kb up	-	3kb up	Myb family transcription factor
AT5G47310	-	3kb up	-	3kb up	At5g4731
AT5G47300	-	in gene	-	in gene	Probable F-box protein At5g473
AT5G48905	-	3kb up	-	3kb up	Putative defensin-like protein 165
AT5G48910	-	3kb down	-	3kb down	Pentatricopeptide repeat-containing protein At5g4891
AT5G48900	-	3kb down	-	3kb down	Probable pectate lyase 2
AT5G52060	-	3kb up	+	3kb up	BAG family molecular chaperone regulator 1

	Atsahh1		*Atgsnor1-3*		
TE ID	CH₃	TE family	CH₃	TE family	Superfamily
AT1TE37390	-	HELITRONY2	-	HELITRONY2	RC/Helitron
AT1TE61180	-	RP1_AT	-	RP1_AT	DNA
AT1TE93270	-	ATHAT2	+	ATHAT2	DNA/HAT
AT1TE93275	-	HELITRON1	+	HELITRON1	RC/Helitron
AT2TE26410	-	ATLINE1_6	-	ATLINE1_6	LINE/L1
AT4TE34260	+	ATREP9	+	ATREP9	RC/Helitron

Supplemental Table 10. List of GO-terms significantly enriched in the set of DEGs in *Atgsnor1-3*. GO-terms for molecular function and biological processes were determined. GO-term enrichment analysis (Fisher´s Exact test with FDR correction) was performed in R version 3.6.0 using the following R packages org.At.tair.db (version 3.8.2) and package Go.db (version 3.8.2). GO terms with adjusted p-value less than 0.05 are listed. In case of terms with identical sets of genes, terms, which are less significant, are not listed. Terms with less than 3 annotated genes are not listed. Overlapping genes with the corresponding GO term are not listed due to space limitation. GO term analysis was performed by Dr. Elisabeth Georgii (Institute of Biochemical Plant Pathology Munich).

Molecular function

Atgsnor1-3 upregulated genes		p-value	FDR-adjusted p-value
GO:0046527	glucosyltransferase activity	9,8E-09	2,3E-05
GO:0003824	catalytic activity	3,6E-08	3,0E-05
GO:0035251	UDP-glucosyltransferase activity	3,8E-08	3,0E-05
GO:0008194	UDP-glycosyltransferase activity	3,3E-07	2,0E-04
GO:0080044	quercetin 7-O-glucosyltransferase activity	3,1E-06	1,4E-03
GO:0016757	transferase activity, transferring glycosyl groups	4,1E-06	1,6E-03
GO:0016765	transferase activity, transferring alkyl or aryl (other than methyl) groups	8,4E-06	2,5E-03
GO:0004364	glutathione transferase activity	1,0E-05	2,6E-03
GO:0016491	oxidoreductase activity	6,0E-05	1,4E-02
GO:0048037	cofactor binding	2,1E-04	3,7E-02

Atgsnor1-3 downregulated genes		p-value	FDR-adjusted p-value
GO:0016301	kinase activity	2,7E-16	6,3E-13
GO:0016772	transferase activity, transferring phosphorus-containing groups	5,9E-14	6,9E-11
GO:0003824	catalytic activity	1,1E-12	8,7E-10
GO:0016740	transferase activity	1,9E-12	1,1E-09
GO:0003674	molecular_function	2,2E-08	1,0E-05

Biological Process

Atgsnor1-3 upregulated genes		p-value	FDR-adjusted p-value
GO:0010224	response to UV-B	1,5E-14	6,8E-11
GO:0009718	anthocyanin-containing compound biosynthetic process	6,6E-14	1,5E-10
GO:0009411	response to UV	9,4E-13	1,4E-09
GO:0010583	response to cyclopentenone	5,3E-12	4,7E-09
GO:0009744	response to sucrose	1,9E-11	1,4E-08
GO:0042221	response to chemical	2,7E-11	1,5E-08
GO:0009813	flavonoid biosynthetic process	5,1E-11	2,5E-08

GO:0098754	detoxification	9,3E-11	4,1E-08
GO:0009407	toxin catabolic process	4,4E-10	1,6E-07
GO:0009636	response to toxic substance	9,5E-10	3,0E-07
GO:0010033	response to organic substance	1,9E-09	5,6E-07
GO:0046148	pigment biosynthetic process	3,6E-09	1,0E-06
GO:0050896	response to stimulus	3,9E-09	1,0E-06
GO:0014070	response to organic cyclic compound	2,3E-07	4,9E-05
GO:1901700	response to oxygen-containing compound	5,2E-07	1,0E-04
GO:0009314	response to radiation	8,6E-06	1,7E-03
GO:0009416	response to light stimulus	1,3E-05	2,4E-03
GO:0046482	para-aminobenzoic acid metabolic process	6,3E-05	1,1E-02
GO:0009628	response to abiotic stimulus	8,7E-05	1,5E-02
GO:0010030	positive regulation of seed germination	9,6E-05	1,6E-02
GO:0034614	cellular response to reactive oxygen species	1,1E-04	1,8E-02
GO:0071241	cellular response to inorganic substance	1,2E-04	1,9E-02
GO:0034605	cellular response to heat	1,8E-04	2,6E-02
GO:0071732	cellular response to nitric oxide	2,1E-04	3,0E-02
GO:0001708	cell fate specification	2,8E-04	3,1E-02
GO:0034599	cellular response to oxidative stress	2,8E-04	3,1E-02
GO:0008152	metabolic process	3,7E-04	3,9E-02
GO:0009408	response to heat	4,3E-04	4,2E-02
GO:0010038	response to metal ion	5,0E-04	4,8E-02
GO:0071470	cellular response to osmotic stress	5,1E-04	4,8E-02

Atgsnor1-3 downregulated genes		p-value	FDR-adjusted p-value
GO:0006952	defense response	3,3E-159	1,4E-155
GO:0002376	immune system process	1,2E-140	2,6E-137
GO:0009607	response to biotic stimulus	2,5E-133	3,8E-130
GO:0043207	response to external biotic stimulus	2,0E-132	1,8E-129
GO:0042493	response to drug	2,4E-128	1,8E-125
GO:0006950	response to stress	8,5E-120	4,2E-117
GO:0098542	defense response to other organism	8,3E-117	3,7E-114
GO:0010200	response to chitin	2,9E-114	1,2E-111
GO:0050896	response to stimulus	9,2E-114	3,4E-111
GO:0009814	defense response, incompatible interaction	1,8E-113	6,1E-111
GO:0010243	response to organonitrogen compound	4,6E-112	1,4E-109
GO:0009605	response to external stimulus	4,2E-111	1,2E-108
GO:0010033	response to organic substance	1,1E-108	3,1E-106
GO:0009627	systemic acquired resistance	1,3E-104	3,5E-102
GO:1901700	response to oxygen-containing compound	1,6E-103	3,9E-101
GO:0042221	response to chemical	2,0E-99	4,6E-97
GO:1901698	response to nitrogen compound	1,4E-98	3,1E-96
GO:0051704	multi-organism process	1,9E-98	3,9E-96
GO:0007165	signal transduction	2,5E-97	4,9E-95
GO:0031347	regulation of defense response	6,5E-93	1,3E-90
GO:0042446	hormone biosynthetic process	1,2E-92	2,2E-90
GO:0070887	cellular response to chemical stimulus	1,6E-92	2,8E-90
GO:0071310	cellular response to organic substance	4,4E-92	7,2E-90
GO:0042445	hormone metabolic process	1,1E-90	1,8E-88
GO:0071229	cellular response to acid chemical	3,7E-87	5,4E-85
GO:0051716	cellular response to stimulus	9,2E-87	1,3E-84
GO:0009719	response to endogenous stimulus	1,7E-85	2,4E-83
GO:0009620	response to fungus	9,2E-85	1,2E-82
GO:0007154	cell communication	1,1E-84	1,5E-82
GO:0071495	cellular response to endogenous stimulus	2,4E-84	3,0E-82
GO:0009725	response to hormone	3,3E-84	4,1E-82
GO:0032870	cellular response to hormone stimulus	6,6E-83	7,9E-81
GO:0001101	response to acid chemical	7,7E-83	8,9E-81

GO:0009697	salicylic acid biosynthetic process	4,8E-82	5,4E-80
GO:0009751	response to salicylic acid	2,5E-81	2,8E-79
GO:0071236	cellular response to antibiotic	4,9E-81	5,2E-79
GO:0009863	salicylic acid mediated signaling pathway	1,7E-80	1,8E-78
GO:0002682	regulation of immune system process	9,8E-80	9,6E-78
GO:0035690	cellular response to drug	1,2E-79	1,2E-77
GO:0045088	regulation of innate immune response	3,5E-79	3,3E-77
GO:1901701	cellular response to oxygen-containing compound	1,1E-78	9,6E-77
GO:0046677	response to antibiotic	2,3E-78	1,9E-76
GO:0071407	cellular response to organic cyclic compound	2,7E-78	2,3E-76
GO:0048583	regulation of response to stimulus	1,0E-76	8,5E-75
GO:0035556	intracellular signal transduction	1,2E-75	9,4E-74
GO:0010941	regulation of cell death	1,0E-74	7,9E-73
GO:0008219	cell death	3,1E-74	2,4E-72
GO:0009753	response to jasmonic acid	4,6E-74	3,5E-72
GO:0050832	defense response to fungus	5,1E-74	3,7E-72
GO:0012501	programmed cell death	1,9E-72	1,4E-70
GO:0014070	response to organic cyclic compound	4,7E-72	3,4E-70
GO:0031348	negative regulation of defense response	5,6E-72	3,9E-70
GO:0043067	regulation of programmed cell death	2,7E-71	1,8E-69
GO:0010363	regulation of plant-type hypersensitive response	2,7E-71	1,8E-69
GO:0009626	plant-type hypersensitive response	5,2E-71	3,5E-69
GO:0009617	response to bacterium	7,8E-67	4,7E-65
GO:0009867	jasmonic acid mediated signaling pathway	4,7E-66	2,7E-64
GO:0016999	antibiotic metabolic process	7,8E-65	4,5E-63
GO:0009755	hormone-mediated signaling pathway	1,1E-63	6,0E-62
GO:0048585	negative regulation of response to stimulus	5,3E-62	2,9E-60
GO:0033554	cellular response to stress	9,6E-61	5,2E-59
GO:0072330	monocarboxylic acid biosynthetic process	1,1E-60	5,9E-59
GO:0065008	regulation of biological quality	2,4E-56	1,3E-54

Supplemental Table 11. List of GO-terms significantly enriched in the set of DEGs in *Atsahh1*. GO-terms for molecular function and biological processes were determined. GO-term enrichment analysis (Fisher´s Exact test with FDR correction) was performed in R version 3.6.0 using the following R packages org.At.tair.db (version 3.8.2) and package Go.db (version 3.8.2). GO terms with adjusted p-value less than 0.05 are listed. In case of terms with identical sets of genes, terms, which are less significant, are not listed. Terms with less than 3 annotated genes are not listed. Overlapping genes with the corresponding GO term are not listed due to space limitation. GO term analysis was performed by Dr. Elisabeth Georgii (Institute of Biochemical Plant Pathology Munich).

Molecular function			
***Atsahh1* upregulated genes**		**p-value**	**FDR-adjusted p-value**
GO:0016798	hydrolase activity, acting on glycosyl bonds	1,99E-05	2,85E-02
GO:0016713	oxidoreductase activity, acting on paired donors, with incorporation or reduction of molecular oxygen, reduced iron-sulfur protein as one donor, and incorporation of one atom of oxygen	2,44E-05	2,85E-02
GO:0016762	xyloglucan:xyloglucosyl transferase activity	3,64E-05	2,85E-02
GO:0004601	peroxidase activity	8,41E-05	4,45E-02
***Atsahh1* downregulated genes**		**p-value**	**FDR-adjusted p-value**
GO:0003700	**DNA-binding transcription factor activity**	7,86E-08	1,19E-04
GO:0046872	metal ion binding	4,56E-07	2,04E-04
GO:0003674	molecular_function	9,03E-07	2,37E-04
GO:0005488	binding	1,56E-05	3,65E-03
GO:0043167	ion binding	1,91E-05	4,08E-03
GO:0008270	zinc ion binding	3,97E-05	7,76E-03
GO:0046914	transition metal ion binding	7,40E-05	1,34E-02
GO:0005509	calcium ion binding	1,65E-04	2,77E-02

Biological process

Atsahh1 upregulated genes	p-value	FDR-adjusted p-value
GO:0042221 response to chemical	2,6E-11	1,16E-07
GO:1901700 response to oxygen-containing compound	1,4E-10	3,10E-07
GO:0009718 anthocyanin-containing compound biosynthetic process	3,7E-10	5,47E-07
GO:0050896 response to stimulus	7,6E-09	6,75E-06
GO:0010033 response to organic substance	3,0E-08	2,21E-05
GO:0001101 response to acid chemical	1,7E-06	1,06E-03
GO:0009813 flavonoid biosynthetic process	3,1E-06	1,58E-03
GO:0006694 steroid biosynthetic process	3,2E-06	1,58E-03
GO:0033993 response to lipid	4,5E-06	2,01E-03
GO:1901617 organic hydroxy compound biosynthetic process	9,7E-06	3,09E-03
GO:0014070 response to organic cyclic compound	9,8E-06	3,09E-03
GO:0009725 response to hormone	1,4E-05	3,83E-03
GO:0009628 response to abiotic stimulus	1,5E-05	3,83E-03
GO:0009741 response to brassinosteroid	1,6E-05	3,83E-03
GO:0016126 sterol biosynthetic process	1,6E-05	3,83E-03
GO:0010035 response to inorganic substance	4,1E-05	8,62E-03
GO:0008150 biological_process	4,4E-05	8,90E-03
GO:0009698 phenylpropanoid metabolic process	5,2E-05	9,97E-03
GO:0010224 response to UV-B	5,4E-05	1,00E-02
GO:0009744 response to sucrose	8,7E-05	1,48E-02
GO:0009414 response to water deprivation	1,4E-04	2,14E-02
GO:0009830 cell wall modification involved in abscission	1,5E-04	2,19E-02
GO:0031540 regulation of anthocyanin biosynthetic process	1,5E-04	2,19E-02
GO:0009962 regulation of flavonoid biosynthetic process	2,1E-04	2,76E-02
GO:0010167 response to nitrate	3,2E-04	4,08E-02
GO:0055072 iron ion homeostasis	3,4E-04	4,18E-02

Atsahh1 downregulated genes	p-value	FDR-adjusted p-value
GO:0010200 response to chitin	2,23E-61	9,9E-58
GO:0042493 response to drug	1,12E-55	1,6E-52
GO:1901698 response to nitrogen compound	2,25E-53	2,5E-50
GO:1901700 response to oxygen-containing compound	2,17E-42	1,9E-39
GO:0010033 response to organic substance	7,45E-42	5,5E-39
GO:0042221 response to chemical	9,88E-41	6,2E-38
GO:0006952 defense response	4,64E-38	2,6E-35
GO:0070887 cellular response to chemical stimulus	8,98E-35	4,4E-32
GO:0002376 immune system process	2,12E-34	9,4E-32
GO:0042446 hormone biosynthetic process	1,49E-33	6,0E-31
GO:0050896 response to stimulus	1,20E-32	4,4E-30
GO:0042445 hormone metabolic process	1,06E-31	3,6E-29
GO:0006950 response to stress	1,34E-31	4,2E-29
GO:0071310 cellular response to organic substance	9,81E-31	2,9E-28
GO:0001101 response to acid chemical	1,76E-28	4,1E-26
GO:0009607 response to biotic stimulus	1,53E-27	3,4E-25
GO:0032870 cellular response to hormone stimulus	5,49E-27	1,2E-24
GO:0071495 cellular response to endogenous stimulus	7,08E-27	1,4E-24
GO:0071229 cellular response to acid chemical	8,02E-27	1,5E-24
GO:0043207 response to external biotic stimulus	1,29E-26	2,3E-24
GO:0007165 signal transduction	1,42E-25	2,4E-23
GO:1901701 cellular response to oxygen-containing compound	2,88E-25	4,7E-23
GO:0009605 response to external stimulus	3,16E-25	5,0E-23
GO:0009725 response to hormone	6,42E-25	9,8E-23
GO:0071236 cellular response to antibiotic	2,55E-24	3,5E-22
GO:0035556 intracellular signal transduction	2,95E-24	4,0E-22
GO:0065008 regulation of biological quality	5,38E-24	7,0E-22
GO:0051716 cellular response to stimulus	6,58E-24	8,3E-22

GO:0009620	response to fungus	8,53E-24	1,0E-21
GO:0045087	innate immune response	6,42E-23	7,5E-21
GO:0046677	response to antibiotic	7,78E-23	8,8E-21
GO:0009755	hormone-mediated signaling pathway	2,12E-22	2,3E-20
GO:0007154	cell communication	5,70E-22	6,0E-20
GO:0009751	response to salicylic acid	2,47E-21	2,5E-19
GO:0009753	response to jasmonic acid	3,24E-21	3,3E-19
GO:0098542	defense response to other organism	4,40E-21	4,3E-19
GO:0009863	salicylic acid mediated signaling pathway	4,71E-21	4,5E-19
GO:0014070	response to organic cyclic compound	4,87E-21	4,6E-19
GO:0051704	multi-organism process	2,58E-20	2,0E-18
GO:0050832	defense response to fungus	4,94E-20	3,8E-18
GO:0065007	biological regulation	1,92E-19	1,4E-17
GO:0009611	response to wounding	2,31E-19	1,7E-17
GO:0010363	regulation of plant-type hypersensitive response	2,61E-18	1,8E-16
GO:0031347	regulation of defense response	9,98E-18	5,7E-16
GO:0072330	monocarboxylic acid biosynthetic process	1,25E-17	7,1E-16

Supplemental Table 12. Expression levels of differentially methylated TEs in *Atgsnor1-3* and *At*sahh1. Expression analysis was performed on TE family level. Members of differentially expressed TE families identified as differentially methylated TEs are listed. Abbreviations: padj., adjusted p-value; Chr, Chromosome; start, DMR start position; bp, length of overlapping DMR with genomic feature.

Correlation of TE expression and DNA methylation in *Atgsnor1-3*									
TE Family	log2FC	padj	Chr	Start	bp	CH$_3$	TE family	Locus ID	TE superfamily
ATLINEIII	-1,62	7,32E-09	Chr1	24675742	99	+	ATLINEIII	AT1TE81045	LINE/L1
			Chr1	24675841	52	+	ATLINEIII	AT1TE81045	LINE/L1
			Chr3	15648044	53	+	ATLINEIII	AT3TE63270	LINE/L1
			Chr5	7185139	194	+	ATLINEIII	AT5TE25975	LINE/L1
ATHATN3	-1,16	4,6E-03	Chr1	7224970	96	+	ATHATN3	AT1TE23350	DNA/HAT
HELITRONY1A	-1,07	4,9E-02	Chr2	9492568	101	+	HELITRONY1A	AT2TE40385	RC/Helitron
Correlation of TE expression and DNA methylation in *Atsahh1*									
TE Family	log2FC	padj	Chr	Start	bp	CH$_3$	TE Family	LocusID	TE Superfamily
ATCOPIA89	3,33	3,8E-04	Chr1	13559846	18	-	ATCOPIA89	AT1TE44380	LTR/Copia
ATHILA2	2,24	2,2E-05	Chr3	14065878	90	-	ATHILA2	AT3TE57660	LTR/Gypsy
HELITRONY1A	1,05	2,9E-02	Chr1	3427848	70	-	HELITRONY1A	AT1TE11150	RC/Helitron
			Chr4	7218018	59	-	HELITRONY1A	AT4TE31425	RC/Helitron

Supplemental Table 13. List of transcription factors differentially expressed in *Atgsnor1-3* as analyzed by RNA-seq.

Gene ID	log2FC	padj.	Description
AT3G25730	1,56	1,5E-06	AP2/ERF and B3 domain-containing transcription factor ARF14
AT5G03680	1,50	1,0E-07	Trihelix transcription factor PTL
AT4G34590	1,32	9,0E-16	bZIP transcription factor 11
AT3G54990	1,04	4,5E-03	AP2-like ethylene-responsive transcription factor SMZ
AT5G22570	-3,34	1,2E-20	Probable WRKY transcription factor 38
AT4G34410	-3,14	6,3E-86	Ethylene-responsive transcription factor ERF109
AT5G64810	-2,93	5,3E-19	Probable WRKY transcription factor 51
AT2G46400	-2,67	1,8E-98	Probable WRKY transcription factor 46
AT5G26170	-2,45	3,5E-15	Probable WRKY transcription factor 50
AT5G24110	-2,43	3,7E-15	Probable WRKY transcription factor 30
AT4G23810	-2,37	1,4E-125	Probable WRKY transcription factor 53
AT1G18570	-2,36	1,7E-105	Transcription factor MYB51
AT3G23250	-2,32	8,4E-15	Transcription factor MYB15
AT3G50260	-2,22	4,9E-28	Ethylene-responsive transcription factor ERF011
AT1G80840	-2,09	3,1E-95	Probable WRKY transcription factor 40
AT2G43000	-2,07	3,8E-09	Transcription factor JUNGBRUNNEN 1
AT4G31800	-2,00	4,3E-55	WRKY like transcription factor

AT2G44840	-1,99	3,7E-18	Ethylene-responsive transcription factor 13
AT4G17490	-1,82	7,1E-34	Ethylene-responsive transcription factor 6
AT4G17500	-1,80	5,4E-53	Ethylene-responsive transcription factor 1A
AT1G74930	-1,75	7,5E-36	Ethylene-responsive transcription factor ERF018
AT4G36990	-1,75	7,2E-59	Heat stress transcription factor B-1
AT3G23230	-1,68	6,2E-08	Ethylene-responsive transcription factor ERF098
AT5G65080	-1,55	7,2E-04	K-box region and MADS-box transcription factor family protein
AT2G40750	-1,54	8,3E-36	Probable WRKY transcription factor 54
AT1G22810	-1,47	2,8E-04	Ethylene-responsive transcription factor ERF019
AT2G23320	-1,45	3,8E-89	Probable WRKY transcription factor 15
AT1G42990	-1,40	2,7E-46	bZIP transcription factor 60
AT3G23240	-1,37	7,0E-04	Ethylene-responsive transcription factor 1B
AT3G51910	-1,37	6,1E-07	Heat stress transcription factor A-7a
AT1G67970	-1,34	2,9E-34	Heat stress transcription factor A-8
AT4G11070	-1,33	1,3E-03	Probable WRKY transcription factor 41
AT2G30250	-1,30	8,7E-85	Probable WRKY transcription factor 25
AT1G02340	-1,28	3,0E-14	Transcription factor HFR1
AT3G16770	-1,23	2,9E-31	Ethylene-responsive transcription factor RAP2-3
AT3G15210	-1,21	7,9E-28	Ethylene-responsive transcription factor 4
AT4G36900	-1,07	1,7E-12	Ethylene-responsive transcription factor RAP2-10
AT1G23965	-1,02	6,9E-03	Transcription factor
AT2G01818	-1,01	2,1E-03	PLATZ transcription factor family protein

7.3 Accession numbers

Analysis of differentially methylated or differentially expressed genes related to DNA and histone methylation and metaboloepigenetic processes interacting with DNA and histone methylation were performed based on literature and KEGG database[292]. Gene accession numbers of proteins involved in active DNA demethylation[58,111–114,293,294], canonical RdDM[58,107], and non-canonical RdDM[107,295], maintenance DNA methylation in CG, CHH, and CHG context[58], crosstalk DNA/H3K9me2 methylation[91,153], histone methylation and histone demethylation[85,88–90,95] were used. Further, proteins involved in metabolic pathways providing substrates for DNA and histone methylation processes namely the methylation cycle [117], and the TCA cycle[292], folate biosynthesis[116], cysteine and methionine biosynthesis, S-methylmethionine cycle (SMM), methionine salvage cycle, biosynthesis of nicotianamine, polyamines, and ethylene[117] were taken into account.

Active DNA demethylation

Active DNA demethylases
AT2g36490 REPRESSOR OF SILENCING 1 (ROS1)
AT5g04560 TRANSCRIPTIONAL ACTIVATOR DEMETER (DME)
AT3g10010 DEMETER-LIKE PROTEIN 2 (DML2)
AT4g34060 DEMETER-LIKE PROTEIN 3 (DML3)
Base excision repair process - active DNA demethylation machinery
AT3G48425 DNA-(APURINIC OR APYRIMIDINIC SITE) LYASE (APE1L)
AT3G14890 ZINC FINGER DNA 3'-PHOSPHOESTERASE (ZDP)
AT1G08130 DNA LIGASE 1 (LIG1)
Cytosolic iron-sulfur assembly pathway
AT1G68310 PROTEIN AE7 (CIA2/AE7)
AT5G48120 MET18 HOMOLOG/MMS19-LIKE PROTEIN (MET18/MMS19)
AT4G16440 NUCLEAR ARCHITECTURE RELATED 1 (NAR1)
AT5G18400 FE-S CLUSTER ASSEMBLY PROTEIN DRE2 HOMOLOG (DRE2)
AT5G50960 CYTOSOLIC FE-S CLUSTER ASSEMBLY FACTOR NBP35 (NBP35)
AT2G26060 PROTEIN CIA1 (CIA1)
AT3G02280 NADPH-DEPENDENT DIFLAVIN OXIDOREDUCTASE 1 (TAH18/ATR3)
ROS1 targeting
AT5G58130 REPRESSOR OF SILENCING (ROS3)
Increase in DNA methylation complex (ROS targeting)
AT3G14980 INCREASED DNA METHYLATION 1 (IDM1); also named ROS4
AT1G54840 INCREASED DNA METHYLATION 2 (IDM2); also named ROS5
AT1G20870 INCREASED DNA METHYLATION 3 (IDM3)
AT5G59800 METHYL-CPG-BINDING DOMAIN-CONTAINING PROTEIN 7 (MBD7)
AT1G72270 HARBINGER TRANSPOSON-DERIVED PROTEIN 1 (HDP1)
AT4G31270 HARBINGER TRANSPOSON-DERIVED PROTEIN 2 (HDP2)

AT3G25655 IDM2-LIKE PROTEIN (IDL1)
Facilitates chromatin transaction (FACT) chromatin remodeler - DME targeting
AT3G28730 STRUCTURE SPECIFIC RECOGNITION PROTEIN 1 (SSRP1)
AT4G10710 SUPPRESSOR OF TY16 (SPT16)
AT1G06760 HISTONE H1.1
AT2G30620 HISTONE H1.2
DNA methylation
Components of the non-canonical RdDM
AT4G35800 RNA Polymerase II (NRPB1, Pol II)
AT3G43920 DICER-LIKE 3 (DCL3)
AT3G03300 DICER-LIKE2 (DCL2)
AT5G20320 DICER-LIKE4 (DCL4)
AT1G01040 DICER-LIKE1 (DCL1)
AT1G48410 ARGONAUTE 1 (AGO1)
AT3G49500 RNA-DEPENDENT RNA POLYMERASE 6 (RDR6)
AT1G05460 SILENCING DEFECTIVE (SDE3)
AT1G14790 RNA-DEPENDENT RNA POLYMERASE 1 (RDR1)
AT1G31280 ARGONAUTE 2 (AGO2)
AT2G16485 NEEDED FOR RDR2-INDEPENDENT DNA METHYLATION (NERD)
AT5G23570 SUPPRESSOR OF GENE SILENCING 3 (SDGS3)
AT4G11130 RNA-DEPENDENT RNA POLYMERASE 1 (RDR2)
Components of the canonical RdDM pathway
AT1G63020 NUCLEAR RNA POLYMERASE D1 (NRPD1)
AT2G40030 NRPE1
AT3G23780 NRPD2/NRPE2
AT4G15950 NRPD4/NRPE4
AT3G57080 NRPE5
AT4G16265 NRPE9B
AT4G35800 NRPB1
AT4G11130 RNA-DEPENDENT RNA POLYMERASE 2 (RDR2)
AT3G43920 DICER-LIKE 3 (DCL3)
AT4G20910 HUA ENHANCER 1 (HEN1)
AT2G27040 ARGONAUTE 4 (AGO4)
AT2G32940 ARGONAUTE 6 (AGO6)
AT5G21150 ARGONAUTE 9 (AGO9)
AT3G42670 CLASSY 1 (CLSY1)

AT2G16390 DEFECTIVE IN RNA-DIRECTED DNA METHYLATION 1 (DRD1)

AT3G49250 DEFECTIVE IN MERISTEM SILENCING 3 (DMS3), INVOLVED IN DE NOVO (IDN1)

AT3G22680 RNA-DIRECTED DNA METHYLATION 1 (RDM1)

AT5G04290 KOW DOMAIN-CONTAINING TRANSCRIPTION FACTOR 1 (KTF1/RDM3)

AT3G48670 INVOLVED IN DE NOVO 2 (IDN2)

AT1G15910 IDN2 PARALOGUE 1 (IDP1)

AT4G00380 IDN2 PARALOGUE 2 (IDP2)

AT2G30280 DEFECTIVE IN MERISTEM SILENCING 3 (DMS4)

AT5G14620 DOMAINS REARRANGED METHYLTRANSFERASE 2 (DRM2)

AT2G33290 SU(VAR)3–9 HOMOLOG (SUVH2)

AT4G13460 SU(VAR)3–9 HOMOLOG 9 (SUVH9)

AT5G43990 SU(VAR) 3–9 RELATED 2 (SUVR2)

AT4G36290 MICRORCHIDIA 1 (MORC1)

AT1G19100 MICRORCHIDIA 6 (MORC6)

AT1G15215 SAWADEE HOMEODOMAIN HOMOLOGUE 1 (SHH1)

AT5G63110 HISTONE DEACETYLASE 6 (HDA6)

AT4G20400 JUMONJI 14 (JMJ14)

AT1G62830 LYSINE-SPECIFIC HISTONE DEMETHYLASE 1 (LDL1)

AT3G13682 LYSINE-SPECIFIC DEMTHYLASE 1 – LIKE 2 (LDL2)

AT3G49600 UBIQUITIN-SPECIFIC PROTEASE 26 (UBP26)

AT4G19020 CHROMOMETHYLASE 2 (CMT2)

AT1G69770 CHROMOMETHLASE 3 (CMT3)

AT5G49160 METHYLTRANSFERASE 1(MET1)

AT5G13960 SU(VAR)3–9 HOMOLOG 4 (SUVH4)

AT5G66750 DECREASED DNA METHYLATION 1 (DDM1)

AT1G54440 RIBOSOMAL RNA PROCESSING 6 - LIKE 1 (RRP6L1)

AT4G03430 STABILIZED1

AT1G28060 RNA-DIRECTED DNA METHYLATION 16 (RDM16)

AT5G52640 HSP90-1

AT5G56030 HSP90-2

AT5G56010 HSP90-3

AT5G56000 HSP90-4

<u>CG methylation</u>

AT5g49160 Methyltransferase 1 (MET1)

AT1G57820 VARIANT IN METHYLATION 1 (VIM1)

AT1G66050 VARIANT IN METHYLATION 2 (VIM2)

AT5G39550 VARIANT IN METHYLATION 3 (VIM3)

AT1G66050 VARIANT IN METHYLATION 3 (VIM4)

AT1G57800 VARIANT in METHYLATION 5 (VIM5)

<u>CHG methylation</u>

AT4G19020 CHROMOMETHYLASE 2 (CMT2)

AT1G69770 CHROMOMETHYLASE 3 (CMT3)

AT5G13960 SU(VAR)3–9 HOMOLOG 4 (SUVH4)

AT2G35160 SU(VAR)3–9 HOMOLOG 5 (SUVH5)

AT2G22740 SU(VAR)3–9 HOMOLOG 6 (SUVH6)

<u>CHH methylation</u>

AT5G14620 DOMAINS REARRANGED METHYLTRANSFERASE 2 (DRM2)

AT4G19020 CHROMOMETHYLASE 2 (CMT2)

AT1G06760 HISTONE H1.1

AT2G30620 HISTONE H1.2

AT5G66750 DECREASED DNA METHYLATION 1 (DDM1)

<u>Additional components for heterochromatin formation</u>

AT5G66750 DECREASED DNA METHYLATION 1 (DDM1)

AT1G06760 HISTONE H1.1

AT2G30620 HISTONE H1.2

AT5G59870 H2A.W6 (HTA6)

AT5G27670 H2A.W7 (HTA7)

Histone methylation

<u>Histone variants and gene regulation</u>

AT1G06760 HISTONE H1.1

AT2G30620 HISTONE H1.2

AT2G38810 H2A.Z (HTA8)

AT1G52740 H2A.Z (HTA9)

AT3G54560 H2A.Z (HTA11)

AT5G65360 H3.1 (HTR1)

AT1G09200 H3.1 (HTR2)

AT3G27360 H3.1 (HTR3)

AT5G10400 H3.1 (HTR9)

AT5G10390 H3.1 (HTR13)

AT4G40030 H3.3 (HTR4)

AT4G40040 H3.3 (HTR5)

AT5G10980 H3.3 (HTR8)

AT1G01370 CENH3 (HTR12)

<u>INCREASE IN BONSAI METHYLATION 1 (IBM1) - full-length functional transcript processing</u>

AT3G07610 IBM1 (JMJ25)

AT5G11470 ANTI-SILENCING 1 (ASI1)

AT5G55390 ENHANCED DOWNY MILDEW 2 (EDM2)

AT1G05970 ASI1- IMMUNOPRECIPITATED PROTEIN 1 (AIPP1)

AT3G02890 ASI1- IMMUNOPRECIPITATED PROTEIN 2 (AIPP2)

AT4G11560 ASI1- IMMUNOPRECIPITATED PROTEIN 3 (AIPP3)

AT5G01270 POL II CARBOXY- TERMINAL DOMAIN PHOSPHATASE CARBOXY- TERMINAL PHOSPHATASE- LIKE 2 (CPL2)

<u>AGDP1 links H3K9me2 to DNA methylation</u>

AT1G09320 AGENET DOMAIN (AGD)-CONTAINING P1 (AGDP1)

Histone methyltransferases

<u>Histone lysine methyl transferases</u>

Class I - Enhancer of Zeste homologs E(Z)

AT2G23380 CLF/CURLY LEAF (SDG1, SET1)

AT4G02020 SWN/SWINGER (SDG10)

AT1G02580 MEDEA (SDG5)

Class II - ASH1 homologs and related (ASH)

AT1G76710 ASHH1 (SG26)

AT1G77300 ASHH2 (SG8)

AT2G44150 ASHH3 (SG7)

AT3G59960 ASHH4 (SG24)

AT4G30860 ASHR3 (SG4)

Class III – TRITHORAX homologs and related (TRX)

AT2G31650 ATX1 (SG27)

AT1G05830 ATX2 (SDG30)

AT3G61740 ATX3 (SDG14)

AT4G27910 ATX4 (SDG16)

AT5G53430 ATX5 (SDG29)

AT4G15180 ATXR3 (SDG2)

AT5G42400 ATXR7 (SDG25)

Class IV – Arabidopsis TRX related (ATXR)

AT5G09790 ATXR5 (SDG15)

AT5G24330 ATXR6 (SDG34)

Class V – Suppressor of variegation (SU(VAR) homologs and related

AT5G04940   SUVH1 (SDG32)
AT2G33290   SUVH2 (SDG3)
AT1G73100   SUVH3 (SDG19)
AT5G13960   SUVH4 (SDG33)
AT2G35160   SUVH5 (SDG9)
AT2G22740   SUVH6 (SDG23)
AT1G17770   SUVH7 (SDG17)
AT2G24740   SUVH8 (SDG21)
AT4G13460   SUVH9 (SDG22)
AT2G05900   SUVH10 (SDG11)
AT1G04050   SUVR1 (SDG13)
AT5G43990   SUVR2 (SDG18)
AT3G03750   SUVR3 (SDG20)
AT3G04380   SUVR4 (SDG31)
AT2G23740   SUVR5 (SDG6)

<u>Protein arginine methyltransferases (PRMT)</u>
AT2G19670   PRMT1A
AT4G29510   PRMT1B
AT3G12270   PRMT3
AT5G49020   PRMT4A
AT3G06930   PRMT4B
AT3G20020   PRMT6
AT1G04870   PRMT10
AT4G31120   PRMT5/SKB1
AT4G16570   PRMT7

<u>Jumonji domain-containing histone demethylases (JHDM/JMJ)</u>
KDM4/JHDM3 Group
AT5G04240   JMJ11
AT3G48430   JMJ12/REF6
AT5G46910   JMJ13
KDM5/JARID1 Group
AT4G20400   JMJ14
AT2G34880   JMJ15
AT1G08620   JMJ16
AT1G63490   JMJ17
AT1G30810   JMJ18
AT2G38950   JMJ19
JMJD6 Group
AT1G78280   JMJ21
AT5G06550   JMJ22
KDM3/JHDM2 Group
AT1G09060   JMJ24
AT3G07610   IBM1 (JMJ25)
AT1G11950   JMJ26
AT4G00990   JMJ27
AT4G21430   JMJ28
AT1G62310   JMJ29
JmjC domain-only Group
AT5G63080   JMJ20
AT3G20810   JMJ30
AT5G19840   JMJ31
AT3G45880   JMJ32

<u>Lysine-specific demethylase family (LSD) – LIKE (LDL)</u>
AT3G10390   FLD
AT3G13682   LDL2
AT1G62830   LDL1
AT4G16310   LDL3

DNA methylation
<u>DNA methyltransferases (DMTs)</u>
AT5G49160   METHYLTRANSFERASE 1(MET1
AT4G19020   CHROMOMETHYLASE 2 (CMT2)
AT1G69770   CHROMOMETHLASE 3 (CMT3)

AT5G14620   DOMAINS REARRANGED METHYLTRANSFERASE 2 (DRM2)
AT5G15380   DRM1 (NON-FUNCTION)
AT1G80740   CMT1 (NON-FUNCTION)
AT4G08990   MET2 (NON-FUNCTION)
<u>DNA demethylase</u>
AT5G04560   DEMETER (DME)
AT2G36490   REPRESSOR OF SILENCING 1 (ROS1)
AT3G10010   DEMETER-LIKE 2 (DML2)
AT4G34060   DEMETER-LIKE 3 (DML3)
Methylation cycle and metabolic pathways downstream and upstream
<u>Folate biosynthesis</u>
AT3G07270   GTP CYCLOHYDROLASE I (GTPCHI)
AT3G11750   DIHYDRONEOPTERINE ALDOLASE (DHNA1)
AT5G62980   DIHYDRONEOPTERINE ALDOLASE (DHNA2)
AT3G21730   DIHYDRONEOPTERINE ALDOLASE (DHNA3)
AT4G30000   HYDROXYMETHYLDIHYDROPTERIN PYROPHOSPHOKINASE/ DIHYDROPTEROATE SYNTHASE (HPPK/DHPS1)
AT1G69190   HYDROXYMETHYLDIHYDROPTERIN PYROPHOSPHOKINASE/ DIHYDROPTEROATE SYNTHASE (HPPK/DHPS2)
AT5G41480   DIHYDROFOLATE SYNTHETASE (DHFS)
AT2G16370   DIHYDROFOLATE REDUCTASE - THYMIDYLATE SYNTHASE 1 (DHFR-TS1)
AT4G34570   DIHYDROFOLATE REDUCTASE - THYMIDYLATE SYNTHASE 3 (DHFR-TS3)
AT2G21550   DIHYDROFOLATE REDUCTASE - THYMIDYLATE SYNTHASE 2 (DHFR-TS2)
AT5G05980   FOLYLPOLYGLUTAMATE SYNTHASE 1 (FPGS1 PLASTIDIC)
AT3G10160   FOLYLPOLYGLUTAMATE SYNTHASE 2 (FPGS2 MT)
AT3G55630   FOLYLPOLYGLUTAMATE SYNTHASE 3 (FPGS3 CYTOSOLIC)
AT2G28880   AMINODEOXYCHORISMATE SYNTHASE (ADCS)
AT5G57850   AMINODEOXYCHORISMATE LYASE (ADCL)
AT1G78660   GAMMA-GLUTAMYL HYDROLASE 1 (GGH1)
AT1G78680   GAMMA-GLUTAMYL HYDROLASE 2 (GGH2)
AT1G78670   GAMMA-GLUTAMYL HYDROLASE 3 (GGH3)
<u>Synthesis and interconversion of C1-THF</u>
AT4G37930   SERINE TRANSHYDROXYMETHYLTRANSFERASE 1 (SHMT1, MT)
AT5G26780   SERINE HYDROXYMETHYLTRANSFERASE 2 (SHMT2, MT)
AT4G32520   SERINE HYDROXYMETHYLTRANSFERASE 3 (SHMT3, CP)
AT4G13930   SERINE HYDROXYMETHYLTRANSFERASE 4 (SHMT4, CYT)
AT4G13890   SERINE HYDROXYMETHYLTRANSFERASE 5 (SHMT5, CYT)
AT1G22020   SERINE HYDROXYMETHYLTRANSFERASE 6 (SHMT6)
AT1G36370   SERINE HYDROXYMETHYLTRANSFERASE 7 (SHMT7/MSA1)
AT2G26080   GLYCINE DECARBOXYLASE P-PROTEIN 2 (GLDP2)
AT4G33010   GLYCINE DECARBOXYLASE P-PROTEIN (GLDP1)
AT1G11860   GLYCINE DECARBOXYLASE T-PROTEIN (GDT1)
AT1G60990   GLYCINE DECARBOXYLASE T-PROTEIN

AT1G48030 GLYCINE DECARBOXYLASE L-PROTEIN (LPD1)

AT3G17240 GLYCINE DECARBOXYLASE L-PROTEIN (LPD2)

AT2G35120 GLYCINE DECARBOXYLASE - H PROTEIN 2 (GDH2)

AT2G35370 GLYCINE DECARBOXYLASE - H PROTEIN 1 (GDH1)

AT1G32470 GLYCINE DECARBOXYLASE - H PROTEIN 3 (GDH3)

AT2G38660 5,10-METHYLENE THF DEHYDOGENASE/ 5,10-METHYLENE THF CYCLOHYDROLASE 1 (DHC1/MTHFD2/FOLD1)

AT4G00620 5,10-METHYLENE THF DEHYDOGENASE/ 5,10-METHYLENE THF CYCLOHYDROLASE 2 (DHC4/FOLD4)

AT3G12290 5,10-METHYLENE THF DEHYDOGENASE/ 5,10-METHYLENE THF CYCLOHYDROLASE 3 (DHC2/MTHFD1)

AT4G00600 5,10-METHYLENE THF DEHYDOGENASE/ 5,10-METHYLENE THF CYCLOHYDROLASE 4 (DHC3/FOLD3)

AT1G50480 10-FORMYLTETRAHYDROFOLATE SYNTHETASE (FTHFS)

AT5G13050 5-FORMYLTETRAHYDROFOLATE CYCLO-LIGASE (5FCL)

AT3G59970 5,10-METHYLENETETRAHYDROFOLATE REDUCTASE (MTHFR1)

AT2G44160 5,10-METHYLENETETRAHYDROFOLATE REDUCTASE (MTHFR2)

AT4G17360 FORMYLTETRAHYDROFOLATE DEFORMYLASE 2 (PURU2)

AT5G47435 FORMYLTETRAHYDROFOLATE DEFORMYLASE 1 (PURU1)

Cysteine and Methionine biosynthesis

AT1G55920 SERINE ACETYLTRANSFERASE 1 (SAT1)

AT2G17640 SERINE ACETYLTRANSFERASE 2 (SAT2)

AT3G13110 SERINE ACETYLTRANSFERASE 3 (SAT3)

AT2G17640 SERINE ACETYLTRANSFERASE 4 (SAT4)

AT5G56760 SERINE ACETYLTRANSFERASE 5 (SAT5)

AT4G14880 O-ACETYLSERINE(THIOL)LYASE (OAS-A1)

AT2G43750 O-ACETYLSERINE(THIOL)LYASE (OAS-B)

AT3G59760 O-ACETYLSERINE(THIOL)LYASE (OAS-C)

AT3G61440 O-ACETYLSERINE(THIOL)LYASE (CYS-C1)

AT3G04940 O-ACETYLSERINE(THIOL)LYASE (CYS-D1)

AT5G28020 O-ACETYLSERINE(THIOL)LYASE (CYS-D2)

AT5G28030 O-ACETYLSERINE(THIOL)LYASE (DES1)

AT3G03630 O-ACETYLSERINE(THIOL)LYASE (CS26)

AT3G01120 CYSTATHIONINE GAMMA -SYNTHASE (CGS)

AT3G57050 CYSTATHIONINE ß-LYASE (CBL)

AT1G64660 MET GAMMA-LYASE (MGL)

Methylation cycle

AT5G17920 METHIONINE SYNTHASE 1 (MS1)

AT3G03780 METHIONINE SYNTHASE 2 (MS2)

AT5G20980 METHIONINE SYNTHASE 3 (MS3)

AT1G02500 METHIONINE S-ADENOSYLTRANSFERASE 1 (MAT1)

AT4G01850 METHIONINE S-ADENOSYLTRANSFERASE 2 (MAT2)

AT2G36880 METHIONINE S-ADENOSYLTRANSFERASE 3 (MAT3)

AT3G17390 METHIONINE S-ADENOSYLTRANSFERASE 4 (MAT4)

AT4G13940 S-ADENOSYLHOMOCYSTEINE HYDROLASE 1 (SAHH1)

AT3G23810 S-ADENOSYLHOMOCYSTEINE HYDROLASE 2 (SAHH2)

AT3G09820 ADO KINASE (ADK1)

AT5G03300 ADO KINASE (ADK2)

S-Methylmethionine cycle (SMM) cycle

AT5G49810 MET S-METHYLTRANSFERASE (MMT)

AT3G25900 HCYS S-METHYLTRANSFERASE 1 (HMT1)

AT3G63250 HCYS S-METHYLTRANSFERASE 2 (HMT2)

AT3G22740 HCYS S-METHYLTRANSFERASE 3 (HMT3)

Methionine salvage cycle

AT4G38800 MTA NUCLEOSIDASE (MTN1)

AT4G34840 MTA NUCLEOSIDASE (MTN2)

AT1G49820 METHYLTHIORIBOSE KINASE (MTK1)

AT2G05830 METHYLTHIORIBOSE-1-PHOSPHATE ISOMERASE (MTI1)

AT5G53850 DEHYDRATASE/ENOLASE/PHOSPHATASE (DEP1)

AT4G14716 ACIREDUCTONE DIOXYGENASE 1 (ARD1)

AT4G14710 ACIREDUCTONE DIOXYGENASE 2 (ARD2)

AT2G26400 ACIREDUCTONE DIOXYGENASE 3 (ARD3)

AT5G43850 ACIREDUCTONE DIOXYGENASE 4 (ARD4)

Nicotianamine biosynthesis

AT5G04950 NICOTIANAMINE SYNTHASE 1 (NAS1)

AT5G56080 NICOTIANAMINE SYNTHASE 2 (NAS2)

AT1G09240 NICOTIANAMINE SYNTHASE 3 (NAS3)

AT1G56430 NICOTIANAMINE SYNTHASE 4 (NAS4)

Polyamine biosynthesis

AT3G02470 S-ADENOSYL-L-METHIONINE DECARBOXYLASE 1 (SAMDC1)

AT5G15950 S-ADENOSYL-L-METHIONINE DECARBOXYLASE 2 (SAMDC2)

AT3G25570 S-ADENOSYL-L-METHIONINE DECARBOXYLASE 3 (SAMDC3)

AT5G18930 S-ADENOSYL-L-METHIONINE DECARBOXYLASE 4 (SAMDC4)

AT1G23820 SPERMIDINE SYNTHASE 1 (SPDS1)

AT1G70310 SPERMIDINE SYNTHASE 2 (SPDS2)

AT5G19530 THERMOSPERMINE SYNTHASE (ACL5, TSPMS)

AT5G53120 SPERMINE SYNTHASE (SPMS)

AT5G13700 POLYAMINE OXIDASE 1 (PAO1)

AT2G43020 POLYAMINE OXIDASE 2 (PAO2)

AT3G59050 POLYAMINE OXIDASE 3 (PAO3)

AT1G65840 POLYAMINE OXIDASE 4 (PAO4)

AT4G29720 POLYAMINE OXIDASE 5 (PAO5)

AT2G23510 SPERMIDINE DISINAPOYL TRANSFERASE (SDT)

Ethylene Biosynthesis

AT3G61510 1-AMINOCYCLOPROPANE-1-CARBOXYLATE SYNTHASE-LIKE PROTEIN 1 (ACS1)

AT1G01480 1-AMINOCYCLOPROPANE-1-CARBOXYLATE SYNTHASE-LIKE PROTEIN 2 (ACS2)

AT5G28360 1-AMINOCYCLOPROPANE-1-CARBOXYLATE SYNTHASE-LIKE PROTEIN 3 (ACS3) PSEDOGENE

AT3G22810 1-AMINOCYCLOPROPANE-1-CARBOXYLATE SYNTHASE-LIKE PROTEIN 4 (ACS4)

AT5G65800 1-AMINOCYCLOPROPANE-1-CARBOXYLATE SYNTHASE-LIKE PROTEIN 5 (ACS5)

AT4G11280 1-AMINOCYCLOPROPANE-1-CARBOXYLATE SYNTHASE-LIKE PROTEIN 6 (ACS6)

AT4G26200 1-AMINOCYCLOPROPANE-1-CARBOXYLATE SYNTHASE-LIKE PROTEIN 7 (ACS7)

AT4G37770 1-AMINOCYCLOPROPANE-1-CARBOXYLATE SYNTHASE-LIKE PROTEIN 8 (ACS8)

AT3G49700 1-AMINOCYCLOPROPANE-1-CARBOXYLATE SYNTHASE-LIKE PROTEIN 9 (ACS9)

AT1G62960   1-AMINOCYCLOPROPANE-1-CARBOXYLATE SYNTHASE-LIKE PROTEIN 10 (ACS10)

AT4G08040   1-AMINOCYCLOPROPANE-1-CARBOXYLATE SYNTHASE-LIKE PROTEIN 11 (ACS11)

AT5G51690   1-AMINOCYCLOPROPANE-1-CARBOXYLATE SYNTHASE-LIKE PROTEIN 12 (ACS12)

AT2G19590   1-AMINOCYCLOPROPANE-1-CARBOXYLATE OXIDASE 1 (ACO1)

AT1G62380   1-AMINOCYCLOPROPANE-1-CARBOXYLATE OXIDASE 2 (ACO2)

AT1G12010   1-AMINOCYCLOPROPANE-1-CARBOXYLATE OXIDASE 3 (ACO3)

AT1G05010   1-AMINOCYCLOPROPANE-1-CARBOXYLATE OXIDASE 4 (ACO4)

AT1G77330   1-AMINOCYCLOPROPANE-1-CARBOXYLATE OXIDASE 5 (ACO5)

GSH biosynthesis and GSNO turnover

AT4G23100   γ—GLUTAMYLCYSTEINE SYNTHASE (GSH1)
AT5G27380   GLUTATHIONE SYNTHETASE (GSH-S)
AT5G43940   GSNO REDUCTASE 1 (GSNOR1)
AT3G24170   GLUTATHIONE REDUCTASE (GR1)
AT3G54660   GLUTATHIONE REDUCTASE (GR2)

Chlorophyll - SAM as methyl donor

At4g25080 Magnesium protoporphyrin IX methyltransferase (CHLM)

Tricarboxylic acid (TCA) Cycle

AT4G35830   ACONITASE 1 (ACO1)
AT4G26970   ACONITASE 2 (ACO2)
AT2G05710   ACONITASE 3 (ACO3)
AT1G54340   ISOCITRATE DEHYDROGENASE, PEROXISOMAL (ICDH)
AT5G14590   ISOCITRATE/ISOPROPYLMALATE DEHYDROGENASE FAMILY PROTEIN
AT2G17130   ISOCITRATE DEHYDROGENASE, (IDH2) [NAD]
AT4G35650   ISOCITRATE DEHYDROGENASE (IDH3) [NAD]
AT4G35260   ISOCITRATE DEHYDROGENASE (IDH1) [NAD]
AT1G32480   ISOCITRATE DEHYDROGENASE, PUTATIVE (IDH4) [NAD]
AT3G09810   ISOCITRATE DEHYDROGENASE (IDH6) [NAD]
AT1G65930   ISOCITRATE DEHYDROGENASE, CYTOSOLIC (CICDH)
AT5G03290   ISOCITRATE DEHYDROGENASE(IDH5) [NAD]
AT3G55410   2-OXOGLUTARATE DEHYDROGENASE, E1 SUBUNIT-LIKE PROTEIN (OGDC-E1-L)
AT4G26910   2-OXOGLUTARATE DEHYDROGENASE E2 COMPONENT (OGDC-E2-2)
AT5G65750   2-OXOGLUTARATE DEHYDROGENASE, E1 COMPONENT (OGDC-E1)
AT5G55070   2-OXOGLUTARATE DEHYDROGENASE E2 COMPONENT (OGDC-E2-1)
AT5G23250   SUCCINYL-COA SYNTHETASE ALPHA 2 SUBUNIT (SCS-A-2)
AT2G20420   SUCCINYL-COA SYNTHETASE BETA SUBUNIT (SCS-B)
AT5G08300   SUCCINYL-COA SYNTHETASE ALPHA 1 SUBUNIT (SCS-A-1)
AT5G66760   SUCCINATE DEHYDROGENASE (SDH1-1)
AT3G27380   SUCCINATE DEHYDROGENASE (SDH2-1)

AT2G18450   SUCCINATE DEHYDROGENASE (SDH1-2)
AT5G40650   SUCCINATE DEHYDROGENASE (SDH2-2)
AT4G32210   SUCCINATE DEHYDROGENASE (SDH3-2)
AT5G09600   SUCCINATE DEHYDROGENASE (SDH3-1)
AT5G65165   SUCCINATE DEHYDROGENASE (SDH2-3)
AT2G47510   FUMARASE (FUM1)
AT5G50950   FUMARASE (FUM2)
AT5G56720   MALATE DEHYDROGENASE, cp (CMDH3)
AT1G04410   MALATE DEHYDROGENASE, cp (CMDH1)
AT1G53240   MALATE DEHYDROGENASE, mt (MMDH1)
AT5G43330   MALATE DEHYDROGENASE, cp (CMDH2)
AT3G15020   MALATE DEHYDROGENASE, mt (MMDH2)
AT2G22780   MALATE DEHYDROGENASE, PEROXISOMAL (PMDH1)
AT3G47520   MALATE DEHYDROGENASE, cp (CPMDH)
AT5G09660   MALATE DEHYDROGENASE, PEROXISOMAL (PMDH2)
AT2G44350   CITRATE SYNTHASE (CSY4)
AT3G60100   CITRATE SYNTHASE (CSY5)
AT3G58740   CITRATE SYNTHASE (CSY1)
AT3G58750   CITRATE SYNTHASE (CSY2)
AT2G42790   CITRATE SYNTHASE (CSY3)
AT1G09430   ATP-CITRATE LYASE (ACLA3)
AT1G10670   ATP-CITRATE LYASE (ACLA1)
AT1G60810   ATP-CITRATE LYASE (ACLA2)
AT3G06650   ATP-CITRATE LYASE (ACLB -1)
AT5G49460   ATP-CITRATE LYASE (ACLB -2)
AT1G01090   PYRUVATE DEHYDROGENASE E1 COMPONENT SUBUNIT ALPHA-3, cp (CPPDHE1-A3)
AT1G24180   PYRUVATE DEHYDROGENASE E1 COMPONENT SUBUNIT ALPHA-2, MT(MTPDHE1-A2)
AT1G30120   PYRUVATE DEHYDROGENASE E1 COMPONENT SUBUNIT BETA-2, cp (CPPDHE1-B2)
AT1G59900   PYRUVATE DEHYDROGENASE E1 COMPONENT SUBUNIT ALPHA-1, mt (MTPDHE1-A1)
AT2G34590   PYRUVATE DEHYDROGENASE E1 COMPONENT SUBUNIT BETA-3, CP (CPPDHE1-B3)
AT5G50850   PYRUVATE DEHYDROGENASE E1 COMPONENT SUBUNIT BETA-1, mt (MTPDHE1-B)
AT1G34430   PYRUVATE DEHYDROGENASE E2 COMPONENT (PDCE2-5)
AT1G54220   PYRUVATE DEHYDROGENASE E2 COMPONENT (PDCE2-3)
AT3G13930   PYRUVATE DEHYDROGENASE E2 COMPONENT (PDCE2-2)
AT3G25860   PYRUVATE DEHYDROGENASE E2 COMPONENT (PDCE2-4)
AT3G52200   PYRUVATE DEHYDROGENASE E2 COMPONENT (PDCE2-1)
AT1G48030   DIHYDROLIPOAMIDE DEHYDROGENASE, mt (MTLPD1)
AT3G16950   DIHYDROLIPOAMIDE DEHYDROGENASE (LPD1)
AT3G17240   DIHYDROLIPOAMIDE DEHYDROGENASE, mt (MTLPD2)
AT4G16155   DIHYDROLIPOAMIDE DEHYDROGENASE (LPD2)

8 References

1. Taylor, B. N. & Thompson, A. The International System of Units. *Nist Spec. Publ. 330 2008 Ed.* 92 (2008).
2. Buet, A. & Simontacchi, M. Nitric oxide and plant iron homeostasis. *Ann. N. Y. Acad. Sci.* **1340**, 39–46 (2015).
3. Fancy, N. N., Bahlmann, A.-K. & Loake, G. J. Nitric oxide function in plant abiotic stress. *Plant. Cell Environ.* **40**, 462–472 (2017).
4. Trapet, P. *et al.* NO signaling in plant immunity: A tale of messengers. *Phytochemistry* **112**, 72–79 (2015).
5. Yu, M., Lamattina, L., Spoel, S. H. & Loake, G. J. Nitric oxide function in plant biology: a redox cue in deconvolution. *New Phytol* **202**, 1142–1156 (2014).
6. Ageeva-Kieferle, A., Rudolf, E. E. & Lindermayr, C. Redox-Dependent Chromatin Remodeling: A New Function of Nitric Oxide as Architect of Chromatin Structure in Plants. *Front. Plant Sci.* **10**, (2019).
7. Mur, L. A. J. *et al.* Nitric oxide in plants: an assessment of the current state of knowledge. *AoB Plants* **5**, pls052 (2013).
8. Floryszak-Wieczorek, J., Milczarek, G., Arasimowicz, M. & Ciszewski, A. Do nitric oxide donors mimic endogenous NO-related response in plants? *Planta* **224**, 1363–1372 (2006).
9. Gross, F., Durner, J. & Gaupels, F. Nitric oxide, antioxidants and prooxidants in plant defence responses. *Front Plant Sci* **4**, 419 (2013).
10. Astier, J., Gross, I. & Durner, J. Nitric oxide production in plants: an update. *J. Exp. Bot.* 1–11 (2018).
11. Mohn, M., Thaqi, B. & Fischer-Schrader, K. Isoform-Specific NO Synthesis by Arabidopsis thaliana Nitrate Reductase. *Plants* **8**, 67 (2019).
12. Tejada-Jimenez, M., Llamas, A., Galván, A. & Fernández, E. Role of Nitrate Reductase in NO Production in Photosynthetic Eukaryotes. *Plants* **8**, 56 (2019).
13. Chaki, M. *et al.* Identification of nuclear target proteins for S-nitrosylation in pathogen-treated Arabidopsis thaliana cell cultures. *Plant Sci.* **238**, 115–126 (2015).
14. Begara-Morales, J. C. *et al.* Nitric oxide buffering and conditional nitric oxide release in stress response. *J. Exp. Bot.* **69**, ery072 (2018).
15. Buet, A., Galatro, A., Ramos-Artuso, F. & Simontacchi, M. Nitric oxide and plant mineral nutrition: current knowledge. *J. Exp. Bot.* 1–16 (2019).
16. Kolbert, Z., Feigl, G., Bordé, Á., Molnár, Á. & Erdei, L. Protein tyrosine nitration in plants: Present knowledge, computational prediction and future perspectives. *Plant Physiol. Biochem.* **113**, 56–63 (2017).
17. Kovacs, I. & Lindermayr, C. Nitric oxide-based protein modification: formation and site-specificity of protein S-nitrosylation. *Front Plant Sci* **4**, 137 (2013).
18. Feng, J., Chen, L. & Zuo, J. Protein S-Nitrosylation in plants: Current progresses and challenges. *J. Integr. Plant Biol.* **61**, 1206–1223 (2019).
19. Kovacs, I., Ageeva, A., König, E.-E. & Lindermayr, C. Chapter Two - S-Nitrosylation of Nuclear Proteins: New Pathways in Regulation of Gene Expression. in *Nitric Oxide and Signaling in Plants* (ed. Wendehenne, D. B. T.-A. in B. R.) vol. 77 15–39 (Academic Press, 2016).
20. Mengel, A., Chaki, M., Shekariesfahlan, A. & Lindermayr, C. Effect of nitric oxide on gene transcription - S-nitrosylation of nuclear proteins. *Front Plant Sci* **4**, 293 (2013).
21. León, J., Costa, Á. & Castillo, M. C. Nitric oxide triggers a transient metabolic reprogramming in Arabidopsis. *Sci. Rep.* **6**, 1–14 (2016).
22. Freschi, L. Nitric oxide and phytohormone interactions: current status and perspectives. *Front Plant Sci* **4**, 398 (2013).
23. Simontacchi, M., García-Mata, C., Bartoli, C. G., Santa-María, G. E. & Lamattina, L. Nitric oxide as a key component in hormone-regulated processes. *Plant Cell Rep.* **32**, 853–866 (2013).
24. Wang, B. L. *et al.* Nitric oxide is involved in phosphorus deficiency-induced cluster-root development and citrate exudation in white lupin. *New Phytol.* **187**, 1112–1123 (2010).
25. Planchet, E., Jagadis Gupta, K., Sonoda, M. & Kaiser, W. M. Nitric oxide emission from tobacco leaves and cell suspensions: rate limiting factors and evidence for the involvement of mitochondrial electron transport. *Plant J.* **41**, 732–743 (2005).
26. Planchet, E. & Kaiser, W. M. Nitric oxide production in plants: facts and fictions. *Plant Signal. Behav.* **1**, 46–51 (2006).
27. Gupta, K. J., Kumari, A., Florez-Sarasa, I., Fernie, A. R. & Igamberdiev, A. U. Interaction of nitric oxide with the components of the plant mitochondrial electron transport chain. *J. Exp. Bot.* **69**, 3413–3424 (2018).
28. Jasid, S., Simontacchi, M., Bartoli, C. G. & Puntarulo, S. Chloroplasts as a nitric oxide cellular source. Effect of reactive nitrogen species on chloroplastic lipids and proteins. *Plant Physiol.* **142**, 1246–1255 (2006).
29. Bethke, P. C. Apoplastic Synthesis of Nitric Oxide by Plant Tissues. *Plant Cell Online* **16**, 332–341 (2004).
30. Eick, M. & Stöhr, C. Denitrification by plant roots? New aspects of plant plasma membrane-bound nitrate reductase. *Protoplasma* **249**, 909–918 (2012).
31. Chamizo-Ampudia, A. *et al.* A dual system formed by the ARC and NR molybdoenzymes mediates nitrite-dependent NO production in Chlamydomonas. *Plant Cell Environ.* **39**, 2097–2107 (2016).
32. Yang, J. *et al.* Oxyl and hydroxyl radical transfer in mitochondrial amidoxime reducing component-catalyzed nitrite reduction. *J. Am. Chem. Soc.* **137**, 5276–5279 (2015).
33. Chamizo-Ampudia, A., Sanz-Luque, E., Llamas, A., Galvan, A. & Fernandez, E. Nitrate Reductase Regulates Plant Nitric Oxide Homeostasis. *Trends Plant Sci.* **22**, 163–174 (2017).
34. Zaffagnini, M. *et al.* Protein S-nitrosylation in photosynthetic organisms: A comprehensive overview with future

perspectives. *Biochim. Biophys. Acta - Proteins Proteomics* **1864**, 952–966 (2016).

35. Corpas, F. J. & Palma, J. M. Assessing Nitric Oxide (NO) in Higher Plants: An Outline. *Nitrogen* **1**, 12–20 (2018).

36. Gross, I. & Durner, J. In Search of Enzymes with a Role in 3', 5'-Cyclic Guanosine Monophosphate Metabolism in Plants. *Front. Plant Sci.* **7**, 1–9 (2016).

37. Zhang, J. *et al.* Phytoglobin overexpression promotes barley growth in the presence of enhanced level of atmospheric nitric oxide. *J. Exp. Bot.* (2019).

38. Jahnová, J., Luhová, L. & Petřivalský, M. S-Nitrosoglutathione Reductase—The Master Regulator of Protein S-Nitrosation in Plant NO Signaling. *Plants* **8**, 48 (2019).

39. Lindermayr, C. Crosstalk between reactive oxygen species and nitric oxide in plants: Key role of S -nitrosoglutathione reductase. *Free Radic. Biol. Med.* 1–6 (2017).

40. Mengel, A. *et al.* Nitric oxide modulates histone acetylation at stress genes by inhibition of histone deacetylases. *Plant Physiol.* pp.01734.2016 (2016).

41. Broniowska, K. A., Diers, A. R. & Hogg, N. S-nitrosoglutathione. *Biochim. Biophys. Acta* **1830**, 3173–81 (2013).

42. Kovacs, I. *et al.* ROS-Mediated Inhibition of S-nitrosoglutathione Reductase Contributes to the Activation of Anti-oxidative Mechanisms. *Front. Plant Sci.* **7**, 1–17 (2016).

43. Guerra, D., Ballard, K., Truebridge, I. & Vierling, E. S-Nitrosation of Conserved Cysteines Modulates Activity and Stability of S-Nitrosoglutathione Reductase (GSNOR). *Biochemistry* **55**, 2452–2464 (2016).

44. Hu, J. *et al.* Site-specific nitrosoproteomic identification of endogenously S-nitrosylated proteins in Arabidopsis. *Plant Physiol.* **167**, 1731–1746 (2015).

45. Feechan, A. *et al.* A central role for S-nitrosothiols in plant disease resistance. *Proc Natl Acad Sci U S A* **102**, 8054–8059 (2005).

46. Lee, U., Wie, C., Fernandez, B. O., Feelisch, M. & Vierling, E. Modulation of nitrosative stress by S-nitrosoglutathione reductase is critical for thermotolerance and plant growth in Arabidopsis. *Plant Cell* **20**, 786–802 (2008).

47. Chen, R. *et al.* The Arabidopsis PARAQUAT RESISTANT2 gene encodes an S-nitrosoglutathione reductase that is a key regulator of cell death. *Cell Res.* **19**, 1377–1387 (2009).

48. Kawabe, H., Ohtani, M., Kurata, T., Sakamoto, T. & Demura, T. Protein S-Nitrosylation Regulates Xylem Vessel Cell Differentiation in Arabidopsis. *Plant Cell Physiol.* **59**, 17–29 (2018).

49. Yun, B. W. *et al.* Nitric oxide and S-nitrosoglutathione function additively during plant immunity. *New Phytol* **211**, 516–526 (2016).

50. Zhan, N. *et al.* S-Nitrosylation Targets GSNO Reductase for Selective Autophagy during Hypoxia Responses in Plants. *Mol. Cell* **71**, 142-154.e6 (2018).

51. Imran, Q. M. *et al.* Transcriptome profile of NO-induced Arabidopsis transcription factor genes suggests their putative regulatory role in multiple biological processes. *Sci. Rep.* **8**, 1–14 (2018).

52. Tada, Y. *et al.* Plant immunity requires conformational changes [corrected] of NPR1 via S-nitrosylation and thioredoxins. *Science (80-.).* **321**, 952–956 (2008).

53. Lindermayr, C., Sell, S., Muller, B., Leister, D. & Durner, J. Redox regulation of the NPR1-TGA1 system of Arabidopsis thaliana by nitric oxide. *Plant Cell* **22**, 2894–2907 (2010).

54. Tavares, C. P. *et al.* S-nitrosylation influences the structure and DNA binding activity of AtMYB30 transcription factor from Arabidopsis thaliana. *Biochim. Biophys. Acta - Proteins Proteomics* **1844**, 810–817 (2014).

55. Serpa, V. *et al.* Inhibition of AtMYB2 DNA-binding by nitric oxide involves cysteine S-nitrosylation. *Biochem Biophys Res Commun* **361**, 1048–1053 (2007).

56. Wang, S. *et al.* Nitric oxide activation of Erk1/2 regulates the stability and translation of mRNA transcripts containing CU-rich elements. *Nucleic Acids Res.* **34**, 3044–3056 (2006).

57. Schvartzman, J. M., Thompson, C. B. & Finley, L. W. S. Metabolic regulation of chromatin modifications and gene expression. **217**, 2247–2259 (2018).

58. Zhang, H., Lang, Z. & Zhu, J. K. Dynamics and function of DNA methylation in plants. *Nat. Rev. Mol. Cell Biol.* **19**, 489–506 (2018).

59. Vasudevan, D. *et al.* Nitric oxide regulates gene expression in cancers by controlling histone posttranslational modifications. *Cancer Res.* **75**, 5299–5309 (2015).

60. Nott, A. & Riccio, A. Nitric oxide-mediated epigenetic mechanisms in developing neurons. *Cell Cycle* vol. 8 725–730 (2009).

61. Li, H. *et al.* Plant-specific histone deacetylases HDT1/2 regulate GIBBERELLIN 2-OXIDASE2 expression to control arabidopsis root meristem cell number. *Plant Cell* **29**, 2183–2196 (2017).

62. Ou, X. *et al.* DNA Methylation Changes Induced in Rice by Exposure to High Concentrations of the Nitric Oxide Modulator, Sodium Nitroprusside. *Plant Mol. Biol. Report.* (2015).

63. Hickok, J. R., Vasudevan, D., Antholine, W. E. & Thomas, D. D. Nitric oxide modifies global histone methylation by inhibiting Jumonji C domain-containing demethylases. *J Biol Chem* **288**, 16004–16015 (2013).

64. Shen, Y., Issakidis-Bourguet, E. & Zhou, D. X. Perspectives on the interactions between metabolism, redox, and epigenetics in plants. *J. Exp. Bot.* **67**, 5291–5300 (2016).

65. Hussain, A. *et al.* Nitric Oxide Mediated Transcriptome Profiling Reveals Activation of Multiple Regulatory Pathways in Arabidopsis thaliana. *Front. Plant Sci.* **7**, 1–18 (2016).

66. Gibbs, D. J. *et al.* Nitric Oxide Sensing in Plants Is Mediated by Proteolytic Control of Group VII ERF Transcription Factors. *Mol. Cell* **53**, 369–379 (2014).

67. He, Y., Xue, H., Li, Y. & Wang, X. Nitric oxide alleviates cell death through protein S-nitrosylation and transcriptional regulation during the ageing of elm seeds. *J. Exp. Bot.* **69**, 5141–5155 (2018).

68. Palmieri, M. C. *et al.* Nitric oxide-responsive genes and promoters in Arabidopsis thaliana: A bioinformatics approach. *J. Exp. Bot.* **59**, 177–186 (2008).

69. Puyaubert, J. *et al.* Identification of endogenously S-nitrosylated proteins in Arabidopsis plantlets: effect of cold stress on cysteine nitrosylation level. *Plant Sci* **215**–**216**, 150–156 (2014).

70. Maldonado-Alconada, A. M. *et al.* Proteomic analysis of Arabidopsis protein S-nitrosylation in response to inoculation with Pseudomonas syringae. *Acta Physiol. Plant.* **33**, 1493–1514 (2011).

71. Fares, A., Rossignol, M. & Peltier, J. B. Proteomics investigation of endogenous S-nitrosylation in Arabidopsis. *Biochem Biophys Res Commun* **416**, 331–336 (2011).

72. Lindermayr, C., Saalbach, G. & Durner, J. Proteomic identification of S-nitrosylated proteins in Arabidopsis. *Plant Physiol* **137**, 921–930 (2005).

73. Lozano-Juste, J., Colom-Moreno, R. & León, J. In vivo protein tyrosine nitration in Arabidopsis thaliana. *J. Exp. Bot.* **62**, 3501–3517 (2011).

74. Chaki, M. *et al.* Protein targets of tyrosine nitration in sunflower (Helianthus annuus L.) hypocotyls. *J. Exp. Bot.* **60**, 4221–4234 (2009).

75. Begara-Morales, J. C. *et al.* Protein tyrosine nitration in pea roots during development and senescence. *J. Exp. Bot.* **64**, 1121–1134 (2013).

76. Abat, J. K. & Deswal, R. Differential modulation of S-nitrosoproteome of Brassica juncea by low temperature: change in S-nitrosylation of Rubisco is responsible for the inactivation of its carboxylase activity. *Proteomics* **9**, 4368–4380 (2009).

77. Navarre, D. a, Wendehenne, D., Durner, J., Noad, R. & Klessig, D. F. Nitric oxide modulates the activity of tobacco aconitase. *Plant Physiol.* **122**, 573–582 (2000).

78. Palmieri, M. C., Lindermayr, C., Bauwe, H., Steinhauser, C. & Durner, J. Regulation of plant glycine decarboxylase by s-nitrosylation and glutathionylation. *Plant Physiol* **152**, 1514–1528 (2010).

79. Romero-Puertas, M. C. *et al.* Proteomic analysis of S-nitrosylated proteins in Arabidopsis thaliana undergoing hypersensitive response. *Proteomics* **8**, 1459–1469 (2008).

80. Benoit, M. *et al.* Replication-coupled histone H3.1 deposition determines nucleosome composition and heterochromatin dynamics during Arabidopsis seedling development. *New Phytol.* **221**, 385–398 (2019).

81. Fan, G. & Li, J. Regions identity between the genome of vertebrates and non-retroviral families of insect viruses. *Virol. J.* **8**, 511 (2011).

82. Begara-Morales, J. C. *et al.* Differential transcriptomic analysis by RNA-seq of GSNO-responsive genes between arabidopsis roots and leaves. *Plant Cell Physiol.* **55**, 1080–1095 (2014).

83. Mills, B. B., McBride, C. M. & Riddle, N. C. Chapter 8 - Epigenetic inheritance. in (eds. Huang, S., Litt, M. D. & Blakey, C. A. B. T.-E. G. E. and R.) 183–208 (Academic Press, 2015). doi:https://doi.org/10.1016/B978-0-12-799958-6.00008-1.

84. Linder, S. J. & Mostoslavsky, R. *Interaction Between Cellular Metabolic States and Chromatin Dynamics*. *Chromatin Regulation and Dynamics* vol. 384 (Elsevier Inc., 2016).

85. Pontvianne, F., Blevins, T. & Pikaard, C. Arabidopsis Histone Lysine Methyltransferases. *Adv. Bot. Res.* **53**, 1–22 (2010).

86. Forneris, F. *et al.* A highly specific mechanism of histone H3-K4 recognition by histone demethylase LSD1. *J. Biol. Chem.* **281**, 35289–35295 (2006).

87. Shi, Y. G. & Tsukada, Y. The discovery of histone demethylases. *Cold Spring Harb. Perspect. Biol.* **5**, 2–4 (2013).

88. Liu, C., Lu, F., Cui, X. & Cao, X. Histone Methylation in Higher Plants. *Annu. Rev. Plant Biol.* **61**, 395–420 (2010).

89. Xiao, J., Lee, U. S. & Wagner, D. Tug of war: adding and removing histone lysine methylation in Arabidopsis. *Curr. Opin. Plant Biol.* **34**, 41–53 (2016).

90. Thorstensen, T., Grini, P. E. & Aalen, R. B. SET domain proteins in plant development. *Biochim. Biophys. Acta - Gene Regul. Mech.* **1809**, 407–420 (2011).

91. Du, J., Johnson, L. M., Jacobsen, S. E. & Patel, D. J. DNA methylation pathways and their crosstalk with histone methylation. *Nat. Rev. Mol. Cell Biol.* **16**, 519–532 (2015).

92. Harris, C. J. *et al.* A DNA methylation reader complex that enhances gene transcription. *Science (80-.).* **362**, 1182–1186 (2018).

93. Berr, A., Ménard, R., Heitz, T. & Shen, W. H. Chromatin modification and remodelling: A regulatory landscape for the control of Arabidopsis defence responses upon pathogen attack. *Cell. Microbiol.* **14**, 829–839 (2012).

94. Stroud, H., Greenberg, M. V. C., Feng, S., Bernatavichute, Y. V & Jacobsen, S. E. Comprehensive analysis of silencing mutants reveals complex regulation of the Arabidopsis methylome. *Cell* **152**, 352–364 (2013).

95. Huang, Y., Chen, D., Liu, C., Shen, W. & Ruan, Y. Evolution and conservation of JmjC domain proteins in the green lineage. *Mol. Genet. Genomics* **291**, 33–49 (2016).

96. Ishihara, H. *et al.* Primed histone demethylation regulates shoot regenerative competency. *Nat. Commun.* **10**, (2019).

97. Martignago, D. *et al.* The four FAD-dependent histone demethylases of arabidopsis are differently involved in the control of flowering time. *Front. Plant Sci.* **10**, 1–15 (2019).

98. Walport, L. J. *et al.* Arginine demethylation is catalysed by a subset of JmjC histone lysine demethylases. *Nat. Commun.* **7**, 1–12 (2016).

99. Koehntop, K. D., Emerson, J. P. & Que, L. The 2-His-1-carboxylate facial triad: A versatile platform for dioxygen activation by mononuclear non-heme iron(II) enzymes. *J. Biol. Inorg. Chem.* **10**, 87–93 (2005).

100. Qian, S., Wang, Y., Ma, H. & Zhang, L. Expansion and Functional Divergence of Jumonji C-Containing Histone Demethylases: Significance of Duplications in Ancestral Angiosperms and Vertebrates. *Plant Physiol.* **168**, 1321–1337 (2015).

101. Kabelitz, T. *et al.* A JUMONJI Protein with E3 Ligase and Histone H3 Binding Activities Affects Transposon Silencing in Arabidopsis. *Plant Physiol.* **171**, 344–358 (2016).

102. Deng, S. *et al.* JMJ24 binds to RDR2 and is required for the basal level transcription of silenced loci in Arabidopsis. *Plant J.* **83**, 770–782 (2015).

103. Audonnet, L., Shen, Y. & Zhou, D. X. JMJ24 antagonizes histone H3K9 demethylase IBM1/JMJ25 function and interacts with RNAi pathways for gene silencing. *Gene Expr. Patterns* **25**–**26**, 1–7 (2017).

104. Cheng, K. *et al.* Histone tales: lysine methylation, a protagonist in Arabidopsis development. *J. Exp. Bot.* (2019).

105. Inagaki, S. *et al.* Gene-body chromatin modification dynamics mediate epigenome differentiation in Arabidopsis. *EMBO J.* e201694983 (2017).

106. Bewick, A. J. & Schmitz, R. J. Gene body DNA methylation in plants. *Curr. Opin. Plant Biol.* **36**, 103–110 (2017).

107. Matzke, M. A. & Mosher, R. A. RNA-directed DNA methylation: an epigenetic pathway of increasing complexity. *Nat Rev Genet* **15**, 394–408 (2014).

108. Song, X. & Cao, X. Context and Complexity: Analyzing Methylation in Trinucleotide Sequences. *Trends Plant Sci.* **22**, 351–353 (2017).

109. Lei, M. *et al.* Regulatory link between DNA methylation and active demethylation in Arabidopsis. *Proc. Natl. Acad. Sci. U. S. A.* **112**, 3553–7 (2015).

110. Williams, B. P., Pignatta, D., Henikoff, S. & Gehring, M. Methylation-Sensitive Expression of a DNA Demethylase Gene Serves As an Epigenetic Rheostat. *PLoS Genet.* **11**, 1–18 (2015).

111. Duan, C. G. *et al.* A pair of transposon-derived proteins function in a histone acetyltransferase complex for active DNA demethylation. *Cell Res.* **27**, 226–240 (2017).

112. Zheng, X. *et al.* ROS3 is an RNA-binding protein required for DNA demethylation in Arabidopsis. *Nature* **455**, 1259–1262 (2008).

113. Wang, X. *et al.* The cytosolic Fe-S cluster assembly component MET18 is required for the full enzymatic activity of ROS1 in active DNA demethylation. *Sci. Rep.* **6**, 1–15 (2016).

114. Li, Y., Kumar, S. & Qian, W. Active DNA demethylation: mechanism and role in plant development. *Plant Cell Rep.* **37**, 77–85 (2018).

115. Su, X., Wellen, K. E. & Rabinowitz, J. D. Metabolic control of methylation and acetylation. *Curr. Opin. Chem. Biol.* **30**, 52–60 (2016).

116. Gorelova, V., Ambach, L., Rébeillé, F., Stove, C. & Van Der Straeten, D. Folates in Plants: Research Advances and Progress in Crop Biofortification. *Front. Chem.* **5**, 1–20 (2017).

117. Sauter, M., Moffatt, B., Saechao, M. C., Hell, R. & Wirtz, M. Methionine salvage and S-adenosylmethionine: essential links between sulfur, ethylene and polyamine biosynthesis. *Biochem J* **451**, 145–154 (2013).

118. Yan, X. *et al.* METHIONINE SYNTHASE1 Is Involved in Chromatin Silencing by Maintaining DNA and Histone Methylation. *Plant Physiol.* **181**, 249–261 (2019).

119. Huang, X.-Y., Li, M., Luo, R., Zhao, F.-J. & Salt, D. E. Epigenetic regulation of sulfur homeostasis in plants. *J. Exp. Bot.* **70**, 4171–4182 (2019).

120. Baubec, T. *et al.* Cooperation of multiple chromatin modifications can generate unanticipated stability of epigenetic States in Arabidopsis. *Plant Cell* **22**, 34–47 (2010).

121. Ouyang, B. *et al.* Transcriptome profiling and methyl homeostasis of an Arabidopsis mutant deficient in S-adenosylhomocysteine hydrolase1 (SAHH1). *Plant Mol Biol* **79**, 315–331 (2012).

122. Fulnecek, J. *et al.* Inhibition of SAH-hydrolase activity during seed germination leads to deregulation of flowering genes and altered flower morphology in tobacco. *Mol Genet Genomics* **285**, 225–236 (2011).

123. Rocha, P. S. *et al.* The Arabidopsis HOMOLOGY-DEPENDENT GENE SILENCING1 gene codes for an S-adenosyl-L-homocysteine hydrolase required for DNA methylation-dependent gene silencing. *Plant Cell* **17**, 404–417 (2005).

124. Li, C. H. *et al.* Down-regulation of S-adenosyl-L: -homocysteine hydrolase reveals a role of cytokinin in promoting transmethylation reactions. *Planta* **228**, 125–136 (2008).

125. Jordan, N. D., West, J. P., Bottley, A., Sheikh, M. & Furner, I. Transcript profiling of the hypomethylated hog1 mutant of Arabidopsis. *Plant Mol Biol* **65**, 571–586 (2007).

126. Tanaka, H. *et al.* Morphological changes and hypomethylation of DNA in transgenic tobacco expressing antisense RNA of the S-adenosyl-L-homocysteine hydrolase gene. *Plant Mol. Biol.* **35**, 981–986 (1997).

127. Fojtová, M., Kovarík, A., Votruba, I. & Holý, A. Evaluation of the impact of S-adenosylhomocysteine metabolic pools on cytosine methylation of the tobacco genome. *Eur. J. Biochem.* **252**, 347–352 (1998).

128. Kovǎřík, A., Koukalová, B., Holý, A. & Bezděk, M. Sequence-specific hypomethylation of the tobacco genome induced with dihydroxypropyladenine, ethionine and 5-azacytidine. *FEBS Lett.* **353**, 309–311 (1994).

129. Meng, J. *et al.* METHIONINE ADENOSYLTRANSFERASE 4 mediates DNA and histone methylation. *Plant Physiol.* **177**, 652 LP – 670 (2018).

130. González, B. & Vera, P. Folate Metabolism Interferes with Plant Immunity through 1C Methionine Synthase-Directed Genome-wide DNA Methylation Enhancement. *Mol. Plant* **12**, 1227–1242 (2019).

131. Zhou, H.-R. *et al.* Folate Polyglutamylation Is Involved in Chromatin Silencing by Maintaining Global DNA Methylation and Histone H3K9 Dimethylation in Arabidopsis. *Plant Cell* **25**, 2545–2559 (2013).

132. Zhang, H. *et al.* Sulfamethazine suppresses epigenetic silencing in Arabidopsis by impairing folate synthesis. *Plant Cell* **24**, 1230–1241 (2012).

133. Groth, M. *et al.* MTHFD1 controls DNA methylation in Arabidopsis. *Nat Commun* **7**, 11640 (2016).

134. Huang, X. Y. *et al.* Nuclear Localised MORE SULPHUR ACCUMULATION1 Epigenetically Regulates Sulphur Homeostasis in Arabidopsis thaliana. *PLoS Genet.* **12**, 1–29 (2016).

135. Shi, Y. Y. Y. Y. *et al.* Histone demethylation mediated by the nuclear amine oxidase homolog LSD1. *Cell* **119**, 941–953 (2004).

136. Abdulla, A. *et al.* Regulation of lipogenic gene expression by lysine-specific histone demethylase-1 (LSD1). *J. Biol. Chem.* **289**, 29937–29947 (2014).

137. Pan, D., Mao, C. & Wang, Y. X. Suppression of Gluconeogenic Gene Expression by LSD1-Mediated Histone Demethylation. *PLoS One* **8**, 1–9 (2013).

138. Xiao, M. *et al.* Inhibition of α-KG-dependent histone and DNA demethylases by fumarate and succinate that are accumulated in mutations of FH and SDH tumor suppressors. *Genes Dev.* **26**, 1326–1338 (2012).

139. Palczewski, M. B., Petraitis, H. & Thomas, D. D. Nitric oxide is an epigenetic regulator of histone post-translational modifications in cancer. *Curr. Opin. Physiol.* **9**, 94–99 (2019).

140. Bovee, R. C., Hickok, J. R., Vasudevan, D. & Thomas, D. D. *Mechanisms of Epigenetic Regulation by Nitric Oxide*. *Nitric Oxide* (Elsevier Inc., 2017).

141. Socco, S., Bovee, R. C., Palczewski, M. B., Hickok, J. R. & Thomas, D. D. Epigenetics: The third pillar of nitric oxide signaling. *Pharmacol. Res.* **121**, 52–58 (2017).

142. Vasudevan, D., Bovee, R. C. & Thomas, D. D. Nitric oxide, the new architect of epigenetic landscapes. *Nitric Oxide - Biol. Chem.* **59**, 54–62 (2016).

143. Costa-Broseta, Á. *et al.* Nitric Oxide Controls Constitutive Freezing Tolerance in Arabidopsis by Attenuating the Levels of Osmoprotectants, Stress-Related Hormones and Anthocyanins. *Sci. Rep.* **8**, 1–10 (2018).

144. Gupta, K. J. *et al.* Inhibition of aconitase by nitric oxide leads to induction of the alternative oxidase and to a shift of metabolism towards biosynthesis of amino acids. *J. Exp. Bot.* **63**, 1773–1784 (2012).

145. Zhao, H. *et al.* Epigenetic effects of RRx-001: a possible unifying mechanism of anticancer activity. *Oncotarget* **6**, 43172–81 (2015).

146. Hmadcha, B. A., Bedoya, F. J., Sobrino, F. & Pintado, E. Methylation-dependent Gene Silencing Induced by Interleukin 1β Via Nitric Oxide Production. **190**, 1595–1603 (1999).

147. Huang, F. Y. *et al.* Helicobacter pylori induces promoter methylation of E-cadherin via interleukin-1β activation of nitric oxide production in gastric cancer cells. *Cancer* **118**, 4969–4980 (2012).

148. Bovee, R., Pham, V., Fernandez, J., Tretyakova, N. & Thomas, D. D. Nitric oxide is an epigenetic regulator of gene expression by directly controlling DNA methylation patterns. *Free Radic. Biol. Med.* **120**, S114 (2018).

149. Sen, N. & Snyder, S. H. Neurotrophin-mediated degradation of histone methyltransferase by S-nitrosylation cascade regulates neuronal differentiation. *Proc. Natl. Acad. Sci.* **108**, 20178–20183 (2011).

150. Parani, M. *et al.* Microarray analysis of nitric oxide responsive transcripts in Arabidopsis. *Plant Biotechnol. J.* **2**, 359–366 (2004).

151. Ahlfors, R., Brosché, M., Kollist, H. & Kangasjärvi, J. Nitric oxide modulates ozone-induced cell death, hormone biosynthesis and gene expression in Arabidopsis thaliana. *Plant J.* **58**, 1–12 (2009).

152. Shi, H., Ye, T., Zhu, J. K. & Chan, Z. Constitutive production of nitric oxide leads to enhanced drought stress resistance and extensive transcriptional reprogramming in Arabidopsis. *J. Exp. Bot.* **65**, 4119–4131 (2014).

153. Zhang, C. *et al.* Arabidopsis AGDP1 links H3K9me2 to DNA methylation in heterochromatin. *Nat. Commun.* **9**, 4547 (2018).

154. Yan, D., Zhang, Y., Niu, L., Yuan, Y. & Cao, X. Identification and characterization of two closely related histone H4 arginine 3 methyltransferases in Arabidopsis thaliana. *Biochem. J.* **408**, 113–121 (2007).

155. Hu, J. *et al.* Nitric Oxide Regulates Protein Methylation during Stress Responses in Plants. *Mol. Cell* **67**, 702-710.e4 (2017).

156. Yang, H. *et al.* A companion cell-dominant and developmentally regulated H3K4 demethylase controls flowering time in Arabidopsis via the repression of FLC expression. *PLoS Genet* **8**, e1002664 (2012).

157. Deng, X. *et al.* Arginine methylation mediated by the Arabidopsis homolog of PRMT5 is essential for proper pre-mRNA splicing. *Proc. Natl. Acad. Sci. U. S. A.* **107**, 19114–9 (2010).

158. Vernis, L. *et al.* Fe-S Clusters Emerging as Targets of Therapeutic Drugs. *Oxid. Med. Cell. Longev.* **2017**, (2017).

159. Danishpajooh, I. O. *et al.* Nitric Oxide Inhibits Methionine Synthase Activity in Vivo and Disrupts Carbon Flow through the Folate Pathway. *J. Biol. Chem.* **276**, 27296–27303 (2001).

160. Lindermayr, C., Saalbach, G., Bahnweg, G. & Durner, J. Differential inhibition of Arabidopsis methionine adenosyltransferases by protein S-nitrosylation. *J Biol Chem* **281**, 4285–4291 (2006).

161. Pérez-Mato, I., Castro, C., Ruiz, F. A., Corrales, F. J. & Mato, J. M. Methionine adenosyltransferase S-nitrosylation is regulated by the basic and acidic amino acids surrounding the target thiol. *J. Biol. Chem.* **274**, 17075–17079 (1999).

162. Pikaard, C. S. & Mittelsten Scheid, O. Epigenetic Regulation in Plants. *Cold Spring Harb. Perspect. Biol.* **6**, (2014).

163. Arnold, K., Bordoli, L., Kopp, J. & Schwede, T. The SWISS-MODEL workspace: A web-based environment for protein structure homology modelling. *Bioinformatics* **22**, 195–201 (2006).

164. Brzezinski, K., Dauter, Z. & Jaskolski, M. High-resolution structures of complexes of plant S - Adenosyl-l-homocysteine hydrolase (Lupinus luteus). *Acta Crystallogr. Sect. D Biol. Crystallogr.* **68**, 218–231 (2012).

165. DeLano, L. W. *The PyMOL Molecular Graphics System (2002) DeLano Scientific, Palo Alto, CA, USA. http://www.pymol.org*. (2002).

166. Badri, D. V. *et al.* Transcriptome analysis of Arabidopsis roots treated with signaling compounds: A focus on signal transduction, metabolic regulation and secretion. *New Phytol.* **179**, 209–223 (2008).

167. García-Giménez, J. L., Romá-Mateo, C., Pérez-Machado, G., Peiró-Chova, L. & Pallardó, F. V. Role of glutathione in the regulation of epigenetic mechanisms in disease. *Free Radic. Biol. Med.* **112**, 36–48 (2017).

168. Lu, C. & Thompson, C. B. Metabolic regulation of epigenetics. *Cell Metab.* **16**, 9–17 (2012).

169. Sambrook, J. & Russell, D. W. *Molecular cloning: a laboratory manual*. (Cold Spring Harbor Laboratory Press, 2001).

170. Wu, X. *et al.* A mutant deficient in S-adenosylhomocysteine hydrolase in Arabidopsis shows defects in root-hair development. *Botany* **87**, 571–584 (2009).

171. Morel, J.-B., Mourrain, P., Béclin, C. & Vaucheret, H. DNA methylation and chromatin structure affect transcriptional and post-transcriptional transgene silencing in Arabidopsis. *Curr. Biol.* **10**, 1591–1594 (2000).

172. Murashige, T. & Skoog, F. A Revised Medium for Rapid Growth and Bio Assays with Tobacco Tissue Cultures. *Physiol Plant.* **15**, 473–497 (1962).

173. Chomczynski, P. & Sacchi, N. Single-Step Method of RNA Isolation by Acid Guanidinium Extraction. **159**, 156–159 (1987).

174. Koncz, C. & Schell, J. The promoter of TL-DNA gene 5 controls the tissue-specific expression of chimaeric genes carried by a novel type of Agrobacterium binary vector. *MGG Mol. Gen. Genet.* **204**, 383–396 (1986).

175. Weber, S., Horn, R. & Friedt, W. Isolation of a low-copy plasmid from agrobacterium using QIAprep® technology. *Qiagen News* 11–12 (1998).

176. Clough, S. J. & Bent, A. F. Floral dip: a simplified method for Agrobacterium-mediated transformation of Arabidopsis thaliana. *Plant J.* **16**, 735–743 (1998).

177. Earley, K. W. *et al.* Gateway-compatible vectors for plant functional genomics and proteomics. *Plant J.* **45**, 616–629 (2006).

178. Lyska, D., Engelmann, K., Meierhoff, K. & Westhoff, P. pAUL: A Gateway-Based Vector System for Adaptive Expression and Flexible Tagging of Proteins in Arabidopsis. *PLoS One* **8**, 1–12 (2013).

179. Bimboim, H. C. & Doly, J. A rapid alkaline extraction procedure for screening recombinant plasmid DNA. *Nucleic Acids Res.* **7**, 1513–1523 (1979).

180. O'Malley, R. C., Barragan, C. C. & Ecker, J. R. A user's guide to the arabidopsis T-DNA insertion mutant collections. *Plant Funct. Genomics Methods Protoc. Second Ed.* 323–342 (2015).

181. Sutherland, E., Coe, L. & Raleigh, E. A. McrBC: a multisubunit GTP-dependent restriction endonuclease. *J. Mol. Biol.* **225**, 327–348 (1992).

182. Stewart, F. J., Panne, D., Bickle, T. A. & Raleigh, E. A. Methyl-specific DNA binding by McrBC, a modification-dependent restriction enzyme. *J. Mol. Biol.* **298**, 611–622 (2000).

183. Krueger, F. & Andrews, S. R. Bismark: A flexible aligner and methylation caller for Bisulfite-Seq applications. *Bioinformatics* **27**, 1571–1572 (2011).

184. Langmead, B. & Salzberg, S. L. Fast gapped-read alignment with Bowtie 2. *Nat. Methods* **9**, 357–359 (2012).

185. Barturen, G., Rueda, A., Oliver, J. L. & Hackenberg, M. MethylExtract: High-Quality methylation maps and SNV calling from whole genome bisulfite sequencing data. *F1000Research* 1–23 (2014).

186. Becker, C. *et al.* Spontaneous epigenetic variation in the Arabidopsis thaliana methylome. *Nature* **480**, 245–249 (2011).

187. Hagmann, J. *et al.* Century-scale Methylome Stability in a Recently Diverged Arabidopsis thaliana Lineage. *PLoS Genet.* **11**, (2015).

188. Richards, C. L. *et al.* Ecological plant epigenetics: Evidence from model and non-model species, and the way forward. *Ecol. Lett.* **20**, 1576–1590 (2017).

189. Bray, N. L., Pimentel, H., Melsted, P. & Pachter, L. Near-optimal probabilistic RNA-seq quantification. *Nat. Biotechnol.* **34**, 525–527 (2016).

190. Love, M. I., Huber, W. & Anders, S. Moderated estimation of fold change and dispersion for RNA-seq data with DESeq2. *Genome Biol.* **15**, 550 (2014).

191. Cheng, Y. T. *et al.* Nuclear pore complex component MOS7/Nup88 is required for innate immunity and nuclear accumulation of defense regulators in Arabidopsis. *Plant Cell* **21**, 2503–2516 (2009).

192. Feller, C., Forné, I., Imhof, A. & Becker, P. B. Global and specific responses of the histone acetylome to systematic perturbation. *Mol. Cell* **57**, 559–572 (2015).

193. Rappsilber, J., Mann, M. & Ishihama, Y. Protocol for micro-purification, enrichment, pre-fractionation and storage of peptides for proteomics using StageTips. *Nat Protoc* **2**, 1896–1906 (2007).

194. Peri, S., Steen, H. & Pandey, A. GPMAW – a software tool for analyzing proteins and peptides. *Trends Biochem. Sci.* **26**, 687–689 (2001).

195. Laemmli, U. K. Cleavage of Structural Proteins during the Assembly of the Head of Bacteriophage T4. *Nature* **227**, 680–685 (1970).

196. Towbin, H., Staehelin, T. & Gordon, J. Electrophoretic transfer of proteins from polyacrylamide gels to nitrocellulose sheets: procedure and some applications. *Proc. Natl. Acad. Sci. U. S. A.* **76**, 4350–4 (1979).

197. Pereira, L. A. *et al.* Methyl recycling activities are co-ordinately regulated during plant development. *J Exp Bot* **58**, 1083–1098 (2007).

198. Jaffrey, S. R. & Snyder, S. H. The Biotin Switch Method for the Detection of S-Nitrosylated Proteins. *Sci. Signal.* **2001**, pl1–pl1 (2001).

199. Forrester, M. T. *et al.* Proteomic analysis of S-nitrosylation and denitrosylation by resin-assisted capture. *Nat. Biotechnol.* **27**, 557–559 (2009).

200. Bradford, M. M. A rapid and sensitive method for the quantitation of microgram quantities of protein utilizing the principle of protein-dye binding. *Anal. Biochem.* **72**, 248–254 (1976).

201. Fujioka, M. & Takata, Y. S-Adenosylhomocysteine hydrolase from rat liver. Purification and some properties. *J. Biol. Chem.* **256**, 1631–1635 (1981).

202. Takata, Y. *et al.* Catalytic mechanism of S-adenosylhomocysteine hydrolase. Site-directed mutagenesis of Asp-130, Lys-185, Asp-189, and Asn-190. *J Biol Chem* **277**, 22670–22676 (2002).

203. Sakamoto, A., Ueda, M. & Morikawa, H. Arabidopsis glutathione-dependent formaldehyde dehydrogenase is an S-nitrosoglutathione reductase. *FEBS Lett.* **515**, 20–24 (2002).

204. Jefferson, R. A., Kavanagh, T. A. & Bevan, M. W. GUS fusions: beta-glucuronidase as a sensitive and versatile gene fusion marker in higher plants. *EMBO J.* **6**, 3901–7 (1987).

205. Lichtenthaler, H. K. & Wellburn, A. R. Determinations of total carotenoids and chlorophylls a and b of leaf extracts in different solvents. *Biochem. Soc. Trans.* **11**, 591–592 (1983).

206. Piknova, B. & Schechter, A. N. Measurement of Nitrite in Blood Samples Using the Ferricyanide-Based Hemoglobin Oxidation Assay. *Methods Mol. Biol.* **704**, 39–56 (2011).

207. Groß, F., Rudolf, E. E., Thiele, B., Durner, J. & Astier, J. Copper amine oxidase 8 regulates arginine-dependent nitric oxide production in Arabidopsis thaliana. *J. Exp. Bot.* **68**, 2149–2162 (2017).

208. Hermanson, G. T. B. *Bioconjugate Techniques*. (Academic Press, 2013).

209. Baubec, T., Finke, A., Mittelsten Scheid, O. & Pecinka, A. Meristem-specific expression of epigenetic regulators safeguards transposon silencing in Arabidopsis. *EMBO Rep* **15**, 446–452 (2014).

210. Corpas, F. J., Alché, J. D. & Barroso, J. B. Current overview of S-nitrosoglutathione (GSNO) in higher plants. *Front. Plant Sci.* **4**, 126 (2013).

211. Thalineau, E. *et al.* Cross-Regulation between N Metabolism and Nitric Oxide (NO) Signaling during Plant Immunity. *Front. Plant Sci.* **7**, (2016).

212. Corpas, F. J. *et al.* Metabolism of reactive nitrogen species in pea plants under abiotic stress conditions. *Plant Cell Physiol.* **49**, 1711–1722 (2008).

213. Van Wilder, V. *et al.* C1 metabolism and chlorophyll synthesis: the Mg-protoporphyrin IX methyltransferase activity is dependent on the folate status. *New Phytol* **182**, 137–145 (2009).

214. Szyf, M. Epigenetics, DNA methylation, and chromatin modifying drugs. *Annu Rev Pharmacol Toxicol* **49**, 243–263 (2009).

215. Noctor, G. *et al.* Glutathione in plants: An integrated overview. *Plant, Cell Environ.* **35**, 454–484 (2012).

216. Fan, J., Krautkramer, K. A., Feldman, J. L. & Denu, J. M. Metabolic regulation of histone post-translational modifications. *ACS Chem Biol* **10**, 95–108 (2015).

217. Smith, C. M. *et al.* Mass spectrometric quantification of acetylation at specific lysines within the amino-terminal tail of histone H4. *Anal. Biochem.* **316**, 23–33 (2003).

218. Thompson, J. D., Higgins, D. G. & Gibson, T. J. CLUSTAL W: Improving the sensitivity of progressive multiple sequence alignment through sequence weighting, position-specific gap penalties and weight matrix choice. *Nucleic Acids Res.* **22**, 4673–4680 (1994).

219. Hall, T. A. BioEdit: a user-friendly biological sequence alignment editor and analysis program for Windows 95/98/NT. *Nucleic Acids Symposium Series* vol. 41 95–98 (1999).

220. Elmayan, T., Proux, F. & Vaucheret, H. Arabidopsis RPA2: A Genetic Link among Transcriptional Gene Silencing, DNA Repair, and DNA Replication. *Curr. Biol.* **15**, 1919–1925 (2005).

221. Lippman, Z., May, B., Yordan, C., Singer, T. & Martienssen, R. Distinct Mechanisms Determine Transposon Inheritance and Methylation via Small Interfering RNA and Histone Modification. *PLoS Biol.* **1**, e67 (2003).

222. Mathieu, O., Probst, A. V & Paszkowski, J. Distinct regulation of histone H3 methylation at lysines 27 and 9 by CpG methylation in Arabidopsis. *EMBO J.* **24**, 2783–2791 (2005).

223. Mull, L., Ebbs, M. L. & Bender, J. A histone methylation-dependent DNA methylation pathway is uniquely impaired by deficiency in Arabidopsis S-adenosylhomocysteine hydrolase. *Genetics* **174**, 1161–1171 (2006).

224. Krueger, F., Kreck, B., Franke, A. & Andrews, S. R. DNA methylome analysis using short bisulfite sequencing data. *Nat. Methods* **9**, 145 (2012).

225. Cokus, S. J. *et al.* Shotgun bisulphite sequencing of the Arabidopsis genome reveals DNA methylation patterning. *Nature* **452**, 215–219 (2008).

226. Veiseth, S. V. *et al.* The SUVR4 histone lysine methyltransferase binds ubiquitin and converts H3K9me1 to H3K9me3 on transposon chromatin in arabidopsis. *PLoS Genet.* **7**, (2011).

227. Dutta, A., Choudhary, P., Caruana, J. & Raina, R. JMJ27, an Arabidopsis H3K9 histone demethylase, modulates defense against Pseudomonas syringae and flowering time. *Plant J.* **91**, 1015–1028 (2017).

228. Lu, F. *et al.* Comparative analysis of JmjC domain-containing proteins reveals the potential histone demethylases in Arabidopsis and rice. *J Integr Plant Biol* **50**, 886–896 (2008).

229. Li, C. *et al.* Concerted genomic targeting of H3K27 demethylase REF6 and chromatin-remodeling ATPase BRM in Arabidopsis. *Nat. Genet.* **48**, 687–693 (2016).
230. Ye, R. *et al.* Cytoplasmic Assembly and Selective Nuclear Import of Arabidopsis ARGONAUTE4/siRNA Complexes. *Mol. Cell* **46**, 859–870 (2012).
231. Cho, J. N. *et al.* Control of Seed Germination by Light-Induced Histone Arginine Demethylation Activity. *Dev. Cell* **22**, 736–748 (2012).
232. Hang, R. *et al.* Arabidopsis protein arginine methyltransferase 3 is required for ribosome biogenesis by affecting precursor ribosomal RNA processing . *Proc. Natl. Acad. Sci.* **111**, 16190–16195 (2014).
233. Xu, S., Guerra, D., Lee, U. & Vierling, E. S-nitrosoglutathione reductases are low-copy number, cysteine-rich proteins in plants that control multiple developmental and defense responses in Arabidopsis. *Front Plant Sci* **4**, 430 (2013).
234. Rusterucci, C., Espunya, M. C., Diaz, M., Chabannes, M. & Martinez, M. C. S-Nitrosoglutathione Reductase Affords Protection against Pathogens in Arabidopsis, Both Locally and Systemically. *Plant Physiol.* **143**, 1282–1292 (2007).
235. Mnatsakanyan, R. *et al.* Proteome-wide detection of S-nitrosylation targets and motifs using bioorthogonal cleavable-linker-based enrichment and switch technique. *Nat. Commun.* **10**, 1–12 (2019).
236. Puyaubert, J. & Baudouin, E. New clues for a cold case: nitric oxide response to low temperature. *Plant Cell Env.* **37**, 2623–2630 (2014).
237. Kolbert, Z. *et al.* S-Nitrosothiol Signaling Is involved in Regulating Hydrogen Peroxide Metabolism of Zinc-Stressed Arabidopsis. *Plant Cell Physiol.* **60**, 2449–2463 (2019).
238. Marchand, C. H. *et al.* Thioredoxin targets in Arabidopsis roots. *Proteomics* **10**, 2418–2428 (2010).
239. Smith, J. N. & Dasgupta, T. P. Kinetics and Mechanism of the Decomposition of S-Nitrosoglutathione by l-Ascorbic Acid and Copper Ions in Aqueous Solution to Produce Nitric Oxide. *Nitric Oxide* **4**, 57–66 (2000).
240. Keisham, M. *et al.* Deciphering the nitric oxide, cyanide and iron-mediated actions of sodium nitroprusside in cotyledons of salt stressed sunflower seedlings. *Nitric Oxide - Biol. Chem.* **88**, 10–26 (2019).
241. Zhou, J. *et al.* Genome-wide profiling of histone H3 lysine 9 acetylation and dimethylation in arabidopsis reveals correlation between multiple histone marks and gene expression. *Plant Mol. Biol.* **72**, 585–595 (2010).
242. Hoffman, D. R., Cornatzer, W. E. & Duerre, J. A. Relationship between tissue levels of S-adenosylmethionine, S-adenosylhomocysteine, and transmethylation reactions. *Can. J. Biochem.* **57**, 56–64 (1979).
243. Vanin, A. F. *et al.* Endogenous superoxide production and the nitrite/nitrate ratio control the concentration of bioavailable free nitric oxide in leaves. *J. Biol. Chem.* **279**, 24100–24107 (2004).
244. Ramirez, L., Simontacchi, M., Murgia, I., Zabaleta, E. & Lamattina, L. Nitric oxide, nitrosyl iron complexes, ferritin and frataxin: A well equipped team to preserve plant iron homeostasis. *Plant Sci.* **181**, 582–592 (2011).
245. Simontacchi, M., Buet, A., Lamattina, L. & Puntarulo, S. Exposure to nitric oxide increases the nitrosyl-iron complexes content in sorghum embryonic axes. *Plant Sci.* **183**, 159–166 (2012).
246. Nozoye, T. The Nicotianamine Synthase Gene Is a Useful Candidate for Improving the Nutritional Qualities and Fe-Deficiency Tolerance of Various Crops. *Front. Plant Sci.* **9**, 1–7 (2018).
247. Sivitz, A. B., Hermand, V., Curie, C. & Vert, G. Arabidopsis bHLH100 and bHLH101 Control Iron Homeostasis via a FIT-Independent Pathway. *PLoS One* **7**, e44843 (2012).
248. Tzvetkova-Chevolleau, T. *et al.* The light stress-induced protein ELIP2 is a regulator of chlorophyll synthesis in Arabidopsis thaliana. *Plant J.* **50**, 795–809 (2007).
249. Speckmann, B. *et al.* Selenium increases hepatic DNA methylation and modulates one-carbon metabolism in the liver of mice. *J. Nutr. Biochem.* **48**, 112–119 (2017).
250. Luka, Z., Capdevila, A., Mato, J. M. & Wagner, C. A Glycine N-methyltransferase knockout mouse model for humans with deficiency of this enzyme. *Transgenic Res.* **15**, 393–397 (2006).
251. Detich, N., Hamm, S., Just, G., Knox, J. D. & Szyf, M. The methyl donor S-Adenosylmethionine inhibits active demethylation of DNA. A candidate novel mechanism for the pharmacological effects of S-Adenosylmethionine. *J. Biol. Chem.* **278**, 20812–20820 (2003).
252. Crack, J. C., Green, J., Thomson, A. J. & Brun, N. E. L. Iron-sulfur clusters as biological sensors: The chemistry of reactions with molecular oxygen and nitric oxide. *Acc. Chem. Res.* **47**, 3196–3205 (2014).
253. Ara, A. I., Xia, M., Ramani, K., Mato, J. M. & Lu, S. C. S-Adenosylmethionine Inhibits Lipopolysaccharide-Induced Gene Expression via Modulation of Histone Methylation. *Hepatology* **47**, 1655–1666 (2008).
254. Lu, F., Cui, X., Zhang, S., Jenuwein, T. & Cao, X. Arabidopsis REF6 is a histone H3 lysine 27 demethylase. *Nat Genet* **43**, 715–719 (2011).
255. Crevillen, P. *et al.* Epigenetic reprogramming that prevents transgenerational inheritance of the vernalized state. *Nature* **515**, 587–590 (2014).
256. Gan, E. S. *et al.* Jumonji demethylases moderate precocious flowering at elevated temperature via regulation of FLC in Arabidopsis. *Nat Commun* **5**, 5098 (2014).
257. Hewezi, T. *et al.* Cyst Nematode Parasitism Induces Dynamic Changes in the Root Epigenome. *Plant Physiol.* **174**, 405 LP – 420 (2017).
258. Zhang, X. *et al.* Genome-wide high-resolution mapping and functional analysis of DNA methylation in arabidopsis. *Cell* **126**, 1189–1201 (2006).
259. Takuno, S. & Gaut, B. S. Gene body methylation is conserved between plant orthologs and is of evolutionary consequence. *Proc. Natl. Acad. Sci.* **110**, 1797–1802 (2013).
260. Dowen, R. H. *et al.* Widespread dynamic DNA methylation in response to biotic stress. *Proc. Natl. Acad. Sci. U. S. A.*

109, (2012).

261.   Li, P. *et al.* The Arabidopsis UDP-glycosyltransferases UGT79B2 and UGT79B3, contribute to cold, salt and drought stress tolerance via modulating anthocyanin accumulation. *Plant J.* **89**, 85–103 (2017).

262.   Gollhofer, J., Schläwicke, C., Jungnick, N., Schmidt, W. & Buckhout, T. J. Members of a small family of nodulin-like genes are regulated under iron deficiency in roots of Arabidopsis thaliana. *Plant Physiol. Biochem.* (2011).

263.   Greenberg, M. V. C. & Bourc'his, D. The diverse roles of DNA methylation in mammalian development and disease. *Nat. Rev. Mol. Cell Biol.* **20**, 590–607 (2019).

264.   Stroud, H. *et al.* DNA methyltransferases are required to induce heterochromatic re-replication in Arabidopsis. *PLoS Genet.* **8**, e1002808 (2012).

265.   Fouché, S. *et al.* Stress-driven transposable element de-repression dynamics and virulence evolution in a fungal pathogen. *Mol. Biol. Evol.* (2019).

266.   Vaillant, I. & Paszkowski, J. Role of histone and DNA methylation in gene regulation. *Curr. Opin. Plant Biol.* **10**, 528–533 (2007).

267.   Underwood, C. J., Henderson, I. R. & Martienssen, R. A. Genetic and epigenetic variation of transposable elements in Arabidopsis. *Curr. Opin. Plant Biol.* **36**, 135–141 (2017).

268.   Zilberman, D. An evolutionary case for functional gene body methylation in plants and animals. *Genome Biol.* **18**, 17–19 (2017).

269.   Manavella, P. A. *et al.* Cross-talk between ethylene and drought signalling pathways is mediated by the sunflower Hahb-4 transcription factor. *Plant J.* **48**, 125–137 (2006).

270.   Shook, M. S. & Richards, E. J. VIM proteins regulate transcription exclusively through the MET1 cytosine methylation pathway. *Epigenetics* **9**, 980–986 (2014).

271.   Kim, J., Kim, J. H., Richards, E. J., Chung, K. M. & Woo, H. R. Arabidopsis VIM proteins regulate epigenetic silencing by modulating DNA methylation and histone modification in cooperation with MET1. *Mol. Plant* **7**, 1470–1485 (2014).

272.   Stroud, H. *et al.* The roles of non-CG methylation in Arabidopsis. *Nat Struct Mol Biol* **21**, 64–72 (2014).

273.   Locato, V., Cimini, S. & De Gara, L. ROS and redox balance as multifaceted players of cross-tolerance: Epigenetic and retrograde control of gene expression. *J. Exp. Bot.* **69**, 3373–3391 (2018).

274.   Green, L. S. *et al.* Mechanism of inhibition for N6022, a first-in-class drug targeting S-nitrosoglutathione reductase. *Biochemistry* **51**, 2157–2168 (2012).

275.   Liu, Z. W. *et al.* Two Components of the RNA-Directed DNA Methylation Pathway Associate with MORC6 and Silence Loci Targeted by MORC6 in Arabidopsis. *PLoS Genet.* **12**, 1–24 (2016).

276.   Xue, Y. *et al.* GPS-SNO: Computational prediction of protein s-nitrosylation sites with a modified GPS algorithm. *PLoS One* **5**, 1–7 (2010).

277.   Lee, T. Y., Chen, Y. J., Lu, T. C., Huang, H. Da & Chen, Y. J. Snosite: Exploiting maximal dependence decomposition to identify cysteine S-Nitrosylation with substrate site specificity. *PLoS One* **6**, (2011).

278.   Xu, Y., Shao, X.-J., Wu, L.-Y., Deng, N.-Y. & Chou, K.-C. iSNO-AAPair: supplementary material. *PeerJ* **1**, e171 (2013).

279.   Xu, Y., Ding, J., Wu, L. Y. & Chou, K. C. iSNO-PseAAC: Predict Cysteine S-Nitrosylation Sites in Proteins by Incorporating Position Specific Amino Acid Propensity into Pseudo Amino Acid Composition. *PLoS One* **8**, 1–7 (2013).

280.   Zhu, J. K., Kapoor, A., Sridhar, V. V., Agius, F. & Zhu, J. K. The DNA Glycosylase/Lyase ROS1 Functions in Pruning DNA Methylation Patterns in Arabidopsis. *Curr. Biol.* **17**, 54–59 (2007).

281.   Sako, K. *et al.* Arabidopsis RPT2a, 19S proteasome subunit, regulates gene silencing via DNA methylation. *PLoS One* **7**, e37086 (2012).

282.   Jeong, I. S. *et al.* Arabidopsis C-terminal domain phosphatase-like 1 functions in miRNA accumulation and DNA methylation. *PLoS One* **8**, e74739 (2013).

283.   He, X. J. *et al.* An Effector of RNA-Directed DNA Methylation in Arabidopsis Is an ARGONAUTE 4- and RNA-Binding Protein. *Cell* **137**, 498–508 (2009).

284.   Gao, Z. *et al.* An RNA polymerase II- and AGO4-associated protein acts in RNA-directed DNA methylation. *Nature* **465**, 106–109 (2010).

285.   Durut, N. *et al.* A duplicated NUCLEOLIN gene with antagonistic activity is required for chromatin organization of silent 45S rDNA in Arabidopsis. *Plant Cell* **26**, 1330–44 (2014).

286.   Johnson, L. M. *et al.* The SRA methyl-cytosine-binding domain links DNA and histone methylation. *Curr. Biol.* **17**, 379–384 (2007).

287.   Kuhlmann, M. & Mette, M. F. Developmentally non-redundant SET domain proteins SUVH2 and SUVH9 are required for transcriptional gene silencing in Arabidopsis thaliana. *Plant Mol. Biol.* **79**, 623–633 (2012).

288.   Pontier, D. *et al.* Reinforcement of silencing at transposons and highly repeated sequences requires the concerted action of two distinct RNA polymerases IV in Arabidopsis. *Genes Dev.* **19**, 2030–2040 (2005).

289.   Steimer, a *et al.* Endogenous targets of transcriptional gene silencing in Arabidopsis. *Plant Cell* **12**, 1165–1178 (2000).

290.   Xia, R. *et al.* ROR1/RPA2A, a putative replication protein A2, functions in epigenetic gene silencing and in regulation of meristem development in Arabidopsis. *Plant Cell* **18**, 85–103 (2006).

291.   Soldi, M. *et al.* Chromatin proteomics reveals novel combinatorial histone modification signatures that mark distinct subpopulations of macrophage enhancers. *Nucleic Acids Res.* **45**, 12195–12213 (2017).

292.   Kanehisa, M., Sato, Y., Furumichi, M., Morishima, K. & Tanabe, M. New approach for understanding genome variations in KEGG. *Nucleic Acids Res.* **47**, D590–D595 (2019).

293. Li, Q. *et al.* Regulation of Active DNA Demethylation by a Methyl-CpG-Binding Domain Protein in Arabidopsis thaliana. *PLoS Genet.* **11**, e1005210 (2015).
294. Frost, J. M. *et al.* FACT complex is required for DNA demethylation at heterochromatin during reproduction in Arabidopsis. *Proc. Natl. Acad. Sci.* **115**, E4720–E4729 (2018).
295. Cuerda-Gil, D. & Slotkin, R. K. Non-canonical RNA-directed DNA methylation. *Nat. Plants* **2**, 16163 (2016).

Eidesstattliche Erklärung

Ich erkläre an Eides statt, dass ich die bei der promotionsführenden Einrichtung

Wissenschaftszentrum Weihenstephan für Ernährung, Landnutzung und Umwelt (WZW)

Lehrstuhl für Biochemische Pflanzenpathologie

Der TUM zur Promotionsprüfung vorgelegt Arbeit mit dem Titel:

"Loss of S-NITROSOGLUTATHIONE REDUCTASE 1 (GSNOR1) function leads to an altered DNA and histone methylation pattern in *Arabidopsis thaliana*"

unter der Anleitung und Betreuung durch Prof. Dr. Jörg Durner ohne sonstige Hilfe erstellt und bei der Abfassung nur die gemäß § 6 Abs. 6 und 7 Satz 2 angegebenen Hilfsmittel benutzt habe.

Ich habe keine Organisation eingeschaltet, die gegen Entgelt Betreuerinnen und Betreuer für die Anfertigung von Dissertationen sucht, oder die mir obliegenden Pflichten hinsichtlich der Prüfungsleistungen für mich ganz oder teilweise erledigt.

Ich habe die Dissertation in dieser oder ähnlicher Form in keinem anderen Prüfungsverfahren vorgelegt.

Ich habe den angestrebten Doktorgrad noch nicht erworben und bin nicht in einem früheren Promotionsverfahren für den angestrebten Doktorgrad endgültig gescheitert.

Die öffentlich zugängliche Promotionsordnung der TUM ist mir bekannt, insbesondere habe ich die Bedeutung von § 28 (Nichtigkeit der Promotion) und § 29 (Entzug des Doktorgrades) zur Kenntnis genommen. Ich bin mir der Konsequenzen einer falschen Eidesstaatlichen Erklärung bewusst.

Mit der Aufnahme meiner personenbezogenen Daten in die Alumni-Datei bei der TUM bin ich einverstanden.

München, am 30.01.2020

Eva Rudolf